International Conference on Green and Human Information Technology 2016

Proceedings of ICGHIT 2016

Feb. 24 ~ Feb. 26, 2016

Clark, Angeles City, Philippines

http://icghit.org/

IEIE

IEEE SEOUL SECTION

Organized by

THE INSTITUTE OF ELECTRONICS AND INFORMATION ENGINEERS
Computer Information Society

Technically co-sponsored by

IEEE
SEOUL SECTION

Contents

ICGHIT 2016 Committee

I. International Advisory Committee

Hyunsik Ahn (Tongmyong Univ., President of IEIE CIS, Korea)
SangHyun Lee (Univ.of Michigan, USA)
Ebroul Izquierdo (Queen Mary Univ. of London, UK)
Abbas Jamalipour (Univ. of Sydney, Australia)

II. Organizing Committee

General Co-Chairs
- Beongku An (Hongik University, Korea)
- Kyutae Lee (Kongju National University, Korea)

Organizing Chair
- Seungcheon Kim(Hansung University, Korea)

Local Management Chair
- Gilbert M. Tumibay(AUF, Philippines)

Publication Co-Chairs
- Soyoung Rho (Wolsong Publication, Korea)
- Chansu Lee (Youngnam University, Korea)

Finance Chair
- Einjeon Hwang (Myungji Hospital, Korea)

Administration Co-Chairs
- Jinhong Kim (Sungkyunkwan Univ., Korea)

International Cooperation Co-Chairs
- Franklin Bien (UNIST, Korea)
- Wang Ye (Lishui Univ., China)
- Jongyun Kim (Kyungdong Univ.)

Promotion Co-Chairs

- Moonsik Kang (Gangneung Nat. Univ., Korea)

Exhibition & Recruiting Co-Chairs

- Soonyoung Chun (Dongyang University, Korea)
- Byungsoon Cho (C&C Instrument, Korea)

Industrial Cooperation Co-Chairs

- Yousik Hong (Sangji Univ., Korea)
- Byongmin Im (New International Limited, Korea)
- Le Quoc Cuong (Department of Information and Communications of HoChiMinh, Vietnam)

III. Technical Program Committee

• TPC Co-Chairs
  - Hoon JIN (Kyonggi University, Korea)
  - Yongsoo Choi (Sungkyul Univercity, Korea),
  - Soo-Hyun Park (Kookmin University, Korea),
  - Sathaporn Promwong (King Mongkut's Institute of Tech. Ladkrabang, Thailand)

• TPC Members
  - Minho Jo (Korea University, Korea)
  - Jong-Yun Kim (Kyungdong University, Korea)
  - Abderrahim Benslimane (University of Avignon, France)
  - Alan Liew (Griffith University, Australia)
  - Jun Jo (Griffith University, Australia)
  - V. Mani (Indian Institute of Science, India)
  - Sundaram Suresh (Nanyang Technological University, Singapore)
  - Qianni Zhang (Queen Mary University of London, UK)
  - Shijun Xiang (Jinan University, China)
  - Ned Koch (Texas A&M International University, USA)
  - Bela Stantic (Griffith University, Australia)
  - Xiping Ma (BeiHua University, China)

- Dumitru Dan Burdescu (University of Craiova, Romania)
- Ahmed Al-Dubai (University of Glasgow, UK)
- Nørregaard Jørgensen (University of Southern Denmark, Denmark)
- Woontack Woo (KAIST, Korea)
- Jungyeon Shim (Kangnam University, Korea)
- Min-Ho Lee (Kyungpook National University, Korea)
- Moon-Goo Lee (Kimpo College, Korea)
- Chang Hyun Oh (Korea University, Korea)
- Byung Seo Kim (Hongik University, Korea)
- Seong Oun Hwang (Hongik University, Korea)

Conference Venue Information

HOTEL INFORMATION

The conference will be held at which is located in the free port zone of Angeles City.

XENIA HOTEL(http://xeniahotel.com.ph)
CLARK FREEPORT ZONE

When visiting Angeles City and Clark, you'll feel right at home at Xenia Hotel Clark, which offers quality accommodation and great service. From here, guests can enjoy easy access to all that the lively city has to offer. With its convenient location, the hotel offers easy access to the city's must-see nature and business destinations.

Xenia Hotel Clark Philippines offers impeccable service and all the essential amenities to invigorate travelers. For the comfort and convenience of guests, the hotel offers 24-hour front desk, room service, complimentary Wi-Fi, car park, airport transfer.

Guests can choose from 200 rooms, all of which exude an atmosphere of total peace and harmony with fantastic views of greeneries and tropical elegance from guestroom verandas.

The hotel offers wonderful recreational facilities such as an outdoor pool with a poolside bar to make your stay truly unforgettable. Whatever your purpose of visit, Xenia Hotel Clark Philippines is an excellent choice for your stay in Angeles city, Clark.

Program Schedule

Time	Room: Sapphire	Room: Diamond	Room: Emerald
Wednesday, Feb. 24			
09:30 ~ 10:00	Registration(Feb24-26 9:30 AM to 17:00 PM)		
10:00 ~ 10:20	Opening Ceremony		
10:20 ~ 11:10		Plenary Talk Ⅰ : Prof. Gilbert M. Tumibay (AUF, Philippines)	
11:10 ~ 11:20	Break Time		
11:20 ~ 12:10		Plenary Talk Ⅱ : Prof. Franklin Bien(UNIST, Korea)	
12:10 ~ 13:40	Lunch		
13:40 ~ 14:40	Session Ⅰ-1 : (Oral) Communication and Ubiquitous Ⅰ		Session Ⅰ-2 : (Poster) Convergence Ⅰ
13:40 ~ 16:10			
16:10 ~ 16:20	Break Time		
16:20 ~ 17:20		Welcome Reception (Snack&Tea Party)	
Thursday, Feb. 25			
09:30 ~ 10:00	Registration		
10:00 ~ 12:10	Session Ⅱ-1 : (Oral) Convergence Ⅱ		Session Ⅱ-2 : (Oral) Communication and Ubiquitous Ⅱ
12:10 ~ 13:40	Lunch		
13:40 ~ 15:50	Session Ⅲ-1 : (Oral) Convergence Ⅲ		Session Ⅲ-2 : (Oral) Control Information System
15:50 ~ 16:00	Break Time		
16:00 ~ 17:20	Recruit Session	Session Ⅳ : (Poster) Convergence Ⅳ	
17:20 ~ 20:00	Banquet		
Friday, Feb. 26			
09:30 ~ 10:00	Registration		
09:30 ~ 10:40	Session Ⅴ : (Poster) Multimedia and Signal Processing		
10:40 ~ 11:00	Break Time		
11:00 ~ 13:30	International corporation work		

Program Details

Wednesday, February 24

09:30 ~ 10:00

Registration(Feb24-26 9:30 AM to 17:00 PM)

10:00 ~ 10:20

Opening Ceremony

Room: Diamond

Chair: Seungcheon Kim (Hansung University, Korea)

-Welcome Address

-Congratulatory Address

10:20 ~ 11:10

Plenary Talk Ⅰ : Prof. Gilbert M. Tumibay

Title: "Research and educational opportunity in Philippines. "

Room: Diamond

Chair: Beongku An (Hongik University, Korea)

11:20 ~ 12:10

Plenary Talk Ⅱ : Prof. Franklin Bien

Title: "Enhancing the Human Life with Bio-medical IT"

Room: Diamond

Chair: Kyutae Lee (Kongju National University, Korea)

12:10 ~ 13:40

Lunch

13:40 ~ 16:10

Session I-1 : (Oral) Communication and Ubiquitous Ⅰ

Room: Sapphire

Chair: Beongku An (Hongik University, Korea), Sanguk Kang (Sangmyung University, Korea)

Yan-Ming Cheng (College of Electrical & Information Engineering Beihua University , China, P.R. China); Ye Wang (Lishui University, P.R. China); Il-Kyoo Lee (Kongju National University, Korea); Zhen-Xiong Zhou (Beihua University, P.R. China)

13:40 ~ 14:40

Session I-2 : (Poster) Convergence I

Room: Emerald

Chair: Franklin Bien (UNIST, Korea), Jongyun Kim (Kyungdong University, Korea)

16:10 ~ 16:20

Break Time

16:20 ~ 17:20

Welcome Reception (Snack&Tea Party)

Thursday, February 25

09:30 ~ 10:00

Snack & Morning Tea

10:00 ~ 12:10

Session Ⅱ-1 : (Oral) Convergence Ⅱ

Room: Sapphire

Chair: Jinhong Kim (Sungkyunkwan University, Korea), Sehwan Park (KIST, Korea)

10:00 ~ 12:10

Session Ⅱ-2 : (Oral) Communication and Ubiquitous Ⅱ

Room: Emerald

Chair: Moonsik Kang (Gangneung-Wonju University, Korea), Chair: Seungcheon Kim (Hansung University, Korea)

12:10 ~ 13:40

Lunch

13:40 ~ 15:50

Session Ⅲ-1 : (Oral) Convergence Ⅲ

Room: Sapphire

Chair: Chan-Su Lee (Youngnam University, Korea), Janggeun Ki (Kongju National University, Korea)

13:40 ~ 15:50

Session Ⅲ-2 : (Oral) Control Information System

Room: Emerald

Chair: Hyunsik Ahn (Tongmyoung University, Korea), Yousik Hong (Sangji University, Korea)

15:50 ~ 16:00

Break Time

16:00 ~ 17:20

Session IV : (Poster) Convergence IV

Room: Diamond

Chair: Yongsu Choi (Sungkyul University, Korea), Einjeong Hwang (Myungji Hospital)

17:20 ~ 20:00

Banquet

Friday, February 26

09:30 ~ 10:00

Snack & Morning Tea

09:30 ~ 10:40

Session V : (Poster) Multimedia and Signal Processing

Room: Sapphire

Chair: Kyutae Lee (Kongju National University, Korea), Sanguk Kang (Sangmyung University, Korea)

10:40 ~ 11:00

Break Time

11:00 ~ 13:30

International Cooperation Work

Wednesday, Feb. 24

Session I-1 : (Oral) Communication and Ubiquitous I

Applying Beamforming to LTE Base Station for Reducing Interference Impact and Saving Frequency

Yan-Ming Cheng
College of Electrical & Information Engineering
Beihua University
Jilin, China
mycheng@kongju.ac.kr

Ye Wang
The Department of Electronic and Information Engineering Lishui University Zhejiang, China
wychina_2007@ hotmail.com

Il-Kyoo Lee†
Division of Electrical, Electronics & Control Engineering
Kongju National University
Cheonan, Korea
leeik@ kongju.ac.kr

Zhen-Xiong Zhou
College of Electrical & Information Engineering
Beihua University
Jilin, China
742884852@qq.com

***Abstract*—This paper assumes that Long Term Evolution (LTE) will be deployed in TV White Spaces (TVWSs) and beamforming is applied to LTE base station (BS) for reducing interference impact of LTE on DTV. A simulation method based on Monte Carlo is proposed to evaluate the interference probability in DTV receiver in the case of interference impact of LTE BS on DTV receiver. As a result, the interference impact of LTE BS on DTV receiver is efficiently mitigated and the guard band remarkably reduced when LTE BS uses beamforming.**

Keywords- Long Term Evolution (LTE); TV White Spaces (TVWSs); beamforming; DTV;interference probability

I. INTRODUCTION

The compatibility between LTE and DTV has to be taken into account before LTE is deployed in practice in TV White Spaces (TVWSs). In this paper, only interference from LET base stations (BSs) to DTV is considered. Beamforming as one of interference mitigation techniques is assumed to be applied to LTE BS for reducing interference impact on DTV. On the basis of the assumption, the performance of DTV receiver is evaluated with Monte Carlo method.

II. PROPOSED SIMULATION METHOD

The interference probability is chosen as criteria to evaluate the performance of DTV receiver (Rx). Referring to the principle of calculation of the interference probability in victim in Spectrum Engineering Advanced Monte Carlo Analysis Tool (SEAMCAT)[1], the interference probability (P_I) in DTV Rx can be calculated by suing Eq.(1).

$$P_I = 1 - P_{NI} \tag{1}$$

Where P_{NI} is the probability of non interference (NI) of in DTV Rx .

In the case of LTE interfering with DTV, ratio of the desired receiver signal level (C) in DTV Rx to the received interfering signal level (I) in DTV Rx is chosen as protection criteria. Therefore, PIN is defined as

$$P_{NI} = P\left((C/I)_{trial} > (C/I)_{criteria} \left| \mathrm{C}_{\mathrm{trial}} >= \mathrm{Sensitivity} \right.\right) \tag{2}$$

Here $(C/I)_{trial}$ is one trial C/I. $(C/I)_{criteria}$ represents protection criteria of DTV receiver. C_{trial} is desired received signal strength in DTV at one trial and sensitivity is the sensitivity of DTV Rx.

By definition of $P(A|B)=P(A \cap B)/P(B)$, P_{NI} becomes

$$P_{NI} = \frac{P\left((C/I)_{trial} > (C/I)_{criteria}, C_{trial} >= Sensitivity\right)}{P(C_{trial} >= Sensitivity)} \tag{3}$$

Due to LTE BS uses beamforming in scenario of LTE interfering with DTV Rx, only the interference of LTE BS into DTV Rx is analyzed. $(C/I)_{trial}$ in DTV Rx can be expressed as

$$\left(C/I\right)_{\substack{trial \\ LTE\ BS \to DTV\ Rx}} = \frac{Desired\ signal\ in\ DTV\ Rx}{\sum_{j=1}^{n}\sum_{i=1}^{N}\left(10^{\frac{P_{BS_i}}{10}} \times 10^{\frac{G(Beamformig)_j}{Between\ BS_i\ and\ DTV\_Rx}} \times 10^{-\frac{PL(d_i)}{10}} \times 10^{-\frac{Shaowing(\xi_i)}{10}}\right)} \tag{4}$$

Where considering the worst case, DTV Rx is assumed to locate at the edge of DTV transmitter coverage. Therefore, sensitivity of DTV Rx is used as the minimum desired received signal level in DTV Rx. The j represents the number of the jth MS_j in each LTE Cell and the i represents the number of the ith BS_i in each LTE cell. P_{BSi} is the transmit power of the ith LTE BSi. $PL(d_i)$ is path loss (PL) corresponding to the ith path loss from the ith BS_i to DTV Rx. The ξ_i is the distortion due to shadowing between the ith BS_i and DTV Rx.

Eq.(5) represents the jth beamforming gain from the ith LTE BS_i to DTV Rx, which is determined by the jth LTE MS_j in each LTE cell.

Sponsors: Scientific and Technological Planning Project of Jilin Province of China (No.20150519023JH); Scientific and Technological Research Project of Department of Education of Jilin Province of China (No.2014167).

†Corresponding author: Il-Kyoo Lee

$$G(Beamformig)_{\substack{j \\ Between\ BS_i\ and\ DTV\_Rx}} = G_{HB_i}(\theta_{HRx}) + G_{VB_i}(\phi_{VRx}) + G_{HRx}(\theta_{HB_i}) + G_{VRx}(\phi_{VB_i}) \quad (5)$$

Where the symbol $G_{HBi}(\theta_{HRx})$ represents horizontal antenna gain of the ith LTE BS_i toward θ_{HRx}, where θ_{HRx} is direction of DTV Rx from the ith LTE BSi in horizontal direction. The symbol G_{VBi} (Φ_{VRx}) represents vertical antenna gain of the ith LTE BS_i toward Φ_{VRx} , where φ_{VRx} is vertical direction from LTE BS_i to DTV Rx. In the same way, $G_{HRx}(\theta_{HBi})$ represents the horizontal antenna gain of DTV Rx toward θ_{HBi}, where θ_{HBi} is the horizontal direction from DTV Rx to BSi. The symbol $GVRx(\varphi_{VBi})$ is the vertical antenna gain of DTV toward φ_{VBi}, where φ_{VBi} is the vertical direction from DTV Rx to BS_i [2].

III. Simulations and Results

In scenario of LTE BS interfering with DTV Rx, the 19-cell LTE structure is assumed. Frequency reuse is not applied in this study. 24 LTE mobile stations (MSs) in each LTE cell are assumed to be active. For comparing the performance of DTV Rx between the case of LTE BS applying beamforming and the case of LTE BS without applying beamforming, the simulations will be implemented in two cases as following:

Case 1: Beamforming technology is applied to LTE BS.

Case 2: Beamforming technology is not applied to LTE BS.

Fig.1 shows one simulation status that 24 MSs are randomly distributed in each LTE cell when snapshot is 1 and the separation distance between the central LTE BS (the reference LTE BS) is 500 m.

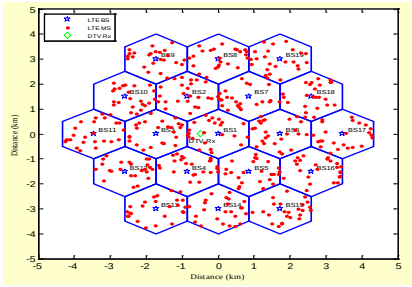

Figure 1. Simulation status

According to LTE BS emission mask [3,4], the guard band of 0 and 10 MHz are respectively selected, the interference probability in DTV Rx and the maximum allowable transmit power of LTE BS are respectively evaluated along with the increase of separation distance between DTV Rx and the reference LTE BS.

Fig.2 shows when LTE BSs are transmitting signal at the maximum allowable transmit power of 46 dBm, the interference probability in DTV Rx can be efficiently reduced when DTV Rx locates within LTE network.

Fig.3 shows that if the interference probability of 5% in DTV Rx is acceptable, the corresponding maximum allowable transmit power of LTE BS can be figured out when the different guard bands are defined and the different separation distances between DTV Rx and the reference LTE BS are required. Comparing to the maximum allowable transmit power of LTE in the case of LTE BS without applying beamforming, more than 5 dB of the maximum allowable transmit power of LTE in the case of LTE BS applying beamforming can be improved to meet the interference probability of 5%.

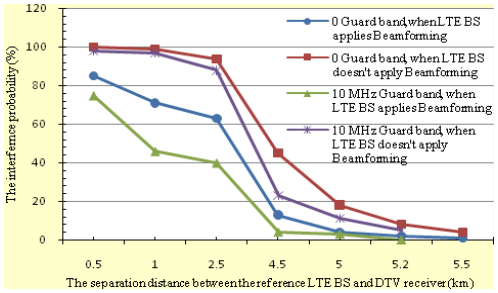

Figure 2. The relationship between the interference probability in DTV Rx and the separation distance between the reference LTE BS and DTV Rx

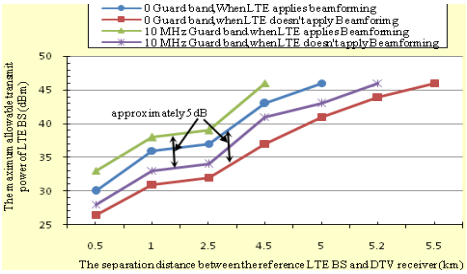

Figure 3. The relationship between the maximum allowable transmit power of LTE BS and the separation distance between DTV Rx and the reference LTE BS

IV. Conclusions

LTE was assumed to be deployed in TVWSs. For reducing interference from LTE BS to DTV Rx, beamforming is assumed to be applied by LTE BS. On the basis on of the assumption, a simulation method is proposed to evaluate the interference probability in DTV Rx impacted by LET BS with or without beamforming. As a result, the maximum allowable transmit power of LTE BS is improved about 5 dB when beamforimg is applied to LTE BS to meet the interference probability of 5%.

References

[1] *SEAMCAT Handbook*, ECO, January 2010.

[2] Hiroshi Harada, Ramjee Prasad, *Simulation and Software Radio for Mobile Communications*, Artech House, 2002, p.456-364.

[3] Report 40, Compatibility study for LTE and WiMAX operating within the bands 880-915 MHz / 925-960 MHz and 1710-1785 MHz / 1805-1880 MHz (900/1800 MHz bands), , CEPT, November 2010, p.50-51.

[4] 3GPP TR 36.942 V10.1.0, Technical Specification Group Radio Access Network; Evolved Universal Terrestrial Radio Access (E-UTRA);Radio Frequency (RF) system scenarios(Release 10), 3GPP TR, Sep.2009, p.14-15.

A Joint Optimization Algorithm for PAPR Reduction in AF Cooperative Multicarrier System

Yingshan Li[1*], Wenbo Yu[1], Haiyue Li[1], Changyoung An[2], Heung-Gyoon Ryu[2]
[1] Department of Communication engineering, College of Electronic Information and Optical Engineering, Nankai University, Tianjin, 300071, China
[2] Department of Electronic Engineering, Chungbuk National University, Korea
yingsl1122@nankai.edu.cn; 2012yuwb@mail.nankai.edu.cn; 1325158794@qq.com; acy890217@naver.com; ecomm@cbu.ac.kr

Abstract — A SLM-TR joint optimization algorithm based on CAZAC sequence is proposed. Simulation results show, proposed method can reduce PAPR considerably and improve BER performance effectively, with insurance of high spectrum efficiency, low complexity and low loss in power efficiency.

Index Terms—PAPR, SLM, TR, CAZAC Sequence

I. INTRODUCTION

Currently, there are several PAPR reduction methods, such as, signal pre-distortion technique, coding technique and non-distortion scrambling technique [1-3].

Until now, few studies has been made about PAPR problem in the cooperative communication scenario. In this paper, a new SLM-TR joint optimization algorithm based on CAZAC(Constant Amplitude Zero Auto-Correlation) sequence is proposed in the cooperative communication system. Simulation results show that, by applying proposed method, PAPR can be reduced significantly, further with the insurance of high spectrum efficiency and relatively low complexity.

II. SYSTEM DESCRIPTION

A. Cooperative Diversity

Fig. 1 and Fig. 2 describe the system model and time slot structure which is applied in this paper.

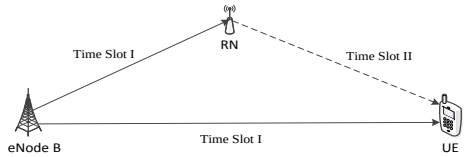

Fig.1. Cooperative System model

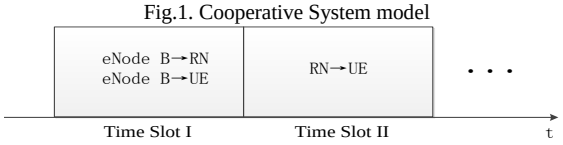

Fig.2. Time slot structure diagram

This work was supported by the TianJin Natural Science Foundation of China under Grant No. 14JCYBJC16100.
Corresponding author email: yingsl1122@nankai.edu.cn.

III. A JOINT OPTIMIZATION ALGORITHM BASED ON CAZAC SEQUENCE

In this paper, to reduce PAPR in AF(amplify-and-forward) cooperative multicarrier system, a SLM-TR joint optimization algorithm based on CAZAC sequence is proposed. The algorithm of proposed SLM-TR joint optimization algorithm can be summarized as follows:

Step1: N_{TR} tone carriers and $N-N_{TR}$ data carriers are divided first. tone carriers are reserved for tone candidates, data carriers are prepared for data transmission. n_{cazac} CAZAC sequences with length $N-N_{TR}$ are generated and stored in the memory, ready for use as the initial phase vector candidates of SLM procedure;

Step2: Select one CAZAC sequence as the initial phase vector candidate, multiply (point-wise multiplication) the data sequence with the first phase vector $P^{(0)}$ (selected CAZAC sequence), perform IFFT and then compute PAPR. Set this PAPR to $PAPR_{min}$;

Step3: Multiply the first element of phase vector ($P_n^{(0)}$, n=0) with three phase rotation factors $\left(\exp(j\pi/2), \exp(j\pi), \exp(j(3\pi/2))\right)$, multiply the data sequence with these modified phase rotation factors respectively, perform IFFT and compute PAPR, name them as PAPR2, PAPR3, PAPR4;

Step4：Compare $PAPR_{min}$ with PAPR2, PAPR3, and PAPR4 computed in step3. If $PAPR_{min}$ is still the smallest, store the $PAPR_{min}$ and corresponding phase vector, If PAPR2 is the smallest, let $PAPR_{min}$=PAPR2, and store corresponding $PAPR_{min}$ and phase vector, If PAPR3 is the smallest, let $PAPR_{min}$=PAPR3, and store corresponding $PAPR_{min}$ and phase vector, If PAPR4 is the smallest, let $PAPR_{min}$=PAPR4, and store corresponding $PAPR_{min}$ and phase vector;

Step5: Repeat the same procedure from step3 to step4 for the remaining elements of the first phase vector $P^{(0)}$;

Step6: Change the phase vector to $P^{(1)}$ and compute PAPR, compare $PAPR_{min}$ with the PAPR in step6, if PAPR>$PAPR_{min}$, then maintain $PAPR_{min}$; If PAPR<$PAPR_{min}$, update $PAPR_{min}$ as the PAPR computed in step6.

Step7: Repeat the procedure from step3 to step5 for the phase vector $P^{(1)}$.

Step8: Change the phase vector from $P^{(2)}$ to $P^{(D-1)}$ one by one, repeat step6, and then continually repeat the procedure from step3 to step5. Finally, select the modified time domain data signal with final minimum PAPR, and select final achieved phase vector $P_{selceted}$ as side information. The modified time domain data signal is considered as the initial transmission signal.

Step9: In TR procedure, randomly generate tone sequence of length N satisfying following formula, $P(m)=\begin{cases}1, & 0\le m\le N_{TR}-1\\ 0, & N_{TR}\le m\le N-1\end{cases}$, and achieve corresponding time domain tone signal through IFFT.

Step10: Find max value $x_{\max}$ and its position $m_{\max}$ of initial transmission signal, find corresponding phase and amplitude information, name it as amplitude and phase factor α , $\alpha = x_{\max}\cdot\exp(j\cdot phase(x_{\max}))$.

Step11: Time domain tone signal is optimized using cyclic transposition algorithm, that is, the max value position of time domain tone signal is cyclic trans posited to the position $m_{\max}$, then multiplied with corresponding amplitude and phase factor α computed in step10, generated signal is named as modified time domain peak-cancelling tone signal;

Step12: Above modified time domain peak-cancelling tone signal in step11 is subtracted from the initial transmission signal, residual signal is considered as the modified initial transmission signal.

Step13: Repeat the procedure k_{loop} (small value of k_{loop} is considered to reduce complexity.) times from step9 to step 12, update initial transmission signal, compute PAPR, finally achieve optimized transmission signal with lowest PAPR, transmit final optimized transmission signal, and simultaneously transmit phase vector $P_{selceted}$ for side information.

IV. Performance Results

In this paper, in order to evaluate the performance of the proposed SLM-TR joint optimization algorithm, CCDF of PAPR and BER (bit error rate) are discussed in AF cooperative communication system.

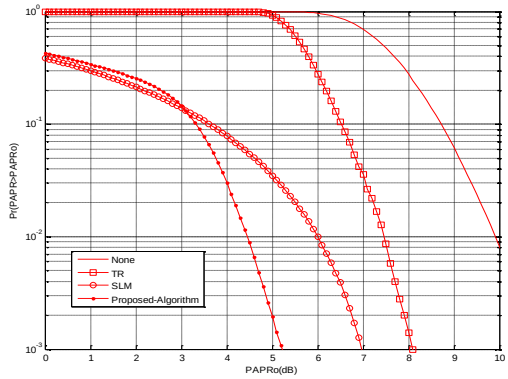

Fig.3. CCDFs of PAPR of different algorithms

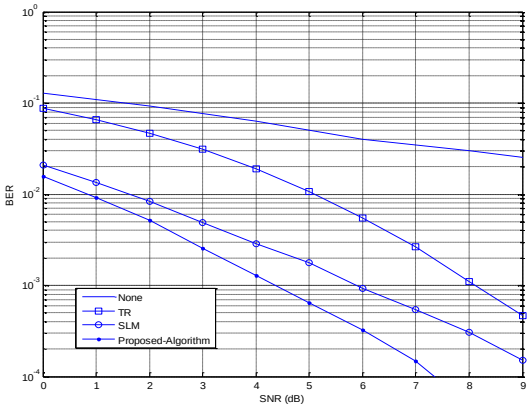

Fig.4. BER performances of different algorithms

V. Conclusions

In this paper, a new SLM-TR joint optimization algorithm based on CAZAC sequence is proposed to reduce PAPR in AF cooperative multicarrier system.

Simulation results show, proposed method can reduce PAPR considerably and improve BER performance effectively, with insurance of high spectrum efficiency, low complexity and low loss in power efficiency. Further discussion proves that, with the increase of initial phase vector number and tone carrier number, PAPR and BER performances can be improved, but it is not appropriate to increase number too much in the reason of system complexity and spectrum efficiency, about 2 or 4 is enough. Additionally, further studies must be continued to find optimum sequences as CAZAC sequence to improve system QoS.

Acknowledgment

The authors wish to thank Professor Jiaxiang Zhao. This work was supported in part by a grant from TianJin Natural Science Foundation of China.

References

[1] K. Fazel, S. Kaiser: 'Multi-Carrier and Spread Spectrum Systems'(J.Wiley House, 2003)

[2] Seung Hee Han, Jae Hong Lee: 'An overview of peak-to-average power ratio reduction techniques for multicarrier transmission', Wireless Communications, IEEE Transactions on, April 2005, Volume: 12 , Issue: 2, pp: 56 – 65.

[3] Ochiai, H, Imai, H.: 'On the distribution of the peak-to-average power ratio in OFDM signals', Communications, IEEE Transactions on, 2001, Volume: 49 , Issue: 2, pp: 282 – 289.

A Connection-Time Analysis of Vehicle-to-Mobile RSU (V2MR) Communications with a Bus Stop

Magdalena Trie Purnaningtyas
Department of Electrical and Computer Engineering
Pusan National University
Busan, 609-735 Republic of Korea
magdalena@pusan.ac.kr

Han-You Jeong
Department of Electrical and Computer Engineering
Pusan National University
Busan, 609-735 Republic of Korea
hyjeong@pusan.ac.kr

***Abstract*—We study the connection time of vehicle-to-mobile roadside unit (V2MR) communications which can reduce the significant cost of the fixed RSU by installing a gateway of mobile network into a transit bus called the mobile RSU. In the V2MR communications, the connectivity of a commute vehicle can be improved via ad-hoc connection to a nearby mobile RSU. In this paper, we present a new analysis model to estimate the connection time between a commute vehicle and a mobile RSU, when there is a bus stop in their overlapping route. Since the connection time between two vehicles is highly dynamic and unpredictable, our analysis will provide a fundamental basis of connection-time estimation of V2MR communications. Numerical results show that our analysis can estimate the connection time of V2MR communications with the average error below 1.0 percent.**

Keywords*: *V2MR communications, mobile RSU, connection time.

I. Introduction

Vehicular ad-hoc networks (VANETs) have recently considered the attention of both academia and industry [1]. To support emerging vehicle safety and transportation efficiency applications, the VANETs enable a vehicle, as a mobile node, to communicate with each other via vehicle-to-vehicle (V2V) communication, and/or with a fixed roadside unit (RSU) via vehicle-to-infrastructure (V2I) communication. The unique characteristic of the VANET is a rapid change of connectivity due to the high mobility of vehicles, which leads to a dynamic topology change, as well as a short connection time.

In general, the fixed RSU (FR) plays the role of gateway between a VANET and a legacy network, such as the Internet. However, the high cost of deploying and operating the FR is the main obstacle to enhance the penetration rate of the FR. Moreover, the short connection time of the V2I communication lowers the cost efficiency of the FR.

In this paper, we advocate the use of vehicle-to-mobile RSU (V2MR) communications for providing the connectivity to the legacy network. We refer to a transit bus equipped with a gateway to the legacy network as the *mobile RSU (MR)*. The MR has a few advantages over the FR. First, the MR has much lower deployment/operational cost than the FR. Since the public transport timetable is carefully determined based on the demands of public transportation, the MR can better support the demands of the VANETs. Finally, the MR can support a longer connection time to a vehicle of the same direction. We focus on the connection time of vehicle-to-MR (V2MR) communications.

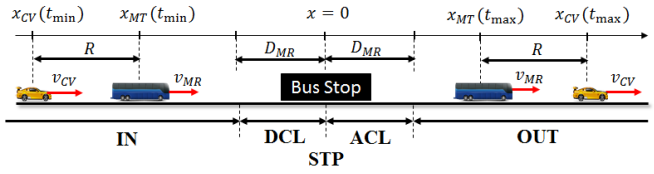

Fig. 1. Model for V2MR communications (*Case 4*).

We present a new *connection-time analysis (CTA) model* for V2MR communications when there is a bus stop in the overlapping route. Since the MR decelerates, stops, and accelerates around the bus stop, the CTA divide the mobility of an MR into five different phases. For a practical setting of parameters, we derive seven cases of V2MR communications, and then propose a detailed analysis for the connection time of each case. From the numerical results obtained from a vehicle mobility simulator, we show that the average estimation error of the CTA model is at most 1.0 percent of the connection time.

II. Connection-Time Analysis (CTA) Model

A. Model for V2MR Communications with a Bus Stop

Fig. 1 shows a straight road of length L on which both an MR of a bus line and a commute vehicle (CV) are running at the same direction. The MR and the CV move at their own constant speeds v_{MR} and v_{CV}, respectively. We assume that the speed of CV is higher than that of MR ($v_{CV} > v_{MR}$). We denote the horizontal location of MR and CV at time t by $x_{MR}(t)$ and $x_{CV}(t)$, respectively. We consider a two-ray ground reflection model for the radio channel model of V2MR communications [2]. Then, the CV is connected to the MR, if

$$\Delta x(t) = |x_{MR}(t) - x_{CV}(t)| \leq R, \tag{1}$$

where R is the transmission range of V2MR communications. The connection time is also represented by $C_{V2MR} = t_{\max} - t_{\min}$, where $t_{\max}$ and $t_{\min}$ are the leaving time (LT) and the encounter time (ET) of a V2MR communication, respectively.

A bus stop is located at the middle of this road which is the origin of the x-axis. We assume that the MR approaches

TABLE I
SEVEN CASES OF V2MR COMMUNICATIONS

LT \ ET	IN	DCL	STP	ACL	OUT
IN	D/C	N/A	N/A	N/A	N/A
DCL	*Case 1*	N/A	N/A	N/A	N/A
STP	*Case 2*	N/A	N/A	N/A	N/A
ACL	*Case 3*	N/A	N/A	N/A	N/A
OUT	*Case 4*	*Case 5*	*Case 6*	*Case 7*	N/A

to (departs from) the bus stop at a constant deceleration (acceleration) denoted by a_{MR}. We also denote the stopping time at the station by t_{ST}. Then, we can classify the mobility of an MR into five different phases as shown in Fig. 1: **IN**, **DCL**, **STP**, **ACL**, and **OUT**. We denote the distance between the bus stop and the boundary between **IN** (**ACL**) and **DCL** (**OUT**) by D_{MR}. Table 1 summarizes seven different cases of V2MR communications with a practical parameter settings: $v_{MR} = 12$ m/sec, $v_{CV} = 15$ m/sec, $a_{MR} = 2$ m/sec^2, $R = 300$ m, and $t_{ST} = 20$ sec. The case marked with D/C (*don't care*) corresponds to the case whose connection time is the same as that without bus stop, i.e. $2R/\Delta v$, where $\Delta v = v_{CV} - v_{MR}$. The case marked with N/A (*not available*) means that it is not feasible with our parameter settings.

B. Connection-Time Analysis of V2MR Communications

We derive the boundary condition and the connection time of each phase in Fig. 1, where

$$C_{V2MR} = C_{\mathbf{IN}} + C_{\mathbf{DCL}} + C_{\mathbf{STP}} + C_{\mathbf{ACL}} + C_{\mathbf{OUT}}. \quad (2)$$

We denote the position of an MR at the ET by $x_{ET} = x_{MR}(t_{\min})$. The connection time of **IN** phase is given by

$$C_{\mathbf{IN}} = \frac{-D_{MR} - x_{ET}}{v_{MR}}, \text{ for } x_{ET}^{\min} \le x_{ET} < -D_{MR}, \quad (3)$$

where $x_{ET}^{\min} = -2R\frac{v_{MR}}{\Delta v} - D_{MR}$. Next, the connection time of **DCL** phase consists of three cases, as follows:

$$C_{\mathbf{DCL}} = \begin{cases} \frac{2R-\Delta x_D}{v_D}, & x_{ET}^{\min} \le x_{ET} < x_D \\ \frac{2D_{MR}}{v_{MR}}, & x_D \le x_{ET} < -D_{MR} \\ \sqrt{-\frac{2x_{ET}}{a_{MR}}}, & -D_{MR} \le x_{ET} < 0, \end{cases} \quad (4)$$

where $x_D = -D_{MR} - \frac{2R-(v_{CV}-\frac{1}{2}v_{MR})\frac{v_{MR}}{a_{MR}}}{\Delta v}v_{MR}$, $\Delta x_D = \frac{-D_{MR}-x_{ET}}{v_{MR}}\Delta v$, $v_D = \frac{1}{2}(v_{MR} + v_{MR}^D)$ and $v_{MR}^D = \sqrt{v_{MR}^2 - 2a_{MR}(2R - \Delta x_D)}$. The connection time of **STP** phase is also given by

$$C_{\mathbf{STP}} = \begin{cases} \frac{2R-\Delta x_D-\Delta x_S}{v_{CV}}, & x_D \le x_{ET} < x_S \\ t_{ST}, & x_S \le x_{ET} < 0, \\ \frac{1}{2}t_{ST}, & x_{ET} = 0, \end{cases} \quad (5)$$

where $x_S = x_D + t_{ST}\frac{v_{CV}}{\Delta v}v_{MR}$, and $\Delta x_S = \frac{2D_{MR}(v_{CV}-\frac{1}{2}v_{MR})}{v_{MR}}$. The connection time of **ACL** phase is similarly expressed by

$$C_{\mathbf{ACL}} = \begin{cases} \frac{2R-\Delta x_A}{v_{A1}}, & x_S \le x_{ET} < x_A \\ \frac{2D_{MR}}{v_{MR}}, & x_A \le x_{ET} < 0, \\ \frac{D_{MR}-x_{ET}}{v_{A2}}, & 0 \le x_{ET} < D_{MR}, \end{cases} \quad (6)$$

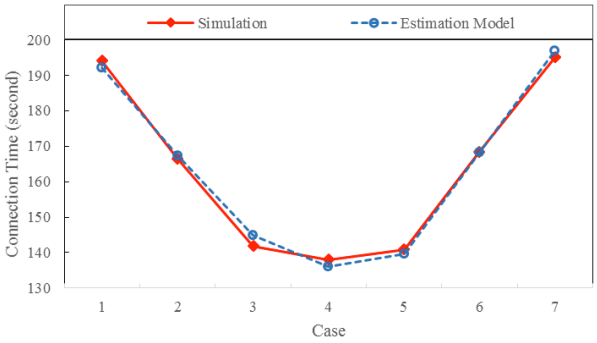

Fig. 2. Average Connection Time

where $x_A = x_S + \frac{(v_{CV}-\frac{1}{2}v_{MR})\frac{v_{MR}}{a_{MR}}}{\Delta v}v_{MR}$, $\Delta x_A = \Delta x_D + \Delta x_S + t_{ST}v_{CV}$, $v_{A1} = \frac{1}{2}(v_{MR}^{A1})$, $v_{MR}^{A1} = \sqrt{v_{MR}^2 - 2a_{MR}(2R - \Delta x_A)}$, $v_{A2} = \frac{1}{2}(v_{MR} + v_{MR}^{A2})$ and $v_{MR}^{A2} = \sqrt{v_{MR}^2 - 2a_{MR}(D_{MR} - x_{ET})}$. Finally, the connection time of **OUT** phase is formulated as

$$C_{\mathbf{OUT}} = \begin{cases} \frac{2R-\Delta x_A-\Delta x_S}{\Delta v}, & x_A \le x_{ET} < -D_{MR} \\ \frac{2R-\Delta x_{O1}}{\Delta v}, & -D_{MR} \le x_{ET} < 0, \\ \frac{2R-\Delta x_{O2}}{\Delta v}, & x_{ET} = 0, \\ \frac{2R-\Delta x_{O3}}{\Delta v}, & 0 < x_{ET} < D_{MR}, \end{cases} \quad (7)$$

where $\Delta x_{O1} = \sqrt{-\frac{2x_{ET}}{a_{MR}}}(v_{CV} - \sqrt{-\frac{a_{MR}x_{ET}}{2}}) + t_{ST}v_{CV} + \Delta x_S$, $\Delta x_{O2} = \frac{1}{2}t_{ST}v_{CV} + \Delta x_S$, and $\Delta x_{O3} = \frac{(v_{CV}-v_{A2})(D_{MR}-x_{ET})}{v_{A2}}$.

III. NUMERICAL RESULTS AND DISCUSSION

We demonstrate the accuracy of our CTA in comparison with the numerical results obtained from the Simulation of Urban MObility (SUMO) simulator [3]. We generate 14 MRs and 3500 CVs. Fig. 2 plots the average connection time between an MR and a CV against the case of V2MR communications. We observe that our CTA matches well with the simulation results, to . The average estimation error of our CTA is limited to only 1.0 percent of the connection time.

To summarize, we present a CTA model for the connection-time of V2MR communications. Since the connection time between two vehicles is highly dynamic and unpredictable, our CTA will provide a fundamental basis of connection-time estimation of V2MR communications.

ACKNOWLEDGEMENT

This research was supported by National Research Foundation of Korea (NRF) Grant (No. 2009-0083495) and by Basic Science Research Program (No. 2013R1A1A1012290) through the NRF, which is funded by the Ministry of Science, ICT & Future Planning.

REFERENCES

[1] R. Daher and A. Vinel, *Roadside networks for vehicular communications: Architecture, applications, and test fields,* IGI Global, Oct. 2012.

[2] Wikipedia "Two-ray ground-reflection model," online available: https://en.wikipedia.org/wiki/Two-ray_ground-reflection_model

[3] Institute of Transportation Systems, *SUMO - Simulation of Urban MObility*, online available: http://www.dlr.de/ts/en/ desktopdefault.aspx/tabid-9883/16931_read-41000/

Interference analysis between WPT devices at ISM bands and Radio Modem

SeungNam Kim
Information & Communication Engineering
Kongju National University
ChungNam, Korea
ksn1989@kongju.ac.kr

*IlKyoo Lee
Dept. Electricity Electronic Control Engineering
Kongju National University
ChungNam, Korea
leeik@kongju.ac.kr

KeeYoung Kwon
Dept. Electricity Electronic Control Engineering
Kongju National University
ChungNam, Korea
kky@kongju.ac.kr

JangGeun Ki
Dept. Electricity Electronic Control Engineering
Kongju National University
ChungNam, Korea
kjg@kongju.ac.kr

***Abstract*—Recently the interest of Wireless Power Transmission (WPT) has been increased for mobile device applications. It is necessary to analyze the interference between WPT devices and other wireless devices for the efficient use of frequency resource. In this paper, the impact of the 3rd order harmonics of the wireless charger for cellular phone on the existing radio modem was analyzed. As a result, the separation distance and the allowable number of interferer on the basis of service radius were obtained to protect the Radio Modem from the wireless charger for cellular phone.**

Keywords-component: WPT, Frequency, Interference, MCL, MC

I. INTRODUCTION

The technology for Wireless Power Transmission (WPT) has been developed in the area of cellular phone, electric vehicle and home appliances these days. Especially, wireless charger for cellular phone has been developed rapidly. It is also necessary to analyze interference between WPT devices and other wireless devices for the efficient use of frequency resource. In this paper, the impact of the 3rd order harmonics of the wireless charger for cellular phone on the existing radio modem was analyzed. For the interference analysis, interference scenario was setup and system performance parameters were applied. The results were obtained through the Minimum Coupling Loss (MCL) method and Monte Carlo(MC) method.

II. INTERFERENCE SCENARIO AND ANALYSIS DESCRIPTIONS

A. Interference scenario

Interference scenario is shown in Fig. 1. Here, dRss is the desired Received signal strength and iRss is the interference Received signal strength. The interference impact can be determined according to the ratio of dRss to iRss.

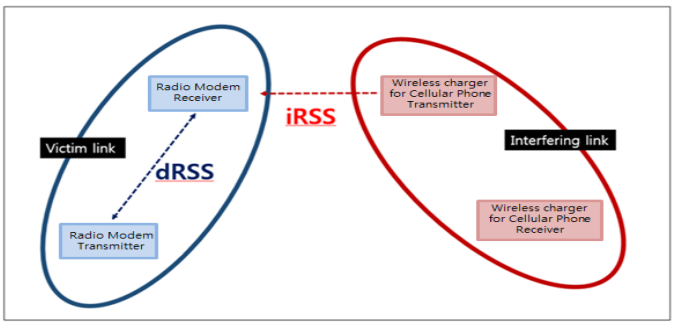

Figure 1. Interference scenario

B. MCL method

Wireless chargers for cellular phones are generally for the local area network using a loop antenna. The power level is attributed to the near field which was made by the magnetic field loop antennas. The related antenna's radiation power is H field and E field. It is indicated in Eq. (1) and Eq. (2), respectively [1].

$$|H_{av}| \cong \frac{IS}{2\pi R^3}(1+\beta^2R^2)^{1/2} \quad (1)$$

$$|E_{av}| \cong \frac{60\pi r_1^2 I}{R^3}(1+\beta^2R^2)^{1/2} \quad (2)$$

The radiation power is calculated as in Eq. (3).

$$P = |H_{av}| \cdot |E_{av}| \quad (3)$$

Path Loss (PL) is the power loss between a transmitter and a receiver. Received power can be calculated as in Eq. (4) by applying the intrinsic impedance of 120π .

$$P = 120\pi[\frac{I^2S^2}{4\pi^2R^6}(1+\beta^2R^2)] \quad (4)$$

Here, I is the current of a loop antenna, S is the extent, $4\pi^2$ is the unit sphere surface area of the receiving antenna, β is $\frac{2\pi}{\lambda}$

This work was supported by the research grant(2014-1252-01) of the Kongju National University in 2014
*Corresponding author

and R is the distance. Received power under the condition of $\beta R \gg 1$ can be achieved with Eq. (5).

$$P_r = P_t \frac{\beta^2 R^2}{4\pi^2 R^6} \quad (5)$$

Here, P_t is the transmitting power.

Therefore, the PL is calculated with Eq. (6).

$$\mathrm{PL} = P_t - P_r = \frac{4\pi^2 R^4}{\beta^2} \quad (6)$$

C. MC method

As an interference analysis tool, Spectrum Engineering Advanced Monte-Carlo Analysis Tool (SEAMCAT) was used [2][3]. In random event, the ratio of iRss to dRss is calculated though many times of repetition and then the interference probability is achieved by comparing dRss/iRss with the required Carrier to Interference (C/I).

III. THE RESULTS OF INTERFERENCE ANALYSIS

A. System characteristics of a victim and an interferer

The performance characteristics of a victim (Radio Modem) and an interferer (wireless charger for cellular phone) are summarized in Table 1 and Table 2, respectively.

TABLE I. THE CHARACTERISTICS OF RADIO MODEM

Parameters	Value	Unit
Frequency	40.695	MHz
Thermal Noise	-134.5	dBm/Hz
Sensitivity	-85	dBm
Bandwidth	4	kHz
C/I	10	dB
Propagation Model	Free space	-

TABLE II. THE CHARACTERISTICS OF CHARGER

Parameters	Value	Unit
Frequency	13.56	MHz
Frequency 3rd	40.68	MHz
Thermal Noise	-131.7	dBm/Hz
Out Power	36.99	dBm
Out Power 3rd	-23.1	dBm
Bandwidth	17	kHz
Antenna gain	-30	dBi
Propagation Model	Free space	-

B. The Spectrum emission mask of Interference

Spectrum emission mask used in the SEAMCAT is shown in Fig. 2.

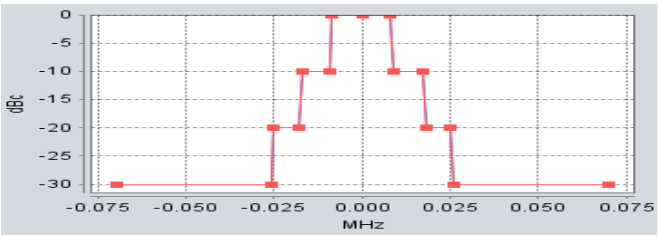

Figure 2. Spectrum emission mask

C. The result of MCL method

Considering of the transmission power of 36.99 dBm, the antenna gain of -30 dBi and the emission mask characteristics of -80 dBc, the PL of 21.37 dB was calculated. In order to get the separation distance, Eq. (6) can be described as Eq. (7).

$$21.37\mathrm{dB} = P_t - P_r = 10\log(\lambda^2 R^4) \quad (7)$$

The separation distance to protect the radio modem from the interference of 3rd order harmonics of wireless charger for cellular phone is around 1.2 m.

D. The rusult of MC Method

The allowable number of interferers meeting an interference probability less than 5 % was computed at the radii of 0.5 m and 1.0 m by applying performance parameters of a victim and an interferer. The analysis results are summarized in Table 3.

TABLE III. THE ANALYSIS RESULTS WITH MC METHOD

Radius (m)	Interference Number	Interference Probability (%)
2	1	2.99
3	1	1.25
4	1	0.85
4	2	2.49
5	1	0.52
5	2	1.63
5	3	2.84

As a result, the allowable number of interferer was 1 at radius of 2 m, 1 at radius of 3 m, 2 at radius of 4 m and 3 at radius of 5 m to meet an interference probability less than 5 %.

IV. CONCLUSION

This paper presents the impact of the 3rd order harmonics of the wireless charger for cellular phone on radio modem by considering practical performance parameters. The protection distance of 1.2 m was obtained for the case of single victim and single interferer through MCL method. The allowable number of interferer was 1 at radius of 2 m, 1 at radius of 3 m, 2 at radius of 4 m and 3 at radius of 5 m for the case of multiple interferes through MC method. The analysis results are expected to be used as a guideline for the coexistence of wireless devices.

REFERENCES

[1] Frank M. Greene, "The Near-Zone Magnetic Field of a Small Circular-Loop Antenna" , JOURNAL OF RESEARCH of the National Bureau of Standards – C. Engineering and Instrumentation, Vol. 71C, No. 4, Oct-Dec. 1967

[2] European Radio communications Office, "SEAMCAT SoftwareVersion2.1 User Manual", European Radio Communications office, 23 February. 2004.

[3] ERC REPORT 68, "Monte-Carlo simulation methodology for the use in sharing and Compatibility studies between different radio services or system", European radio communications committee (ERC), February. 2000.

50 Mbps data rate/ low power transmission near-field communication system via metal walls

***Abstract*—This paper presents the investigation results of the sheet like waveguide transmitter and spiral coil receiver to transmit high data rate (50 $Mbps$ binary)/ power via metal structures. The evanescent field generated by the presented transmitter forms surface waves on the metal structures. The proposed system was designed to operate at a frequency of 25 MHz. The receiver was designed to pick-up the surface waves from the metal to power a 8 W LED load with an efficiency of 93.3% at any arbitrary position across the metal structure. The proposed system can be used to transmit and receive data in ships, where the traditional wireless radio waves are unable to propagate for communication. Additionally low power sensors can be wirelessly powered using the proposed system.**

I. Introduction

The traditional wireless radio equipment does not work reliably in the presence of extremely low opening metal cabins such as the ships [1]- [5]. As a result, the shipping industry extensively utilizes cables for their communication equipment. In order to install the cables, drilling of metal cabins is inevitable. Modern ships have hundreds of such walls where drilling has to be done, as a result the production time and the man-hours take a toll on the efficiency of the rate of manufacturing. The power cables are unavoidable, but the additional burden of cables for communication device adds up to the overall weight, cable consumption and production cost. Apart from this, low power sensors installed at hard to access locations require cabling as well [2]. Hence, it is desirable to opt for wireless solution for communication systems and low power equipment, such as the sensors.

Some of the research groups have come up with solutions, utilizing piezoelectric transducers and electromagnetic acoustic transducers (EMAT) [1] and [2]. Although, these are effective solutions, they pose some limitations as compared to wireless RF systems. (a.) efficiency 4% in case of EMATs (b) frequency or data rate 12.4 Mbps in case of piezoelectric transducer based systems and 1Mbps in case of EMATS and (c.) coaxial alignment of the transceivers.

Certain research groups have considered wireless power transfer (WPT) as a possible solution, they have considered inductive power transfer (IPT) [3]. But the frequency of optimum efficiency is between several hundred hertz to several hundred kilo hertz. In this paper we investigated the concept of sheet like waveguides which were first reported by [6]- [8]. In this paper we powered-up an 8 W load across varied test conditions. The fig 1, shows the scheme in which the proposed WPT system can be used to carry out data or power transmission.

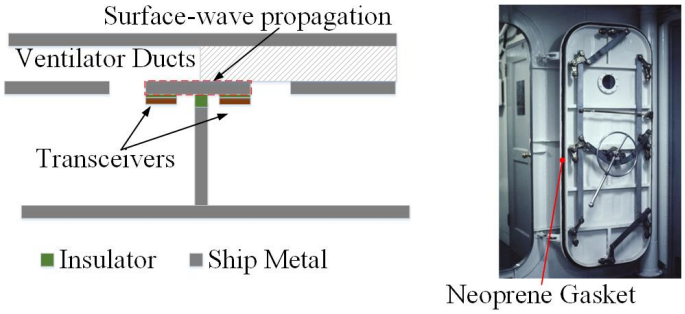

Fig. 1. Metal-Dielectric Interfaces.

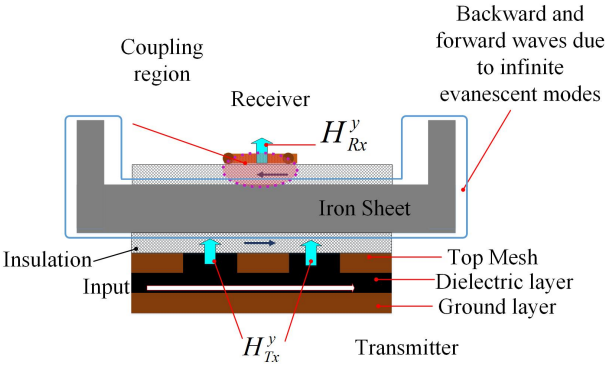

Sheet Like Wave-guide transmitter generates evanescent field

Fig. 2. Metal-Dielectric Interfaces.

A. Theory

The fig.2 shows the details of the principle of operation of the sheet like wave guide which has been presented in this paper. The electromagnetic field profile immediately above the waveguide can be described by the following equations. First, we define the electric field profile in z-direction :

$$E = \frac{k_2^2}{k_1} V_0 exp(-k_1 z) exp(-jkx) exp(j\omega t) \qquad (1)$$

$k_1^2 = (\mu\epsilon - \mu_0\epsilon_0)\omega^2 - \frac{j\sigma\epsilon\omega}{h}$, $k_2^2 = \frac{j\sigma\epsilon\omega}{h}$, $k^2 = \mu\epsilon\omega^2 - \frac{j\sigma\mu\omega}{h}$

Where, E is the electric field, ϵ is the permittivity, μ is the magnetic permeability, h is the distance between the ground plate and top mesh layer of the sheet like waveguide. ω is the angular frequency of the EM wave exciting the waveguide transmitter. V_0 is the peak value of the voltage of

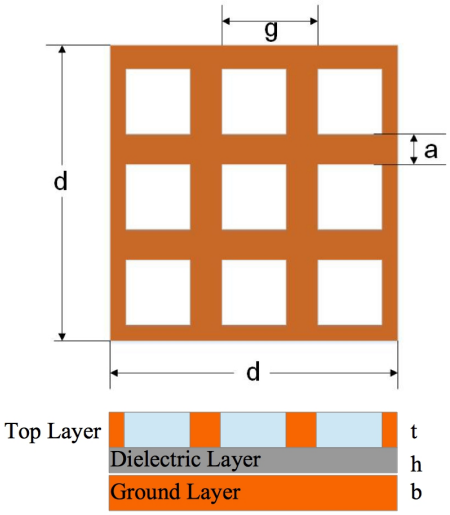

Fig. 3. Sheet Like Waveguide Transmitter and Receiver.

the sinusoidal excitation.

Field profile along the metal surface is given by:

$$E_z = \begin{cases} e^{-ikx} + \sum_{n=-\infty}^{+\infty} A_n e^{i\alpha y} e^{ib_{1n}x}, & x > 0 \\ \sum_{n=-\infty}^{\infty} B_n e^{i\alpha y} e^{ib_{2n}x}, & x < 0 \end{cases} \quad (2)$$

where A_n and B_n are unknown amplitudes of spatial harmonics of diffraction fields.

II. EXPERIMENTS AND RESULTS

Fig.3. shows the proposed Transmitter, receiver used for the experiments in this paper. The dimensions of transmitter and receiver are enlisted in table I .The fig.4shows the experimental demonstration of the concept. An LED load of 8 watts was illuminated along 1.2 m of metal and across 80 mm metal. As soon as the transmitter or receiver is lifted off from the metal surface, the power transfer ceases to occur. The power into the transmitter was fed by using an RF amplifier. The efficiency of transmission is 93.3%. There was no effect of the surface waves on the human body and hence it is safe for operation. The entire system can be redesigned for ISM band frequency.

III. CONCLUSION

A sheet like waveguide as a transmitter and receiver for wireless high data rate/low power transmission via metal walls was investigated in this paper. It was demonstrated that it is possible to carry out power and high speed data rate wireless transmission of up 8 W and 50 $Mbps$ (binary), respectively. There is no degradation in the system performance despite of the alignment of the transmitter and receiver. Hence such a system can be put to effective use, wherever there are very small openings in the metal cabins e.g. ventilation ducts, insulated metal doors in ships.

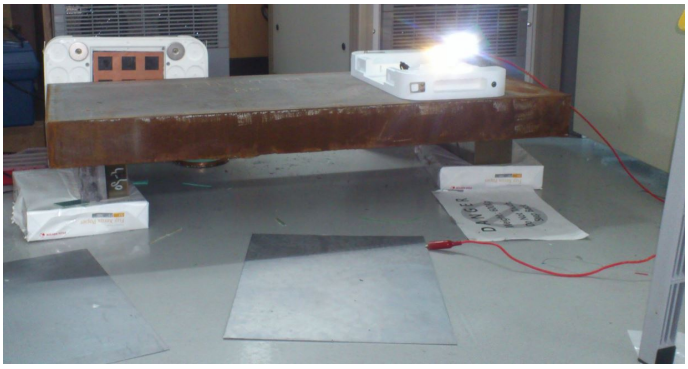

Fig. 4. Power Transfer Demo.

REFERENCES

[1] Lawry, T.J., Saulnier, G.J., Ashdown, J.D., Wilt, K.R., Scarton, H.A., Pascarelle, S. and Pinezich, J.D., "Penetration-free system for transmission of data and power through solid metal barriers," MILITARY COMMUNICATIONS CONFERENCE, vol., no., pp.389-395, 7-10 Nov. 2011

[2] Graham, D.J., Neasham, J.A. and Sharif, B.S., "Investigation of Methods for Data Communication and Power Delivery Through Metals," IEEE Transactions on Industrial Electronics, vol.58, no.10, pp.4972-4980, Oct. 2011

[3] Zangl, H.; Fuchs, A.; Bretterklieber, T.; Moser, M.J.; Holler, G., "Wireless Communication and Power Supply Strategy for Sensor Applications Within Closed Metal Walls," Instrumentation and Measurement, IEEE Transactions on , vol.59, no.6, pp.1686,1692, June 2010.

[4] Oruganti, S.K. and Bien, F., "Investigation of near-field wireless energy transfer for through metal-wall applications," in Wireless Power Transfer Conference (WPTC), 2014 IEEE , vol., no., pp.247-250, 8-9 May 2014.

[5] Oruganti, S.K., Heo, S.H., Ma, H. and Bien, F., "Wireless energy transfer-based transceiver systems for power and/or high-data rate transmission through thick metal walls using sheet-like waveguides," in Electronics Letters , vol.50, no.12, pp.886-888, June 5 2014.

[6] Noda, A.; Shinoda, H., "Selective Wireless Power Transmission Through High- Q Flat Waveguide-Ring Resonator on 2-D Waveguide Sheet," in Microwave Theory and Techniques, IEEE Transactions on , vol.59, no.8, pp.2158-2167, Aug. 2011

[7] Liang He; Linghe Kong; Yu Gu; Jianping Pan; Ting Zhu, "Evaluating the On-Demand Mobile Charging in Wireless Sensor Networks," in Mobile Computing, IEEE Transactions on , vol.14, no.9, pp.1861-1875, Sept. 1 2015

[8] Yoneyama, N.; Arai, H., "A power collecting circuit for WPT system using sheet-like waveguide," in Microwave Workshop Series on Innovative Wireless Power Transmission: Technologies, Systems, and Applications (IMWS), 2012 IEEE MTT-S International , vol., no., pp.119-122, 10-11 May 2012

Development of IaaS-Based Cloud Co-location and Management System using Open Source Cloud Stack

Sang-Min, Bae
Gyeongbuk Research Institute of Vehicle Embedded Technology
G.I.V.E.T
Gyeongbuk, Korea
smbae@givet.re.kr

Kyoung-Hwoan, Cho
ICT Convergence Team, Mobile Technology Convergence Center
Daegu, Korea
hani6085@ttp.org

Dong- Ki, Lee
Gyeongbuk Research Institute of Vehicle Embedded Technology
G.I.V.E.T
Gyeongbuk, Korea
dklee@givet.re.kr

Hyun-Ki, Ryu
Gyeongbuk Research Institute of Vehicle Embedded Technology
G.I.V.E.T
Gyeongbuk, Korea
hkryu@givet.re.kr

***Abstract*—The weakness of server-based hosting is that it has low usability because it is limited by server unit operation. It is very difficult to maximize the efficiency of the entire server and have a limited number of manpower to manage multiple servers. Server hosting-based management from setting to troubleshooting gives a huge burden on manpower. This paper states that IaaS (Infrastructure as a Service)-based cloud co-location and management system using open source Cloud Stack can be developed to solve such problems, and can help ease the burden of managing manpower by maximizing the usability of server and enhancing the efficiency of hosting management**

Keywords-component; formatting; Cloud, Virtualization, Open Source, Web Services, Ajax, VID, Co_Location

I. INTRODUCTION

The weakness of server-based hosting is that it has low usability because it is limited server unit operation. It is in face difficult to use it completely for all users who cannot reach a mutual consensus. This paper describes that the development of IaaS-based cloud co-location and management system using open source Cloud Stack to easily manage the entire cloud hosting support by maximizing the usability of server and enhancing the efficiency of hosting management.

A. Importance of Technology Development

While the current IT system has been operating separate servers for general work or by application service, cloud-computing environment continuously develops the virtualization of server and storage devices that are IT equipment. Users of cloud-based S/W can have hundreds of server and storage devices through the virtualization technology by cloud computing providers. S/W based on cloud server need to be provided as a service concept to user in the virtualized clouding environment [1]. This has led to the acceleration of the development of SaaS(software as a Service) that are becoming more activated, as the operating system and software platform are expanding for computer-base to web-base [2].

B. Necessity of Technology Development

In general, the weakness of server-based hosting is limited operation of server unit and has low usability. It is also difficult to use it completely for all servers or even more so to maximize the efficiency of server hosting for all users who cannot reach a mutual consensus. Since a limited number of manpower management multiple servers, server hosting-based operation from setting to problems give a huge burden on the manpower. This paper explains that such problems can be solved at once if all cloud-hosting resources are managed. In addition, it will describe about IaaS-based cloud co-location and management system using open source Cloud Stack, which can maximize the usability of server and enhance the efficiency of hosting management [4].

II. SYSTEM STRUCTURE

The core of the development is to create an IaaS system that becomes the basis of cloud system and develop a device based on the IaaS system. Show in Figure 1. As for VID device, USB mouse and keyboard is supported and a regular monitor of RGB and DIV port is used. The establishment of interoperability between the VID devices and entire system are verified, and communication module for VID devices, network environment, interface, and display module are developed. Also, the cloud system is stabilized and DB is dualized, and a cloud system related to improving vulnerabilities is developed through S/W firewall upgrade.

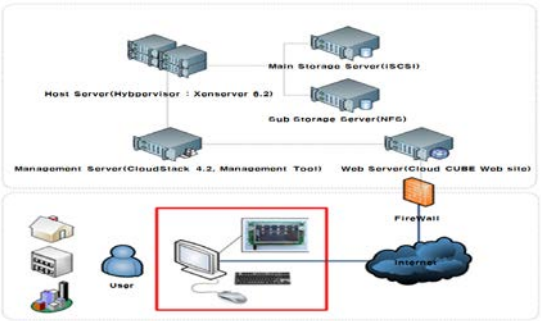

Fig 1. VID Client-only system configuration

III. EXPERIMENTAL RESULT

The performance will be verified by using AIDA64 Extreme Edition and Crystal Disk Mark, which is used the most often for the performance test of CPU and its device in famous hardware venture site at home and abroad [5], [6]. The system performance of CPU will be test by the operation

ability of CPU floating point ability of cloud system, and a higher value means more excellent performance. The measurement of CPU performance tests the performance of system with the CPU floating point ability of cloud system, and a higher value means more excellent performance.

TABLE I. CPU MEASURING RESULTS (UNIT : FPG VP8)

	1	2	3	4	5
CPU Test	2838	2326	2642	2405	2615
6	**7**	**8**	**9**	**10**	***Avg.***
2372	2492	2632	2360	2341	2557

During the measurement of memory performance, a shorter delay time exhibits a better performance and a lower value means an excellent performance. The test environment is the same as a CPU test and the measurement results are as in Table 3.

TABLE II. MEMORY DELAY TIME MEASUREMENT RESULTS (UNIT : NS)

	1	2	3	4	5
Delay	106	85	133	133	133
6	**7**	**8**	**9**	**10**	***Avg.***
133	81	80	80	80	108

The results of memory read and write test are as in Table 4 and 5. A higher value in the table means more excellent performance.

TABLE III. MEMORY READ MEASURING RESULTS (UNIT : MBPS)

	1	2	3	4	5
Read	16710	11122	16644	16960	16978
6	**7**	**8**	**9**	**10**	***Avg.***
16978	11150	11111	16948	16871	15134

TABLE IV. MEMORY WRITE MEASURING RESULTS (UNIT : MBPS)

	1	2	3	4	5
Write	5047	7195	5036	7202	7200
6	**7**	**8**	**9**	**10**	***Avg.***
7201	5036	4935	5033	5038	5892

The Write and Read test of a storage measures the Read and Write performance of 4K, which is the most frequently occurring capacity. A higher value means a better performance; the test environment is the same as that of CPU and memory performance test, and Crystal Disk Mark program was use for measurement.

The measurement results were as in Table6 and 7.

TABLE V. STORAGE 4K READ MEASURING RESULTS (UNIT : MB/S)

	1	2	3	4	5
4K Read	11.3	12.0	11.4	11.6	11.7
6	**7**	**8**	**9**	**10**	***Avg.***
11.7	13	11.7	11.8	13.7	12.0

TABLE VI. MEMORY 4K WRITE MEASURING RESULTS (UNIT : MB/S)

	1	2	3	4	5
4K Write	10.4	10.3	10.1	10.3	10.2
6	**7**	**8**	**9**	**10**	***Avg.***
10.2	12.3	10.0	10.1	11.5	10.6

The simultaneous access test per server created and registered VM for 10 new accounts of cloud cube homepage, and confirmed the creation nodes of the VM using the manager tools. It confirmed the realization of system design considering traffic and physical elements, and checked the development of automatic VM allocation function considering resource allotment quote when creating a new account.

IV. CONCLUSION

The IaaS-based cloud co-location and management system using open source Cloud Stack in this paper is a computing system that provides virtualized IT resources as a service. This computing system allows users to borrow IT resources (software, storage, server, and network) as much they need and receive support for real-time expandability depending on service load. It is a computing system in which only input/output work are mainly done through a personal device while performing information analysis and processing, storage, management, and distribution in a third space. The development of Internet in 2000s came with the age of cloud computing of software, platform, infra environment in a virtual space, according to user requests. This age progressed with the advancement of wired and wireless communication, evolution of smartphone, and development of virtualized technology. As a server-based hosting was limited operation of server unit, had a low usability, and was very difficult to be used completely for all servers and maximize the efficiency of server hosting for all user who could not reach a mutual consensus. In addition, since many servers were managed by limited manpower, having the entire manpower to work on it was not enough, and server hosting-based operation from configuration to problem occurrences gave a huge burden on manpower. However, an IaaS-based cloud co-location and management system using an open source Cloud Stack could solve such problems at once when managing the entire hosting resources, maximize the usability of server, and increase the efficiency of hosting management to ease the burden of managing manpower. From now on, the cloud system could be adopt quickly with the development of individual system, reduction of equipment purchase cost, etc., to service the centralized software smoothly and strengthen the interwork with the network field and security field.

ACKNOWLEDGMENT

This research was financially supported by the Ministry of Trade, Industry and Energy(MOTIE) and Korea Institute for Advancement of Technology(KIAT) through the Infrastructure Project for Industrial Technology Development (No. N0001156).

REFERENCES

[1] I. Jung, S. Lee, Y. Eom, “Comparative Analysis of OpenSource Cloud Computing Platforms”, KIISE, 2012, pp.382-384.

[2] OpenStack, http://www.openstack.org.

[3] Johan Trosson, Ruben S.Montero, Rafael Moreno-Vozmediano, Ignacio M. Llorente, “Cloud brokering machines across multiple providers”, Future Generation Computer Systems, vol 28, 2012, pp.358-367.

[4] J. Ra, S. Hang, B. Sung, Y. Kim, “Open Source Cloud Platforms : OpenStack and CloudStack”, KIISE, 2012, pp.259-261.

[5] AIDA64 Extreme Deition, http://www.aida64.com

[6] CryStalDiskMark, http://crystalmark.info.

Wednesday, Feb. 24

Session I-2 : (Poster) Convergence I

Robot-Assisted Sensor Relocation to Reduce Sensing Hole in Wireless Sensor Networks

Junyoung Heo
Dept. of Computer Engineering,
Hansung University,
South Korea
Email: jyheo@hansung.ac.kr

Hong Min
School of Computer and
Information Engineering,
Hoseo University,
South Korea
Email: hmin@hoseo.edu

Jinman Jung
Dept. of Information and
Communication Engineering,
Hannam University,
South Korea
Email: jmjung@hnu.ac.kr

***Abstract*—Wireless sensor networks are useful to various unmanned monitoring application such as monitoring environments, surveillance system, unmanned space exploration, and so on. Due to the inappropriate placement of sensor nodes, there are some problems, for example, low connectivity and high overlapped sensing area. These problems can make it difficult for the data collection and lead to a waste of energy. In this paper, we propose a robot-assisted sensor relocating method to resolve the inappropriate placement of sensor nodes. The robot has capabilities to carry nodes, collect nodes placed in the monitoring area, and place nodes. Given monitoring area, we place sensor nodes randomly and find sensing holes using data from the nodes. The robot relocates the nodes and resolves the sensing holes. To evaluate the proposed method, we use simulation. Through the simulation, We show that the proposed method is viable and efficient compared with the existing randomly locating method.**

***Keywords*—Sensing Hole, Robot-Assisted, Sensor Node Relocation, Wireless Sensor Networks**

I. Introduction

Wireless sensor networks are wireless networks which are composed of many sensor nodes. These nodes gather data using its sensors and transmit the data to sink node via wireless networks. Based on the data collected in the sink node, automatically the sink reacts or gives some useful information to users. Wireless sensor networks are able to operate normally even when some nodes are failed because nodes build networks automatically by communicating each other. A lot of sensor nodes are required to build networks, and the cost of each node should be as low as possible. The low cost requirement makes a node equip a constrained hardware such as a 8-bit CPU and a very small amount of memory. In addition, a node uses battery power, and low power consumption must be considered when we design nodes and networks. [1], [2]

In general, there is a random placement and placement in a fixed position for the sensor node placement. Random placement method sprays randomly the nodes on the means of transportation such as aircraft or vehicle. Fixed method installs the nodes one by one calculating the position of them in advance. [3]. In the latter case, we can replace the node easily because we calculate the optimum position of the sensors in advance. There is no problem even when the battery is discharged or the node failure. However, because it requires an information about the monitoring area in advance it cannot be used in unknown monitoring area [4].

Random placement method causes excessive redundant nodes and sensing holes. Sensing holes mean that a specific sensing area can not be sensed at all because the area is out of the sensing range of all the nodes. Excessive redundant nodes mean that the number of nodes in a specific sensing area is too much and even though leaving some of them sleep state does not affect the lifetime of the entire networks [1].

We can utilize nodes more effectively by moving the excessive redundant nodes to the sensing holes. This relocation can be performed by the person directly, or it is also possible to use an autonomous mobile system, such as a robot. In particular, in an application utilizing sensor networks in a dangerous area such as the volcanic activity area or the alien planet, the relocation by a robot is necessary [1], [4], [5], [6].

In this paper, we find the sensing holes and excessive redundant nodes based on the data collected from sensor networks, where sensors are placed randomly. And we propose a method for relocation of a sensor by a robot, based on the information efficiently.

II. Proposed Scheme

This paper is based on the following assumptions:

- Sensor nodes know their location through the location detection technique such as GPS.
- A sensing range(Rs) is longer than the communication range(Rc).
- The sensor nodes can always communicate with the robot or sink. That is, the isolated node is not present.

The proposed method is composed of finding sensing holes, excessive redundant nodes, and optimal robot movement path for relocating nodes. The detailed explanation of each step is as follows.

A. Finding Sensing Holes

First, we divide the monitoring area as a grid like Fig. 1. Then, we set the cross point as a representative sensing point, $(p_{i,j})$. If there is a sensing point which is not covered by any nodes, we call the point sensing hole. The calculation time and accuracy of the algorithm is affected by the size of the grids.

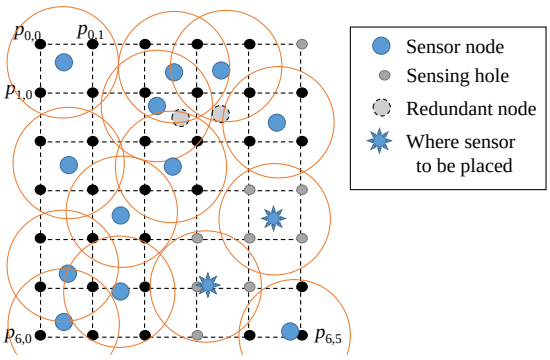

Fig. 1. Sensing holes and redundant sensor nodes

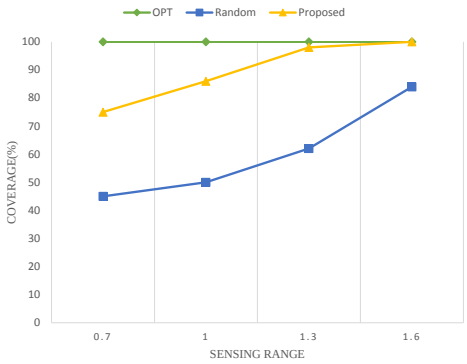

Fig. 2. Sensing coverage(%)

Each sensor node(blue one in the figure) knows the sensing points placed in its sensing range. We define the set of the sensing points can be reached by the sensor as S_i. For example, S_i of the sensor at the left-topmost in the figure is $S_i = \{p_{0,0}, p_{0,1}, p_{1,0}, p_{1,1}\}$. We define a sensing hole as the sensing point that is not belong to any S_i for every sensors:

$$SensingHole = P - \bigcup_{sensori} S_i$$

If two adjacent sensing holes can be covered by one sensor, the sensing holes are merged to one. And it merges sensing hole until the sensing holes can be no longer merged. In the Fig. 1, $SensingHole = \{\{p_{3,4}, p_{3,5}, p_{4,4}, p_{4,5}\}, \{p_{4,3}, p_{5,3}, p_{5,4}, p_{6,3}\}\}$

B. Finding Excessive Redundant Nodes

We define the essential node which covers a sensing point sensed by only the essential single node. A node other than these essential nodes is defined as a redundant node. If there are more than a certain number of redundant nodes within the sensing range, we determined that the redundant nodes are excessive redundant nodes. These excessive redundant nodes will be collected and moved to sensing holes by a robot. In Fig.1, two nodes painted in a gray dashed border will be collected. Here, we simply determined that all the redundant nodes are the excessive ones.

The robot moves the excessive redundant nodes to the area of sensing holes efficiently. In this paper, we use genetic algorithm to determine the optimal path of the robot.

III. Experiment

To evaluate the proposed method, we conducted a simulation. We compared the proposed method with OPT, which places sensors in optimal location by hand. We randomly placed 100 sensors in 10x10 area, and applied the proposed method. We measure the increased size of possible sensing area after applying the proposed method. We also compared the sensing area of the proposed method with that of the OPT.

Fig. 2 shows the comparison results of the proposed method, random placed method, and OPT. The x-axis is the sensing range, and the y-axis is the resulting coverage of each method. The sensing range is relative distance when the width of grid is 1. For OPT, the coverage is 100% when the sensing range 0.7 at least. As shown in the figure, the proposed method increased the coverage of the random placed method by relocating nodes.

IV. Conclusion

The monitoring performance of a sensor networks depend on how well locating nodes. The lifetime of the sensor networks can be increased through the cooperation with each other nodes. In this paper, we find the sensing holes and excessive redundant nodes based on data gathered from other nodes in randomly placed sensor networks. In the proposed method, the robot relocates the excessive redundant nodes on the basis of this information efficiently. The further study of the heuristic algorithms to determine the efficient path of the robot and the proper size of a grid is necessary. Further research is needed also on how to restore the network through the relocation in the context of being disconnected sensor nodes.

References

[1] Y. Wang and C.-H. Wu, "Robot-assisted sensor network deployment and data collection," in *Computational Intelligence in Robotics and Automation, 2007. CIRA 2007. International Symposium on*. IEEE, 2007, pp. 467–472.

[2] J. Wu and S. Yang, "Smart: a scan-based movement-assisted sensor deployment method in wireless sensor networks," in *INFOCOM 2005. 24th Annual Joint Conference of the IEEE Computer and Communications Societies. Proceedings IEEE*, vol. 4. IEEE, 2005, pp. 2313–2324.

[3] G. Wang, G. Cao, and T. La Porta, "Movement-assisted sensor deployment," *Mobile Computing, IEEE Transactions on*, vol. 5, no. 6, pp. 640–652, 2006.

[4] G. Fletcher, X. Li, A. Nayak, and I. Stojmenovic, "Randomized robot-assisted relocation of sensors for coverage repair in wireless sensor networks," in *Vehicular Technology Conference Fall (VTC 2010-Fall), 2010 IEEE 72nd*. IEEE, 2010, pp. 1–5.

[5] X. Li, G. Fletcher, A. Nayak, and I. Stojmenovic, "Randomized carrier-based sensor relocation in wireless sensor and robot networks," *Ad hoc networks*, vol. 11, no. 7, pp. 1951–1962, 2013.

[6] P. Corke, S. Hrabar, R. Peterson, D. Rus, S. Saripalli, and G. Sukhatme, "Deployment and connectivity repair of a sensor net with a flying robot," in *Experimental robotics IX*. Springer, 2006, pp. 333–343.

Secure Bootstrapping Scehem for IoT devices

Namhi Kang
Digital Media Department,
Duksung Women's University
Seoul, Korea
Email: kang@duksung.ac.kr

***Abstract* — This paper proposes a secure configuration (i.e. bootstrapping) scheme for resource constrained devices such as sensors or actuators. The scheme is activated when both a new device initially installs and re-installs to network that is currently in operation. The method is suited for a scenario, where resource constrained nodes are interconnected with each other and thus formed Internet of Things.**

Keywords; Secure bootstrapping, Internet of Things, Resource constrained devices, Pre-shared Key

I. INTRODUCTION

The technical trend toward Internet of Things (IoT) has received increasing attention in these days, where a rapidly growing number of smart devices are trying to connect to the Internet. The IoT can be used in wide industry fields such as industrial control, smart home and building services, healthcare services and several other industries. However, if there is no proper security mechanism, private and sensitive data around humans can be revealed to the public Internet [1].

This paper presents an efficient and secure scheme to configure a resource constrained IoT device. Especially, we focus on secure key configuration. Most IoT devices are embedded in objects of daily life and operate with minimal resources (i.e. 8 bit processing microcontrollers with limited amounts of memory). The network is also constrained one (e.g. 6LoWPAN having high packet error rates and a typical throughput of 10s of kbit/s). We assumed that communications of IoT nodes are based on TCP/IP protocols and the nodes use the constrained application protocol (CoAP) [2].

Pre-shared key (PSK) based secure schemes are well known and widely used for various security services in Internet. All such schemes strictly assume that the PSK is only known to the two communication entities involved in current security service. However, it is still not clear how PSK of resource constrained node can be initially configured in a secure manner.

As a conceptual solution, this paper presents an initial setup method that might be a part of secure bootstrapping scheme. The basic idea of the proposed scheme is motivated from a lock of suitcase. Simple and default password such as '0000' or '1234' is initially setup on a lock of suitcase in selling. Owner can change the password after purchasing. In our method, similarly, initial key of a node is configured by installer during bootstrapping phase. When the node join to an existing network, the key (i.e. PSK) can be securely reconfigured. The proposed scheme does not cover all operations of secure bootstrapping for IoT networks, but it is intended to securely support self-reconfiguration of the pre-installed temporary key of joined node.

II. PROPOSED SCHEME

A. *Preliminary*

Secure bootstrapping is regarded as a difficult problem in Internet of Things. This is mainly because lots of things connected to Internet are resource constrained. IETF classified constrained devices with consideration of data size and code size as shown in the following table.

TABLE 1. CLASSES OF CONSTRAINED DEVICES [3]

Name	data size (i.e. RAM)	code size (i.e., Flash ROM)
Class 0	<< 10 KiB	<< 100 KiB
Class 1	~ 10 KiB	~ 100 KiB
Class 2	~ 50 KiB	~ 250 KiB

In addition, user-device interfaces of resource constrained device are not enough for doing configurations manually by person (i.e. inadequate or even no input/output equipment such as display or keyboard).

To solve the problem, we propose a scheme to securely re-configure a symmetric key (i.e. pre-installed key in manufacturing phase) automatically upon joining to existing network. After the secure configuration phase, an installer (or manufacturer) cannot read/modify/insert any communication data even though he did initial pre-setup of secure credential of the communicating nodes. We do not assume that a system administrator trusts an installer (or manufacturer) even though he makes orders for the installer. This is because trust and responsibility of installer, who buys and install devices, are different from those of system administrator.

The following transactions are done prior to the secure key reconfiguration (i.e. procedures in enrolment Phase).

1) System administrator makes orders and requests initial setup of devices to an installer. Pre-setup information is a set of values that include ID and network socket ID (NID) of controller for each of the devices, and a temporary key used as

an initial key (IK_N). All devices handled by a single installer may share the same IK_N.

2) System administrator also stores the same initial information for each of nodes in authentication server. A controller can perform operations of an authentication server in case of a small network.

3) Installer purchases devices and then configures the information requested by the administrator in doing installation phase. Some of the information for a node may be pre-configured by manufacturer.

4) When a node joins to network, it knows NID of its associated controller with which he can communicate. Also, authentication server has lists including node ID and pre-installed key for new nodes.

5) PSK reconfiguration phase can be then started.

B. Secure Bootsrtapping Procedures

There are three message exchanges between a new node SBI(i) and network node(s) (i.e. SBR(c) and SBS(s)). A controller SBR(c) may include functions of both SBR(c) and SBS(s) depending on the size of application domain or the ability of SBR (i.e. computing power and memory). Mutual authentication and PSK reconfiguration procedures are shown in Figure 1.

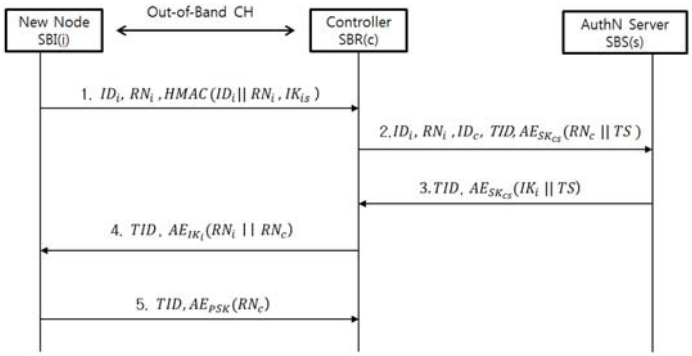

Figure 1. Secure Bootstrapping Procedures

When a new node SBI(i) joins an existing network, he generates a random number RNi and sends it with his identifier IDi to his controller SBR(c) over OOB (Out-of-Band) channel. QR code, NFC, light, audio can be used as the OOB CH that is relatively more secure than wireless channels with wide communication coverage such as WiFi, Bluetooth, etc. This is due to the fact that user can make sure that there is no attacker (i.e. man in the middle attacker) nearby him. In Figure 1, we use the notation AE (Authenticated Encryption), but the two nodes transmit plaintext depending on the secure strength of the OOB CH. The NID of SBR(c) (i.e. IP address and port number) has been pre-configured by installer of the SBI(i) in the enrolment phase as specified in subsection A of this chapter.

Upon receiving the message, SBR(c) generates a random number RNc and a sequence number used as a transaction ID (i.e. TID). Then he sends the values with his IDc, time stamp (TS) and the message received from SBI(i) to the authentication server SBS(s). TS allows SBR(s) to derive the valid time of key and verify the freshness of the arrived message.

The authentication server SBS(s) first discovers the IKi for node IDi in his secure repository. SBS(s) now can derive a new PSK for the node SBI(i) and replace the IKi with the PSKi, where the PSK for SBI(i) is derived as follows.

PSKi = E(RNi XOR RNc, IKi)

After the reconfiguration of PSK for node SBI(i), he encrypts the concatenation value of IKi and TS with the symmetric key SKcs which is a shared key between SBS(s) and SBR(c). Then he sends the encryption value with TID to SBR(c). This is because SBR(c) does not have the key IKi at this moment.

On receiving the encrypted value from SBS(s), SBR(c) can know the key IKi. He can verify the received message by using the decrypted TS. Then, SBR(c) encrypts the concatenation value of RNi and RNc with the key IKi. He sends both the encrypted value and TID to SBI(i). Note that, SBR(c) must not transmit the derived PSK over the public network.

SBI(i) can verify the authenticity of SBR(c) by using the decrypted RNi value from the received message. Finally, SBI(i) can configure his PSK thereafter sending the encryption value of RNc with the new key PSK to SBR(c) for the authenticity validation. SBI(i) derives a session key SKi from the PSK and then reconfigures his secure credential.

III. CONCLUSION

In this paper, we present a secure key setup method that is a part of secure bootstrapping scheme. Currently, we are designing and implementing the proposed scheme by using various types of OOB CH. In particular, we believe that NFC and audio are the best solutions for resource constrained IoT devices. That is mainly because the two interfaces are widely used for lots of daily objects and thus the cost is very low.

ACKNOWLEDGMENT

This work was partly supported by Institute for Information & communications Technology Promotion (IITP) grant funded by the Korea government (MSIP) (No.B0126-15-1018). Also, this research was partly supported by the MSIP (Ministry of Science, ICT and Future Planning), Korea, under the ITRC (Information Technology Research Center) support program (IITP-2015-H8501-15-1008) supervised by the IITP (Institute for Information & communications Technology Promotion).

REFERENCES

[1] N. Kang, et. al., “ESSE: Efficient Secure Session Establishment for Internet-Integrated Wireless Sensor Networks,” J. Distributed Sensor Networks, vol.501, 393754, 2015.

[2] Shelby, Z., Hartke, K., and Bormann, C., "The Constrained Application Protocol (CoAP)", RFC 7252, June 2014.

[3] Bormann, C., Ersue, M., Keranen, A.: Terminology for Constrained-Node Networks. IETF. RFC 7228, June 2014.

Characteristics of ESPAR Antenna with Circumferential Slot Active Element

Kang Pyo Lee
Dankook University
Youngin-si, South Korea
iamdhkfvy@naver.com

Sang Min Han
Soonchunhyang University
Asan-si, South Korea
auspice0@gmail.com

Jung Hun Oh
Electronics and Telecommunications Research Institute
Daejeon-si, South Korea
jhoh70@etri.re.kr

Hak Keun Choi
Dankook University
Youngin-si, South Korea
hkchoi@dankook.ac.kr

Ye Myo Kyaw
Dankook University
Youngin-si, South Korea
yemyokyaw326@gmail.com

***Abstract*—In this paper, a five-element ESPAR antenna with a circumferential slot feed structure is proposed. The central active element consists of two copper cylinders, a dielectric cylinder, and a short copper cylinder for implementing the slot. The parasitic element has a structure surrounding the active element using an FR-4 substrate. The active element facilitates impedance matching with various parameters. In this structure has a bandwidth of about 60 MHz at the return loss of -10 dB or lower. Each parasitic element forms radiation patterns in four directions at 2.45 GHz through adjustment of the reactance load.**

Keywords—Component, ESPAR, Slot antenna, Cylindrical dielectric, Beamforming, Reconfigurable beam pattern

I. INTRODUCTION

The development of wireless communication has enabled us to enjoy fast communication and a wide range of content. However, with the increasing number of users, antennas that support large capacity high-speed communication and beamforming are required to provide convenient communication services [1]. Beamforming refers to a technology for arranging multiple antennas and sending them in a desired direction. Conventional antennas include digital beamforming array antennas and phased array antennas. Because multiple antennas must be arranged, digital beamforming array antennas and phased array antennas require many RF chains, consume a great deal of power, and involve high costs [2]. To improve these drawbacks, the Electronically Steerable Parasitic Array Radiators (ESPAR) antenna was proposed [3]. The ESPAR antenna has a structure of multiple parasitic elements arranged around one active element. It can generate, change, and rotate multiple radiation patterns by adjusting the reactance of a parasitic element [4]. As an active element has one RF chain, the number of RF chains, the power consumption, and the cost have been reduced. However, impedance matching is difficult with the ESPAR antenna due to the effect of the coupling of the active element and the parasitic elements [5]. Therefore, in this paper, an ESPAR antenna with a circumference slot active element is proposed. The proposed active element consists of a circumferential slot, a dielectric cylinder, and a copper cylinder. Impedance matching is easy using such parameters as slot thickness and position, dielectric height, the height and radius of the copper cylinder, and the distance between the slot and the cylinder.

II. ANTENNA CONFIGURATIONS

In this chapter, an ESPAR antenna with a circumference slot active element is described. A five-element ESPAR antenna with one active element and four parasitic elements was designed to work at the central frequency of 2.45 GHz. In the past, dipole- or monopole-type active elements were used. Impedance matching was difficult because these two active elements were structurally simple and had a small number of changeable parameters. Therefore, an active element having several parameters is proposed to improve impedance matching and is compared with a conventional dipole active element.

Figure 1 compares the return loss of the dipole active element and the circumferential slot active element. The dipole active element has a bandwidth of about 100 MHz at a return loss of -10dB or lower, whereas the proposed active element has a bandwidth of about 180 MHz at a return loss of -10dB or lower. The circumferential slot active element showed improved return loss due to changes in various parameters under the same conditions.

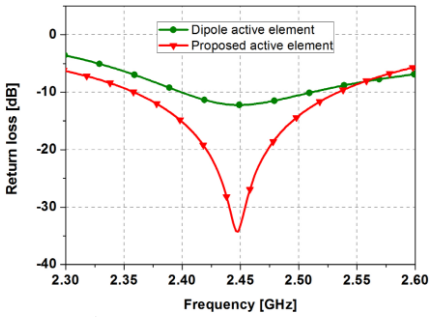

Fig 1. Comparison of return loss between dipole active element and proposed active element

Figure 2(a) shows the overall structure of the ESPAR antenna with a circumferential slot active element. The

active element is located at the center of the antenna, and the parasitic element consists of four FR-4 elements of 0.8 mm thickness (εr=4.3); these adjust the reactance load. Figure 2(b) shows the sectional view of the circumference slot active element, while (c) shows the top view of the antenna. Starting inside and moving outward, this element consists of an Inner conductor cylinder with a thickness of 0.35 mm, a Teflon cylinder with a thickness of 2.24 mm (εr=2.1), and a separated Outer conductor cylinder with a thickness of 0.35 mm. In the Outer conductor cylinder, an FR-4 element serves as the slot. Impedance matching is possible using the height, thickness, and radius of each component as well as the existence and location of the slot.

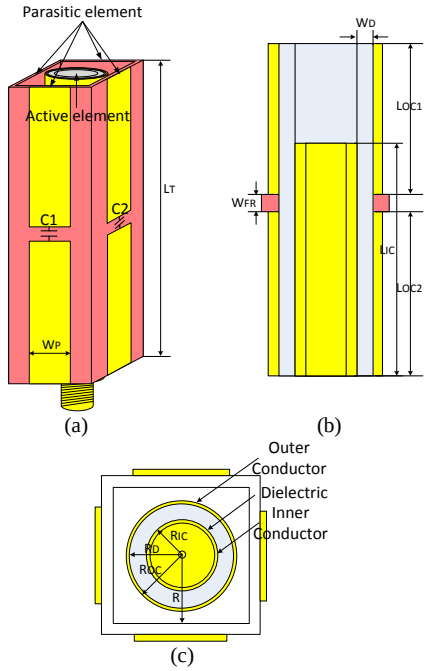

Fig 2. (a) ESPAR Antenna (b) Sectional view of active element (c) Top view

III. CHARACTERISTICS OF THE ESPAR ANTENNA

Figure 3 shows the return loss characteristics of the ESPAR antenna with the simulated circumference slot active element. It shows a bandwidth of about 60 MHz at the return loss of -10dB or lower.

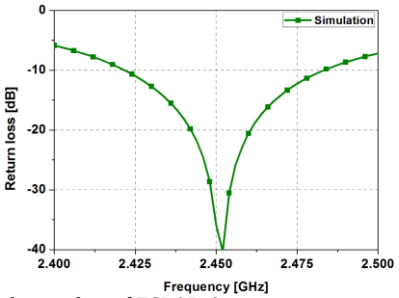

Fig 3. Simulated return loss of ESPAR Antenna

Figure 4 shows the radiation pattern of the ESPAR antenna with the circumference slot active element at the central frequency of 2.45 GHz. At 2.45 GHz, it produced directional radiation patterns in four directions with the adjustment of the reactance load based on four C-values. This means that the proposed active element can be applied to the ESPAR antenna for better performance of the technology.

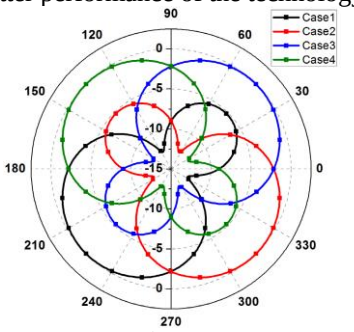

Fig 4. Simulated radiation pattern of ESPAR antenna at 2.45 GHz

IV. CONCLUSION

In this paper, we tested an ESPAR antenna and its characteristics using a cylinder radiating through a circumferential slot as the active element. The original ESPAR antenna had difficulty in impedance matching due to the arrangement distance between the active element and the parasitic element, which generated a coupling effect. However, the proposed circumference slot active element facilitates impedance matching using various parameters such as slot position and thickness and the height and diameter of the dielectric and the copper cylinder. The cylindrical feed structure is also applicable to the ESPAR antenna due to its omnidirectional pattern.

ACKNOWLEDGMENT

This work was supported by an Institute for Information & Communications Technology Promotion (IITP) grant funded by the Korean government (MSIP) [No. R0101-15-244, Development of 5G Mobile Communication Technologies for Hyper-connected smart services].

REFERENCES

[1] Bellofiore, S., Balanis, C., Foufz, J., and Spanias, A.S., "Smart antenna systems for mobile communication networks part 1: Overview and Antenna Design," IEEE, Antennas and Propagation Magazine, vol. 44, pp. 145–154, 2002

[2] Ghouse Basha, T.S., Aloysius, G., Rajakumar, B.R., Giri Prasad, M.N., and Sridevi, P.V., "A constructive smart antenna beam forming technique with spatial diversity," IEEE, Microwaves, Antennas & Propagation, IET, vol. 6, pp. 773–780, 2012

[3] Kawakami, H. and Ohira, T., "Electrically steerable passive array radiator (ESPAR) antennas," IEEE Antennas and Propagation Magazine, vol.47, pp. 43–50, 2005

[4] Sun, C., Hirata, A., Ohira, T., and Karmakar, N.C., "Fast beamforming of electrically steerable parasitic array radiator antennas: theory and experiment," IEEE Trans. On Antennas and Propagation, vol. 52, no.7, pp. 1819–1832,JULY. 2004

[5] Sol-li Yoo, Kwang-Seok Kim, Tae-Dong Yeo, Soo-Ji Lee, Dong-Jin Lee, and long-Won Yul, "A compact and reconfigurable beam pattern ESPAR antenna with automatic impedance matching system," Microwave Conference (EuMC), 44th European, pp. 56–56, 2014

Satellite Mobile Terminal Design having Hybrid Antenna Structure

Young-Bae Jung
Electronics and Control Engineering
Hanbat National University
Daejeon, R.O.Korea
ybjung@hanbat.ac.kr

Soon-Young Eom
Radio Technology Research Department
Electronics and Telecommunications Research Institute
Daejeon, R.O.Korea
syeom@etri.re.kr

***Abstract*—It is proposed that a hybrid antenna (HA) for mobile satellite communications. This antenna has the merit of the high-gain performance using a cassegrain reflector and the rapid two-dimensional beam tracking using a small phased array antenna. This antenna can be operated in 3-bands for a Korean satellite called as Mugungwha, Ka-/K-band for multimedia service and Ku-band for direct broadcast satellite (DBS) service. In this antenna design, we reduced the role of the phased array with a motional sub-reflector and applied a simple satellite tracing algorithm for low cost and structural simplicity.**

Keywords—component; satellite, communications, cassegrain, phased array

I. INTRODUCTION

After 1990s, because the various demands of many people for mobile multimedia service, terrestrial mobile communications via satellite has been widespread till now and vehicle antenna system via satellite will be more populated before long[1]. And the recent Internet growth has resulted in new generation of applications with higher throughput requirements and communication demands. By this reason, vehicle antenna system technologies to access various multimedia service regardless where one is has been rapidly developed with people's high attention, and the technical concerns have focused in the development of the antenna system having high gain and accurate satellite tracking ability at minimum cost [2–4].

In this paper, novel HA with high gain and fast beam steering capability is described. The HA has a modified structure on the basis of the two-reflector scheme with a rotating sub-reflector. The large aperture of the main reflector provides high gain performance, and the rotating sub-reflector enhances the beam steering capacity. Proposed HA mainly performs the beam steering like a conventional HA by the mechanical control of main reflector with the electrical one of a feeder (phased array). The rotating sub-reflector can quickly move to any direction in the reference of fixed center point, so the incident angle of radiated signal from the feeder to the sub-reflector can be controlled by rotation angle of the sub-reflector. This method makes beam steering angle wide and beam steering speed fast in comparison with conventional mechanical method like the movement of whole antenna system is controlled by motors.

II. HYBRID ANTENNA DESIGN

HA is designed to be operated in K-band with right hand circular polarization and Ka-band with left hand circular polarization P). The HA is mainly operated by mechanical method, but electrical beam scanning compensates the shortages of the mechanical one in tracking speed and error. The satellite tracking is electrically realized by the control of a tracking beam in K-band. The proposed HA structure and the beam scanning methods using a feed array and a rotating sub-reflector are summarized in Fig. 1.

To realize the high performance antenna system with low

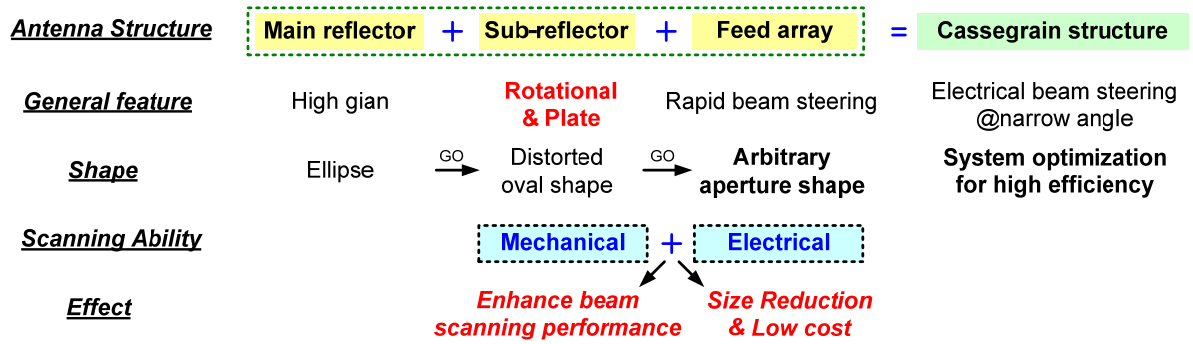

FIG. 1. SUMMARY OF PROPOSED HYBRID ANTENNA STRUCTURE AND BEAM SCANNING ABILITY

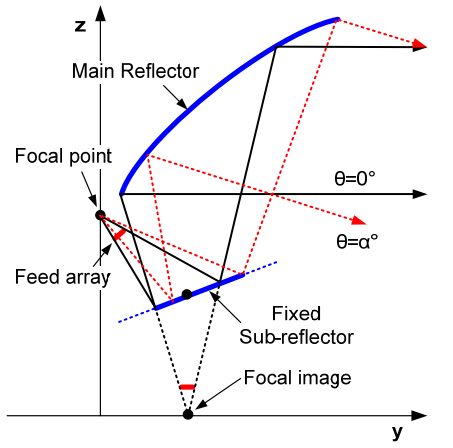

(a)

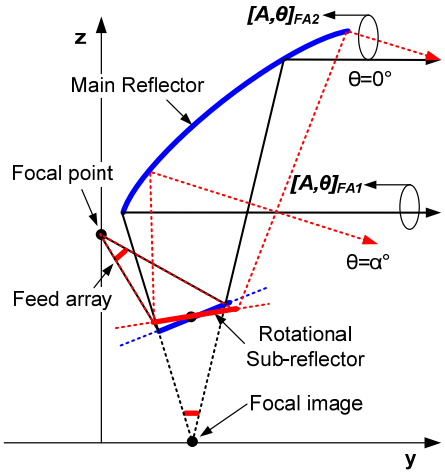

(b)

FIG. 2. OPERATIONAL BEAM CONTROL SCHEME OF PROSED HYBRID ANTENNA.(a) BEAM CONTROL USING A FEED ARRAY (b) BEAM CONTROL USING A SUB-REFLECTOR

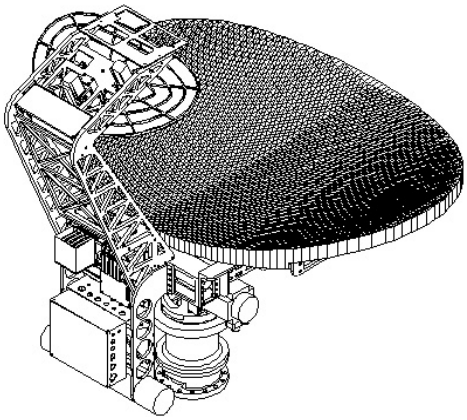

TABLE I. FIG. 2. PROPOSED HYBRID ANTENNA SYSTEM.

cost, we proposed a HA structure shown in Fig. 2. Proposed structure is electrically composed of two parts. The one is communication part for the Ka-/K-band multimedia service using a reflector antenna, and the other is broadcasting part for the Ku-band DBS service using a planar microstrip array antenna. As shown in the figure, the main role of the HA is focused on the multimedia service and the DBS service can be simply realized by the microstrip antenna placed on the back side of the sub-reflector. From Fig. 2, it can be known that the operational beam control scheme of the HA. Fig. 2(a) shows the beam control using a feed array. The feed array is composed of 20 elements with multi-channel active modules. Fig. 2(b) shows the beam control using a rotational sub-reflector. With The required rotation angle of the sub-reflector to make beam steering angles of ±2° in the elevation direction is ∓3°, and the required rotation angle to make angle ±2° in azimuth is ∓3° as well. The wide beam scanning can be also realized by controlling the array feed and the sub-reflector simultaneously.

The fabricated HA was tested in far-field measurement system and the detail HA structure is depicted in Fig. 2. The HA has a minimum gain of 47.2 dBi for TX (30.085~30.885 GHz) and 44.7 dBi for RX (20.335 ~ 21.155 GHz). And the beam width is 1.2° × 0.6°. The side-lobe levels (SLL) of all patterns are less than 15 dB and the maximum pointing error of 0.11° with maximum pointing loss of 1.6 dB. Whole antenna size is 170 cm (diameter) × 170 cm (height) which is smaller than conventional mechanical tracking antennas by about 20%.

III. CONCLUSIONS

A mobile satellite communication antenna with hybrid beam scanning scheme is proposed. This antenna is composed of two reflectors and a feed array like a cassegrain structure. The parabolic main reflector of the HA is designed for high gain, and the sub-reflector is rotational in the elevation and azimuth direction for 2-dimensional beam scanning. Using the proposed structure, we can realize a high performance antenna having high gain and rapid beam scanning ability. And the fabricated antenna size can be reduced by 20% compared with conventional mechanical antennas and the fabrication cost also can be reduced considerably compared with full phased arrays.

ACKNOWLEDGMENT

This research was supported by the MSIP(Ministry of Science, ICT and Future Planning), Korea, under the Global IT Talent support program (NIPA-2014-H0904-14-1002) supervised by the NIPA(National IT Industry Promotion Agency) and the research fund of Hanbat National University in 2013.

REFERENCES

[1] K. Fujimoto, J.R. James, *Mobile Antenna Systems Handbook*, Artech House, 1994

[2] V. Schena and F. Ceprani, "FIFTH project solutions demonstrating new satellite broadband communication system for high speed train," IEEE Vehicular Technology Conference, vol. 5, pp. 2831–2835, May 2004

[3] A. Densmore and V. Jamnejad, "A satellite-tracking K- and Ka-band mobile vehicle antenna system," IEEE Trans. on Vehicular Technology., vol. 42, no. 4, pp. 502–513, Nov. 1993

[4] L.D.Bachrah and G.K.Galimov, *Scanning reflector antennas*, Moscow, Science, 1981

A Study on An Efficient Electricity Saving Scheme for Mobile Cloud Computing

Jun Heo
Dept. of Information & Communication
Kyungmin College
Uijeongbu, South Korea
heojun@kyungmin.ac.kr

Kyung-Shin Kim
School of Mobile Communications
ChungKang College
Icheon, South Korea
kskim@ck.ac.kr

Moon-Sik Kang
Dept. of Electronic Engineering
GangneungWonju Nat'l University
Gangneung&Wonju
South Korea
mskang@gwnu.ac.kr

Abstract - In r*ecent years, many studies have been in progress around the world to solve the problem of global warming. The reduction of CO_2 would be important to solve the global warming problem. Probably the energy production and conservation might be considered to be highly crucial. In addition, the efficient use of energy is also important issue. Therefore, this paper focused on the development of electricity saving scheme as a primary energy source for mobile cloud computing, which can be utilized in homes, shops, buildings and so on. Here, an efficient electricity saving scheme is proposed for reducing the electricity consumption using SARIMA model. Performance analysis is carried out for showing the effectiveness of the proposed system.*

Keywords-electricity saving scheme, SARIMA model, Mobile Cloud Computing, global warming, inference algorithm

I. INTRODUCTION

The energy management system for buildings and factories can collect or analyze both the energy usage and facility operating history through various sensor devices.[1][2] Also it reduces electrical energy by providing the driving information of the building energy devices. The electricity saving device would be mostly introduced when constructing new buildings, moreover when being installed additionally in existing buildings. In any case the electricity device requires a number of additional facilities. Therefore it is challenging to manage energy efficiently, by comparing with the investment costs. Mobile Cloud Computing (MCC) is the combination of cloud computing, mobile computing and wireless networks to bring rich computational resources to mobile users, network operators, as well as cloud computing providers. MCC might provide business opportunities for mobile network operators as well as cloud providers. In order to design a high-efficiency electric device, it is essential to develop the method for electric energy reduction. Such an electric device consists of both a predictive engine and a predictive control engine. The predictive engine on a server is designed to activate predictive algorithm for the management of available power usage. This model is operated based on mobile cloud system including the fixed data, external data and internal data. The predictive control engine on the client system is composed to activate the predictive control algorithm for reducing the energy consumption. The electricity saving scheme is designed by using the precise prediction method as well as SARIMA model, based upon the predicted data at server for mobile cloud computing.

Ⅱ. ELECTRICITY SAVING SCHEME USING SARIMA MODEL

The ARIMA model is used to estimate the demand of the various industrial or social sectors. But becasuse it is impractical to apply ARIMA model to the periodic and seasonal condition, we have applied a SARIMA(Seasonal Autoregressive Integrated Moving Average) model, the extended version for ARIMA model. Furthermore, MCC uses computational augmentation approaches by which resource-constraint mobile devices can utilize the computational resources. There are four types of cloud-based resources, namely, the distant immobile clouds, the proximate immobile computing entities, the proximate mobile computing entities, and the hybrid entities. Smartphones, tablets, handheld devices, and wearable computing devices are part of another group of cloud-based resources. These are the proximate mobile computing entities. The SARIMA model will be the suitable technique for the seasonal and periodic procedure. The equation(1) is related to the model of SARIMA(p,d,q)(P,D,Q)s.

$$\Phi_p(L)\Phi_p(L^s)(1-L)^d(1-L^s)^D Z_t = \delta + \theta_q(L)\Theta_Q(L^s)\epsilon_t \quad (1)$$

Where P,Q,D mean the degree of seasonal AR terms, the degree of seasonal MA terms, and the degree of seasonal difference respectively. The SARIMA model can be divided into three steps such as identification, estimation, and forecasting. In identification phase, the required model is set by analyzing the input data according to conversion, differences, and seasonal variations. In estimation phase, by calculating a statistics, the accuracy of the parameter will be estimated and determined for any forecasting. Based on SARIMA model, in the previous works, the predictive algorithm was tested on MCC environment. Here we use the collected data, in other words a one-year period of historical data for five years. The collected data is composed of month and year, parking, day, time, temperature, weather, and the number of visitors. After

preparing the historical annual data, we compared the predictable data for predicting the time(weather, temperature) with the collected historical data for 5 years in order to predict the number of visitors on one day.[3] Finally, the number of expected visitors on that day is predicted as 4. We will predict the amount of usage in cold / heating operation temperature and illumination data on that day based on the predicted number of visitors, the fixed data, the external data and the internal data. In predictive engine, various simulations can be added under the varied environment. In this paper, however, we will only treat the illumination simulation and the temperature one.

A. Illumination Temperature case

In the initial process, we have predicted the number of visitors on that day. In illumination simulation, we will predict illumination value on the same condition by using the all data which have gathered up as the procedure proceeded so far. The associated attributes of illumination simulation will vary from sunset, sunrise, prediction, the number of predicted visitors, and the fixed contract electrical power. To predict the illumination value, the illumination must be set in accordance with the sunset and sunrise times by comparing with those times and checking current illumination value. Also illumination value has to be set by the number of visitors. With the difference between the contract and currently using electric power, the marginal electric power per hour can be calculated. With the difference between the internal cumulative power and the target power, we will calculate the monthly average margin power and divide your monthly power margin back to 24 the number of shares remaining days, and finally calculate the hourly average margin progressive power. This illumination value extracts the predicted illumination value by adjusting illumination value based upon sunset, sunrise, and the number of visitors. Along with illumination simulation, temperature simulation extracts the prediction value of the coolers / heaters for 1 hour at a point after the current time. Here several values are used such as the predicted number of visitors, the fixed data, external data, and internal data. Temperature simulation has an environment property that the properties for usage management are month, the highest external temperature, the lowest external temperature, fixed contract electric power, internal electric power, the internal cumulative power and the target power.

III. PERFORMANC EVALUATION

In order to evaluate the performance for the proposed scheme, we selected a convenience store which is easily found anywhere as the experimental environment. In the setting phase of SARIMA model, we used the measured value of the same time zone. The measured value is composed of the fixed data, the external data and the internal data. The target is a 24-hour convenience store located in Seoul. The contract power is 20KW. Power consumption was set depending on the size of a convenience store refrigerator, freezer, open-chilled fruit and vegetables, air conditioning, and fluorescent lights. The contract power consumption was determined by the electricity use per hour between KEPCO and convenience store.

Figure 1 shows the results for the illumination and cooling/heating operation based on the temperature came up with extraction, which is obtained by using a predictive control algorithm of prediction and by using the prediction engine control algorithm of the intelligent BEMS server. In this experiment, the use of power savings for a year was compared with the predicted data of five years based on the data 2013. From the figure 1, we can estimate the trend of electric power usage that while electric power usage tends to increase in summer and winter, it tends to decrease in spring and winter. In case of using the space division intelligent BEMS, the same results can be obtained. Besides, the electricity reduction effect under the existing environment is about 7~8%, which is due to use the various data attributes. Furthermore, if we use self-learning method, there will be a possibility of considerable reduction.

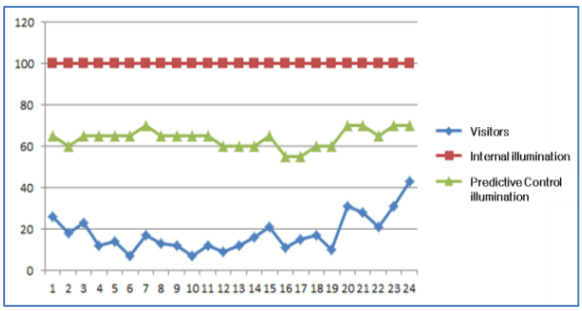

Fig. 1.The predicted control illumination results

IV. CONDULSION AND FURTURE WORKS

The energy reduction would be achieved by saving tiny stuff rather than saving big stuff. It might be necessary to approach for energy reduction issue without degrading the quality of human life. By taking advantage of electricity saving with the intelligent inference algorithm for MSS, which is proposed in this paper, the energy consumption can be reduced. This algorithm makes the best use of SARIMA model to predict the estimated data after one hour or after 10minutes by using the existing data. The predicted results can be applied to control electric devices. In the paper, the function of prediction method is proposed and shows that it is efficient and reasonable scheme. Possible future projects include the development of the high-performance electric power saving scheme on IoT (Internet of Things) cloud environment.

REFERENCES

[1] W.K. Park, Y.K. Jeong, I.W. Lee, "Energy Management Technology for High Energy-Efficient Building," ETRI, Electronics and Telecommunications Trends 26(6), 2011.12.

[2] Y. K. Jeong, W. K. Park, J. S. Han, C. S. Choi, H, J. Yoon, I. W. Lee, "An architecture of the remote building management and control platform for high-efficient low-cost building energy management", ETRI Electronics and Telecomm. Trend, 2010.

[3] X. Pang, M. Wetter, P. Bhattacharya, P. Haves, A framework for simulation-based real-time whole building performance assessment, Building and Environment 54, 100-108, 2012

Towards Higher Educational m-Learning Platform for Conceptual STEAM Environment

Jinhong Kim[1], Sungkyunkwan Univ.
College of Information and Communication Eng.
jinhkm@skku.edu

DeugWhan Sa[2], Kyungdong Univ.
Department of Public Administration
sdwhan@kduniv.ac.kr

Jong-Yun Kim[3], Kyungdong Univ.
Department of Computer Engineering
kjyuni@kduniv.ac.kr

***Abstract*—Now a day, the progress of information and communications technology and information of society has made wire/wireless-based communications become a popular approach and widely used methodology for delivering various educational programs and organizational business situations. In our research paper, we present policy and target of educational model using STEAM.**

Keywords-component; formatting; STEAM, Education Model

I. INTRODUCTION

Recently, higher education and life-long human resource development are urgent issues to support the sustainable development of global society. The conventional methods of education are not enough to support the global demands because of limitations in technology, geographical location, and time zone-based resources [1]. Therefore, a suitable use of advanced ICT in education is needed to meet the social demands, especially for developing countries where high-quality Internet service is not available and the prevalent lack of educational resources. It is well recognized that in the future developing countries would play a key role in sustainable development more than before where opportunities on higher education were limited. Therefore, a suitable use of advanced ICT in education is needed to meet the social demands, especially for developing countries where high-quality Internet service is not available and the prevalent lack of educational resources. It is well recognized that in the future developing countries would play a key role in sustainable development more than before where opportunities on higher education were limited. The features of m-Communication for higher education should be also different from those of the undergraduate education. Based-on the requirements and demands of higher education, the goals of this research are defined as follows: 1) To remove the obstacles of both time and place to post-secondary education for individual and corporate by developing and demonstrating innovative, cost-effective approaches in delivering education through the use of rapidly evolving advanced technology. 2) To provide a means for learners to obtain formal recognition of the skills and knowledge obtained outside the traditional higher education context and/or from multiple providers through the assessment and certification of competency. 3) To encourage joint development of new learning and assessment materials among universities in the global scale, and technology standards that ensure connectivity. Trends and methodologies of m-Learning service have been changing, and nowadays, virtual conference-based, so called video conferencing, or streaming-based contents are being sought for. The new technology brings courses alive by allowing online learners to use their visual and auditory senses. Authoring tool for virtual conference-based content is needed to support this new trend and methodology. The tool should give the opportunity to reuse contents or archives which can be shared to learners [2]. For m-Meeting service, stability of the meeting operation in the unreliable network environment is very important. To preserve the meeting operation, the system should perform automatic reconnection for intermittent network especially in areas with low-speed Internet. A lot of requirements from the business sector that need to be addressed, e.g., content privacy and system management issues [3]. In the m-Meeting section, a meeting management system for controlling member groups and contents were implemented. The author designed a new simple group-based structure for easier management. The system can manage the contents on each group by limiting the number of content, limiting the number of concurrent access, and control the behavior of logging-in members [4]. After all, a usual computer with usual operating systems such as Windows, Linux and Mac operating systems is enough for use.

II. M-LEARNING SYSTEM FOR STEAM

Distance education has been utilized to provide instructional access to adult students living in remote areas where traditional education is not available. An m-Learning system is a popular technology for distance education. The m-Learning education system is based on the web-oriented models conventional in-person education by providing equivalent virtual access to classes, contents, and other resources [5]. It is also a social space where students and teacher can interact through threaded discussions or chat, and we show in Fig. 1. There is a variety of benefits to use m-Learning system. Learner who has limitations of time and location can learn by themselves with the distant-learning

system via Internet technology at a lower cost and higher quality in global scale. M-Learning system can be integrated with a physical learning environment which may be referred to as blended learning. It can take place synchronously or asynchronously. In synchronous systems, participants meet in "real-time" and teachers conduct live classes in virtual classrooms [6]. Students can communicate through a microphone, chat rights, or by writing on the board. In asynchronous learning, which is sometimes called "self-virtual environment" learning, students are expected to complete lessons and assignments independently through the system. Asynchronous courses have deadlines just as synchronous courses do, but each student is learning at their own pace.

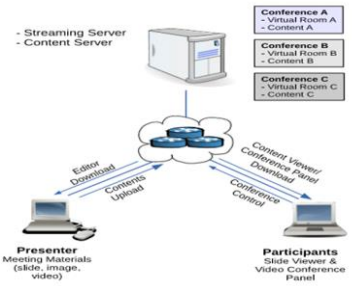

Figure 1. m-Learning system for STEAM

III. M-LEARNING PLATFORM FOR STEAM

There are three main types of the m-Learning platform, i.e., the standalone system, the server-client system and cloud computing system. A lot of applications are working as a standalone system. They do not need the network infrastructure, but they require installation of software application in user's computer. They almost support for a various operating systems. Moreover, the implementation m-Learning on a cloud computing platform has its peculiarities and needs a specific approach. This presented an m-Learning ecosystem based on cloud computing infrastructure. The benefits of the system are reliable, flexible, and cost-efficient. The system also has mechanisms to guarantee the teaching and learning activities, and the quality and the running of the ecosystem. In addition, this measured the positive impact of using cloud computing architectures upon m-Learning solution development. The measured result shows that cloud computing system can reduce the cost of infrastructure maintenance and risk of hardware failure of an m-Learning system.

IV. WIRELESS-BASED CONTENT OF M-LEARNING FOR STEAM

Learning contents are the essential element of an m-Learning system. The prevalent characteristics of learning content can be categorized in three groups: (1) General web-based learning content – is used as a standard e-learning system since web technology was first initiated. It uses standard HTML elements such as text, images and links for making content. (2) Slide-based learning content – is composed of slides with embedded objects, such as text, image and others. Slide is the main element of the content. It is used to control the embedded object changing. (3) wireless-based learning content – is proposed to integrate data stream and slide presentation into a learning content. The wireless-based stream is used as a baseline of a learning content. Presentation slides are automatically changed by operating time. In the educational system, the use of this for student learning has long been discussed since it consist of various multimedia types such as image, audio, animation and teacher actions. This form of technology brings courses alive by allowing online learners to use their visual and auditory senses to learn new concepts. This streaming allows online instructors the opportunity to deliver alternative course materials to learners who use m-Learning system especially in higher education.

V. CONCLUSIONS

The proposed authoring and viewing tools have exhibited numerous advantages as an m-Learning tool for higher education. The total system can help accomplish the purposes of distance learning among universities. It makes learning activities available anytime and anywhere. In addition, cross-platform and cloud computing are supported to break the barriers in various operating systems and application software installation is not necessary at the users' computer. Since using online content is a trend for obtaining knowledge due to the vast availability of information and content from the Internet, then the proposed system can be used to support advanced knowledge by self-learning. It is considered to support the classroom-based learning due to the increasing social demand internationally, and to address the limitations of the traditional learning due to time, location, and cost. Therefore, the author implements a new online authoring tool for m-Learning system using Flash technology. The proposed system is achieved and optimized to support the cloud computing technology since the technology is implemented in a wide variety of architectures, services, models, and other technologies for STEAM.

REFERENCES

[1] Kolodner J. L, Camp P. J , Crismond D (2001) "Problem-based learning meets case-based reasoning in the middle-school science classroom: Putting learning by design into practice" , Journal of the Learning Sciences, Vol.12 (4) ; pp.495-547.

[2] Squire K , Jenkins H , Walter H , Heather M (2003) "Design Principles of Next-Generation Digital Gaming for Education" , Educational Technology, Vol.43 (5) ; pp.17-23.

[3] Kim Engil , Jonghun Kim (2011) "STEAM education curriculum design on project based learning" , Journal of Information Education, Vol.15 (4) ; pp.551-560. in press.

[4] Kim Jueun (2004) "PC game model research for elementary students English education" , Master Thesis of Chung-Ang Univ

[5] Shaffer D. W , Richard Squire H , Gee J. K. R (2005) Video games and the future of learning , WCER Working Paper, Vol.4.

[6] Wi Jong Hyun , Enseok Wohn (2014) "The analysis on the effectiveness of afterschoolprogram at elementary school" , Foreign Language Education, Vol.21 (1) ; pp.75-85.

An Improved Wireless Communication System Using Relay for Signal Transmission

Won-Seok Lee
uT Communication Research Institute
Sejong University
Seoul, Korea
scu008@nate.com

Myoung-Jin Kim
uT Communication Research Institute
Sejong University
Seoul, Korea
keywind@naver.com

Hyoung-Kyu Song [1]
uT Communication Research Institute
Sejong University
Seoul, Korea
songhk0514@gmail.com

***Abstract*— This paper proposes a cooperative communication scheme for improving wireless communication performance. By the distance of between transmitter and receiver, the signal from the transmitter is distorted for various reasons such as inter-cell interference (ICI), power reduction, incorrect channel estimation. In order to solve problems, the proposed scheme uses the relay. By the relay, the communication performance improves. Because the relay is located in between transmitter and receiver In this paper, the relay uses AF scheme for transmitting two signals at the same time.**

Keywords- amplify-and-forward, cooperative communication, OFDM, MMSE

I. INTRODUCTION

Recently, wireless communication system demands high reliability and transmission rate. In order to obtain improved communication performance, many new techniques have been developed.

Orthogonal frequency division multiplexing (OFDM) system is used in latest communication system such as, long term evolution (LTE), wireless local area network (WLAN). The OFDM system uses orthogonal multi carrier for transmission. Therefore, The OFDM system provides high frequency efficiency and robustness for multi-path fading. The multiple-input multiple-output (MIMO) system is studied for improved wireless communication. The MIMO system uses multiple antennas to obtain high data rate and diversity gain. By the number of antennas in the transmitter and receiver, wireless communication system is defined as single-input single-out (SISO), multiple-input multiple-output (MIMO), multiple-input single-out (MISO) and single-input multiple-out (SIMO). The MIMO system is effective scheme to signal's multi-path fading that causes the attenuation and distortion. But there are limits of MIMO system such as device size, transmission power, complexity on the mobile device. The cooperative communication was proposed to solve problems of MIMO system [1].

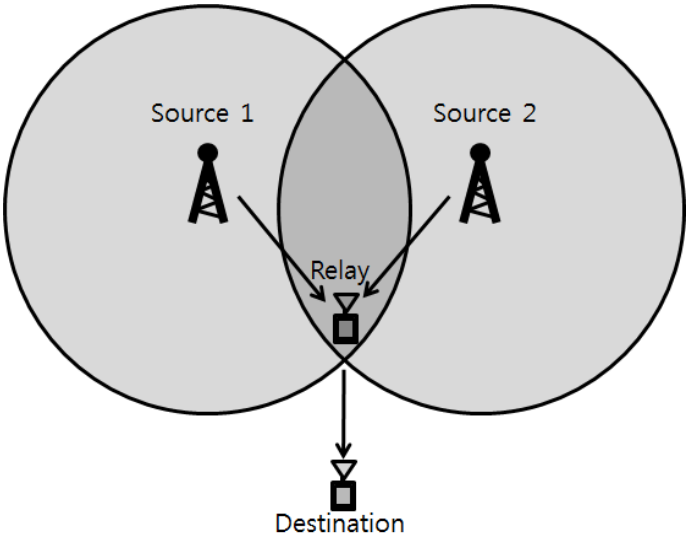

Figure 1. System model of the cooperative communication

In the cooperative communication, devices share the antenna. It makes the virtual MIMO system without additional antenna equip and communication system obtains diversity gain The relay is name of device that shares antenna. The relay receives signal from the source and forwarding to the destination. The destination receives the same signal from both the source and the relay [2].

This paper proposes the cooperative communication scheme for device is located in edge of cell. The proposed cooperative communication scheme adds the relay to obtain diversity gain. The relay is received two signals at the same time by sources and forwarding to the destination. The destination detects the signals using minimum mean square error (MMSE) scheme [3].

II. SYSTEM MODEL OF THE PROPOSED COMMUNICATION SCHEME

Fig.1 shows the system model of considered communication environment. There are two sources, a relay and destination. The circle means reliable cell coverage of source. The reliable cell coverage represents that if destination

1) Corresponding author

is located in circle the communication between source and destination is reliable. But in Fig.1 position of destination is out of circle. Therefore, communication performance is very low. This paper proposes to solve this problem. The relay is located in inner circle both of source 1 and source 2. The relay receives reliable signal than destination and sand to received signals to destination. The relay uses amplify-and-forward (AF) scheme for sanding to destination. The destination demodulates signals by MMSE detection scheme. It is assumed that the destination has two antennas.

The signal from the base station is transmitted by passing through the Rayleigh fading channel. This transmitted signal also suffers complex Gaussian random noise added by receiver. The received signal vector is expressed as follows,

$$Z = HX + n\,, \tag{1}$$

where H is complex channel matrix and X is complex OFDM symbols. n is complex additive white Gaussian noise (AWGN) that has zero mean and variance σ^2.

TABLE I. TRANSMISSION SYSTEM OF THE PROPOSED SCHEME

	Source 1	Source 2	relay
Time slot 1	x_1	x_2	
Time slot 2			$h_1x_1 + h_2x_2$

)

In proposed system transmitted signals are amplified by AF scheme. Table 1 shows Transmission system of the proposed scheme. At the time slot 1, source transmits to relay and relay send to destination at next time slot. The h_1 means channel state between source 1 and relay. Similarly, h_2 means channel state between source 2 and relay. In the destination, received signal are represented in equation as follows,

$$\begin{aligned} y_1 &= h_{r1}(h_1x_1 + h_2x_2) \\ y_2 &= h_{r2}(h_1x_1 + h_2x_2), \end{aligned} \tag{2}$$

The transmitted signals are detected by the minimum mean square error (MMSE) detection scheme. The form of the MMSE matrix is represented as follows,

$$G_{mmse} = (H^HH + \sigma^2I)^{-1}H^H, \tag{3}$$

where H^H is a form the self-adjoint matrix that is composed of a complex square matrix with own conjugate transpose, I means a form of the unit matrix and σ^2 is noise variance. In the cooperative communication, The AF scheme only amplifies the received signal from the source forwarding to destination. The AF scheme is simply realized. But AF scheme has the problem that noise is amplified with signal. The amplified noise degrades the detection performance. When amplified noise is large, the communication system has low performance. In the system model, the relay received reliable signals by assumption.

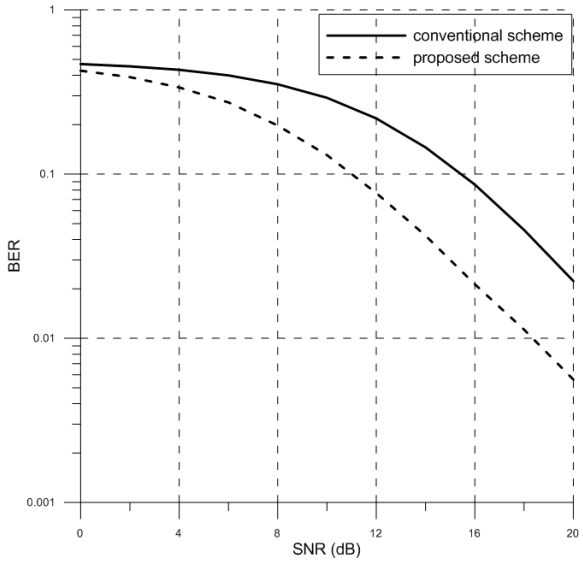

Figure 2. Simulation Result

III. SIMULATION RESULT AND CONCLUSION

The fast Fourier transform (FFT) size is 64, the cyclic prefix size is 16 and 16QAM modulation is used. The signal goes through 7-path Rayleigh fading channel. Fig. 2 shows BER performance of proposed scheme compared with conventional scheme. The proposed scheme has high BER performance among conventional schemes According to the simulation results, the proposed scheme can obtain the improved BER performance. antennas.

In order to achieve high performance in the poor channel state, this paper proposes scheme that using cooperative communication. If the state of channel condition is poor and the path loss is large, the signal from the base station suffers the attenuation. he proposed scheme applies AF scheme and MMSE detection scheme. Therefore, the proposed scheme provides high BER performance. It means the proposed scheme is useful for the wireless communication system.

ACKNOWLEDGMENT

This research was supported by Basic Science Research Program through the National Research Foundation of Korea(NRF) funded by the Ministry of Science, ICT and future Planning(No. 2013R1A2A2A01067708) and the IT R&D program of MOTIE/KEIT [10054819, Development of modular wearable platform technology for the disaster and industrial site].

REFERENCES

[1] L. T. Berger, A. Schwager, P. Pagani,D. M. Schneider, "OMIMO Power Line Communications," IEEE COMMUNICATION SURVEYS & TUTORIALS, VOL. 17, NO. 1, pp. 106–124, 2015.

[2] S. M. Alamouti, "A Simple Transmit Diversity Technique for Wireless Communications," IEEE JOURNAL ON SELECT AREAS IN COMMUNICATIONS, VOL. 16, NO. 8, pp. 1451–1458, OCTOBER 1998.

[3] H. Vincent Poor, S. Verdu, "Probability of Error in MMSE Multiuser Detection," IEEE TRANSACTIONS ON INFORMATION THEORY, VOL. 43, NO. 3, pp. 858–872, MAY 199

An Adaptive Cooperative Transmission Scheme According to the User Location

Chang-Hee Kang
uT Communication Research Institute
Sejong Univeristy
Seoul, Korea
kknaghea@nate.com

Hyun-Jee Yang
uT Communication Research Institute
Sejong University
Seoul, Korea
hjyang206@naver.com

Hyoung-Kyu Song[1]
uT Communication Research Institute
Sejong University
Seoul, Korea
songhk0514@gmail.com

***Abstract*—In this paper, an adaptive cooperative transmission scheme according to the user location is proposed. The proposed cooperative scheme considers the destination user location and applies cooperative scheme properly. If the destination user is located in the cell boundary, the quality of communication is degraded in the broadcasting system. Therefore, the adaptive transmission scheme for the user location is proposed. In the simulation results, the proposed scheme can obtain more improved performance than the conventional scheme.**

Keywords-component; adaptive transmission, broadcasting system, cooperative transmission, improved performance.

I. INTRODUCTION

In wireless communication, the communication quality is degraded by the effect of channel fading and inter-symbol interference. In order to improve the communication quality, multiple-input multiple-output (MIMO) systems which provide high data rate and reliable communication are studied. Since the MIMO system uses a number of antennas, the cost of the system is expensive and the complexity of the hardware is increased [1]. So, the cooperative transmission scheme is studied to resolve the problem of the MIMO system. The cooperative transmission scheme uses single antenna user and build the virtual MIMO system. In the cooperative transmission scheme, composition elements are source, destination user and relay. The relay transfers the signal to the destination with independent path. So, the destination user received the signal additionally by using the relay [2].

The cooperative transmission scheme can obtain diversity gain since the destination user received additional signal from the relay. Also, the reliability of the communication is improved. In this paper, space time block code (STBC) scheme is adapted to improve the performance of the proposed scheme. So, the proposed scheme constructs the virtual MIMO system by cooperating with one antenna users. The STBC scheme uses two time slots to transmit symbols from two transmission antennas. In the STBC scheme, the diversity gain is obtained since the time and space are separated.

The communication performance is influenced from the transmission distance between a base station and a destination user. If a destination user is distant from a base station, the performance of communication is degraded. This paper proposes an adaptive cooperative transmission scheme using relay according to the location of a destination user. In the proposed scheme using relay with STBC scheme, two locations are used and the cooperative transmission scheme is adaptively utilized in each location. Therefore, the propose scheme obtains more high performance than the conventional scheme in the cell boundary.

II. PROPOSED SCHEME

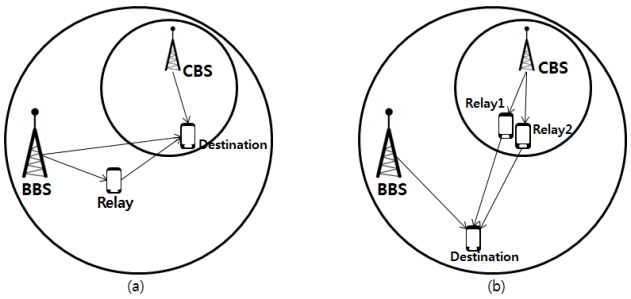

Figure 1. The system model of proposed transmission scheme

In the broadcasting system, the BBS and CBS communicate with each other and the quality of the communication is affected by the location of the destination user. If the destination user is located in the cell boundary, the communication performance is degraded by the distance increase. Therefore, an adaptive cooperative transmission scheme for the reliable transmission is proposed in this paper.

The location (a) and (b) are used in the proposed scheme according the two locations. Each location adapts STBC scheme of cooperative transmission scheme for reliable transmission when the destination user is located in the cell edge. In Fig. 2, the adaptive proposed schemes are represented. Also, the location (a) and (b) are using cooperative transmission scheme with relay for improved performance. In the location (a) of the Fig. 2, the destination user is located in the cell boundary of CBS. On the other hand, the destination user is located in the cell boundary of BBS in the location (b)

1) Corresponding author

of Fig. 2. The adaptive transmission scheme is necessary for reliable transmission since two locations have different environment of communication system. Therefore, this paper proposes an adaptive cooperative transmission scheme with relay to obtain high performance and diversity gain. Also, STBC scheme of cooperative transmission scheme is applied to improve the communication performance when the transmission distance between BBS and the destination user and between CBS and destination user is increased. So, the adaptive cooperative proposed scheme which uses relay between a base station and the destination user is obtained more good BER performance than the conventional scheme.

TABLE I. TRANSMISSION SEQUENCE OF THE LOCATION (A) IN PROPOSED SCHEME

Time slot	BBS	Relay	CBS
T1	X1	X2	X1
T2	-X2*	X1*	X2

TABLE II. TRANSMISSION SEQUENCE OF THE LOCATION (B) IN PROPOSED SCHEME

Time slot	BBS	CBS	Relay
T1	X1	X1	X2
T2	X2	-X1*	X1*

Table. 2 expresses the transmission sequence of the adaptive cooperative transmission scheme about the location (a). Also, Table. 3 expresses the transmission sequence of the adaptive cooperative transmission scheme about the location (b). In Table. 2 and Table. 3, the BBS and CBS transmit the OFDM symbol x1 and c2 during two time slots. X1* and X2* mean the signal suffering STBC scheme which is spatial diversity scheme. In the location (a), the BBS and the relay process the STBC scheme since the destination user is far from the BBS compared with CBS. On the other hand, since the destination user is far from the CBS compared with BBS, the CBS and the relay process the STBC scheme in the location (b).

III. SIMULATION RESULTS

In this section, BER performance is shown. The proposed scheme is compared with the conventional scheme to prove the performance improvement. The OFDM modulated signals are transmitted and the number of subcarrier is 64. The transmitted signals use quadrature phase shift keying (QPSK) modulation and 1/2 convolutional code is also used. The 7-path Rayleigh fading channel is suffered in these simulations. In the simulation, the attenuation rates of the channel condition are expressed 10 and 15 decibel (dB). These two dB values mean that the channel condition between a base station and the destination user is bad since the destination user is located in the cell boundary.

Fig. 3 shows bit error rate (BER) performance of the conventional scheme and proposed scheme. The simulation graph is also expressed according to the destination user location (a) and (b) and conventional scheme. It is confirmed that the proposed scheme has higher BER performance than the conventional scheme in all locations by the simulation results. Therefore, the proposed scheme is more efficiently in the broadcasting system and possible the reliable transmission in the attenuation environment.

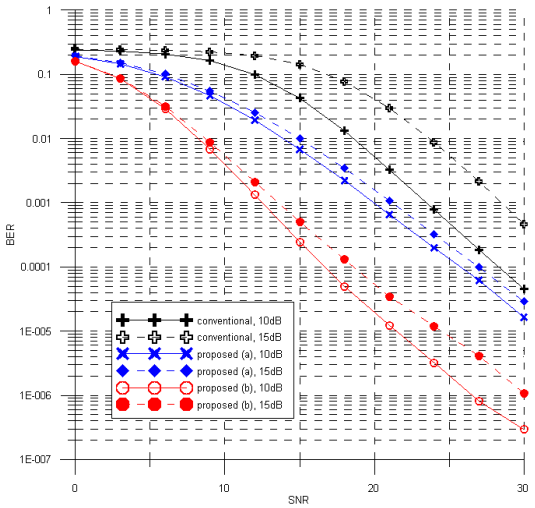

Figure 2. The simulation result of BER performance

IV. CONCLUSION

In this paper, the adaptive cooperative transmission scheme according to the destination location is proposed in order to improve the quality of communication. The conventional scheme can obtain diversity gain since BBS and CBS transmit the signal to the destination user at the same time. However, the performance of the conventional scheme is degraded if the distance between BBS and the destination user and CBS and the destination user is increased and the communication environment is bad. So, this paper proposes the adaptive cooperative transmission scheme with relay according to the destination user location. As a result, the improved performance is provided by proposed scheme since the relay transmits the additional signal by short transmission distance. Also, the application of the suitable transmission scheme considering two locations can obtain good performance. Therefore, the proposed scheme can do reliable communication with relay in the attenuation environment

ACKNOWLEDGMENT

This research was supported by Basic Science Research Program through the National Research Foundation of Korea(NRF) funded by the Ministry of Science, ICT and future Planning(No. 2013R1A2A2A01067708) and ICT R&D program of MSIP/IITP. [R0101-14-0189, Development of the next generation convergence broadcasting and monitoring systems combined with the networks].

REFERENCES

[1] S.H. Jung, D.H. Park, H.K. Song, “Cooperative Beamforming Scheme Using MIMO Antenna Array in LTE-A System”, Journal of Electromagnetic Waves and Applications, vol.29, no.9, pp.1218-1227, May 2015

[2] S.B. Choi, E.H. Lee, J.I. Baik, Y.H. You, H.K. Song, “Cooperative Communication Using the DF Protocol in the Hierarchical Modulation”, IEICE Transactions Fundamentals, vol. E98-A, no.9, pp. 1990-1994, Sep 2015

Run-Time IC Trojan Detection and Isolation Using an SoC Bus

Kanda Guard
Dept. of Information and Communication Engineering
Hanbat National University
Daejeon, South Korea
guardkanda@gmail.com

Kwangki Ryoo
Dept. of Information and Communication Engineering
Hanbat National University
Daejeon, South Korea
kkryoo@gmail.com

***Abstract*— A secure and effective on-chip bus used for detecting hardware Trojan activities by way of modification in the on-chip bus modules such as the arbiter, address decoder, signal multiplexors is proposed. The AMBA AHB is used for this research. The design was modeled with the Xilinx 14.7 ISE and tested on the HBE-SoC-IPD test board equipped with the virtex4 FPGA device. The design operates at a frequency of 250MHz and has a gate count of 42K gates.**

Keywords- Trojan; On-chip bus ; AHB

I. INTRODUCTION

Silicon chips are getting much more complex to design manufacture, fabricate and test. Owing to the prediction of Moore's Law, new generation of ICs are becoming smaller and complex in view of transistor size and has caused IC production process to be independent because for instance designs can be outsourced or third party IP can be used. These ways have introduced an inevitable security and trust issues in the IC design world because a designer has no full control of the design process. DARPA, a defense agency in the US which deals with the hardware security first raised this issue [1-2]. Hardware Trojans which is the addition or modification of an IC for an ill purpose [3-4] can be carried out at any stage in the IC design process. Trojan attacks then come easy through the use of outsourced IPs for example and if these malicious IPs gets undetected, the after effect can be very costly based on the attack type of the Trojan. All Trojans can be placed anywhere in a Hardware design but most adversaries target the system bus which is the main channel of data and control signals to other devices. A successful attack on the on-chip bus means an entire system breakdown. For this reason the proposed architecture for a secured on-chip bus for Systems-on-Chip design is presented in this paper to provide some level of security and detection in an SoC.

II. RELATED RESEARCH

Research into the field of hardware Trojans started not so long ago because formerly, a computers security was only based on the software program running on the computer but currently due to the issue of complexity leading to outsourcing and use of third party IPs this general rule of thumb has changed. A method of handling hardware Trojans pre-deployment was carried out. A method of voting on an even number of same IP from different vendors and calculating the CRC value for each IP to determine the best IP with the least votes was presented in [5]. N. Yoshimuzu detected hardware Trojans by breaking of symmetries and measuring of the path delay as presented in [6]. A Trojan when activated will sensitize functional path whose propagation delay is adversely affected by the malicious circuit inclusion, although the impact of a Hardware Trojan a path delay can be very small. Current Integration methodology was used by [7] to observe Trojan activity in the circuit and a localized current analysis approach to isolate the Trojan. The presence of a Trojan circuit reflects in the current drawn from the power supply even if no switching occurs in the Trojan circuit hence an extra gate will cause a change in the power consumption. L.W Kim detected and halted the operation of the infected IPs in [8]. This paper provides the following modifications to[8]

- Use of a multiple arbitration scheme to improve the operations of the secured bus.
- Use of a simple ROM for specifying all the restricted address ranges masters have to a slaves.
- There is also a self-correcting master to slave mux to check the signals from the original source and if they do not match, corrects them to the appropriate value.

III. PROPOSED BUS ARCHITECTUE

A. Proposed Secure Bus Arbiter

The bus arbiter is the "traffic cop" that dictates which and when a bus master requesting for the bus actually gets to use the bus by the use of request and lock, HBUSREQx and HLOCK signals in the arbiter. When there is a bus grant, the master granted the bus is known from HMASTER signal. The MLD block detects how long a master keeps the bus for based on the threshold value specified by the system architect. If a master occupies the bus more than this threshold value, it is suspicious and the malicious lock detect signal is asserted to register the master HMASTER. This ID is checked against a new request and if the new request is coming from the same master, it is masked out and the default master is granted the bus. Multiple arbitration has the highest priority arbitration as default scheme. The other scheme, fair chance round robin allows every master an equal chance to use the bus and can use the bus again only after all other masters have had their chance to use the bus. If a master keeps the bus in the default arbitration scheme for a threshold time, the arbitration scheme is automatically changed to initially provide a means of preventing the bus lock and if it continues then the MLD block will flag it as a suspicious master and act accordingly.

MSIP (Ministry of Science, ICT and Future Planning), Korea, under the Global IT Talent support program (IITP-2015-R0134-15-1019)

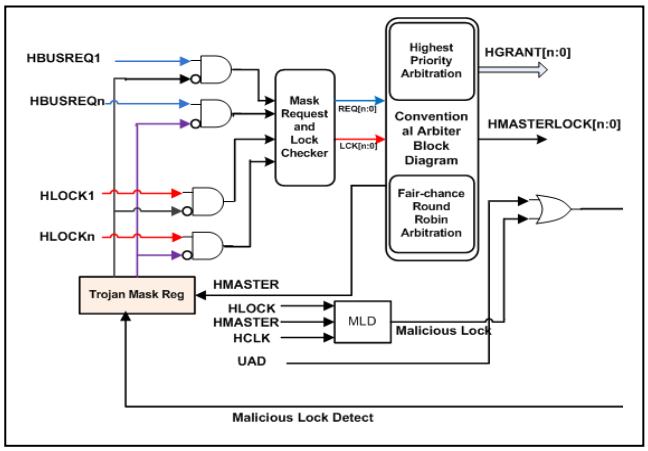

Figure 1. Proposed Secure Address Decoder

B. *Proposed Secure Address Decoder*

Fig. 2 shows the proposed secure address decoder which uses a simple ROM in the comparator to keep the restricted addresses. The Master ID and the slave ID are used together to pick the restricted address of a transaction and checks it against HADDRs if there is no match, UAD signal is asserted which is used to send the transaction to the default slave. A malicious slave ID is registered and checked against all new slave select signals to mask them out if there is a select to the same registered ID. The transfer is then sent to the default slave. The proposed architecture used a 5x144 ROM with each location occupying about 36 bit. First 32 bit is the actual address and the final 4bits is the incremental value to obtain the range.

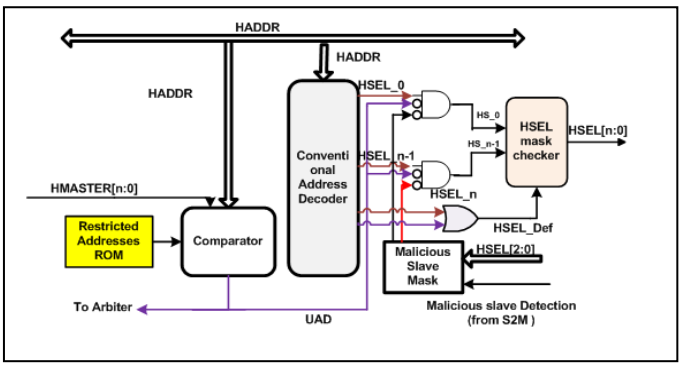

Figure 2. Proposed Secure Address Decoder.

C. *Proposed Secure Slave to Master Mux*

Fig. 3 below shows the proposed secure slave to master mux. Threshold values for how long a slave can keep its ready and response signals low is predetermined by designer. As soon as any of the two response signals goes low the detect logic is triggered and monitors the signal. If it stays low until the threshold value the signal malicious_slave_detect signal is generated, sent to the secure address decoder to enable and register the slave select ID, HSEL of the current slave. If the next slave select is same as the one registered, the ID is used and the default slave select is activated for the transfer. The master to slave mux also checks if the transactions size and burst size have not been altered by checking it against the original value. The original value from the master is restored if there is no match between the two values.

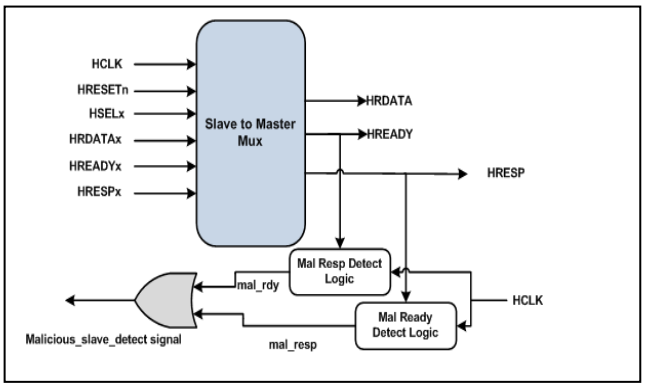

Figure 3. Proposed Secure Slave to Master Mux

IV. EXPERIMENTAL RESULT

TABLE I. RESULT COMPARISON

	Architecture Comparison	
	Conventional Bus	***Proposed Secure Bus***
Bus Size	5 Master, 5 Slaves	5 Masters , 5 Slaves
Process(TSMC)	130nm	130nm
Frequency	300MHz	250MHz
Gate Count	32K	42K

a. compared results.

V. CONCLUSION

Secure bus architecture for detecting and isolating Trojans have been proposed in the paper. Though this modified architecture causes some overhead cost and increase in area it provides a trade off in terms of security.

ACKNOWLEDGMENT

This research was supported by the MSIP (Ministry of Science, ICT and Future Planning), Korea, under the Global IT Talent support program (IITP-2015-R0134-15-1019) supervised by the IITP (Institute for Information and Communication Technology Promotion)

REFERENCES

[1] DARPA BAA 07-24-solicitations-microsyste m s technology office. http://www.darpa. mil/MTO/solicitations/baa07-24/index.html, 2007.

[2] S. Adee, The hunt for the kill switch, Spectr. IEEE 45 (5) May (2008) 34–39.

[3] G. Bloom, E. Leontie, B. Narahari, R. Si mha. Hardware and security: vulnerabilities and solutioins.

[4] S Bhunia, M.S.Hsiao, Mainak B, and Seet haram N "Hardware Trojan attacks - threat analysis and countermeasures"

[5] A. Al-Anwar, Y. Alkabani, M. Watheq El-Kharashi, Hassan Bedour "Hardware Trojan detection methodology for FPGA" IEEE PACRIM,sept 2013.

[6] N. Yoshimizu "Hardware Trojan detection by symmetry breaking in path delays "IEEE international Symposium on Hardware-OrientedSecurity and Trust(HOST),April 2014.

[7] X Wang, H Salmani, M Tehranipoor and J Plusquellic "Hardware Trojan detection and isolation using current integration and localized current analysis" IEEE DFTVS'08

[8] L.W Kim, J.D. Villasenor, "A system-on-chip bus architecture for thwarting integrated circuit Trojan horses" IEEE transaction on VLSI, Oct, 2011

A 12-bit 100kS/s SAR ADC for Biomedical Applications

Sung-Chan Rho, Jae-Suk Kim
Department of Electronics and Computer Engineering
Seokyeong University
Seoul, Korea
scrho@skuniv.ac.kr

Shin-Il Lim
Department of Electronics Engineering
Seokyeong University
Seoul, Korea
silim@skuniv.ac.kr

***Abstract*—This paper describes a 12-bit 100kS/s successive approximation register analog-to-digital converter (SAR ADC) for biomedical system. Both top-plate sampling technique and VCM-based switching technique are applied to the capacitor digital-to-analog converter (CDAC) to implement a 12-bit SAR ADC with 10-b capacitor array DAC. To enhance the linearity of proposed ADC, thermometer decoder is used in capacitor array DAC. Switching-energy minimization technique and asynchronous control with a low-power delay circuit are also adopted to reduce power consumption. Simulation results show that the proposed ADC achieve the SNDR of 70.97dB, the SDFR of 80.23dB and the ENOB of 11.49b with the CMOS 0.18μm technology. Total power consumption is 11.16(W under the supply voltage of 1.8V at the sampling frequency of 100kHz. And the figure of merit (FoM) is 38.79fJ/conversion-step.**

Keywords – Analog-to-digital converter (ADC), SAR ADC, thermometer decoder DAC, dummy Cap switching, biomedical system, energy-efficient

I. INTRODUCTION

Due to the good power efficiency, the SAR type analog-to-digital converter (ADC) is widely used in biomedical system [1]. In biomedical applications such as electrocardiogram (ECG) and electro-encephalogram (EEG), the resolution of ADC over 10-bit to 12-bit is required for high accuracy in analog front-end. Since the SAR ADC is substantially implemented with the capacitor array in internal DAC, the capacitor array in 12-bit DAC requires large chip area if it is implemented with direct binary weighted capacitor array. And as the recent bio-medical devices are implemented with portable form, low power consumption is essential design condition for battery operated system. In accordance with this trend, this paper focus on the implementation of 12-bit SAR type ADC with low power consumption and small chip area.

II. RCHITECTURE OF THE PROPOSED ADC

Fig. 1 shows the block diagram of proposed 12b SAR ADC. It has a differential CDAC, an output offset cancelled comparator, a SAR and an asynchronous control block. The proposed 12-bit SAR ADC used top plate sampling technique [2] and dummy capacitor switching technique based on V_{CM} [3] in order to reduce chip area and power consumption. To reduce chip area, split array with attenuation capacitor is adopted as shown in Fig. 2. In additional, for the enhanced accuracy, output offset cancelled comparator and thermometer decoder DAC are used. And, for the low power consumption in asynchronous digital control block, leakage based low power delay circuit [4] is adopted.

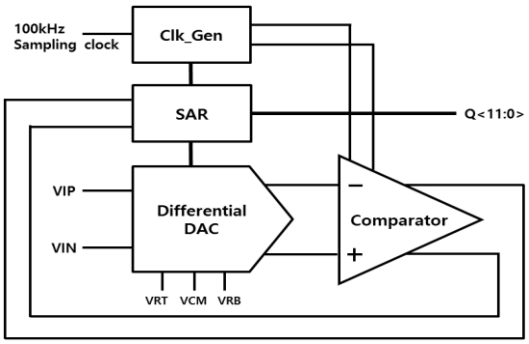

Figure 1. Block diagram of 12-bit SAR ADC

A. Proposed DAC

Fig. 2 shows the thermometer decoder DAC architecture in 12-bit ADC [5]. The thermometer decoder applied to the MSB array in DAC is used to improve the linearity of the SAR ADC. In sampling mode, input signal is applied to the top plate of differential capacitor array. In holding mode, DAC holds VIN and VIP. At this time, the MSB value is determined by comparing the holding values of differential DAC. This technique enables to reduce the total capacitances by half compared to the conventional design. Additional dummy capacitor switching technique based on common mode voltage (V_{CM}) could reduce capacitor array.

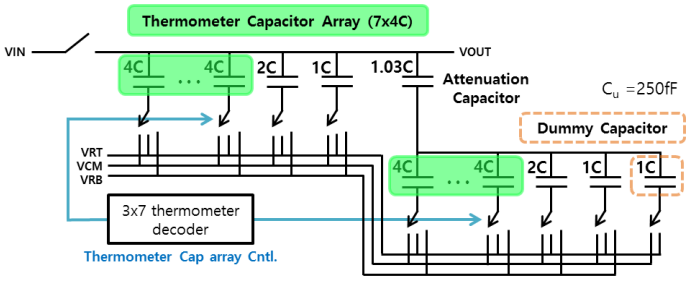

Figure 2. Diagram of the proposed DAC architecture

This technique switches the reference voltage between voltage reference top (VRT) and VCM, instead of VRT and voltage reference bottom (VRB) in last comparison and can reduce the capacitors by half. The number of total capacitors can be reduced to quarter with these two techniques. There is only one switching operation during each conversion step with thermometer decoder. This technique also reduces switching energy compared to the conventional SAR ADC.

B. Implementation of low power delay

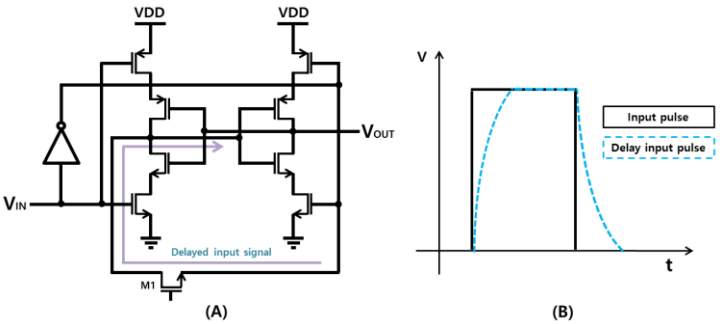

Figure 3. (A) Implementation of low power delay circuit, (B) Input pulse and delayed input pulse

The delay circuit shown in Fig. 3(A) is applied for low power consumption [4]. In conventional inverter chain with load capacitors, a large amount of static current flows in proportion to the output settling time. However, the adopted delay circuits make the longer delay time without large power consumption, because its leakage-based large resistance of MOS transistors and gate capacitance generate the longer RC delay as shown in Fig. 3(B).

III. Simulation Results and Performance Summary

The chip was implemented with a 0.18µm CMOS technology. The core area, as shown in Fig. 4, is 877µm x 479 µm, excluding pads. The FFT simulation results with the 20kHz input signal at sampling rate of 100kHz are shown in Fig. 5. The proposed ADC achieves the SNDR of 70.97dB, the SFDR of 80.23dB and the ENOB of 11.49bits. The power consumes 11.16µW at a sampling frequency of 100kHz under supply voltage of 1.8V. And the figure of merit (FoM) is 38.49fJ/conversion-step. The performance is summarized in Table 1.

IV. Conclusion

The 12-bit 100kS/s SAR ADC was designed with both a top-plate sampling technique and a VCM-based switching technique to reduce chip area. To enhance the performance, thermometer decoder DAC and new delay circuits are applied.

Acknowledgment

This research was supported by the Industrial Core Technology Development Program (10049009) funded by the Ministry of Trade, Industry & Energy (MITIE), Korea. And This work was supported by development program of high-speed test equipment (10047617). The CAD tools were supported by IC Design Education Center (IDEC).

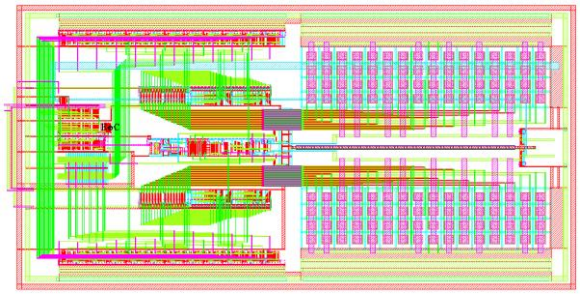

Figure 4. Chip layout (w/o pad)

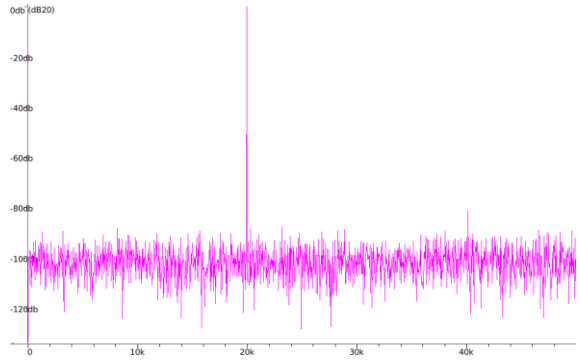

Figure 5. FFT simulation results

TABLE I. Performance Summary

Technology	Magna 0.18µm CMOS
Resolution	12-bit
Power supply	1.8V
Sampling rate	100kHz
FoM	38.79fJ/conv.
SNDR, SFDR	70.97dB, 80.23dB
ENOB	11.49-bit
Layout	877µm x 479µm

References

[1] H. Zhang , Y. Qin , S. Yang and Z. Hong , "Design of an ultra-low power SAR ADC for biomedical applications", Proc. 10th IEEE Int. Conf. Solid-State Integr. Circuit Technol., pp.460 -462 , 2010.

[2] C. Liu, S. Chang, G. Huang and Y. Lin, "A 10-bit 50MS/s SAR ADC with a monotonic capacitor switching procedure", Solid-State Circuits, IEEE Journal of, vol.45, no.4, Apr. 2010.

[3] A. Sanyal and N. Sun , "An energy-efficient low frequency-dependence switchingtechnique for SAR ADCs" , IEEE Trans.Circuit Syst. II, Exp. Briefs , vol. 61 , no. 5 , pp.294 -298 , 2014.

[4] W. Jung, S. Oh, S. Bang, Y. Lee, D. Sylvester and D. Blaauw , "A 3 nW fully integrated energy harvester based on self-oscillating switched-capacitor DC-DC converter" , IEEE ISSCC Dig. Tech. Papers , pp.398 -399.

[5] Y.-Z. Lin , C.-C. Liu , G.-Y. Huang , Y.-T. Shyu and S.-J. Chang , "A 9-bit 150-MS/s 1.53-mW subranged SAR ADC in 90-nm CMOS", IEEE Symp. VLSI Circuits Dig. , pp.243 -244 , 2010.

A Capacitor-less High PSRR LDO with Enhanced Transient Response

Kyung-Chan An, Chan-Kyeong Jung
Department of Electronics and Computer Engineering
Seokyeong University
Seoul, Korea
akcc9491@skuniv.ac.kr

Shin-Il Lim
Department of Electronics and Computer Engineering
Seokyeong University
Seoul, Korea
silim@skuniv.ac.kr

***Abstract*— This paper describes a capacitor-less high PSRR low-dropout (LDO) linear regulator with transition enhancement technique. The proposed LDO adopted the cascode compensation and current buffer compensation techniques within the nested Miller compensation. These compensation techniques not only maintain high stability but also achieve high PSRR with on-chip capacitances. Also, additional voltage-spike detection circuit improves the load transient response. The LDO operates with an input voltage of 3.3V and provides the output voltage of 1.8V. Simulated line and load regulation are 0.26mV/V and 1.8uV/mA, respectively. The power supply rejection ratio (PSRR) is -90dB and –30dB at DC and 1MHz, respectively. The chip area is 240µm x 110µm.**

Keywords- LDO, Regulator, PSRR, Fast Transition, On-Chip System

I. INTRODUCTION

Low-dropout (LDO) regulators are widely used in integrated on-chip power management applications such as handheld devices for clean supply voltage. For on-chip application, an output capacitor-less LDO regulator is needed to reduce printed-circuit-board layout space. However, reduction of the output filtering capacitor will lead to severe output voltage changes during fast load current transients [1]. In addition, to provide a clean voltage source for the noise-sensitive analog/RF blocks, high power supply rejection ratio (PSRR) is required [2]. In this paper, using small internal capacitors, high PSRR capacitor-less LDO with transition enhancement circuit is presented.

II. PROPOSED LDO CIRCUITS

The proposed LDO consists of three gain stages as shown in Figure 1[3]. The first high-gain stage is composed of a differential amplifier. The second gain stage is current mirror amplifier to achieve high PSRR. The third gain stage is power transistor stage. For stable operation, proposed LDO adopted the cascode compensation and current buffer compensation techniques within the nested Miller compensation with small internal capacitors [3]. The cascode compensation is implemented by the source input impedance of MA4 (1/gmA4) and Cc0, and creates the first left half plane zero (LHP zero). Also, the current buffer compensation is implemented by the impedance of transistor MA1 and Cc1, and creates the second left half plane zero [3]. The proposed output capacitor-less LDO guarantees the stability with total internal capacitor of 1.15pF.

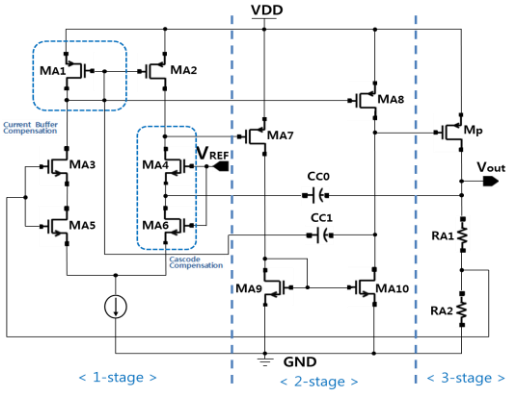

Figure 1. Proposed LDO Circuit

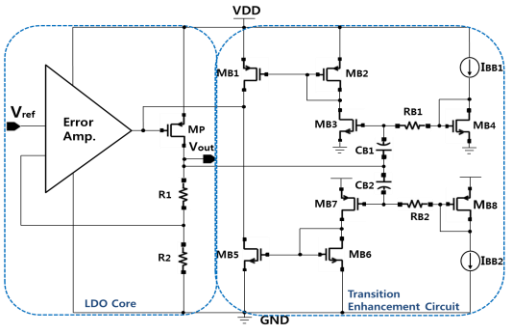

Figure 2. LDO with Transition Enhancement Circuit

Moreover, proposed LDO adopted the transition enhancement circuit as shown in Figure 2 [4]. Resistors (RB1, RB2) and capacitors (CB1, CB2) construct the high-pass filter (HPF) network. Since these HPF network have the function of differentiator, they can detect the voltage spike generated at the output (Vout) when the load current transition occurs. If Vout is lowered due to the increase of load current, the gate voltages of MB3 and MB7 will be lowered. This in turn lowered the gate voltage of driver transistor MP. This lowered gate voltage of MP makes the output voltage of Vout increase. As a result, we can achieve the regulation with this negative feedback loop

in this circuit. Same operation is also achieved in the case of higher Vout. Since the transition enhancement circuit has no high impedance nodes in the loop, it shows higher bandwidth than LDO loop and the fast removal of voltage spike is achieved.

III. SIMULATION RESULTS

The proposed LDO was implemented with the 0.18um CMOS technology. The layout size of the proposed LDO with bandgap reference is 0.026mm2 as shown in Figure 5.

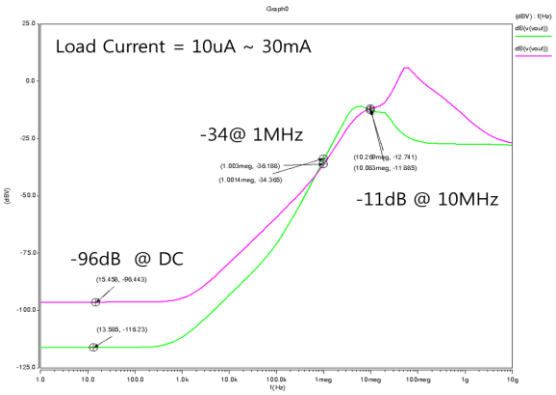

Figure 3. PSR Simulation Results

The PSR simulation results are over -90dB and -34dB at DC and 1MHz with load current 10uA and 30mA, respectively as shown in Figure 3. Figure 4 shows the load transient simulation results as output current has the change of 30mA with rising time of 500ns. With this transition enhancement circuit, undershoot and overshoot of output voltage are reduced from 400mV to 50mV and from 1100mV to 100mV, respectively. The performance summary is presented in Table 1.

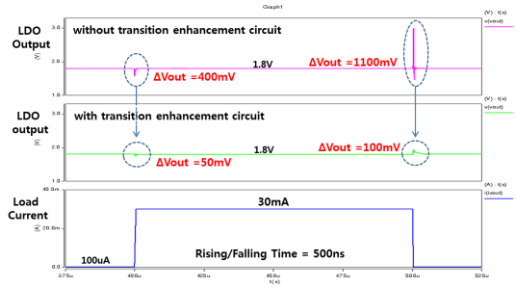

Figure 4. Load Transient Simulation Results

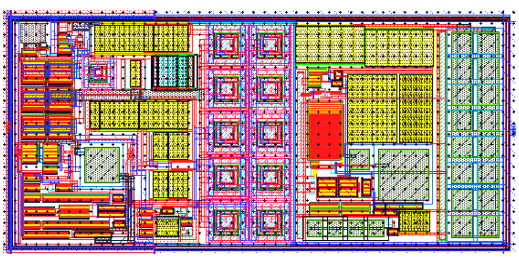

Figure 5. Layout (240μm x 110μm)

TABLE I. PERFORMANCE COMPARISONS

Parameter	[2]	[6]	This Work
$V_{in}(V)/V_{out}(V)$	3.3/1.3	1.5/1.3	3.3/1.8
I_o, Max(mA)	10	50	30
On-Chip Capacitance(pF)	3	NA	5
PSRR(dB)@Hz	-56@DC -10@1MHz	NA	-90dB@DC -30dB@1MHz
Current Consumption(uA)	39	29	40
Chip Area(mm^2)	NA	0.252	0.026

IV. CONCLUSION

The output capacitor-free high PSRR LDO was designed with voltage spike reduction technique. To achieve high PSRR, 2-stage error amplifier is adopted. The stability of LDO guaranteed by using cascode compensation technique and also current buffer compensation technique. To reduce the output voltage change from the load current transition, a spike cancellation circuit is adopted.

ACKNOWLEDGMENT

This research was supported by the Industrial Core Technology Development Program (10049009) funded by the Ministry of Trade, Industry & Energy(MITIE), Korea and also supported by development program of high-speed test equipment (10047617). The CAD tools were supported by IC Design Education Center (IDEC).

REFERENCES

[1] E. N. Y. Ho and P. K. T. Mok, "A capacitor-less CMOS active feedback low-dropout regulator with slew-rate enhancement for portable on-chip application," *IEEE Trans. Circuits and Systems II: Express Briefs*, vol. 57, no. 2, pp. 80-84, Feb. 2010.

[2] J. Day and D. Y. C. Lie, "An output-capacitorless linear regulator for integrate portable power solutions," *Circuits and Systems (MWSCAS), IEEE 54th International midwest Symposium on*, Aug. 2011.

[3] J. W. Kim, S. I. Lim, "An output-capacitorless high PSRR LDO for wide frequency range," *International Conference on Electronics, Information and Communication (ICEIC)*, Jan. 2013.

[4] P. Y. Or and K. N. Leung, "An output-capacitorless low-dropout regulator with direct voltage-spike detection," *IEEE J. Solid-State Circuits*, vol. 45, no. 2, pp. 458-466, Feb. 2010.

[5] Y. I. Kim and S. S. Lee, "A capacitorless LDO regulatior with fast feedback technique and low-quiescent current error amplifier," *IEEE Trans. Circuits and Systems II: Express Briefs*, Vol. 60, no. 6 pp. 326-330, June, 2013.

[6] C. H. Wu and L. R. Chang-Chien, "Full quiescent current enhancement technique for improving transient response on the output-capacitorless low-dropout regulator," *Circuits and Systems (ISCAS) IEEE International Symposium on.* May. 2012.

Thursday, Feb. 25

Session II-1 : (Oral) Convergence I

High Performance of Single Inductor Multiple Output Switching Converter for Cross Regulation Reduction

Jimin Oh, Yilsuk Yang
Power Control Device Research Section
Electronics and Telecommunications Research Institute
Daejeon, Korea
ojmhiin@etri.re.kr

Jung-hee Suk
Mixed Signal Processing Research Section
Electronics and Telecommunications Research Institute
Daejeon, Korea

***Abstract*—this paper demonstrates a high performance of single inductor multiple output (SIMO) converter for cross regulation (CR) reduction. Current compensation and duty control are implemented to reduce CR when output current is varied.**

Keywords-SIMO switching converter, Cross Regulation

I. INTRODUCTION

Single Inductor Multiple Output (SIMO) switching converter has powerful advantages in wearable/IoT devices that these devices have limitations of spaces and one inductor for multiple outputs regulation helps reducing the device size or increasing battery volume. And these battery-powered devices have a restriction on power supply so a high efficiency of converter operation is important factor in wearable/IoT devices.

Many researchers have worked on SIMO converter since 2003. A time-multiplexing (TM) method for multiple outputs is introduced in [1] and a cross regulation is not happened to multiple outputs but a high current operation is limited in DCM mode. PCCM/DCM TM method is also introduced in 2003 [2] and low current driving ability in [1] is overcame by pseudo current operation. For this operation, a size of the freewheel switch in [2] is bigger than one in [1] that cause an increase of conduction loss and drop overall efficiency of converter. To overcome high DC level of the inductor current, in [3], switching frequency is varied to drive high current operation. Lower switching frequency can be implemented to reduce the inductor current and multiple frequency variation helps expectable noise in output filters. Introduced TM methods can reduce the cross regulation but some disadvantages are included; First, switching times are seriously increased when output number increased. TM method works one charge and one discharge for each output regulation so switching loss is increased. Secondly, error amplifier and current compensator are needed to operate TM method that sensitive and complexed techniques are required and bulky analog components may reduce total efficiency. To overcome these, energy sharing (TS) methods are introduced and especially, ordered power distributive control (OPDC) is implemented in [4]. One charge switch is operated and charged current (energy) is distributed to outputs in order that reduces current charge numbers. Furthermore, numbers of analog components (Error amplifier and current compensator) are also reduced to get higher efficiency. In OPDC, one error amplifier and current compensator are used. To reduce all analog components, time-limited power distribution control (TPDC) is introduced in [5]. In the TPDC method, error amplifier and current compensator are totally unnecessary and switching control is implemented with digitally-controlled operation. On the other hand, high current driving or steep current variations are slowly regulated with slow on time control method that makes the cross regulation. A hybrid regulation is introduced with fast current recovery that each output is implemented with linear regulator [6] and one linear regulator is operated in [7].

This paper demonstrates hybrid controls of SIMO switching converter for cross regulation reduction and proper operating algorithm is shown in simulation results.

II. SIMO SWITCHING CONVERTER

A. Overall architecture

Figure 1 shows overall architecture of 3-output SIMO switching converter. An inductor is placed between input voltage (Vi) and outputs (Vo1, Vo2, and Vo3). Five power switches are implemented in the converter that one is for current charging (GN) and another is freewheel switch for conducting same current (GF) and the others are for regulating 3 outputs (G1, G2, and G3). The 3 outputs are compared with 3 reference voltages (ref1, ref2, and ref3) that hysteresis comparators are worked to produce a period of increasing output voltage and error generators are operated to generate a difference between output voltage and reference voltage. A hysteresis comparator composes of two comparator and upper

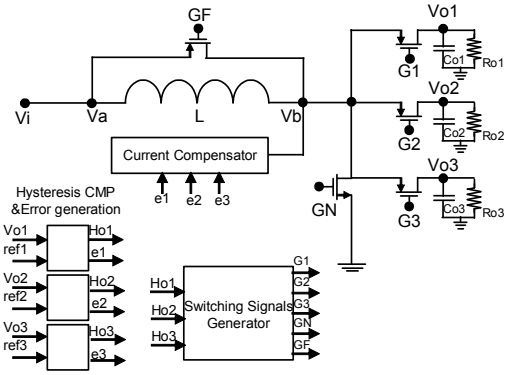

Figure 1. Overall architecture of 3-output SIMO switching converter

/lower windows are determined to be related with output voltage ripple. These signals determine switching on/off timing of power switches and operation of current compensator. Current Compensator is implemented with error signals e1, e2, and e3. This compensator is worked properly when error signals are passed over specific amounts.

B. *Switching Signals Generators*

Switching signals generators include output turn on time controller, voltage rising time controller, and pulse generator. These generators are operated to generate proper switching signals. Figure 2 shows pulse generator for CR reduction. The pulse generator is controlled with duty of switches. A clock, counter and register are composed of the pulse generator. When output 1 duty is decreased with 2Δdt in Fig. 2, other output 2, 3 are increased with 1Δdt. When CR happens, pulse generator and current compensator are operated to reduce CR in outputs.

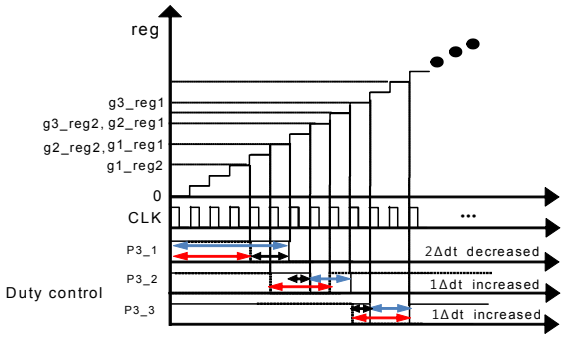

Figure 2. Switching signals generator

III. Simulation and Results

A simulation of SIMO switching converter is operated with PSIM in Fig. 3. In simulation, output 1, 2, and 3 are well regulated to 5, 3.3, and 1.8V. Input voltage is 3.7V and switching frequency is 156 kHz (=20MHz/128). Before 0.0002s, current compensator is not worked so output 3 is not regulated when output 1 current is increasing to 1.5A. An output 1 current is increased to 1.5A at 0.00008s and 0.0003s during 0.00005s. After 0.0002s, current compensator is implemented for reducing output ripple and cross regulation. As results are appeared, output 3 doesn't have CR phenomena when current of output 1 is increasing to 1.5A.

Acknowledgment

This work was supported by Institute for Information & communications Technology Promotion (IITP) grant funded by the Korea government (MSIP) (No.B0186-15-1001, Form factor-free Multi Input and output Power Module Technology for Wearable Devices)

References

[1] D. Ma, W. Ki, and C. Tsui, "Single-Inductor Multiple-Output Switching Conveters With Time-Multiplexing Control in Discontinuous Conduction Mode", IEEE J. of Solid-State Circuits, vol. 38, no. 1, Jan. 2003.

[2] D. Ma, W. Ki, and C. Tsui, "A Pseudo-CCM/DCM SIMO Switching Converter With Freewheel Switching", IEEE J. of Solid-State Circuits, vol. 38, no. 6, June 2003.

[3] X. Jing, P. Mok, M. Lee, "A Wide-Load-Range Constant-Charge-Auto-Hopping Control Single-Inductor-Dual-Output Boost Regulator With Minimized Cross-Regulation", IEEE J. of Solid-State Circuits, vol. 46, no. 10, Oct. 2011.

[4] H. Le, C. Chae, K. Lee, S. Wang, G. Cho, and G. Cho, "A Single-Inductor Switching DC-DC Converter With Five Outputs and Ordered Power-Distributive Control", IEEE J. of Solid-State Circuits, vol. 42, no. 12, Dec. 2007.

[5] J. Kim, D. Kim, and C. Kim, "A Single-Inductor Eight-Channel Output DC-DC Converter With Time-Limited Power Distribution Control and Single Shared Hysteresis Comparator", IEEE Trans. On Circuits and Systems-I:Regular Papers, vol. 60, no. 12, Dec. 2013.

[6] Y. Zhang and D. Ma, "A Fast-Response Hybrid SIMO Power Converter with Adaptive Current Compensation and Minimized Cross-Regulation", IEEE J. of Solid-State Circuits, vol. 49, no. 5, May 2014.

[7] M. Jung, S. Park, J. Bang, D. Park, S. Shin, and G. Cho, "An Error-Based Controlled Single-Inductor 10-Output DC-DC Buck Converter with High Efficiency at Light Load Using Adaptive Pulse Modulation", ISSCC 2015.

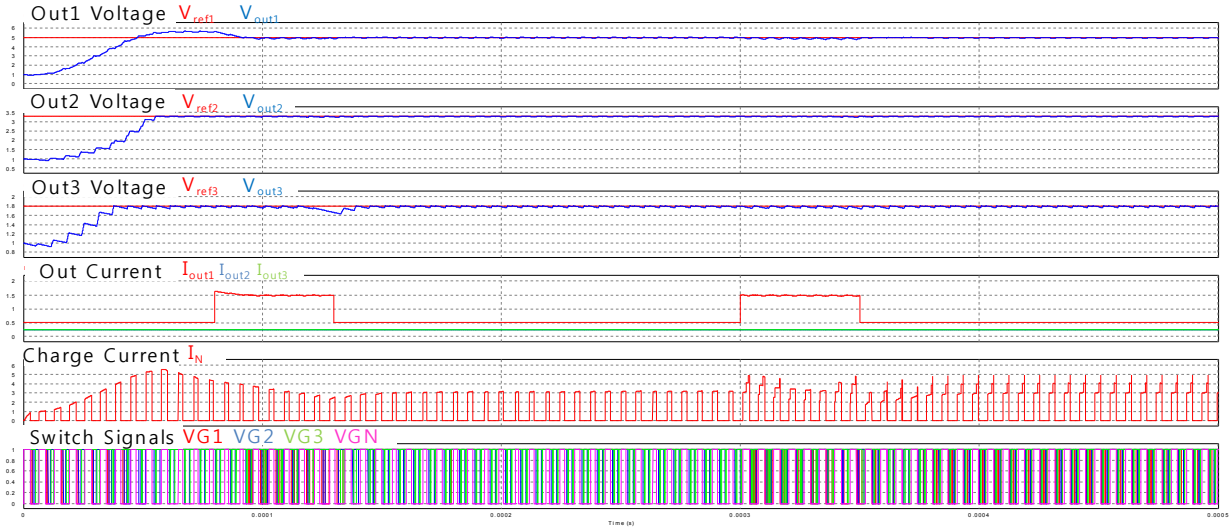

Figure 3. Simulation results

Learning Features through Communication in the Context of Finding an Object

Ryuji Suzuki, Junji Takahashi, and Yoshito Tobe
Department of Integrated Information Technology
Aoyama Gakuin University, Sagamihara, Japan
liuji@rcl-aoyama.jp, takahashi@it.aoyama.ac.jp

***Abstract*—This paper deals with robot's learning both of recognition and communication. We developed an interactive learning system with concentrating a specific situation where a user and a robot cooperatively search an object in real world. We conducted an experiment to evaluate and analyze the process of interactive learning. We confirmed that the entropy is important to analyze the learning and communication process.**

Keywords-component; interactive learning; SOM; Introduction

I. INTRODUCTION

Service robotics has been expected to provide working force to some business which face a manpower shortage such as, an assembly plant, a medical scene, elderly care services, nursery school or expected to support housekeeping. However, the service robots at present are just employed as a demonstration for research or as a performer to attract humans' intention. They are far from practical use.

A service robot at present lacks abilities of object/ environment recognition, conversation understanding, and readiness to new object or event. Although, it is important to study individual ability deeply [1], however, it is also important to study whole abilities simultaneously [2]. According to this thought, our research aims are developing an interactive learning system and analyzing the robot learning and communication process by engineering manner. To do so, we concentrate the specific situation where a user and a robot cooperatively search an object in real world.

II. INTERACTIVE LEARNING

A. A scenario of finding a thing

We designed a human-robot interaction scenario in the context of finding a thing. We assumed the case where a user search an object in a laboratory of university and he/she wants a partner robot to look for it together. But, the robot does not know the visual appearance of the target object. So, the first action the user has to do is to teach the visual appearance of the target object to the partner robot.

This situation also often occurs in daily life between human and human, too. In this case, if a helper is slow learner, the teaching process becomes boring. Even if the helper is replaced with a partner robot, it says the same thing. To prevent the user from boredom, the robot utilizes web knowledge to rapidly estimate and grab the visual appearance of the target object. The robot does image search on web with the keyword given by user and get images. Then, the too much images gathered from the web becomes a problem. To get the image the appearance of which is most similar to the target object, the robot executes cooperative narrow down process. The cooperative narrow down process consists of a categorizing process and a user's selection process. In the selection process, the robot asks to human a simple question based on the results of categorizing result, it is not boring for user. The robot and the user iteratively conduct the narrow down process until the robot recognizes the target appearance.

B. System configuration

The whole picture of interactive learning is shown in Fig. 1. Here, the case, which the user is searching his "key" and the partner robot try to understand the "key" so as to help him to find it, is drawn. The robot system consists of a communication interface with user, a module conducting image search on web, a module categorizing gathered images, and a module asking user which class is nearest to the target object.

C. Objects Classification by Self-Organizing Map

We utilize Self-Organizing Map (SOM) for robot's categorizing process. The SOM is a kind of neural networks of unsupervised classification and has an input layer and an output layer. The SOM automatically categorizes inputted entities based on the similarity of their feature vectors and outputs a Map representing categorized classes. The orthodox SOM algorithm is described as follows,

1. Initialize the MAP with random numbers,
2. Select the closest unit to the input vector,
3. Update the closest and neighbors by adding input vector,
4. Iterate 2 and 3 for all input vectors,
5. Divide the MAP into desired number of classes.

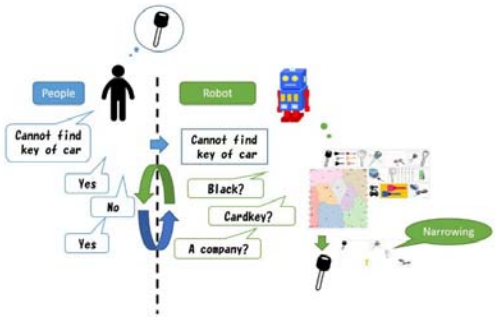

Figure 1. System configuration of Interactive Learning

This research is partially supported by Grant-in-Aid for Scientific Research (C): 25330113

D. *Cooperative narrow down process*

This process is done by the user selecting a likely class. At the class selection, the robot preliminarily nominates one image representing its class, which is a nearest to the center of the class. Therefore, the user just select one likely image from couple of images. This interaction process is not boring for the user, and also brings in a sense of togetherness for the user. Through this interactive process, the robot can approach to the recognition of correct appearance of the target object, but also get understanding of sense of user's worth by analyzing this process afterward.

III. PILOT EXPERIMENT

A. *Experimental setup*

We conducted pilot experiments to evaluate our developed interactive learning system and analyze the cooperative narrow down process. We assumed a situation that the user was looking for his plushie of character. He asked his partner robot to look for the plushie but he forgot the name. So, the robot conducted image search with keyword of "character." Fig. 2 shows the search results including 80 images. In the Ex. I and II, we selected red marked character and blue marked character as a target, respectively. In the Ex. I, the target has several images of different angles, but in the Ex. II, there is one image. We set the number of classes to divide as 4 in all experiment.

B. *Analyze method*

We analyzed the cooperative narrow down process by using a ratio of within-class variance and between-class variance for checking SOM categorization, and an entropy for measure the quantity of information on user selection. Let n, $\boldsymbol{x}$, $\boldsymbol{m}_i$, $\boldsymbol{m}$, c, χ_i denote number of input vectors, an input vector, the center of class i, the center of all vectors, number of classes, a class i, the within-class variance and between-class variance and their ratio are given as follows,

Figure 2. The examples of gathered images by web search: The red marked characte is a target of Ex. I and the blue marked character is a target of Ex. II (These pictures are taken from [3])

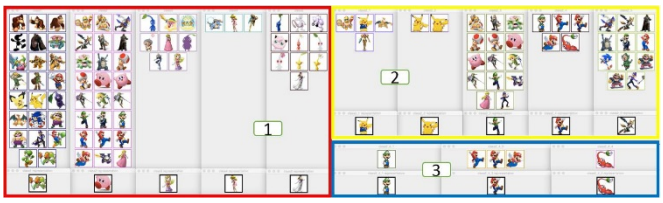

Figure 3. The transition of cooperative narrow down process

TABLE I. THE RESULTS OF EXPERIMENT I AND II

Number of trial	Number of member		Representative ID		Information quantity: $I(T)$		J_σ	
	I	II	I	II	I	II	I	II
0	80	80	-	-	4.00	6.32	-	-
1	39	63	20	2	3.28	5.97	2.41	2.85
2	5	32	37	68	0.73	5.00	1.71	4.52
3	3	10	37	16	0.00	3.32	0.23	0.77
4	-	5	-	8	-	2.32	-	0.21
5	-	4	-	69	-	2.00	-	0.07
6	-	1	-	8	-	0.00	-	0.04

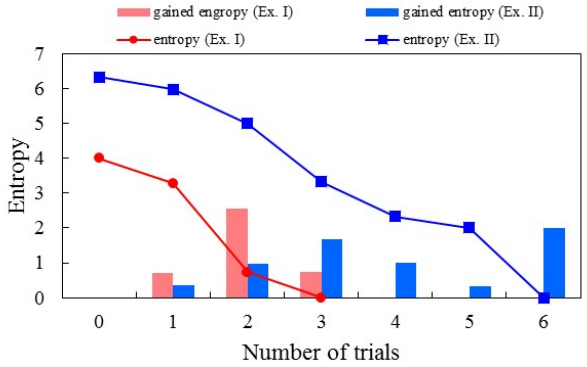

Figure 4. Transition of entropies during the experiments

$$\sigma_w^2 = \frac{1}{n}\sum_{i=1}^{c}\sum_{\boldsymbol{x}\in\chi_i}(\boldsymbol{x}-\boldsymbol{m}_i)^t(\boldsymbol{x}-\boldsymbol{m}_i)\,, \tag{1}$$

$$\sigma_B^2 = \frac{1}{n}\sum_{i=1}^{c}(\boldsymbol{m}_i-\boldsymbol{m})^t(\boldsymbol{m}_i-\boldsymbol{m})\,, \tag{2}$$

$$J_\sigma = \frac{\sigma_B^2}{\sigma_B^2}\,. \tag{3}$$

The probability for hitting target from n images with random selection is given as $P(T)=s/m$, where s is number of target images. Using this probability we can define the entropy as,

$$I(T) = -\log P(T)\,. \tag{4}$$

C. *Experimental results*

Fig. 3 shows the transition of cooperative narrow down process. Table I and Fig. 4 show the analysis results. It is observed that Ex. I reached target image faster than Ex. II. This is because the initial entropy of Ex. I is smaller than that of Ex. II. However, the average entropy given through the selection process (gradient of the graphs) is similar between the two experiments.

IV. SUMMARY

We developed and evaluated an interactive learning system including SOM based categorization process and cooperative narrow down process. One of future works is to declare the relation of entropy and the system parameters.

REFERENCES

[1] K. Lai, et al., "Sparse Distance Learning for Object Recognition Combining RGB and Depth Information," Proc. of ICRA, 2011

[2] J. Takahashi, et al., "Concept Sharing between Different Concept Representation Robots," Proc. IEEE Int. Symp. on System Integration, Tokyo, Japan, pp.118-123, 2009.

[3] Nintendo Co., Ltd. http://www.nintendo.co.jp/ .

Solar Energy Super Capacitor Hybrid Power Source Using in The Patrol Robot

Yuan Guangjun
School of Electric and Information Engineering
BeiHua University
Jilin, China
e-mail: dick780818@163.com

Zhou Zhenxiong
School of Electric and Information Engineering
BeiHua University
Jilin, China
e-mail: 164208749@qq.com

Sun Jiyuan
School of Electric and Information Engineering
BeiHua University
Jilin, China
e-mail: dick780818@163.com

Shi Lichun
School of Electric and Information Engineering
BeiHua University
Jilin, China
e-mail: dick780818@163.com

***Abstract*—the patrol robot needs pollution free and efficient power source. The power source, introduced in this paper, can solve this problem. The power source adopted solar battery and super capacitors as the main module. Super capacitors were divided into two groups, in order to ensured that a group of capacitors charging and another group of capacitors power supply. The voltage of super capacitors needed to be balanced in case the super capacitors were damaged. In order to ensured the quality of the output power of the power source, DC-DC converter was adopted. The experimental results validate that the power take-off of robot is enhanced, and the voltage of super capacitors is balanced, and the power requirement from the power system is reduced.**

Keywords- solar energy, super capacitor, power source, hybrid

I. INTRODUCTION

With the development of social economy, the urban scale expands increasingly. The demand of the security automation of urban is increased by people. The patrol robot is integrated with environment perception, route planning, dynamic decision-making, behavior control and alarm device, and is adopted to regular patrol, fixed-point monitoring or mobile patrol which is a feasible solution.

The power of most patrol robot is supplied by the battery which has limitation of number of charge time, and has water pollution, as well. The heavy current can not be provided by the battery either which is badly needed by the patrol robot when it is started, and accelerated. The battery is charged by the power system that will cause heavier load of the power system. Solar energy, which is a kind of energy that clean and free, can be collected by the power source which is introduced in this paper, and can be stored by the super capacitor. Super capacitor can be charged ten thousands of times which more than the battery. The heavier current can be provided by the super capacitor than the battery which makes patrol robot get better grade ability and accelerating ability. In this paper, the energy is stored in the super capacitor which is coming from solar energy and power system. The performance of the patrol robot can be improved by the solar energy-super capacitor hybrid power source. The power source will be introduced, as follows.

II. THE POWER SOURCE AND THE BALANCE BETWEEN SUPER CAPACITORS

A. *The power source*

The power source is consisted of solar battery, super capacitor, control system and energy regulator, shown as Fig.1. The super capacitors are divided to two groups, capacitor group one and capacitor group two, one group is working at charge state as other is working at discharge state[1]. The solar energy can not meet all the power requirement of the patrol robot. The power system is needed by the power source, too. Therefore, the power

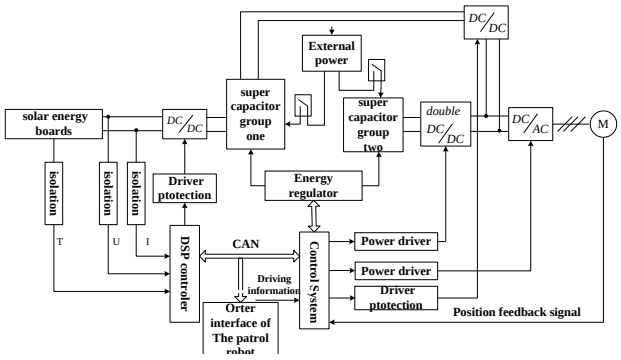

Fig 1. Structure of system

source is charged by both solar battery and power system. TMS320LF2812A is indexed in the control system. The main tasks of control system is ensure the quality of power coming from solar battery through a DC-DC converter, and control the output power through two DC-DC converter, and exchange the information with the driver,

The twelfth five scientific and technological research project of the education department of Jilin province(2014206).
Science and technology planning project of Jilin City(2015131009)
Science and Technology Development Plan project of Jilin Province (20150519023JH)

and keep balance between super capacitors, and ensure the quality of the output power through the energy regulator. The control system need detect the current power of the motor, and match the power with the requirement of the drive, and then give the order to the system

B. Power Supply

The solution introduced in this paper remedy the shortage of the solution three, and solves the problem of balance of super capacitors. The circuit of the solution is shown as Fig.2.

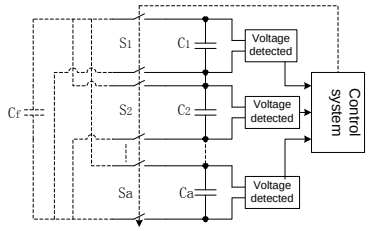

Fig 2. The structure of the balance of the super capacitors

Using super capacitor to provide power to the patrol robot, the enough power can be provided which is meet the requirement of the patrol robot, but the difference of the character of each single super capacitor makes the difference of the voltage of each single super capacitor which can reduce the life span of super capacitors, and depress the efficiency of the system. Therefore, the necessary measure must be taken to make the voltage of super capacitor close to other's as possible when the super capacitor working at discharge state.

Nowadays, there are three efficiency and typical solutions among all the solutions which can keep the balance between the super capacitors. Solution one is connect a divider resistance on the super capacitor. Solution two is connect a conductor on the super capacitor. Solution three is index a third-party capacitor. Solution one and solution two are the way that waste energy which consume the extra energy makes the voltage of super capacitor drops, in order to keep the balance of the super capacitors. Solution three is the most efficiency solution in the three solutions, and it is a workable solution in theory. However, there is a great disfigurement when the solution is reacted. The choice of the third-party capacitor is a big problem. If the value of the third-party is small, the influence of the voltage of super capacitor is small, too. If the value of the third-party capacitor is big, the charge time will be too long. The workable of the solution three is denied.

The C1 to Ca are super capacitors. A store super capacitor is indexed in the system which is connected to each super capacitor in the system through MOSFETs, and its value must be close to the value of each super capacitor. After super capacitors working at discharge state for a little while, the change of voltage of each super capacitor can be detected by the energy regulator, and the extra energy is transmitted from super capacitor to the store super capacitor by the energy regulator, and the energy stored in the store super capacitor can be supplied to the load of patrol robot.

III. THE PROCEDURE OF POWER SOURCE AND BALANCE OF SUPER CAPACITORS

A. The procedure of power source

The power requirement coming from driver is expressed by the Pd. The power of super capacitor group one and super capacitor group two are expressed by the Pb1 and Pb2. The velocity of patrol robot is expressed by the Vche.

The super capacitors are divided into two groups. Super capacitor group one is charged by solar battery and power system. Super capacitor group two is charged by power system. Energy is supplied to the motor through DC-DC converter. The information of voltage and current can be detected by the control system, and the requirement of driver can be detected by control system, too. Therefore, the power requirement can be calculated out. After detected the energy in the super capacitors, and matched it with the power requirement, the decision will be made by the control system that the super capacitors are working at charge state or discharge state.

B. Balance of super source

After charge state, the voltage of super capacitors is detected by the energy regulator, and the super capacitor with lowest voltage will be found. Others super capacitors will be discharged to the store super capacitor till there voltages are same as the lowest one.

C. Super capacitors monitor system

Super capacitors monitor system is set up in the monitor room. Super capacitors monitor system can display the state of the state of each super capacitor.

IV. CONCLUSION

A new type of power source of patrol robot is introduced in this paper which consisted by super capacitor and solar energy mainly. A problem of balance between super capacitors is solved in this paper that makes the quality of output power of the power source introduce in this paper is good. According the detected data, shown as Fig.3, the power source can work well in the patrol robot.

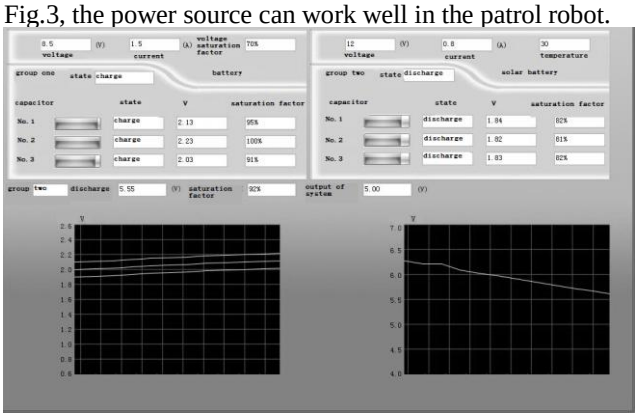

Fig 3. Detect software on the computer

REFERENCES

[1] Kondon J, Ishii I, and Yamaguchi H, "Electrical energy storage systems for energy networks, " Energy Conversion and Management, vol 41, pp. 1863-1874, 2002.

Traffic Type-Aware Power Save Mode Control for Delay-Sensitive Services in IEEE 802.11s based Wireless Mesh Networks

Eun Jung, Lee
School of Electrical Engineering
KAIST
Daejeon, Rep. of Korea
freakone@kaist.ac.kr

Young Min, Kim
Fixed & Mobile Communication
Infrastructure Research Department
ETRI
Daejeon, Rep. of Korea
injesus@etri.re.kr

Hong-Shik, Park
School of Electrical Engineering
KAIST
Daejeon, Rep. of Korea
park1507@kaist.ac.kr

***Abstract*—Previous works on the power save mode control in wireless mesh networks only focused on energy saving without any consideration for delay performance. To overcome this limitation, we propose a new power save mode control (TAPSM) scheme by considering a traffic type to reduce the energy consumption of each wireless mesh station (STA) while supporting delay-sensitive services in IEEE 802.11s based wireless mesh networks.**

***Keywords*—Power save mode control, wireless mesh network, IEEE 802.11s, delay-sensitive services**

I. Introduction

Recently, energy saving, as well as quality of service (QoS), has become a critical issue in wireless mesh networks (WMNs) [1]. As an effort to reduce this energy consumption, the existing IEEE 802.11s standardization defines the power save mode as an option [2]. However, the standardization does not deal with the control policy for the power save mode. This absence has a great challenge for energy-efficient wireless mesh network operators significantly.

To control the power save mode, only few research [3] has studied in recent years. The authors in [3] proposed the Energy Aware Power Save Mode (EAPSM) algorithm that considered the possible energy consumption and the current transmission status of the wireless mesh station (STA). Although the EAPSM algorithm can reduce the energy consumption successfully, it lacks the consideration for the delay performance. When a customer uses the delay-sensitive service, he or she may suffer from the severe degradation of the delay performance.

To overcome this limitation, we newly propose a traffic type-aware power save mode control (TAPSM) algorithm for the wireless mesh networks to reduce the energy consumption while assuring the delay performance of the delay-sensitive services. For achieving this goal, the TAPSM considers the traffic type (i.e., real-time traffic and non-real-time traffic) when controlling the power save mode.

II. Related work

In this section, we explain the previous works on the power save mode control for IEEE 802.11s based wireless mesh networks.

A. Power save mode in IEEE 802.11s

According to IEEE 802.11s in [2], a wireless mesh STA can be have two different power states: $Awake$ state and $Doze$ state. When the mesh STA is in the $Awake$ state, it can transmit or receive frames and operate at its maximum power. Otherwise, it can not do that, and operate very low power. For energy saving, the wireless mesh STA can transit these two states according to the power mode. Basically, a mesh STA can have its power mode for each peering among the below three power modes.

- $Active$ mode - The wireless mesh STA shall be in $Awake$ state all the time. During this mode, it consumes its maximum power all the time.
- $LightSleep$ mode for the power save mode (optional) - The wireless mesh STA shall listen to all the Beacon frames from its peer mesh STA. It wakes up every delivery traffic indication message ($DTIM$) interval and sends data frames to its peer mesh STA during the wake-up window size. After finishing such transmission, the mesh STA falls into $Doze$ state.
- $DeepSleep$ mode for the power save mode (optional) - The basic operation of this mode is same as that of $LightSleep$ mode. The only different thing is that the wireless mesh STA may choose not to listen to the Beacons from its peer mesh STA.

Through the power save mode, the wireless mesh STA can reduce the energy consumption more efficiently. However, the existing IEEE 802.11s only defined the power save mode. Even though it announced that the power save mode control is out-of-scope.

B. Power save mode control in IEEE 802.11s based WMNs

After two years later, *Prakash et. al* in [3] proposed the energy aware power save mode (EAPSM) algorithm that can control the previously defined power save mode in [2]. In particular, the EAPSM algorithm considered the energy consumption and its constraint, and the transmission mode of the wireless mesh STA. Although it was quite effective to reduce the energy consumption, it was hard to support

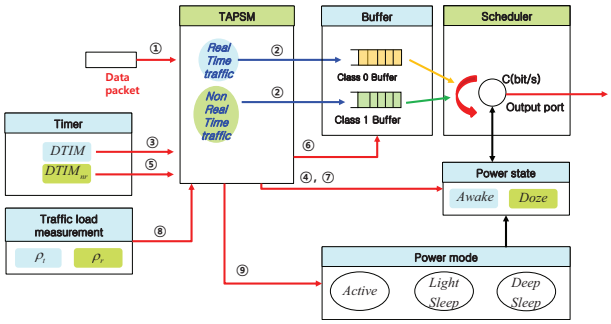

Fig. 1. Operation of the TAPSM scheme in a wireless mesh STA.

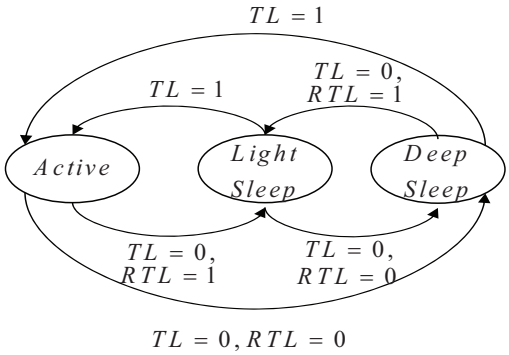

Fig. 2. State transition diagram of the power mode in a wireless mesh STA.

the delay-sensitive services for the same reason of the IEEE 802.11s.

III. Proposed TAPSM Algorithm

In this section, we propose a traffic type-aware power save mode control (TAPSM) algorithm in order to reduce the energy consumption while supporting the delay-sensitive services for IEEE 802.11s based wireless mesh networks.

The fundamental system model of TAPSM is same as that of the IEEE 802.11s. Based on the system model, the TAPSM has one more timer called $DTIM_{nr}$ which is set to the several times of $DTIM$ interval. To consider the delay performance, the TAPSM uses two thresholds: T_{th} for total traffic load and R_{th} for real-time traffic load ($0 \leq R_{th} \leq T_{th} \leq 1$). Furthermore, two buffers exist: class 0 buffer for real-time traffic and class 1 buffer for non-real-time traffic.

Using these characteristics, Fig. 1 shows the basic operation of the TAPSM algorithm. When a data packet arrives at MAC layer in the wireless mesh STA, which is in $Doze$ state (①), the STA checks the type of service (ToS) field of packet's IP header. According to the ToS value, the packet is classified into two classes: class 0 for real-time traffic, and class 1 for non-real-time traffic. After that, each packet is enqueued at its belonging class buffer (②).

When the $DITM$ timer expires (③), the STA changes its state into $Awake$ state (④). After that, it additionally checks whether the $DITM_{nr}$ timer expires or not (⑤). If this timer also expires, the STA dequeues and transmits buffered packets in all buffers (⑥). Otherwise, it only does do that in class 0 buffer (⑥). After finishing the transmission of the buffered packets, the STA changes its state into $Doze$ state (⑦). Then, the STA obtains the total traffic load (ρ_t) and the real-time traffic load (ρ_r) from Traffic load measurement module (⑧). Using these values, the STA calculates TL and RTL values according to E.q. (1) and (2) to control the power mode more easily.

$$TL = \begin{cases} 0, & \text{if } \rho_t \leq T_{th} \\ 1, & \text{otherwise.} \end{cases} \quad (1)$$

$$RTL = \begin{cases} 0, & \text{if } \rho_r \leq R_{th} \\ 1, & \text{otherwise.} \end{cases} \quad (2)$$

Based on the calculated results, the mesh STA control the power mode according to its condition (⑨). Fig. 2 shows the sate diagram of the power mode in the mesh STA. According to this figure, the mesh STA changes its power mode into $Active$ mode when TL equals to 1. Otherwise, it changes its power mode according to RTL value. The main reason for such control is to consider the delay performance of the delay-sensitive services.

IV. Conclusion

In this paper, we proposed the traffic type-aware power save mode management (TAPSM) scheme. Through the TAPSM, mesh network operators can easily saving energy in the mesh STA while accommodating the delay-sensitive services more efficiently in the wireless mesh networks.

Acknowledgment

This work was partly supported by the ICT R&D program of MSIP/IITP, Republic of Korea [B0101-15-1270, Research on Communication Technology using Bio-inspired Algorithm].

References

[1] D. Benyamina, et. al., "Wireless Mesh Networks Design – A Survey," *IEEE Comm. Surv. & Tuto.*, vol. 14, no. 2, 2012.

[2] IEEE, "Draft amendment: ESS mesh networking," IEEE 802.11s Draft 12.00, June 2011.

[3] S. P. S. Prakash, T. N. Nagabhushan, and K. Krinkin, "Energy Aware Power Save Mode Management in Wireless Mesh Networks," Proceeding of *the 14th Conference of Open Innovations Association (FRUCT) 2013*, pp. 122-131, 11-15 Nov. 2013.

Smart Pet Care System based on IoT

Gibert M. Tumibay
College of Computer Studies
Angeles University Foundation (AUF)
Angeles City, Philippines
tumibay.gibo@auf.edu.ph

Seungcheon Kim
Dept. of Information and Communication Eng.
Hansung University, Seoul, Korea
kimsc@hansung.ac.kr

Kyutae Lee
Dept. of Information and Communication Eng.
Kongju National University, Korea
ktlee@kongju.ac.kr

Sungcheol Yu
Domestic Service Team
LG Hitachi LTD, Seoul, Korea
scyu@lghitachi.co.kr

***Abstract*— This paper introduces a smart pet care system that is working in an environment of Internet of Things (IoT). Typical services of the proposed smart pet care system are: Remote feeding, remote controlled automatic defecation, CCTV service and Smart phone APP that can provide the control information of the above services.**

Keywords; smart, pet care, IoT.

I. INTRODUCTION

Recently the interest on the pet-care services is growing as the number of single household increases. The pet care market is also related to the smart technologies such as Internet of Things (IoT) and smart phones, which can provide the convenient services with various aspects for pet owners. However, the current pet care products are restricted in the simple functioning products such as the automatic feeder with timer and monitoring camera.

In order to provide the smart pet care services for pets and pet owners, we need to think about how to check the status of pets with owner's smart phone and provide the proper services for pets such as replacement of defecation pad and feeding bowl recharging. From the perspective of owners, the statistics of feeding and replacement of defecation pad are also one of concerns.

In this paper, we have proposed a new pet care system that can feed the pets while the owners are absent at their homes and can monitor their movement and status and also control its defecation pad through owner's smart phones. The proposed system is distinctive from others in terms of that the proposed system is based on IoT technologies, which uses lots of sensor and wireless communications. Therefore, the proposed system is not restricted in the space and time only if the wireless communications are provided.

II. THE ARCHITECTURE OF SMART PET CARE SYSTEM

The proposed smart pet care system is depicted in fig. 1. As you can see in the figure, the major parts of the smart pet care system is composed of 5 components.

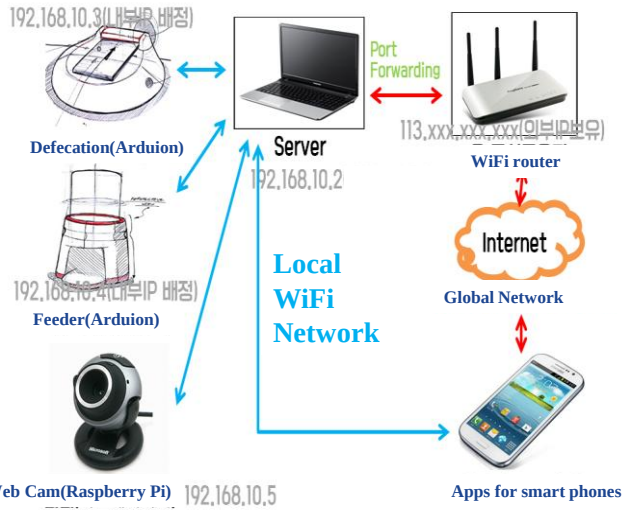

Figure 1. The architecture of Smart pet care system

1. Automatic Feeder

The basic functions of automatic feeder is mostly the same with the product that we can find in the market. The difference laid in the communication ability and sensing ability.

Basically it can act on time basis with timer set. Users can set the regular interval of feeding time for their pets. In addition, users can set the amount of food based on the weight of the amount of onetime food. Every control for setting could be done through user's smart phones. The automatic feeder has been implemented with Arduino MCU. The basic process of jobs in automatic feeder is described in Fig. 2.

2. Automatic Pooping Pad

Recently most of pets are trained to poop in the dedicated area at home. However, while the pet owners are away from their home for a while, the rested area for their pets are hard to be cleaned and get massed easily. For the convenience of the

pet owners, automatic pooping pad has been devised based on IoT technology.

The proposed automatic pooping pad can detect pet's defecation with a help of sensors: temperature sensor, humidity sensor and ultrasonic sensor. Ultrasonic sensor is mostly used to detect the presence of pets on the defecation pad. The automatic pooping pad can be connected to smart phone. It can be controlled and monitored via smart phone. A database has been built to see the temperature and humidity in real time. Fig. 3 shows the operational process of automatic pooping pad.

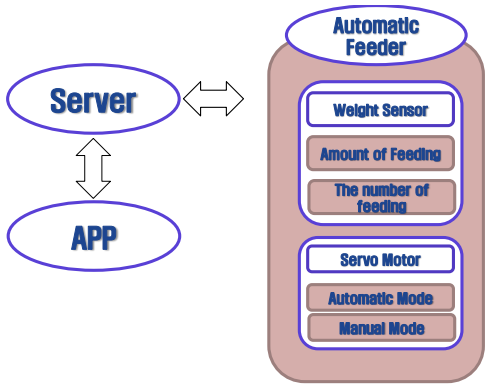

Figure 2 Automatic Feeder

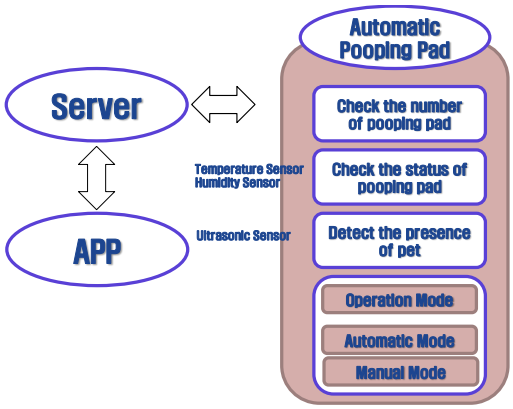

Figure 3 Automatic Pooping Pad

3. Camera with Raspberry Pi

A camera system is added in the smart pet care system. The proposed camera system is specially implemented with Raspberry Pi server. The distinctive feature of the camera system is that it is focused on the pet. Its major interest is to monitor the movement of pet. Therefore, it is usually installed inside of the automatic feeder and automatic pooping pad.

4. Mobile Web and APP for smart phone

The history of feeding or replacement of pooping pad is recorded in the home server and can be displayed through mobile web and APP for smart phone. For these jobs, smart phone APPs are implemented. And the home server is equipped with the functionality of web service.

III. Implementation of the System

The proposed smart pet care system has been implemented based on the architecture shown in Fig. 1. The operational flow between devices in smart pet care system is described in Fig. 4.

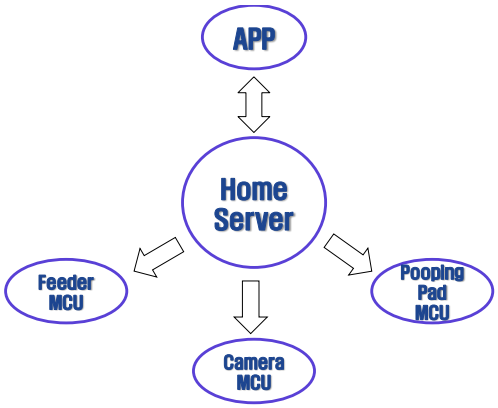

Figure 4 Operational Flow between devices

Fig. 5 shows the implemented automatic feeder and automatic pooping pad. The case of each device were made by using 3D printer.

Figure 5 Smart pet care system

IV. Conclusions

This paper introduces the novel smart pet care system based on IoT technology. The functionalities of smart pet care system will be added with the various new devices.

References

[1] Yongsik Jang, "Step by stpe Android programing", Infinite Books, 2014
[2] Jaesang Lee, "Raspberry Pi white paper: 20 utilization" BJ public, 2013
[3] 3D printer, "Edison Plus User manual", ROKT Inc, 2013.

Thursday, Feb. 25

Session II-2 : (Oral) Communication and Ubiquitous II

Performance Analysis and Implementation of A PMIPv6-based Partially Distributed Mobility Management

Ye Wang
Dept. of Electronic and Information Engineering
Lishui University
Lishui City, China
wychina_2007@hotmail.com

Jang-Geun Ki*, Kyu-Tae Lee
Dept. Information & Communication Engineering
Kongju National University
Cheonan, Korea
kjg@kongju.ac.kr, ktlee@kongju.ac.kr

***Abstract*—This paper provides the implementation mechanism of the pmipv6-based partially distributed mobility management (DMM) and performs extensive simulations under various traffic environments for verification and evaluation of the proposed scheme. The simulation results indicated that Mobility Anchor and Access Router (MAAR) can distribute and manage all IP data packet flow between corresponding node (CN) and mobile node (MN). Therefore, the implementation and performance analysis of proposed mechanism are essential to understand the fundamental features of DMM, which includes method of detecting MN and managing MN's location.**

Keywords-component; DMM; implementation; performance

I. INTRODUCTION

With the increasing volumes of mobile data traffics and massive increase in the number of interconnected devices, especially on demand for "imperceptible latency" with the Tactile internet, and demand millisecond-level latency and nearly 100% reliability with Internet of Thing service [1]. However, conventional IP mobility solutions have adopted a centralized approach that represents a single point of failure, poses scalability issues, and in general, leads to suboptimal routing paths between mobile node and corresponding node [2].

To solve these problems, distributed mobility management (DMM) has recently emerged as a new paradigm to design a flat and flexible mobility architecture, allowing traffic to be broken out locally closer to the edge (i.e., offloading the network core) and exploiting the use of different gateways for traffic with different connectivity and mobility requirements. Apparently, DMM approach is suitable candidates for mobility management in future 5G very dense deployments [3].

A number of the implementation and performance analysis on DMM network have been proposed in the literature. For the implementation issue, Bernardos etc. [4] proposed a method by querying the Central Mobility Database (CMD) to acquire the MN's location information. Yuhong Li etc. [5] introduced AAA server and Software Defined Networking (SDN) to manage MN's location information. Kim etc. [6] presented the multicast and point-to-point searching scheme to get MN's location. However, those proposed mechanism did not give the specific implementation mechanism and feasibility analysis. For the performance analysis issue, Li Yi etc. [7-8] and Kim etc. [9] showed signal control and data transmission cost is lower than PMIPv6 protocol. However, those performances are all cost-based analysis, there are short of the comprehensive and systematic study.

In this paper, the pmipv6-based partially distributed mobility management solution is suggested and the simulator for model verification and performance evaluation of the suggested mechanism is implemented and extensive simulations under various traffic environments are performed.

II. PERFORMANCE ANALYSIS AND DISCUSSION

A. *Distributed Concept in Partially DMM Evaluation*

The partially DMM simulation network architecture is shown in Fig. 1, where three Mobility Anchor and Access Routers (MAARs) are adopted and distance is 2km between each MAARs. The MN will start 2km away from MAAR1 for testing MAAR's detecting procedure and come back from MAAR3 to MAAR1. In this basic DMM performance, the TCP data packet have been choose for evaluating the distributed concept in OPNET.

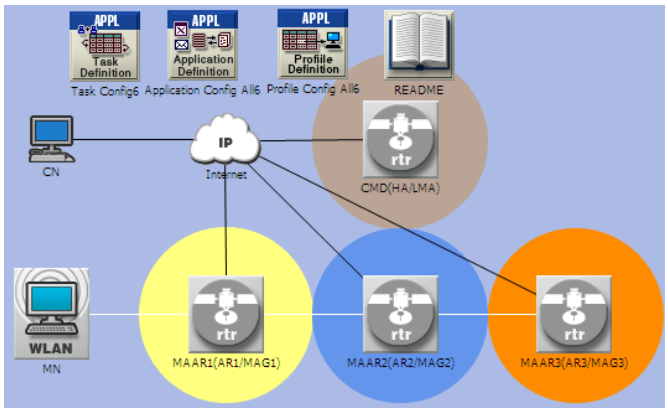

Fig. 1. Partially DMM/MIPv6/PMIPv6 simulation network architecture.

As seen in Fig. 2, CN sends TCP data packets to MN. Once MN moves out its home domain (e.g., attaches MAAR2), the data packets from CN to MN are intercepted by MAAR1. Then MAAR1 sends this tunneled traffic to MAAR2, which will receive this tunneled traffic and then decapsulate this data packet. While MN continues to move to MAAR3, after

distributed-Proxy binding update (d-PBU)/distributed-proxy binding acknowledgment (d-PBA) signaling exchange, MAAR1 intercepts this data packet and then tunnels it to MAAR3, which can receive this tunneled data packet and decapsulate it. It can be seen in Fig. 2 that MAAR1 intercepted all data packets for MN and then sent those tunneled segmented data packets to MAAR2 and MAAR3.

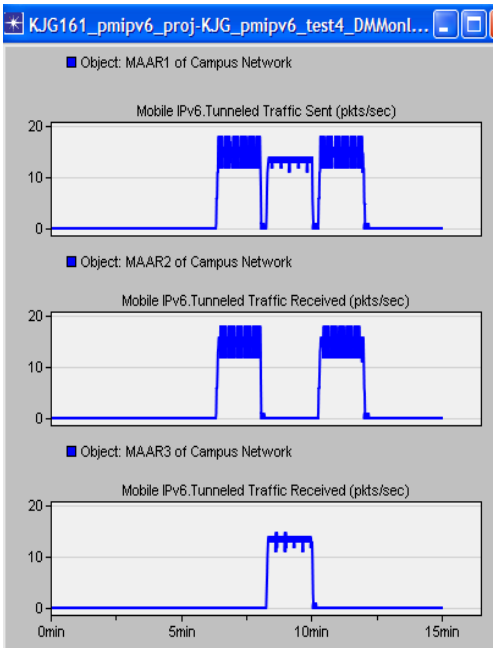

Fig. 2. TCP tunneled data traffic sent/received.

B. Comparative Study of MIPv6, PMIPv6 and DMM

One of the important motivations of DMM mechanism is for solving the increasing volumes of mobile data traffics. In order to better understand DMM performance with the increasing data traffic, the data traffic generated rate is changed from 0.01packet/sec to 20packets/sec. Meanwhile, the mobile node is moving at 60 km/hr with 1 and 10 nodes around MAAR. The performance metric with Packet Delivery Ratio (PDR) is adopted, which is ratio between the number of packets delivered to the receiver and the number of packets sent by the source. With the increasing volumes of data traffics, the Figs. 3-4 show the similar trend of PDR in DMM/PMIPv6/MIPv6.

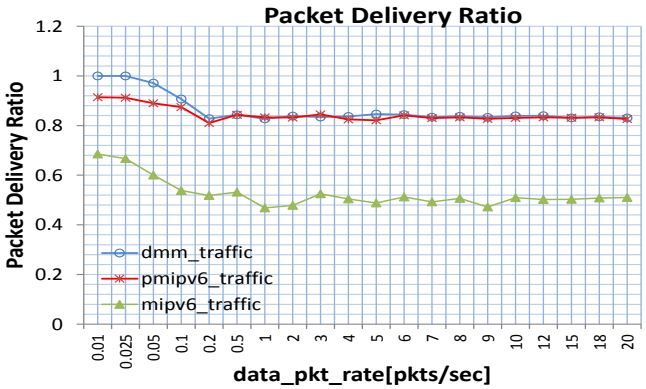

Fig. 3. Effect of data traffics on packet delivery ratio at 1 node.

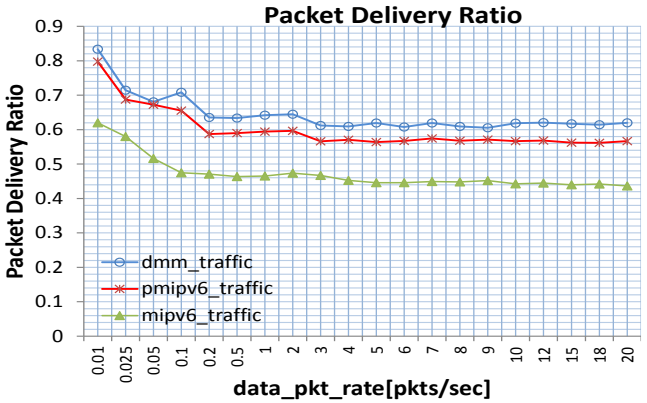

Fig. 4. Effect of data traffics on packet delivery ratio at 10 nodes.

However, with the mobile nodes are increasing, the PDR also decreased, but DMM is performing better than PMIPv6/MIPv6 in PDR. Because extra control traffic caused less available bandwidth for data traffic and increased chances of packet loss due to congestion. It is revealed that DMM mechanism is well suited for higher density network with much more data traffics.

III. CONCLUSIONS

In this paper, as performance results, MAARs in DMM can distribute and manage all IP data packet flow between CN and MN, which is based on where IP data packet flow is established. According to analyzing on the simulation performance with TCP tunneled data packet and PDR, it is concluded that the new modification concept and developed simulation models are logically correct and very useful for studying DMM mechanism.

REFERENCES

[1] IMT-2020 5G Vision and Requirements，IMT-2020 (5G) Promotion Group, White Paper, 2014,1-20

[2] C. Perkins, Ed., D. Johnson and J. Arkko, “Mobility Support in IPv6”, IETF, RFC 6275, 2011.

[3] Fabio Giust, Luca Cominardi and Carlos J. Bernardos, “Distributed Mobility Management for Future 5G Networks: Overview and Analysis of Existing Approaches”. IEEE Communication Magazine, 2015, 53(1): 142-149

[4] CJ. Bernardos, F. Giust and A. de la Oliva, “A PMIPv6-based solution for Distributed Mobility management”. IETF DMM Working Group, draft-bernardos-dmm-pmip-03 (work in progress), 2014

[5] Yuhong Li, Haimeng Wang, Ming Liu and Bofan Zhang, “Software defined networking for Distributed Mobility Management”. IEEE Globecom Workshops, 2013, 885-889

[6] J. Kim, S. Koh, H. Jung and Y. Han, “Use of Proxy Mobile IPv6 for Distributed Mobility Control”. IETF draft-jikim-dmm-pmip-00 (work in progress), 2012

[7] Li Yi, Huachun Zhou, Fei Ren and Hongke Zhang, “Analysis of Route Optimization Mechanism for Distributed Mobility Management”. Journal of Networks, 2012, 7(10) 1662-1669

[8] Li Yi, Huachun Zhou, Daochao Huang and Hongke Zhang, “D-PMIPv6: A distributed mobility management scheme supported by data and control plane separation”. Mathematical and Computer Modelling, 2012, 8(2): 37-45

[9] Ji-In Kim and Seok-Joo Koh, “Distributed Mobility Management in proxy mobile IPv6 using hash function”. Information Networking (ICOIN), 2013, 107-112

A Periodic Garbage Collection to Reduce the Blocking of Vehicular Sensing in the Android Smartphones

Rachmad Nafisholeh, Hoa-Hung Nguyen and Han-You Jeong
Department of Electrical and Computer Engineering
Pusan National University, Busan, 609–735 Republic of Korea
rachmadnafisholeh@gmail.com, nguyenhoahungit@gmail.com, hyjeong@pusan.ac.kr

***Abstract*—Thanks to their multiple sensors, the Android smartphones have drawn significant attention for supporting vehicular sensing apps. These apps usually require continual sampling of sensors to collect the events of driving. However, the standard garbage collection (GC) of the Dalvik virtual machine blocks these apps from collecting sensing information for hundreds of milliseconds, which leads to the failure of detecting vehicular events. To alleviate this problem, we present a scheme that periodically invokes the app-driven GC to reduce the duration of blocking. The experimental results show that we can reduce the number of consecutive sensor losses.**

***Index Terms*—Vehicular sensing, smartphone, Android, garbage collection.**

I. Introduction

Vehicular sensing application is an important functionality in intelligent transportation system. In this application, each vehicle plays a role of sensors to gather, process and share the location-relevant data such as road surface anomaly [1]. These applications require (1) high sampling-rate sensors to gather sufficient samples, (2) processing power to process the raw sensor samples and detect target event, (3) communication ability to share the event information. In this paper, we focus on the road surface anomaly detection application in which the requirement of sensor sampling rate is critical.

In recent years, the Android smartphones have become promising solutions for vehicular sensing applications [2], [3]. They are usually equipped with GPS, accelerometer, gyroscope, and camera, which meets the requirement of vehicular sensing application. For example, they can provide accelerometer sensing whose sampling rate is up to 200 Hz. However, apps in Android-based smartphones are regularly blocked by garbage collection (GC) of the Dalvik virtual machine (VM) which leads to consecutive sensor sample losses.

In Android smartphones, the GC reclaims memory space occupied by objects that are no longer in use. When there is not enough free memory space for a new object, Dalvik VM automatically invokes GC to gather the unused memory space which is known as GC_FOR_ALLOC [6] and blocks the whole app during which GC_FOR_ALLOC runs. As a result, a vehicular sensing app may not get the sensor samples during the blocking time, which leads to the failure in detection.

There exists a few works [4], [5] attempting to alleviate the blocking of GC by modifying the Android operating system (Android OS). In [4], the real-time patch is added to linux kernel of Android OS besides the Android app framework to support the real-time apps, therefore, the apps are not suffered from GC blocking. The authors of [5] suggest to modify Dalvik GC to reduce its blocking time. However, all of these works require to change the Android OS itself, i.e., they cannot be applied to existing Android apps.

In this paper, we propose a solution to reduce the blocking time of GC by periodically calling the explicit GC which is known as GC_EXPLICIT. Since this approach uses the built-in functionality of Android operating system, it is applicable to the existing Android apps. In addition, we attempt to find the optimal calling period in which the GC blocking time is low while GC does not frequently run. The experiment results show that, our solution significantly reduce the amount of consecutive sample losses in vehicular sensing app.

The rest of this paper is organized as follows: In section II, we present detailed description about our approach. The experimental results are discussed in section III.

II. Periodic Garbage Collection

We start this section by describing the different between GC_FOR_ALLOC and GC_EXPLICIT. Then, we describe our periodic GC approach.

To process each sensor sample, the vehicular sensing app needs to create several temporary objects which gradually fill up memory over time. Therefore, GC_FOR_ALLOC is regularly invoked by the Dalvik VM to clean up these objects. In Android smartphones, GC_FOR_ALLOC is called when there is not enough free memory space to allocate an object. During this time, the app is blocked at the object allocation command. As a result, vehicular sensing app cannnot receive and process the sensor samples from the inertial sensors during the blocking time of GC_FOR_ALLOC.

On the other hand, GC_EXPLICIT is called by user app through $System.gc()$ command. It runs on a different thread from user app, therefore, user app can still run in parallel with GC_EXPLICIT on smartphones with multi-core processors which are popular in the recent days. As a result, the blocking time of GC_EXPLICIT is smaller than GC_FOR_ALLOC.

To reduce the blocking time, we utilize the GC_EXPLICIT to gather the temporary objects of vehicular sensing app

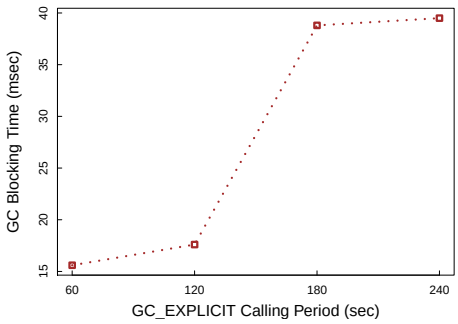

(a) GC blocking time.

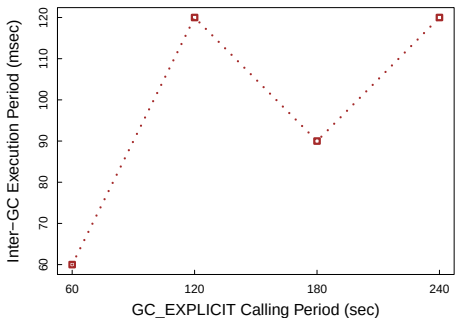

(b) inter-GC execution period.

Fig. 1. GC blocking time and inter-GC execution period of different GC_EXPLICIT calling period.

before memory becomes full and GC_FOR_ALLOC is invoked. When the app starts, we schedule GC_EXPLICIT to run repeatedly every T period using a $Timer$ object. The small T value is expected to cause shorter blocking time but GC_EXPLICIT runs more frequent. The larger T value may increase the blocking time since there are more objects to be freed but GC_EXPLICIT runs less frequent. In the meantime, GC_FOR_ALLOC may be invoked by Dalvik VM before GC_EXPLICIT. The optimal T value variates depending on smartphone model and is determined by the experiment results.

III. Experimental Results

In order to examine the performance of different GC_EXPLICIT calling periods, we develop a vehicular sensing app to detect road anomalies on the Galaxy Note 3 Neo smartphone equipped with 200-Hz sampling rate accelerometer. GC_EXPLICIT calling period T is set as $60, 120, 180$ and 240 sec. We investigate the performance of a GC_EXPLICIT calling period in terms of GC blocking time and inter-GC execution period to find the optimal value.

Fig. 1 shows the GC block time as well as inter-GC execution period for different GC_EXPLICIT calling period T. We can see from Fig. 1(a) that the larger T value leads to higher GC blocking time. The lowest blocking time is achieved at 60 sec. At 180 sec, the GC blocking time significantly increases and keep at high value at 240 sec. At these periods, GC_FOR_ALLOC is invoked before GC_EXPLICIT is called therefore the GC blocking time is high. In Fig. 1(b), we can see that inter-GC execution period is the same

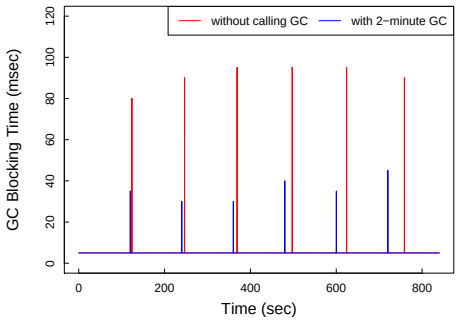

Fig. 2. Sampling period with two-minute GC and without GC_EXPLICIT calling.

with GC_EXPLICIT calling period at 60 and 120 sec but is half of GC_EXPLICIT calling period at higher period since GC_FOR_ALLOC runs in between GC_EXPLICIT. The maximum inter-GC execution period is achieved at 120 and 240 sec. From these results, we see that the optimal GC_EXPLICIT calling period T_{opt} is 120 sec, since it outperforms the higher GC_EXPLICIT calling period in both GC blocking time and inter-GC execution period and has a double inter-GC execution period while slightly higher blocking time comparing to lower GC_EXPLICIT calling period.

Fig. 2 shows the sampling period over time without using GC_EXPLICIT and with the T_{opt} period of GC_EXPLICIT. We can see from the result that without our approach, GC_FOR_ALLOC is call every 130 sec and creates the sampling period up to 100 msec which means that 19 consecutive sensor sample losses. When the optimal GC_EXPLICIT calling period is applied the GC blocking time is reduced to 35 msec which contains six consecutive sample losses. From these results, we can conclude that the proposed solution can significantly reduce the consecutive sample losses while produces a slightly higher inter-GC execution rate.

Acknowledgement

This research was supported by National Research Foundation of Korea (NRF) Grant (No. 2009-0083495) and by Global Frontier Program (No. 2011-0031863) through the NRF, which is funded by the Ministry of Science, ICT & Future Plannig.

References

[1] P. Mohan, V. N. Padmanabhan, R. Ramjee, Nericell: Rich Monitoring of Road and Traffic Conditions Using Mobile Smartphones, ACM SenSys08, pp. 323336, 2008.

[2] G. Strazdins, A. Mednis, G. Kanonirs, R. Zviedris, L. Selavo, Towards vehicular sensor networks with android smartphones for road surface monitoring, 2nd international workshop on networks of cooperating objects, Apr. 2011.

[3] A. Mednis, G. Strazdins, R. Zviedris, G. Kanonirs, and L. Selavo, Real time pothole detection using Android smartphones with accelerometers, DCOSS11, pp. 16, 2011.

[4] I. Kalkov, D. Franke, J. F. Schommer, S. Kowalewski. A real-time extension to the Android platform," ACM JTRES12, pp. 105-114, 2012.

[5] T. Gerlitz, I. Kalkov, J. F. Schommer, D. Franke, S. Kowalewski. "Non-blocking garbage collection for real-time android." ACM JTRES13, pp. 108-117, 2013.

[6] Investigating Your RAM Usage, [online] http://developer.android.com/tools/debugging/debugging-memory.html

Network Status Management Structure based on the Beacon Packet for Wireless Mesh Networks

Sang-Hyun, Lee
School of Electrical Engineering
KAIST
Daejeon, Republic of Korea
capricorns@kaist.ac.kr

Hong-Shik, Park
School of Electrical Engineering
KAIST
Daejeon, Republic of Korea
park1507@kaist.ac.kr

***Abstract*—One of the main issues in wireless mesh networks is throughput degradation caused by hop count increasing and channel interference problem. If each mesh node knows the current networks status such as traffic loads, link delay, and channel assignment information, then it may help to improve network throughput. In this paper, we propose structure and algorithm that can measure the wireless mesh networks status based on an existing beacon packet using the artificial ant concept. Using the measured information, it is applicable to wireless mesh network related algorithm.**

I. Introduction

Wireless mesh networks (WMNs) have been an emerging technology that can respond to the wireless traffic growth for future wireless networking. Also, WMNs have the advantage of scalability, connectivity, and low-cost deployment compared with traditional wired and wireless networks. Although WMNs have deployed in many areas, there are still several research issues.

One of the main issues is the throughput degradation problem caused by hop count increasing and channel interference [1]. Also, performance degradation of the gateway mesh node occurs because the network traffic is centralized to the gateway mesh node rather than edge mesh node due to the mesh network characteristic. If each mesh node knows the network status (such as traffic loads, link delay, channel assignment information, and so on), then the channel assignment for reducing interference and the routing for distributing traffic loads are possible. Furthermore, network throughput can be improved.

To solve this problem, we newly propose structure and algorithm that can measure the network status based on an existing beacon packet for WMNs. Using the measurement information by beacon packets, the each node makes its own a network status database (NS_DB) which consists of end-to-end performance table and neighborhood nodes information table. With this information tables, it is available for efficient routing, channel assignment, and so on. Also, the proposed structure is not hard to deploy to the real WMNs due to the usage of existing beacon packets.

II. Related works and backgrounds

There are two type of methods to measure the WMN status. The first method to measure the network status is the development of new protocol. This approach is possible to measure the network performance efficiently, but it is hard to compatible with existing WMNs for implementation issues. The other method is to add a field for storing the measured information in normal data packet payload. That approach is easy to implement, but it is hard to meet the various QoS requirements. Because this method is difficult to reflect the network status varying in real time.

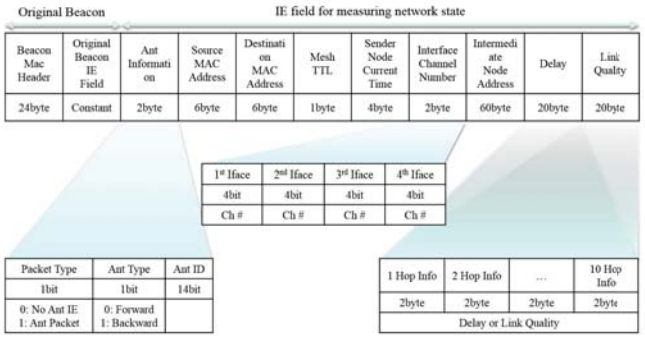

Fig. 1. The structure of artificial ant based on beacon packet

So, we use existing beacon packets for measuring the WMN status. To measure the network status using beacon packets, we utilize the artificial ant concept that consists of forward ant (the broadcasting packet from source node to destination node) and backward ant (the unicasting packet going backward to the path of forward ant) [2]. The forward ant measures and records network status in its packet, and the backward ant updates measured information of forward ant at each node.

III. Proposed Algorithm

In this section, we propose the WMN status measurement structure and algorithm based on the beacon packet to provide the service that meet the end-to-end QoS requirements.

Fig. 1 shows the proposed beacon packet format to measure the WMN status. The beacon packet format that is stipulated in the 802.11s standard consists of a MAC header and a beacon information fields (IE) [3]. The beacon IE, which is a field that has information for a particular role, contains a Mesh ID (the name of mesh node), mesh configuration information for informing the mesh service, and parameters of the transmitting

Algorithm 1 Network status measurement procedure using the beacon of forward ant packet

Create beacon of forward ant role at the sources node
Initialize current node information to the IE
Wait until current node beacon sending time
while $TTL \neq 0$ **do**
    Broadcast the beacon through the wireless link
    Receive the beacon at the neighbor nodes
    $TTL - -$
    if Destination node? **then**
        Go to the Algorithm 2
    else
        Record the measured information at the IE
        Store the received beacons IE at IE_DB
        Wait until current node beacon sending time
        Update current node information to the IE
        Add the IEs (in IE_DB) at the end of beacon
    end if
end while
Discard the artificial ant packet
Terminate the Algorithm 1

mesh nodes [3]. We newly add the IE field that stores the measured network status information as shown in the Fig. 1.

The ant information field consists of packet type (artificial ant or not), ant type (forward ant or backward ant), and ant ID. The Mesh TTL field that limits the lifetime of the artificial ant packet is initialized at the source node according to network size. The interface channel number field contains channel number of neighborhood nodes. When forward ant goes from source to destination node, the address of the intermediate nodes is stored in that field. The measured delay and the link quality values are stored at the each corresponding hop fields.

Generally, the beacon packets are periodically transmitted and received with each neighborhood nodes to announce the presence of the each node. On the other hand, the artificial ant packet should constantly be transmitted from source node to destination node for measuring the end-to-end QoS performances. To solve the above problem, therefore, we propose the beacon packets transmitting method for implementing the artificial ant as shown in algorithm 1 and 2.

The algorithm 1 is the network status measurement procedure using the beacon of forward ant role. Each node has own NS_DB and IE_DB. The NS_DB contains the end-to-end statistic table (delay: $D_i(\mu_D, \sigma_D)$, link quality: $L_i(\mu_L, \sigma_L)$) of each neighborhood nodes according to the destination nodes and neighborhood nodes channel number table ($I_1^i \sim I_4^i$) as shown in Fig. 2. The IE_DB is stored the IEs of forward ants which are received from the neighborhood nodes, and adds the stored IEs to the beacon when next beacon sending time. The forward ants are broadcasted from source to destination node over the measuring network status. The algorithm 2 is the networks status update procedure using the beacon of backward ant role. The backward ants are unicasted through the intermediate nodes over the updating to the NS_DB.

Algorithm 2 Network status update procedure using the beacon of backward ant packet

Record the measured information to the IE
Create beacon of backward ant role equal to forward ant
Wait until current node beacon sending time
while 1 **do**
    Unicast the beacon to path of forward ant packet through the wireless link
    Receive the beacon at the intermediate node
    Update measured information to NS_DB
    if Source node? **then**
        Break
    end if
end while
Discard the artificial ant packet
Terminate the Algorithm 2

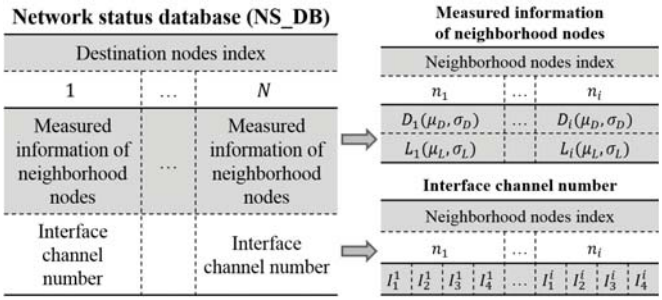

Fig. 2. Structure of network status database

IV. Conclusion

In this paper, we propose the structure and algorithm that can measure the WMN status based on the existing beacon packet using the artificial ant concept. Through the measured network status database, network service provider obtains the help for service providing to guarantee the end-to-end delay performance and to alleviate the channel interference. Also, it is applicable to WMNs related algorithm such as routing, channel assignment, and so on. Now, we are performing complexity analysis of this structure and throughput evaluation using routing algorithm based on the NS-3 simulator.

Acknowledgment

This work was supported by Institute for Information & communications Technology Promotion (IITP) grant funded by the Korea government (MSIP) (B0101-15-1270, Research on Communication Technology using Bio-Inspired Algorithm)

References

[1] Benyamina, D., et al. (2012). "Wireless mesh networks designa survey." Communications Surveys & Tutorials, IEEE 14(2): 299-310.
[2] Di Caro, G. and M. Dorigo (1998). "AntNet: Distributed stigmergetic control for communications networks." Journal of Artificial Intelligence Research: 317-365.
[3] Hiertz, G. R., et al. (2010). "IEEE 802.11 s: the WLAN mesh standard." Wireless Communications, IEEE 17(1): 104-111.

Wireless Communication Performance of the 5G Modulation Systems in the Nonlinear Channel

Changyoung An
Department of Electronics Engineering
Chungbuk National University
Cheongju, Korea 361-763
acy890217@naver.com

Heung-Gyoon Ryu
Department of Electronics Engineering
Chungbuk National University
Cheongju, Korea 361-763
ecomm@cbu.ac.kr

***Abstract*—In this paper, we have focused on spectrum characteristic analysis and performance evaluation of FBMC and UFMC system under the effect of nonlinear HPA. As simulation results, We have confirmed that if HPA nonlinearity rises in each system, OOB power of each system increases, and OOB power increase of FBMC system by strength of HPA nonlinearity is the biggest. Additionally, we have confirmed that performance of every system is degraded by strength of HPA nonlinearity, and FBMC system is the strongest against HPA nonlinearity.**

Keywords— PAPR; OFDM; FBMC; UFMC; HPA nonlinearity

I. INTRODUCTION

Universal filtered multi-carrier (UFMC) and filter bank based multi-carrier (FBMC) are known as the candidate waveform for 5G mobile communication [1-2].

However, these systems based on OFDM are vulnerable to non-linearity of high-power amplifier (HPA), like OFDM. OFDM has high peak-to-average power ratio (PAPR) because multi-carrier signals are overlapped. High PAPR causes nonlinear distortion in HPA because it saturates HPA. Similarly, UFMC and FBMC have high PAPR because these systems are based on multi-carrier [3]. In UFMC and FBMC system, if nonlinear distortion is caused by high PAPR, OOB power of these systems is increased. That is, advantage of these systems vanishes. In this paper, in order to overcome the drawback, we focus on spectrum characteristic analysis and performance evaluation of FBMC and UFMC system under the effect of nonlinear HPA.

II. SYSTEM MODEL

A. OFDM

OFDM system has advantages of orthogonality between each of subcarriers and robustness against ISI effect by CP. That is, OFDM system requires simple equalizer with one tap [4]. However, each subcarrier of OFDM system has high side-lobe power. Additionally, OFDM system has high PAPR characteristic. High PAPR signal is distorted by nonlinear HPA. Because of this, OOB powers can be increased. Also, performance of OFDM system with high PAPR can be degraded. These drawbacks should be overcome for 5G mobile communication.

B. UFMC

UFMC system uses orthogonal multi-carrier, like OFDM system. UFMC filters each sub-band that consists of orthogonal multi-carrier in order to reduce OOB power [1].

C. FBMC

FBMC system uses multi-carrier, like OFDM system. FBMC system filters each sub-carrier in order to reduce OOB power of spectrum [2].

III. HPA NONLINEARITY

We have added HPA nonlinearity model into transmitter of each system. In Saleh model, characteristics of AM-AM and AM-PM are as follows [5].

$$G[A(t)] = \frac{\alpha_A A(t)}{1+\beta_A A(t)^2} \quad (1)$$

$$\Phi[A(t)] = \frac{\alpha_\Phi A(t)^2}{1+\beta_\Phi A(t)^2} \quad (2)$$

Equation (1) shows AM-AM characteristic of Saleh model, nonlinear HPA model. A is amplitude of input signal. α_A and β_A are coefficients for adjusting amplitude of output signal. Equation (2) shows AM-PM characteristic of Saleh model. α_Φ and β_Φ are coefficients for adjusting phase of output signal.

IV. SIMULATION RESULTS AND ANALYSIS

Table 1 shows simulation parameters.

TABLE I. SIMULATION PARAMETERS

Parameter	Value
Modulation	QPSK
# of total subcarrier	64
# of used subcarrier	32
# of null subcarrier	32
Filter for FBMC	Phydyas prototype H0 = 1 H1 = 0.97196 H2 = 0.7071 H3 = 0.235147
Filter for UFMC	Chebyshev Attenuation = 60dB Length = 10
# of sub-band in UFMC	64/8
# of used sub-band in UFMC	4

TABLE II. CONDITION OF HPA NONLINEARITY

Condition	AM-AM	AM-PM
0 (Linear)	$\alpha_A = 1$	$\alpha_\Phi = 0$
	$\beta_A = 0$	$\beta_\Phi = 0$
1	$\alpha_A = 1$	$\alpha_\Phi = 0.26$
	$\beta_A = 0.04$	$\beta_\Phi = 15.9$
2	$\alpha_A = 1$	$\alpha_\Phi = 0.26$
	$\beta_A = 0.2$	$\beta_\Phi = 2.38$
3	$\alpha_A = 1$	$\alpha_\Phi = 0.26$
	$\beta_A = 0.4$	$\beta_\Phi = 0.69$
4	$\alpha_A = 1$	$\alpha_\Phi = 0.26$
	$\beta_A = 0.6$	$\beta_\Phi = 0.127$
5	$\alpha_A = 1$	$\alpha_\Phi = 0.26$
	$\beta_A = 0.8$	$\beta_\Phi = -0.155$

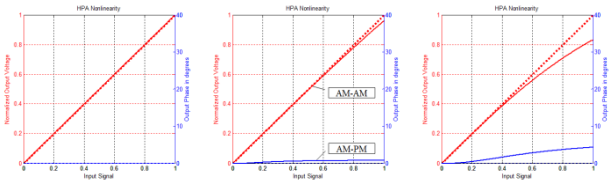

(a) Condition 0 (b) Condition 1 (c) Condition 2

(d) Condition 3 (e) Condition 4 (f) Condition 5

Figure 1. Characteristics of AM-AM and AM-PM in Saleh model.

TABLE III. COMPARISON OF OOB POWER

Condition	OFDM	UFMC	FBMC
0	-26dB	-80dB	-117dB
1	-26dB	-45dB	-48dB
2	-25dB	-32dB	-36dB
3	-24dB	-27dB	-31dB
4	-23dB	-24dB	-28dB
5	-22dB	-23dB	-26dB

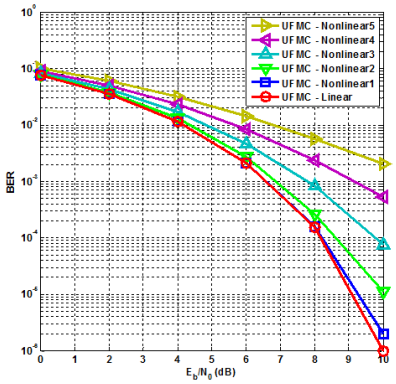

Figure 2. BER performance of UFMC system according to nonlinear HPA conditions.

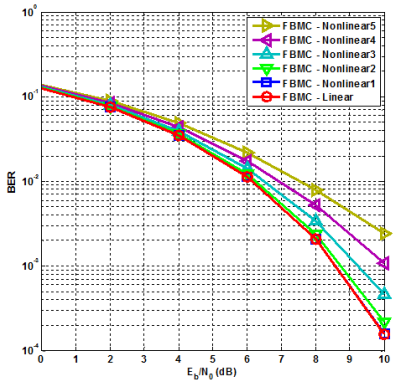

Figure 3. BER performance of FBMC system according to nonlinear HPA conditions.

Under the nonlinear HPA environment, BER performance of every system is degraded. Additionally, FBMC system shows the smallest degradation of BER performance. That is, FBMC system is the strongest against HPA nonlinearity.

V. CONCLUSIONS

In this paper, in order to overcome the drawback, we have focused on spectrum characteristic analysis and performance evaluation of OFDM, FBMC, and UFMC system under the effect of nonlinear HPA. As simulation results, we have confirmed that if HPA nonlinearity rises in each system, OOB power of each system increases, and OOB power increase of FBMC system by strength of HPA nonlinearity is the biggest. Additionally, we have confirmed that performance of every system is degraded by strength of HPA nonlinearity, and FBMC system is the strongest against HPA nonlinearity.

ACKNOWLEDGMENT

"This research was supported by Basic Science Research Program through the National Research Foundation of Korea(NRF) funded by the Ministry of Education, Science and Technology(No.2013R1A2A2A01005849) and this work was supported by Institute for Information & communications Technology Promotion (IITP) grant funded by the Korea government(MSIP) (R0101-15-244, Development of 5G Mobile Communication Technologies for Hyper-connected smart services)"

REFERENCES

[1] Vakilian, V.; Wild, T.; Schaich, F.; ten Brink, S.; Frigon, J.-F., "Universal-filtered multi-carrier technique for wireless systems beyond LTE," in Globecom Workshops (GC Wkshps), 2013 IEEE, pp. 223-228, 9-13 Dec. 2013.

[2] Farhang-Boroujeny, B., "OFDM Versus Filter Bank Multicarrier," in Signal Processing Magazine, IEEE, vol. 28, no. 3, pp. 92-112, May 2011.

[3] Chafii, M.; Palicot, J.; Gribonval, R., "Closed-form approximations of the PAPR distribution for Multi-Carrier Modulation systems," in Signal Processing Conference (EUSIPCO), 2014 Proceedings of the 22nd European, pp. 1920-1924, 1-5 Sept. 2014.

[4] Elshirkasi, A.M.; Siddiqi, M.U.; Habaebi, M.H., "Generalized Discrete Fourier Transform Based Minimization of PAPR in OFDM Systems," in Computer and Communication Engineering (ICCCE), 2014 International Conference on, pp. 205-208, 23-25 Sept. 2014.

[5] P. Drotar, J. Gazda, D. Kocur, and P. Galajda, "MC-CDMA performance analysis for different spreading codes at HPA Saleh model," 18th Int. Conf. Radioelektronika, pp. 1-4, Prague, Apr. 2008.

A Comparative Study on PMIPv6 and Partially DMM Network Architecture

Ye Wang
Dept. of Electronic and Information Engineering
Lishui University
Lishui City, China
wychina_2007@hotmail.com

Jang-Geun Ki*, Kyu-Tae Lee
Dept. Information & Communication Engineering
Kongju National University
Cheonan, Korea
kjg@kongju.ac.kr, ktlee@kongju.ac.kr

***Abstract*—This paper provides the performance analysis and implementation between Proxy Mobile IPv6 (PMIPv6) and partially distributed mobility management (DMM) network architecture. The simulation results indicated DMM network performs better benefits than PMIPv6 network by analyzing packet delivery ratio (PDR) and CPU point-to-point utilization.**

Keywords-component; PMIPv6; DMM; PDR; utilization

I. INTRODUCTION

With the increasing volumes of mobile data traffics and massive increase in the number of interconnected devices, especially on demand for "imperceptible latency" with Tactile internet, and nearly 100% reliability with Internet of Thing service [1], IMT-2020(5G) provides Fifth-Generation (5G) system to meet new and unprecedented demands. Along with these objectives, distributed mobility management (DMM) has recently emerged as a new paradigm to design a flat and flexible mobility architecture, allowing traffic to be broken out locally closer to the edge (i.e., offloading the network core) and exploiting the use of different gateways for traffic with different connectivity and mobility requirements. Apparently, DMM approach is suitable candidates for mobility management in future 5G very dense deployments [2].

A number of distributed mobility management schemes have been proposed in the literature. We are focus on the implementation and performance analysis on DMM network. For the implementation issue, Bernardos etc. [3] proposed a method by querying the Central Mobility Database (CMD) to acquire the MN's location information. Zhengming Ma etc. [4] and Yuhong Li etc. [5] introduced AAA server and Software Defined Networking (SDN) to manage MN's location information, respectively. Kim etc. [6] and Jung etc. [7] presented the multicast and point-to-point searching scheme to get MN's location. However, those proposed mechanism did not give the specific implementation mechanism and feasibility analysis. For the performance analysis issue, Li Yi etc. [8-9] and Kim etc. [10] showed signal control and data transmission cost is lower than PMIPv6 protocol. Seo etc. [11] proposed a multiple LMAs mechanism in DMM and provides lower end-to-end delay. However, those performances are all cost-based analysis, there are short of the comprehensive and systematic study.

In this paper, the partially distributed mobility management (DMM) network and PMIPv6 network were evaluated in OPNET simulator by analyzing the different performance metrics, such as packet delivery ratio (PDR) and CPU point-to-point utilization. The simulation results indicated that performance analysis of DMM network performs better than PMIPv6 network.

II. MATERIALS AND METHODS

A. Simulaiton Environment

The simulation scenarios in OPNET simulator is proposed and illustrated in Fig. 1.

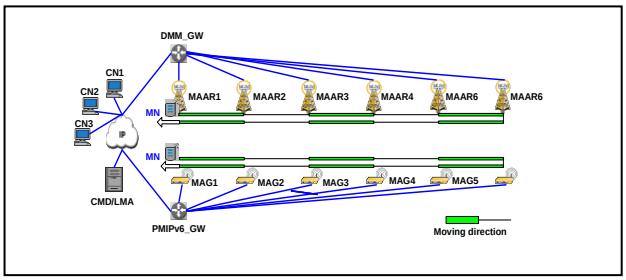

Figure 1. Difference between PMIPv6 and DMM netowrk architecture

In Fig. 1, one scenario is multiple MNs will move from MAAR1 (MAG1) to MAAR6 (MAG6) in both ways in PMIPv6 network and DMM network. The other scenario is MN will communicate with several CNs while performing multiple handoffs in both network.

B. Simulaiton Parameters

The simulation parameters for two scenarios are illustrated in Table I.

TABLE I. THE COMMON SIMULATION PARAMETERS

Parameters	Value
Distance between MAARs and MAGs	2 km
Traffic Generate Rate(packets/sec)	0.01,0.025,0.05,0.1,...,18,20
Traffic Generate Time(sec)	3m, 5m, 7m
Mobility Speed	60 km/h
MN Starts Moving Time	180 sec
Simulation Time	1380 sec

III. PERFORMANCE ANALYSIS AND DISCUSSION

A. Effect of Network Size

The one challenge for DMM solution is related to the frequent movement of MNs and handle with several MNs. It

means MNs can frequently move to several locations and performs several handoffs.

The simulation scenario was proposed as varying number of MNs from 1 to 25. The data traffic generated rate is run 1packet/sec. In general, high density of network size may increase the contention and cause the network congestion, and also increase the data traffic lost.

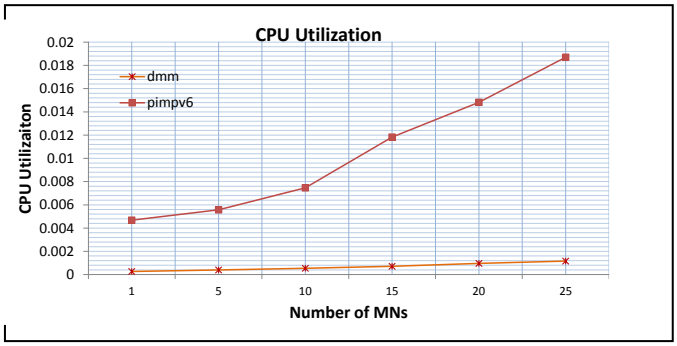

Figure 2. A comparison of CPU utilization as varying MNs from 1to 25

In Fig. 2, the CPU utilization in LMA of PMIPv6 network is higher than it in CMD of DMM network. It also can be seen that CPU utilization will increased sharply as varying the number of MNs from 1 to 25. In DMM network, it seems to be not affected much by increasing the volumes of data traffics. The reason is that all data packets will go through the LMA of PMIPv6 between MNs and CNs with the large number of MNs. However, the data packets will not be managed by CMD of DMM according to the properties of DMM solution.

As depicted in Fig. 3, the performance of packet delivery ratio in DMM and PMIPv6 network shows the similar down trend as increasing the volumes of MNs. However, the PDR of DMM performs better than it in PMIPv6 network. With a large number of concurrent data traffics, extra control traffics causes less available bandwidth for data traffics and increased chances of packet loss due to collisions and interface overflows.

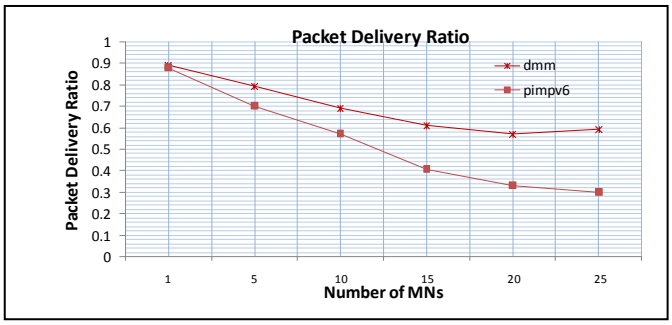

Figure 3. A comparison of packet delivery ratio as varying MNs from 1to 25

IV. CONCLUSIONS

The main difference between PMIPv6 and partially DMM network is the partially distributed category, which consists in de-coupling the entities that participates in the data and the control planes: the data plane becomes distributed and managed by the MAARs near the edge of the network, while the control plane, besides on the MAARs, relies on a central mobility entity.

This paper shows the main differences and comparative study between PMIPv6 and DMM network architecture. As simulation results shown while varying MNs form 1 to 25, it is concluded that DMM performs good benefits than PMIPv6 in the CPU utilization and PDR.

ACKNOWLEDGMENT

This work is supported by Research Fund for PhD early development program of Lishui University (Grant No. QD1405) and the Scientific Research project of Zhejiang Provincial Education (Grant No.Y201534057).

REFERENCES

[1] IMT-2020 5G Vision and Requirements, IMT-2020 (5G) Promotion Group, White Paper, 2014,1-20

[2] Fabio Giust, Luca Cominardi and Carlos J. Bernardos, "Distributed Mobility Management for Future 5G Networks: Overview and Analysis of Existing Approaches". IEEE Communication Magazine, 2015, 53(1): 142-149

[3] CJ. Bernardos, F. Giust and A. de la Oliva, "A PMIPv6-based solution for Distributed Mobility management". IETF DMM Working Group, draft-bernardos-dmm-pmip-03 (work in progress), 2014

[4] Zhengming Ma and Xun Zhang, "An AR-level solution support for Distributed Mobility Management". IETF DMM Working Group, draft-ma-dmm-armip-00 (work in progress), 2012

[5] Yuhong Li, Haimeng Wang, Ming Liu and Bofan Zhang, "Software defined networking for Distributed Mobility Management". IEEE Globecom Workshops, 2013, 885-889

[6] J. Kim, S. Koh, H. Jung and Y. Han, "Use of Proxy Mobile IPv6 for Distributed Mobility Control". IETF draft-jikim-dmm-pmip-00 (work in progress), 2012

[7] Heeyoung Jung, Moneeb Gohar, Ji-ln Kim and Seok-Joo Koh, "Distributed Mobility Control in Proxy Mobile IPv6 Networks". 2011 Institute of Electronics, Information and Communication Engineers (IEICE) TRANS. COMMUN., 2011, E94-B(8): 2216-2224

[8] Li Yi, Huachun Zhou, Fei Ren and Hongke Zhang, "Analysis of Route Optimization Mechanism for Distributed Mobility Management". Journal of Networks, 2012, 7(10) 1662-1669

[9] Li Yi, Huachun Zhou, Daochao Huang and Hongke Zhang, "D-PMIPv6: A distributed mobility management scheme supported by data and control plane separation". Mathematical and Computer Modelling, 2012, 8(2): 37-45

[10] Ji-In Kim and Seok-Joo Koh, "Distributed Mobility Management in proxy mobile IPv6 using hash function". Information Networking (ICOIN), 2013, 107-112

[11] Won-Kyeong SEO, Jae-In CHOI and You-Ze CHO, "Distributed Mobility Management Scheme with Multiple LMAs in Proxy Mobile IPv6". IEICE TRANSACTIONS on Communications, 2014, E97-B(11): 2327-233

Thursday, Feb. 25

Session III-1 : (Oral) Convergence III

Investigating Graphical Passwords: A New Perspective

Kashif Abbasi
PhD Research Fellow
Faculty of Information Science and Technology (FTSM)
University Kebangsaan Malaysia (UKM)
Bangi, Selangor, Malaysia
abbasi.k@gmail.com

Abdullah Mohd. Zin
Faculty of Information Science and Technology (FTSM)
University Kebangsaan Malaysia (UKM)
Bangi, Selangor, Malaysia
amzftsm@ukm.edu.my

Mohd. Rosmadi Mokhtar
Faculty of Information Science and Technology (FTSM)
University Kebangsaan Malaysia (UKM)
Bangi, Selangor, Malaysia
mrm@ukm.edu.my

Abstract – Businesses and Companies comprehend the importance of Green Computing. It is beneficial to reduce operational costs as well as improve customer relations. Within the paradigm of Green Computing, security of devices and resources is highlighted as a potential security risk. Graphical password based authentication is the modern technique for security of computer based information systems. It provides an alternative method to normal text based authentication. Many researchers have introduced their own methods of graphical authentication. They have classified them based on the features and utilization of methods. However, these methods are subject to various security threats and usability problems. In this paper, we have done comparative analysis of graphical authentication methods. We have classified them in a new perspective – based on the security attacks and usability issues. We have tried to highlight main security and usability problems faced by these methods. In the end, solutions to these security and usability problems are given in the discussion section.

Keywords – Green Computing; computer security; user authentication; graphical passwords; security attacks; usability problems

I. INTRODUCTION

During last decade, paradigm of research in the field of Information Technology has shifted from normal desktop computing to mobile based computing. Further it advanced to modern field of Green Computing. With focus on efficient and economical use of resources, Green Computing is getting popularity at all private and public forums. Especially businesses and industries are implementing Green Computing best practices. Consequent upon increased use of energy efficient smart phones and mobile notebooks for day to day activities, the problems of security threats and virus attacks have evolved.

For business and organizations, security of information systems is the basic need of the day. Particularly, keeping the customer data and business records safe and secure on server is very important for them. Only authorized and legitimate users must have access to servers. With the fast growing businesses and demand of the information technology, security threats have also enhanced. As a result, user authentication is considered important factor for data security and computer security.

Conventional methods of authentication require users to enter user name and password through keyboard. These text based passwords must be 8-10 characters long with combination of multiple special characters. It makes the password difficult to remember for normal users [1], [2]. As a result, researchers have introduced graphical passwords. Graphical passwords are considered as alternate to conventional text based passwords.

II. GRAPHICAL PASSWORD METHODS

The graphical passwords are alternative to normal text based passwords. In graphical passwords, pictures, objects and drawings are used for authentication. During last decade various researchers have developed their own graphical password based authentication methods (Refer: Table 1). Graphical passwords are broadly classified as Recognition based passwords and Recall based passwords. In Recognition based passwords, the users are asked to select certain predefined pictures and objects. If user is able to select the pictures then the system will authenticate the user. In Recall based passwords, the users are asked to redraw an image or picture. If user is able to do so, the system will authenticate the user. Psychological Studies have shown that users prefer recognition based methods as compared to the recall based methods [1], [2], [3].

III. SECURITY ATTACKS ON GRAPHICAL PASSWORDS

From operation point of view, graphical passwords are found to be more secure than the normal text based passwords [2], [4], [5]. But graphical passwords are vulnerable to a number of security attacks. Some of these attacks are: Shoulder Surfing Attack, Brute Force Attack, Dictionary Attack, Guessing Attack, Spyware Attack, Frequency of Occurrence Attack, Social Engineering or Description Attack, etc. Among these attacks, the shoulder surfing attack and brute force attack are most critical for graphical passwords. Efforts have been made to make these passwords resistant to these security attacks [6], [7].

IV. CATEGORIZATION OF METHODS

Most of the graphical passwords based authentication methods are focused towards improving the security of methods [8], [9], [10]. Researchers have tried to make the

authentication steps complex so that security attacks can be prevented. However, enhanced security compromises on the usability of the method. Main problem among these methods is that most of them do not cater both security problems and usability problems (Refer: Table 1). If security of method is enhanced, it results in poor usability of method. If focus of work is on improving the usability of method, then the security of method is compromised [11], [12].

In this paper, we have done comparative analysis of graphical authentication methods. Normally latest researchers focus on classifying a graphical method based on its steps / functionality provided, i.e. whether it is recognition based method or recall based method. However, we have classified them in a new perspective. This classification is based on two factors: *a) the security attacks* and *b) the usability* issues. Various graphical methods are listed in the *Table 1* below. These methods are categorized based on the criteria of their usability and security features provided.

V. CATEGORIZTION OF GRAPHICAL METHODS

S. No.	Year	Graphical Method Name	Characteristics Provided	
			Security	***Usability***
1	2015	Authentication Using Session Based Passwords [8]	S	--
2	2015	Prevention of shoulder surfing attack using randomized square matrix virtual keyboard [9]	S	--
3	2015	Graphical Password-Based User Authentication With Free-Form Doodles [10]	S	--
4	2015	A novel way of ICON based authentication methods [1]	S	--
5	2014	Highly Secure Authentication Scheme [6]	S	--
6	2014	Application H-Secure for mobile security [7]	S	--
7	2014	Shoulder-surfing-proof graphical password authentication scheme [2]	S	--
8	2014	Exploring the guessability of hand drawn images based on cultural characteristics [13]	S	--
9	2015	PassBYOP: Bring Your Own Picture for Securing Graphical Passwords [4]	S	U
10	2015	A Comparative Study of Graphical and Alphanumeric Passwords for Mobile Device Authentication [5]	S	U
11	2014	Sequential graphical password framework for mobile devices [14]	S	U
12	2014	A Study of Mnemonic Image Passwords [3]	--	U
13	2014	Challenge Set Designs and User Guidelines for Usable and Secured Recognition-Based Graphical Passwords [15]	S	U

VI. DISCUSSION AND CONCLUSION

In this paper, we have studied latest graphical password based authentication methods. We have compared them in the *Table I* given above. We have compared graphical password based on two main factors which are *Security* and *Usability*. The *Table 1* records which factor is provided by different methods.

Based on the comparison given in the *Table 1*, it is concluded that: Some methods are focused on improving the security of method only [8], [9], [10] while some methods are focused on improving both security and usability of method [4], [5], [14]. It can be observed from the results given in *Table 1* that more researchers have worked on security of graphical passwords and fewer researchers have worked on usability of graphical passwords. Therefore, it can be concluded that there is a strong need to do further research in the area of improving the usability of graphical passwords so that we can have more user friendly authentication methods.

REFERENCES

[1] Devaki, P. and R. Rao. "A novel way of ICON based authentication methods". in IEEE International Advance Computing Conference (IACC). 2015. IEEE.

[2] Wu, T.-S., et al., "Shoulder-surfing-proof graphical password authentication scheme". International Journal of Information Security, 2014. 13(3): p. 245-254.

[3] Chowdhury, S., R. Poet, and L. Mackenzie. "A study of mnemonic image passwords". in Twelfth Annual International Conference on Privacy, Security and Trust (PST). 2014. IEEE.

[4] Bianchi, A., I. Oakley, and H. Kim, "PassBYOP: Bring Your Own Picture for Securing Graphical Passwords". IEEE Transactions on Human-Machine Systems, 2015.

[5] Anwar, M. and A. Imran. "A Comparative Study of Graphical and Alphanumeric Passwords for Mobile Device Authentication". in MAICS. 2015.

[6] Ushir Kishori, N. and R. Joshi, "Highly Secure Authentication Scheme". International Journal of Computer Applications, 2014. 108(14): p. 35-38.

[7] Lopes, H. and M. Chatterjee. "Application H-Secure for Mobile Security". in International Conference on Circuits, Systems, Communication and Information Technology Applications (CSCITA). 2014. IEEE.

[8] Prabhu, S. and V. Shah, "Authentication Using Session Based Passwords". Procedia Computer Science, 2015. 45: p. 460-464.

[9] Nand, P., et al. "Prevention of shoulder surfing attack using randomized square matrix virtual keyboard". in Computer Engineering and Applications (ICACEA), 2015 International Conference on Advances in. 2015. IEEE.

[10] Marcos Martinez-Diaz, J.F., and Javier Galbally, "Graphical Password-Based User Authentication With Free-Form Doodles". IEEE Transactions on Human-Machine Systems, 2015.

[11] Sharifi, E. and M. Shamsi, "Evaluate the security and usability of graphical passwords". International Journal of Advanced Research in Computer Science and Electronics Engineering (IJARCSEE), 2014. 3(8): p. pp: 405-409.

[12] Gao, H., et al., "A survey on the use of Graphical Passwords in Security". Journal of software, 2013. 8(7): p. 1678-1698.

[13] Jebriel, S. and R. Poet. "Exploring the Guessability of Hand Drawn Images based on Cultural Characteristics". in 6th International Conference on Computer Science and Information Technology (CSIT). 2014. IEEE.

[14] Hui, L.T., et al. "Sequential Graphical Password Framework for Mobile Devices". in Fourth World Congress on Information and Communication Technologies (WICT). 2014. IEEE.

[15] Aljahdali, H.M. and R. Poet. "Challenge Set Designs and User Guidelines for Usable and Secured Recognition-Based Graphical Passwords". in 13th International Conference on Trust, Security and Privacy in Computing and Communications (TrustCom), IEEE. 2014. IEEE.

A Fast and Robust Eye-Event Recognition (FRER) for Human-Smartphone Interaction

Ardhiansyah Baskara
School of Electrical and Computer Engineering
Pusan National University
Busan, 609-735 Republic of Korea
ardhiansyah.baskara@gmail.com

Han-You Jeong
School of Electrical and Computer Engineering
Pusan National University
Busan, 609-735 Republic of Korea
hyjeong@pusan.ac.kr

***Abstract*—The human-computer interaction using the computer vision have been extensively studied to provide a chance to access the computers to the people with physical challenges, such as Lou Gehrig's disease or stroke illness. Recently, a smartphone has become one of important gadgets in our daily life. However, there are still many challenges in the computer vision for the human-smartphone interaction (HSI), such as hardware limitation and unstable distance and pose of the smartphone user. In this paper, we present the *fast and robust eye-event recognition (FRER)* scheme that consists of the eye-area extraction, the eye tracking, and the eye-event recognition blocks. We also propose the *slope-based similarity checking (SSC)* algorithm for eye-event recognition of a person with arbitrary eye size. The experimental results show that the FRER scheme can successfully detect the eye events with 99.3 % at frame rate of 19 frames per second.**

Keywords*: *Human-smartphone interaction, computer vision, eye-event recognition.

I. Introduction

The human-computer interaction (HCI) based on the computer vision technology has been one of the hottest research topics, because the eye-event recognition is one of ways to get input command from users by using camera [1] [2]. Many researchers have extensively studied a novel way to establish the interaction between a user and a computer. The seminal paper in [1] presents the framework of eye-event recognition which detects the eye area through motion analysis, tracks the eye area using a similarity measure, and then recognizes the eye events based on the threshold values of the similarity. The authors in [2] present a robust implementation of this framework which supports a frame rate of 30 frames per second (FPS) using a desktop PC equipped with a webcam.

Recently, a smartphone has been a ubiquitous mobile device for web browsing, instant messaging, and streaming services in our daily life. In this paper, we focus on the *human-smartphone interaction (HSI)* using the computer vision technology. The goal of this research is to provide a chance to access the smartphone to the people with severe physical challenges, such as Lou Gehrig's disease and stroke illness. Usually, the HSI faces a couple of additional challenges compared to the HCI: 1) how to detect/track the eye events with computationally efficient way; and 2) how to accurately recognize eye events of a person with arbitrary eye size. The EyePhone in [3] is the first hand-free interaction for driving the apps using the HSI. In [4], the EyeGuardian informs the user if his/her blink rate is exceptionally low. For the template of eye tracking, the EyePhone requires an additional step to collect open-eye templates at the initial phase, whereas the EyeGuardian uses computationally intensive Haar Cascade Classifier. For the eye-blink detection, both apps use the *threshold-based similarity checking (TSC)* which is not robust to a person with different eye size.

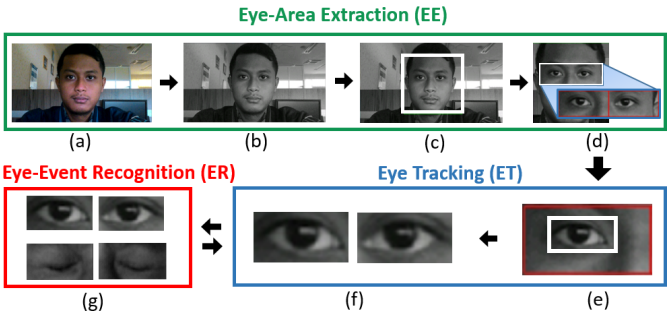

Fig. 1. Overview of the FRER scheme

In this paper, we propose the *fast and robust eye-event recognition (FRER)* scheme. The FRER scheme first extracts the eye-area using the face detection, tracks the location of eye area, and recognizes the eye events regardless of the eye size. The experimental results show that the FRER scheme can detect the eye event with success probability of 99.3 percent at frame rate of 19 FPS.

II. The FRER Scheme

Fig. 1 shows the overview of the FRER scheme consisting of three blocks: the eye-area extraction (EE), the eye-tracking (ET), and eye-event recognition (ER). The EE block obtains the eye area through the following steps: The EE block first converts the RGB frame of smartphone camera in Fig. 1(a) into a grayscale frame as shown in Fig. 1(b). Next, the EE block employs the Haar Cascade Classifier to extract the face area (See Fig. 1(c)), and then obtains the eye area by cropping it from the face area as shown in Fig. 1(d).

Once the eye area is obtained from the EE block, the ET block tracks the movement of the eye area using the Haar Cascade Classifier as shown in Fig. 1(e). To aim this, the ET

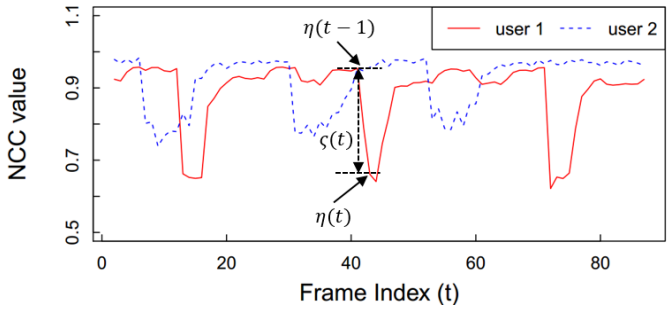

Fig. 2. The NCC of two smartphone users

block considers the extracted eye area as the region of interest (ROI) which includes the open-eye template in Fig. 1(f). This ROI is also used for skipping the computationally intensive EE block, which will be explained at the end of this section.

As shown in Fig. 1(g), we consider two possible states of eye: *open* and *closed*. To recognize an eye event, the ER block uses the open-eye template of the ET block as the reference. The ER block adopts the same similarity measure, called the normalized cross-correlation (NCC), as the existing works in [1–4]. The prime difference of the ER block is the use of *slope-based similarity checking (SSC)* algorithm to detect the eye event. Denoting the NCC value at frame index t by $\eta(t)$, the existing TSC algorithm uses a fixed threshold T of the NCC: An eye is open, if $\eta(t) \geq T$, and closed otherwise. Instead, the SSC toggles its state when the slope of the NCC, denoted by $\varsigma(t)$, exceeds a fixed threshold S: It maintains the current state, if $\varsigma(t) = |\eta(t) - \eta(t-1)| \leq S$, and switches to the other state, otherwise. Fig. 2 plots the NCC of two smartphone users taken from our experiments. We can see that, at the frame of eye closing/opening, both users have a similar slope value while the NCC value is quite different depending on the eye size.

Finally, if $\eta(t)$ is less than 0.5, the FRER scheme interprets that the ET block fails to track the eye area: It goes to the EE block to extract the eye area again. Otherwise, it skips the EE block and directly executes the ET block with the new ROI.

III. Numerical Results and Discussion

In this section, we discuss the numerical results from our experiments with a test app running at the Samsung Galaxy Note 3 Neo. We develop this app using the Android APIs and the OpenCV library.

To demonstrate the computational efficiency, we compare the FRER scheme with the basic scheme that executes all three blocks of FRER at each frame. Table I shows the frame rate of both schemes. At each scenario, we run the test app for three minutes with/without head movements. We can see that the FRER scheme achieves a higher frame rate than the basic scheme; The frame rate of the former is around 19 FPS, while that of the latter is about 15 FPS. We infer that the ET block can reduce the computational load of the face detection.

Fig. 3 show the accuracy of eye-blink recognition of three smartphone users with different eye size. To maximize the

TABLE I
Frame Rate of Eye Tracking

Scheme	Head movement	Frame rate (FPS)		
		Mean	Max	Min
Basic	No	15.04	15.74	13.89
	Yes	15.21	16.12	13.26
FRER	No	18.57	28.39	14.64
	Yes	19.34	29.95	12.01

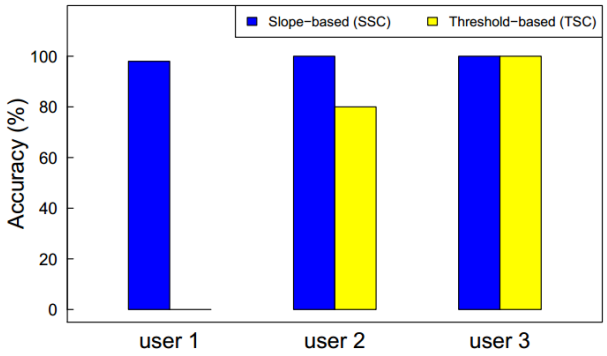

Fig. 3. The accuracy of eye-blink recognition of three users.

accuracy of eye-blink recognition, we set the threshold value of TSC algorithm to $T = 0.865$ and the threshold of SSC algorithm to $S = 0.08$. We observe that the accuracy of SSC algorithm is much higher than the existing TSC algorithm: On average, the former achieves the accuracy of 99.3 % while the latter attains the accuracy of 60.0 %. We can also see that the SSC algorithm achieves a high accuracy regardless of eye size, while the accuracy of TSC algorithm is dependent on the eye size of a user: The maximum difference in the accuracy of SSC algorithm among three users is 2.0 % while that of TSC algorithm is 100 %.

From the above results, we conclude that the FRER scheme is not only computationally efficient for a real-time HSI app, but also robust to the users with different eye sizes.

Acknowledgement

This research was supported by National Research Foundation of Korea (NRF) Grant (No. 2009-0083495) and by Basic Science Research Program (No. 2013R1A1A1012290) through the NRF, which is funded by the Ministry of Science, ICT & Future Planning.

References

[1] K. Grauman, M. Betke, J. Gips, and G. Bradski, "Communication via eye blinks - detection and and duration analysis in real time," in *Proc. IEEE CVPR01*, Kauai, Hawaii, Dec. 2001, pp. 1010 - 1017.

[2] M. Chau and M. Betke, "Real time eye tracking and blink detection with USB cameras," in *Boston University Computer Science Technical Report No. 2005-12*, 2005.

[3] E. Miluzzo, T. Wang, and A. T. Campbell, "Eyephone: activating mobile phones with your eyes," in *Proc. ACM MobiHeld'10*, New Delhi, India, Aug. 2010, pp. 15 - 20.

[4] S. Han, S. Yang, J. Kim, and M. Gerla, "Eyeguardian: a framework of eye tracking and blink detection for mobile device users," in *Proc. ACM HotMobile'12*, San Diego, CA, USA, Feb. 2012.

Research of Motion Control System for Bridge Crane in Copper Electrolysis

Liu Cheng
School of Electric Information Engineering College
BeiHua University
Jilin City, China
yjs_lc@163.com

Cui Yang*
School of Electric Information Engineering College
BeiHua University
Jilin City, China
277968794@qq.com

Abstract—**As a kind of vehicle, mechanical structure and the site operation of bridge crane are relatively simple, it is widely used in industrial applications, such as production workshop and cargo handling field. This paper takes the bridge crane in copper electrolysis workshop as an example, high control performance of their job requirements is analyzed, and active anti-sway motion control system of bridge crane is designed, this paper proposes the bridge crane positioning sliding surface structure control as anti-sway control method, combined with the model and the nonlinear sliding mode control characteristics, a controller for multi-input and multi-output pure mathematical calculation is designed. It is difficult to determine the design parameters of sliding mode, then put forward the parameters optimization of sliding mode using genetic algorithm, and verified the validity of the proposed method, at the same time, it is possible apply sliding mode control anti-sway method for industrial. The MATLAB results show that the scheme has good control effect, and is an ideal control method.**

Keywords- copper electrolysis workshop; bridge crane; sliding mode control

I. INTRODUCTION

In the process of copper electrolysis production as shown in Fig. 1 (a), the work of the bridge crane is mainly to complete the lifting and extraction of the whole plate, and then lift the set of plate to the electrolytic tank, then lift a set of cathode plate lifting to the gap between the anode plate and a cathode plate are arranged at intervals and are not mutually contacted. This is the one electrolytic cycle of the production process, so in the whole workshop production process two cranes have been in the operation of non-stop as shown in Fig. 1 (b).

(a) Copper electrolysis plant

(b) Crane in the work

Figure 1. Working environment of bridge crane in the workshop of copper electrolysis plant

II. DYNAMIC MODEL OF BRIDGE CRANE

Bridge crane has three straight lines running mechanism, which is the cart, the car, and the elevator, bridge crane is always accompanied by the motion of the load, in the process of positioning make the crane positioning model into complex positioning and swing model. In order to solve the problem, the principle of the swing is needed to establish the model of the crane's position and swing. On the basis of analyzing the mechanism of crane movement and swing, the concrete physical model is abstracted, and Lagrange equation is used to establish its dynamic model, which lays a good foundation for the following research.

Mechanism analysis of crane movement

The three main body of the bridge crane operation determines its operating mode and motion characteristics. Due to the car, the car's start, stop or speed change, is big, the acceleration of the car has changed, the load inertia of its own, its movement will lag behind, flexible connecting wire rope will deviate from the lead, which also caused the load swing. Because of the research of crane in the electrolytic copper shop, the influence of the wind load and the wind load is not considered.

The research found that the swing of the large and small car running simultaneously is the synthesis of the vehicle and the direction of the movement. Considering the electrolytic copper plate lifting special sling for four corner hanging structure and engineering experience confirmed the hoisting structure and single point hanging consistent goods does not rotate. Fig. 2 shows sports physical model.

Load anti essence of pendulum is to control the swing angle (sling L and H angle) within the scope of the provisions of, or in larger swing angle can reach the destination or in the car before and after the smaller time zone, weakening to a smaller range of motion or even zero. So that the goods can be accurately and quickly put into the designated point.

Jilin Provincial Department of education project.(104115039)
Research team of high power rectifier equipment patent demonstration(20150312040ZG)
(20150519023JH)
(2014167)

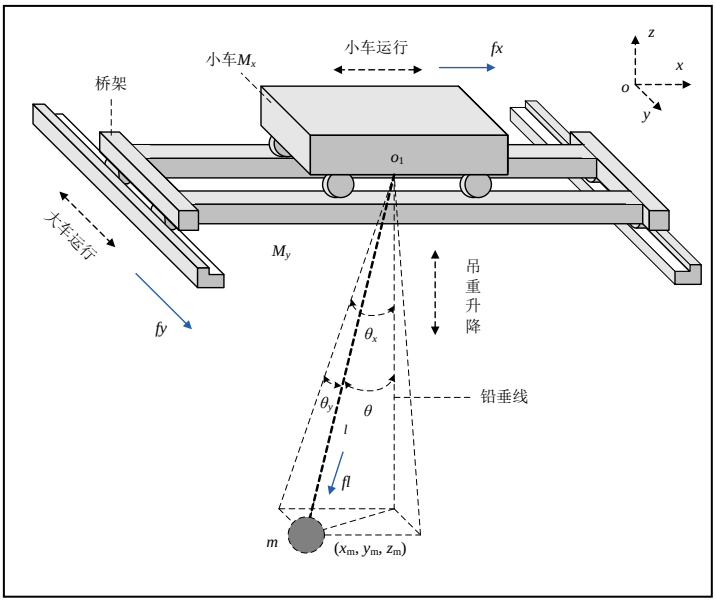

Figure 2. Physical model of bridge crane movement

All of the control of the machine equipment is based on the full study of the mathematical model of the control object. The motion control of the crane is no exception. In the three directions of the coordinate axis, X axis, Y axis and Z axis are the three main mechanisms of the crane, as shown in Fig. 2. Therefore, the dynamic model is established from the angle of geometry and physics, and it is convenient to analyze and control the motion of the whole crane.

III. CRANE POSITIONING AND ANTI SWING CONTROL STRATEGY

In this paper, the sliding mode variable structure control (SMC) strategy is used to control the load of the crane and the precise positioning of the crane. Usually, SMC can change its structure in order to realize the control performance, it has the advantage of reducing the system to the system, strong immunity, and insensitive to the uncertainty, and the response speed is quick.

The sliding mode controller is designed by using the sliding mode variable structure design. Firstly, the sliding mode surface is set to zero and the error vector tends to zero.

Sliding mode control parameter

In the process of evolution, adaptation degree determines the fate of the individual, excellent individuals in the group more and more, to move closer to the problem of the advantages of near, in order to get the best solution, after 150 generation evolution of the genetic algorithm, the optimized results for X=[1.8172, 7.9851, 1.0412, 3.9571, 7.0108, 13.0890, 12.9462, 1.6065, 0.7275, 0.8371, 15.1850, 11.4930, 8.6125].

IV. MOTION SIMULATION RESEARCH

In the simulation experiments, the M_x is 100kg and M_y is 50kg, Dx=0.1kg/s, Dy=0.2kg/s, Dl=0.1kg/s, and m=5kg, respectively. System simulation under two different positioning conditions is given.

Simulation curve can be seen in Fig. 3 system in 13 seconds for car positioning, the load swing is eliminated, in the process of operation, the load swing Angle not more than 10 degrees, also control scheme presented in this paper the three-dimensional system of crane control achieved good control effect, in order to prove that the method can meet the requirements of crane freedom of movement, another set of initial conditions of simulation. Take the system's initial conditions (x_0, y_0, l_0) = (6,8,7), system for a given input (x_d, y_d, l_d) = (1, 2, 3), for its simulation results in Fig.3.

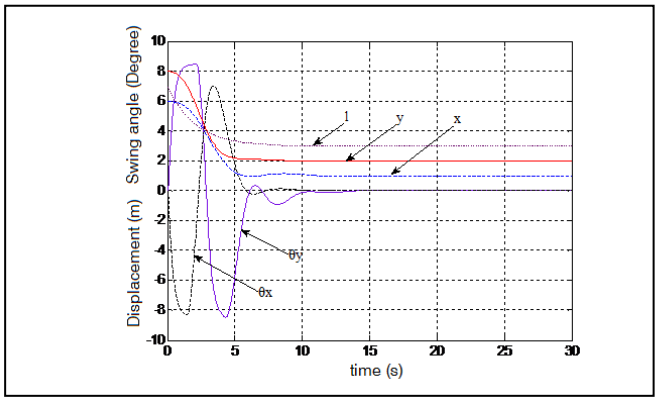

Figure 3. Initial conditions (x_0, y_0, l_0) = (6,8,7), given input (x_d, y_d, l_d) = (1, 2, 3)

Similar to a set of data, the 5 curves in the range of 10~15 seconds to achieve the car's positioning and load swing elimination, in the course of the operation, the load of the maximum swing angle is not more than 10 degrees. Simulation results show that the control scheme proposed in this paper can meet the positioning and anti swing control of the crane system. The control scheme proposed in this paper can meet the positioning and anti swing control of the crane system, and the reciprocating motion can be completed, and the control effect is good, which can meet the requirements of the crane in the operation of the 3D system.

REFERENCES

[1] Li DZ and Wang W. An intelligent sliding mode controller for vibration suppression in flexible structures[J]. Journal of Vibration and Control 2011(17): 2187-2198.

[2] Song B and Sun JQ. Sliding mode control of uncertain dynamical systems with time delay using the continuous time approximation method[J]. Journal of Vibration and Control, 2012(18): 1254-1260.

[3] Solihin MI, Wahyudi and Legowo A, Fuzzy-tuned PID anti-swing control of automatic gantry crane[J]. Journal of Vibration and Control, 2010(16):

[4] Wen Yu, Marco A. Moreno-Armendariz, Floriberto Ortiz Rodriguez. Stable adaptive compensation with fuzzy CMAC for an overhead crane[J]. Information Sciences, 2011(181): 4895-4907.

Experimental Determination on Optimal Resolution of Banknote Image by Considering Serial Number Recognition Accuracy

Young Pyo Hong
Dept. of Computer Science,
Graduate School, Sangmyung University,
Seoul, Republic of Korea
E-mail: coolcoolandy@hanmail.net

Eui Chul Lee
Corresponding author,
Dept. of Computer Science, Sangmyung University,
Seoul, Republic of Korea
E-mail: eclee@smu.ac.kr

Sang-Ug Kang
Dept. of Computer Science, Sangmyung University,
Seoul, Republic of Korea
E-mail: sukang@smu.ac.kr

Daesik Jeong
Kisan Electronics,
Seoul, Republic of Korea
E-mail: jeong.daesik @kisane.com

Abstract— **In this study experimental verification is performed with the product K2 manufactured by Kisan Electronics which can capture banknote as 150 DPI visible image. In the captured Russian ruble banknote image, serial number is recognized for detecting fake or forgery banknote. Generally, high resolution image guarantee high accuracy of serial number recognition. However, high resolution image sensor induce more expensive product. The purpose of this study is to analyze the accuracy of the acquired serial numbers according to resolution. The serial number recognitions are performed through using the images between 80 DPI and 180 DPI with 10 DPI intervals. Although the recognition accuracy of 180 DPI is expected to show the highest one, we will find the optimal resolution by considering both the recognition accuracy and the price of image sensor.**

Keywords-componet; Banknote, Serial number, Bilinear interpolation

I. INTRODUCTION

Since 2003, the credit card industry has been continuously grown. 4.9 credit cards were possessed per economic person and the proportion of payment with a credit card accounted for 59.6 percent of private consumption expenditure in 2011 in South Korea. People use their credit cards more than cash and credit cards are the most active means of payment [1].

However, banknotes are still used in basic financial transactions. The recognition of various kinds of banknotes and the counterfeit discrimination are essential skills in automated banknotes processing unit. There are different kinds of banknotes and various methods of counterfeit discrimination and the discrimination which uses banknotes images from Contact Image Sensor (CIS) or a camera is widely used [2]. Especially, serial number recognition is necessary in order to counterfeit discrimination and tracking banknote distribution.

To detect optimal point between the image resolution and the recognition accuracy of serial number recognition by considering the cost of device, the serial number recognition accuracies are measured using banknote image with various resolutions in this research. For that, banknote images of Russian ruble are acquired by a CIS sensor with 150 DPI by using K2 sorter machine manufactured by Kisan Electronics. The captured images are resized to between 80 DPI and 180 DPI with 10 DPI intervals. Although it is good to utilize high quality images of 180 DPI, this study proposes to investigate the correlation between prices determined by resolution of image sensor and recognition accuracy.

II. IMAGE RESIZING METHOD

As Figure 1 shows, bilinear interpolation which is the most common interpolation algorithm is an operation using the sum of value multiplied by weights on each pixel and four pixels adjacent to the original image mapped with new pixel. At this point, pixel A and B are integers and x and y are real numbers between 0 and 1. The weights are in inverse proportion to the distance from each adjacent pixel.

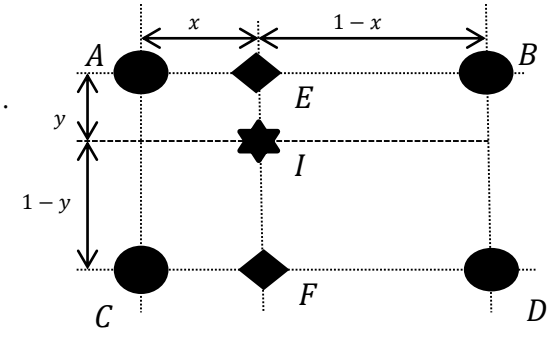

Fig. 1. Conceptual diagram of bilinear Interpolation for determining *I* pixel value

This paper is sponsored by the fund of Employment contract SW master's program from National IT industry Promotion Agency.

Figure 1 is the process of performing bilinear interpolation using the values of four adjacent pixels A, B, C, and D in order to find interpolated pixel I. That is, bilinear interpolation can be explained by performed three times of linear interpolation as equation (1).

$$\begin{aligned} E &= (1-x)A + x\mathrm{B} \\ F &= (1-x)C + xD \\ I &= (1-y)E + y \end{aligned} \qquad (1)$$

As the expression (1), the interpolated pixel E is calculated using the pixel A, pixel B and the weight x on the basis of law of proportions. The interpolated F which refers to the pixel C and D can be calculated by the same way. The final interpolated pixel I is computed using the interpolated pixel E, F and the weight y. Although bilinear interpolation embodies a relatively simple calculation process, it has a weakness that the edge of the expanded image is not smooth [3].

III. EXPERIMENTS

A. The product for banknote image acquistian

In this study, K2 manufactured by Kisan Electronics was used in order to acquire banknote images as 150 DPI. The K2 banknote sorter machine includes several kinds of sensors such as UV (UltraViolet), MG (Magnetic), IR (Infrared) and US (UltraSonic), and visible CIS.

Fig. 2. K2 manufactured by KISAN Electronics which has two output pockets [4]

B. Experimental banknote image

In this experiment, Russian ruble banknotes were used. 150 DPI images were captured by using CIS sensor of K2 machine. The number of images was 4,320. The images include all kinds of ruble (RUB) banknote such as 10 RUB, 50 RUB, 100 RUB, 500 RUB, 1000 RUB and 5000 RUB.

C. Results

In this experiment, it is expected that there is a correlation between the banknote image resolution and the recognition accuracy of serial number. In current stage, serial number recognition accuracy using 150 DPI image is 98.3% which is calculated by dividing false recognized characters by total number of characters. In here, serial number recognition method was our Lab. made supported by Kisan electronics which was based on character image template matching based one.

For experiment, serial number regions were cropped at each banknote image. Then, 4,320 cropped images were resized to 80 ~ 180 DPIs with 10 DPI intervals. As mentioned previous section, interpolation issues during resizing were solved by bilinear interpolation. The examples of resized images are shown in Figure 3.

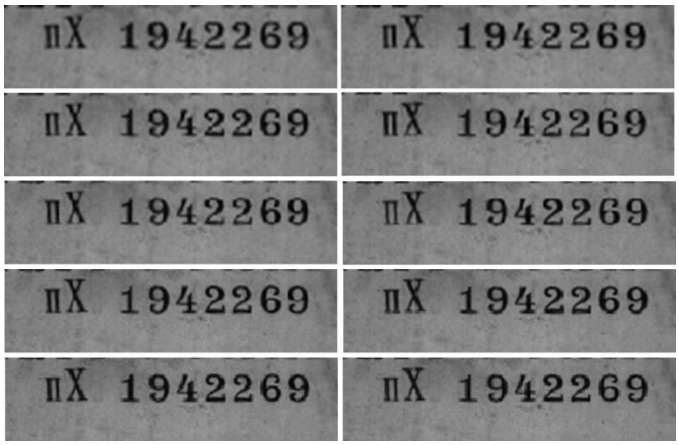

Fig. 3. Resized images from 80 DPI (top-left) to 180 DPI (right-bottom) with 10 DPI interval (150 DPI image is excluded)

With experimentation, this study proposes to seek a good compromise between increment of machine price and recognition performance in relation to high resolution image acquisition.

REFERENCES

[1] Jeon, Hyeon Jin, "Current status of the credit card industry and subsidy effects analysis based on the methods of payment," Konkuk Univ. master's thesis.

[2] Kim Byung Kyun, Seung Byung moon, Lee Gun Jae, Lee Wang Heon, "Remote banknote recognition using smart phone camera and wireless network," Journal of ICROS, 2015, vol.2015, No. 5, pp.169-170.

[3] Hae Min Moon, Sung Bum Pan, "VLSI architecture of digital image scaler combining linear interpolation and cubic convolution interpolation," Journal of IEEK, 2014, vol.51, No.3, pp.112-118.

[4] http://kisane.com/our-service/k2/ (Accessed on 24th Oct., 2015)

A Low Power Subsampling CMOS Image Sensor for a Smart Security System

Hyundong Kim, Yongjun Cho, and Minkyu Song

Dept. of Semiconductor Science, Dongguk University, Seoul, KOREA
mksong@dongguk.edu

***Abstract*— In a security system, it is not always necessary to record a picture in a high resolution mode, when crimes or accidents are not happened. Thus it is possible to take a picture in a low resolution mode to reduce power consumption in a normal state. In this paper, a novel low power sub-sampling CMOS image sensor for a smart security system is discussed. Further, a power shut-down technique is also proposed. The prototype CIS chip is fabricated with a 0.11um CMOS process. While the power consumption is about 3.8mW in a high resolution mode, the power consumption of the proposed subsampling technique is about 1.0mW in a quaternary low resolution mode. Therefore, the power consumption can be extremely reduced, when the subsampling technique is adopted.**

***Keywords*—smart security system; subsampling CMOS image sensor; power shut-down technique; high resolution mode; low resolution mode**

I. INTORDUCTION

Recently, CMOS Image Sensors (CIS) are widely used in the field of industries, broadcast equipment, closed circuit television(CCTV), mobile appliances, digital cameras, and so on. As the market of CIS is growing, many kinds of applications need a lot of requirements such as high pixel resolution, low power consumption, high speed operation, high bit resolution, and so on. [1–4]. In this paper, a low power CIS with a new power reduction technique is discussed.

II. A LOW POWER SUBSAMPLING CIS

Fig.1 shows two kinds of images, a high resolution mode and a low resolution mode. It shows a comparison of each image obtained by changing the mode of the image sensor from a high resolution mode into a low resolution mode [1]-[4]. The low resolution mode reduces power consumption because it converts the image by lowering the existing pixel resolution. Fig. 2 shows the CIS block diagram that was designed in this study. The CIS structure is composed of pixels, column ADCs, and digital control blocks. The pixel converts the amount of light into the corresponding voltage, which then becomes the input for the ADC. The pixel output voltage is transformed into a digital code in the block of ADC. The digital control block controls the pixel, ADC, and output interfaces, respectively. Further, a pixel sub-sampling technique is also included.

(a) (b)

Fig.1. Pixel sub-sampling technique
(a) high resolution mode (b) low resolution mode

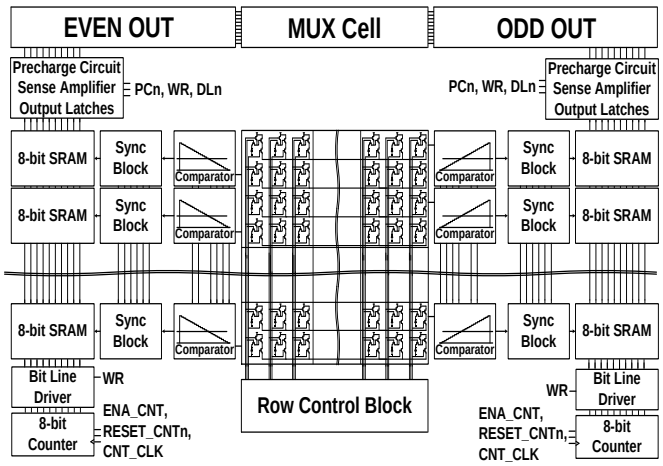

Fig. 2 Block diagram of the proposed CIS

Fig.3 shows the basic operation of a 1/4 pixel sub-sampling technique. Fig.3(a) shows a high resolution mode, where an even column array, an odd column array, and a row control array are working normally. Each row is composed of 2 pixels, and we assume that the pixels are A, B, C, and D. When the first row control is activated, the pixel voltages in A and B are converted into digital codes through each column ADC. Then, the second row control is activated in the same way as the previous one, and the digital codes of pixel C and D are obtained. Fig. 3(b) shows the operating principle of a low resolution mode. It has a 1/4 resolution compared to the high

resolution mode. Basically, the pixel output shown in A has an algorithm to generate the identical output for the other pixels. The simple explanations on the 1/4 pixel sub-sampling are as follows.

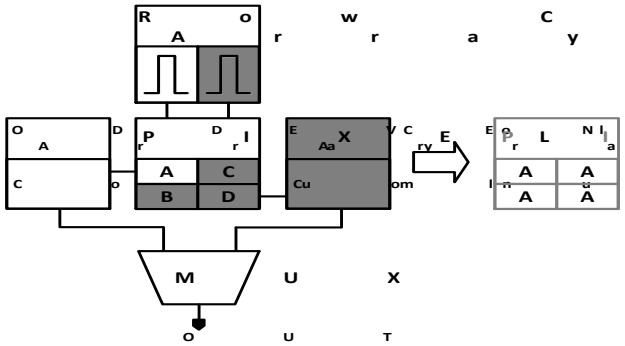

Fig. 3 The principle of 1/4 pixel sub-sampling technique

III. EXPERIMENTAL RESULTS

Fig. 4 shows the chip microphotograph of the designed CIS, and the core area of image sensor is about 6.67mm^2 (2.9 mm × 2.3mm) with a total chip area of 19.11mm^2 (4.9 mm×3.9 mm). The chip in this study has been fabricated with a Dongbu 0.11μm CIS process, which uses an active pixel sensor (APS) with a 4-Tr structure. The pixel size in this paper is 5.0μm×5.0μm. The odd column array is placed on the right side of the pixel array, and the even column array is placed on the left side of the pixel array in order to make a column pitch of 10 μm. Further, to reduce fixed pattern noise, all the columns are designed to have the same repetitive pattern. The CIS has the pixel array of QVGA resolution which has 320×240 pixels.

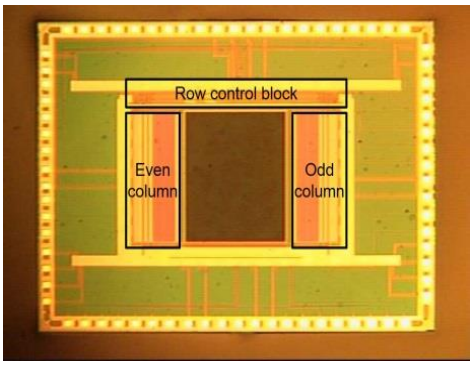

Fig.4 Chip microphotograph of the designed CIS

Fig.5 shows the measured QVGA sample images with the condition of the 8-bit resolution. It achieves the frame rates of 50frame/s at a main clock speed of 10MHz. Fig.5(a) shows the image of high resolution mode, and Fig.5(b) shows the image of low resolution mode. While the number of pixels at the high resolution mode is 64, that of low resolution mode is 16. Thus the proposed 1/4 pixel sub-sampling technique has been successfully verified. Tab.1 shows the performance summary for the CIS measured results.

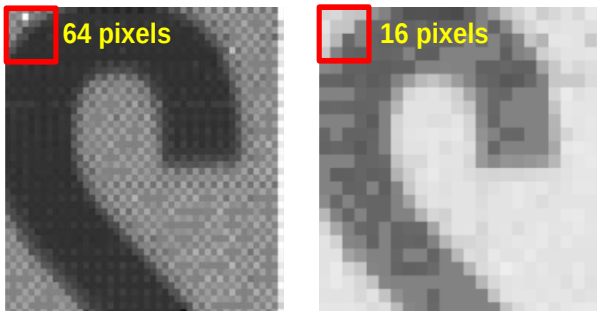

(a) (b)

Fig. 5. Magnified measured sample images
(a) high resolution mode (b) 1/4 low resolution mode

Tab.1 Performance summary of the prototype CIS.

Array Format	320×240
Pixel Size	5.0um×5.0um
ADC	8 bit
Frame Rate	50 frame/s
Power Supply	2.8V(Analog) / 1.5V(Digital)
Power	1.0mW(Low resolution mode)
Core area	19.11mm^2 (4.9mm×3.9mm)
Technology	Dongbu 0.11um CIS

IV. CONCLUSIONS

A low power CIS with a pixel sub-sampling technique for a smart security system was designed. At the high resolution mode, the CIS was based on the QVGA pixel resolution (320×240). However, at the low resolution mode, the pixel array was reduced by the 1/4 pixel sub-sampling technique. Thus the power consumption was also reduced by the ratio of a quarter. When the pixel sub-sampling technique was used at the low resolution mode, the power consumption was about 1.0mW.

ACKNOWLEDGEMENTS

This research was supported by Basic Science Research Program through the National Research Foundation of Korea (NRF) funded by the Ministry of Education.

REFERENCES

[1] H-G. Graf, C. Harendt, T. Engelhardt, C. Scherjon, K. Warkentin, H. Richter, J.N. Burghartz, "High Dynamic Range CMOS Imager Technologiesfor Biomedical Applications," IEEE J. Solid-State Circuits, Vol. 44, pp. 281-289, Jan. 2009.

[2] Scott Hanson, Dennis Sylvester, "A 0.45-0.7V Sub-Microwatt CMOS Image Sensor for Ultra-Low Power Applications," in Symp. VLSI Circuits Dig., pp. 176-177, Jun. 2009.

[3] M.F. Snoeij, A.J.P Theuwissen, K.A.A. Makinwa, J.H. Huijsing, "A CMOS Imager With Column-Level ADC Using Dynamic Column Fixed-Pattern Noise Reduction," IEEE J. Solid-State Circuits, vol. 41, pp. 3007-3015, Dec. 2006.

[4] T. Sugikiet al., "A 60mW 10b CMOS image sensor with column-to-column FPN reduction," in Proc. IEEE ISSCC Dig. Tech. Papers, pp. 108-109,450. Feb. 2000.

Thursday, Feb. 25

Session III-2 : (Oral) Control Information System

Study of High-precision Multi Star Simulator

Xinghua Gao
College of Mechanical Engineering, Beihua University
Jilin, China
e-mail: xhgao1964@126.com

Xinji Gan
College of Mechanical Engineering, Beihua University
Jilin, China
e-mail: ganxinji@sina.com

Abstract — According to application, a high precision digital star simulator has been designed. The star simulator is a device used to test and correct the detectivity and spatial resolution. The working principle of the star simulator is discussed in this paper, and some of the critical section, such as collimator and LED light source are designed and analyzed. The new-type white light LED is used as the light source and the constant current source control system based on PWM is used to control luminance of the light. As the test in the darkroom, the result shows that the star simulator designed in this paper is compact, reasonable and easy to control. The simulated magnitude can reach 0^m~7^m, the spectral range can cover the whole visible light and the control precision can reach $\pm 0.1^m$.

Keywords:star sensor, star simulator, optical system design, LED light source

I. INTRODUCTION

With the deepening of space exploration, star sensor as a kind of high precision attitude control instrument has gradually become the main trend of aerospace aircraft navigation. By detecting the position of the fixed star to determine the attitude of the aircraft, the star sensor is capable of adjusting itself, making the star sensor crucial of the aircraft navigation. In order to test and calibrate properties of the star sensor, star simulation to simulate space infinite pointolite has been applied to test and calibrate properties of measuring ability and spatial resolution. Calibration precision is affected because of the static star simulator's failure of real-time star catalog while position precision of dynamic star simulator is just $\pm 0.3^m$. Meanwhile, star roundness is also difficult to achieve. Therefore, research and development of new type static simulator has been the focus in the field of star simulator.

At present, traditional star simulator mainly selects xenon lamp and halogen lamp as light source. The shortcoming is that mounts of light source have to be added to promote range of star simulator. In reality, mode of multi light source is usually adopted to cover simulator spectrum range, which not only expands volume of the simulator but also increases control difficulty and expense.

II. STRUCTURE DEVELOPMENT OF THE HIGH PRECISION SIMULATOR

A. *Structure Design and Working Principle of Star Simulator*

The new type of static star simulation system is mainly composed of high precision parallel light pipe system, the LED light source system and control system. Its system structure diagram is shown in Fig.1.

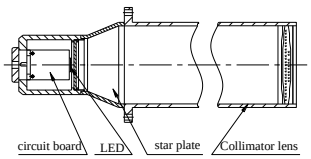

Figure 1. Structure of the Star Simulator

As is shown in Fig.1, considering eliminating system off-axis aberration and practical installation, transmission optical structure has been adopted because the system works in large field and full spectrum band range. In addition, this paper finds a way to install LED drive circuit of the light source to closed chamber of the parallel light pipe. The star board is placed in the focal plane of parallel light pipe and its distance with the LED light source installed in front of the drive circuit is adjusted by nut bolt. Light emitted from the light source is formed in parallel after going through collimator optical system and arrives at the star simulator to accomplish simulations of star atlas from the infinite distance. Via control mode of PWM constant current source , current output has been well controlled to gain the required duty circle and in this way, stellar magnitude simulated by light source is precisely controlled with the final control accuracy of $\pm 0.1^m$.

B. *System Design of the Optics*

According to the index, wave band of the system covers the whole visible light band, namely 400nm~800nm, with system aperture 92mm and distortion, curvature field and color difference will heavily affect imaging equality. Therefore, consideration of eliminating distortion, curvature field and color difference should be taken seriously.The focal length of the optical system can be calculated by equation $f` = L/2\tan\theta/2$ , Where $f`$ is focal length of optical system, L is the size of the star point, 10μm, θ is effective field of parallel light tube, 0.001° .According to the calculation, the effective focal length of the parallel light tube system can be obtained, 550mm and optical system is shown in Fig. 2.

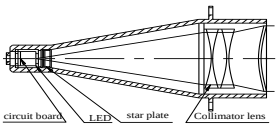

Figure 2. Structure of the Optical System

C. *Modeling and Optimization of Pptical System*

In order to fully verify the imaging quality of the optical system presented in this paper, the modulation transfer function curves of the optical system and spot diagram are produced. We can find that the optical system of the transfer function is close to the diffraction limit and RMS value of the image spot diagram formed by light source under different field of view is below 0.005, gaining good imaging quality and reasonable structure design. (the curves and diagram is omitted in here)

III. DESIGN AND TEST RESULTS OF THE SIMULATOR

A. *Spectral Modulation of LED Light Source*

According to the Hertzsprung-Russel diagram shown, The spectral types of stars have a certain relationship with the luminosity and that's to say, when the luminosity of the main sequence star is 0^m~7^m magnitude, the spectral type is F, G, K, covering the whole spectral band of visible light. As a result, spectral range of LED light source used in the system is the whole visible light.

B. *Calculation of the Luminous Flux of LED*

In order to meet the magnitude change of magnitude simulator, the maximum luminous flux of light is needed to know. According to index requirement, the system design of the collimator aperture diameter φ is 50mm and the star hole diameter is 50μm.Vertical distance, R between LED and star hole is 2mm and when the output magnitude is 2, the maximum light flux needed by the LED light source is 13Lm.

Based on the analysis above, the system selects XLamp@XP-E LED produced by CREE as light source with the spectral range of 400nm~800nm, which covers all the visible spectrum and the maximum light flux is 100ml.Its typical color temperature is 3700K~5000K. The LED has met the requirements of the spectrum range and large dynamic star magnitude.

C. *Control of the Light Source*

The CPU named STM32F103UET6-LQFP100 of the simulator can generate ten path PWM. The LED of the system is driven by PT4115 and the control of the star magnitude from 0 to 7 is realized by adapting PWM control technology. The principle structure of the star simulator controller is shown in Fig. 3.

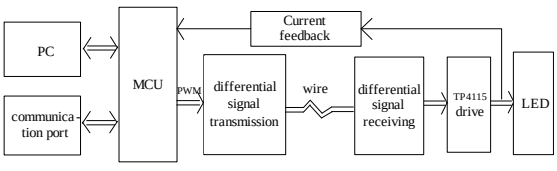

Figure 3. Structure of the Light Source for Star Simulator

In the work process, the LED is controlled by different duty cycle PWM signal generated by the single chip connected with the upper computer. The signal outputs after experiencing power drive and in order to promote the accuracy of the output current, close loop control system is formed and the core controller which generates the PWM signal is 16 bit system. The digital subdivision of PWM signal is 216, which is 65536 when the duty cycle is 100%, making the Illumination ratio of the LED more than 155:1 and finally realizing fine adjustment .Experiments show that control accuracy of the PWM control system arrives at ±0.1%, which has lived up to the accuracy requirement $\pm 0.1^m$ of the 0^m~7^m magnitude dynamics and magnitude simulator. Test Results of Star Simulator. (the material object is omitted in here)

D. *Test Results of Star Simulator*

In order to verify the star simulator, this paper selects to text it in the dark room. When the star simulator works, the luminance meter is placed in the outlet of the parallel light pipe to detect the illumination of the LED and furthermore, the number of PWM pulse needed under different star magnitudes has been correspondingly counted, As depicted in Table 1, Relationship curve of the simulated magnitudes and pulse number is shown in Fig.4.

Table 1 the number of PWM pulse and the corresponding illuminance and magnitude

Test point	1	2	3	4	5	6	7
experimental value of PWM	26108	10394	4139	1644	657	263	103
Intensity of illumination ($\times 10^{-3}$ Lux)	1011	403	160	64	25	10.1	—
Magnitude(m)	1^m	2^m	3^m	4^m	5^m	6^m	7^m

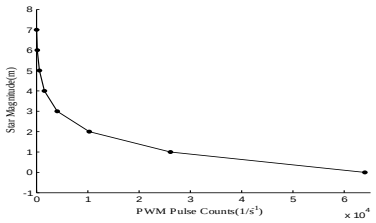

Figure 4. Relation of simulated star magnitudes and PWM pulse counters

Analyzing the test results, we can obtain that simulated magnitudes and distribution of the PWM pulse signal accord with 2.512 times. The relationship of the magnitude illumination and the pulse duty cycle is linear. When the star hole is less than 1mm, the result can get to 2.63 lx～2650 lx, well maintaining the accuracy less than ±0.1% and ensuring stability of the system.

IV. CONCLUSION

This paper has developed a high precision and multiple outputs digital magnitude simulator. The result shows that system design of the high precision simulator is reasonable and satisfies all requirements of design and use with compact structure and simple control. Meanwhile, the simulator rang of the star magnitude is up to 0^m to 7^m , the spectral range is 400nm~800nm and the control accuracy arrives at $\pm 0.1^m$. The simulator designed in this paper not only can solve the test and calibration problems of the star sensor but also greatly meets the calibration and correction requirements of the aerospace detection system, making the simulator more practically valuable.

The Application of PMSM in Motor Drive Control System of Patrol Robot

Yuan Guangjun
School of Electric and Information Engineering
BeiHua University
Jilin, China
e-mail: ygj791223@163.com

Shi Lichun
School of Electric and Information Engineering
BeiHua University
Jilin, China
e-mail: 16420874@qq.com

Zhou Zhenxiong*
School of Information Technology and media
BeiHua University
Jinchuan China
e-mail: 782033955@qq.com

Sun Jiyuan*
School of Electric and Information Engineering
BeiHua University
Jilin, China
e-mail: dick780818@163.com

***Abstract*—In order to reduce the power consume, and enhance the drive ability of robot, the PMSM is adopted in the drive system of patrol robot. The PMSM need a more efficient and cheaper drive system of patrol robot. The hardware platform of drive system of patrol robot based on the MC9S12XS128 is designed, the three-phase inverter is set up based on the BTS7960, PMSM is controlled by vector control algorithm, the three closed-loop control of position, velocity and current is realized. The experiment shows that actual current of axis q traces the setting value fast, and dynamic response of velocity is fast, and the trace of velocity in the steady state is stable, and the position loop is stable.**

Keywords- Microcontroller of free-scale, PMSM, Servo system, Patrol Robot

I. INTRODUCTION

The fire, under the storage rack, can be detected by the fireproofing robot of warehouse more handily than the fix detector [1]. A drive motor with high safety, Low energy consumption and fast response is needed by the robot, in order to fit for the complicated and flammable environment. PMSM can meet this requirement primely.

Because there is no field winding in the rotor, the performance of PMSM is higher than other motor. The efficient rare earth permanent magnet materials excitation is adopted to reduce the volume and the weight of the motor effectively, and realize the higher output torque, and reduce the rotational inertia of the rotor obviously. Therefore, the PMSM is widely used in the high performance alternating current servo drive system [2-4]. With the development of the efficient inverter, digital signal controller, high performance servo motor and control theory, it is inescapable tendency that the alternating current servo system replaces the direct current servo system.

PMSM is adopted in the patrol robot to reduce the power consumption of robot, enhance the drive capability of robot. Therefore, the key problem of this article is how to control the PMSM efficiently. Furthermore, TMS320LF2407 is applied in the reference [2] which is more expensively and more difficulty in nowadays. The MOSFET circuit, over current detect circuit, over voltage detect circuit and etc. are applied in reference [12] which is instability. The MCU of Freescale and the BTS7960 are adopted in the system to solve the problem above, and the vector control algorithm is adopted in the system to improve the efficiency of the control system of the PMSM.

II. POSITION SERVO CONTROL STRATEGY

Follow a series of assumption of the ideal model of the motor, after a series of derivation, the mathematical model of PMSM, under synchronous rotation of rotor and d and q coordinate system, is acquired [5-6].

The equation of the voltage and magnetic linkage of rotor is:

$$\begin{cases} u_{sd} = R_s i_{sd} + p\Psi_{sd} - \Psi_{sq}\omega_r \\ u_{sq} = R_s i_{sq} + p\Psi_{sq} + \Psi_{sd}\omega_r \\ \Psi_{sd} = L_d i_{sd} + \Psi_{fs} \\ \Psi_{sq} = L_q i_{sq} \end{cases} \quad (1)$$

In the equation (1), u_{sd} is voltage of axis d, u_{sq} is voltage of axis q, i_{sd} is current of axis d, i_{sq} is current of axis q, L_d is inductance of axis d of rotor, L_q is inductance of axis q of rotor, R_s is resistance of rotor, ω_r is angular velocity of rotor, $\omega_r=n_p\omega_{m,}$ n_p is the number of pole pairs of motor, ω_m revolving speed of rotor, Ψ_{fs} is magnetic linkage which is a part of excitation magnetic linkage of rotor, and pass through the stator winding, p is differential operator.

Equation of electromagnetic torque is:

$$T_e = 3n_p\left[\Psi_{fs} i_{sq} + \left(L_d - L_q\right) i_{sq} i_{sd}\right]/2 \quad (2)$$

The twelfth five scientific and technological research project of the education department of Jilin province(2014206).
The twelfth five scientific and technological research project of the education department of Jilin province(2014167)
Science and Technology Development Plan project of Jilin Province (20150519023JH)

Equation of motion of motor is:

$$T_e - T_L = Jd\omega_m / dt + B_m\omega_m \tag{3}$$

In the equation (3), B_m is friction coefficient, J is rotational inertia of motor, T_L is load torque.

If the salient pole effect of magnetic circuit is ignored, then L_d=L_q. From the equation of electromagnetic torque (2) above, the maximum torque can be acquired while the included angle between i_s and axis d is 90 °. Meanwhile:

$$T_e - T_L = Jd\omega_m / dt + B_m\omega_m \tag{4}$$

The conclusion can be made from above that the torque can be controlled via the control of i_{sq} to realize linearized control of torque of PMSM, just like control the direct current motor, as long as maintain the i_s be perpendicular to axis d [7].

Topology of the PMSM servo control system, basing on rotor field oriented, is shown as Fig.1.

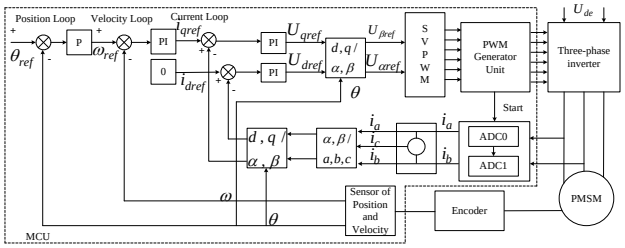

Figure 1. Topology of the PMSM servo control system

III. THE DESIGN OF HARDWARE OF SYSTEM

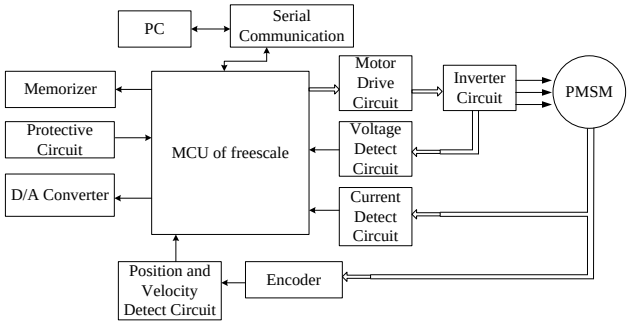

Figure 2. Topology of hardware system

Hardware of the system is mainly composed by six parts, PMSM, MCU, position and velocity detect circuit, main power component, drive circuit and D/A converter circuit. The circuits of main unit will be introduced.

IV. EXPERIMENT RESEARCH

The parameters of the PMSM using in the experiment are listed below: nominal voltage is 36V, rated current is 7.6A, rated speed is 3000min-1, rated power is 200W, number of pole-pairs is 4, d-axis inductance is 0.162mH, q-axis inductance is 0.142mH, stator resistance is 0.215Ω, magnetic linkage of stator side reacted by rotor is 0.012405 Wb. The precision of encoder is 1000 line. In order to verify the feasibility of the design of hardware system, the servo control software is written for the experiment research, the flow chart of software is shown as Figure 4. Software is written in C language.

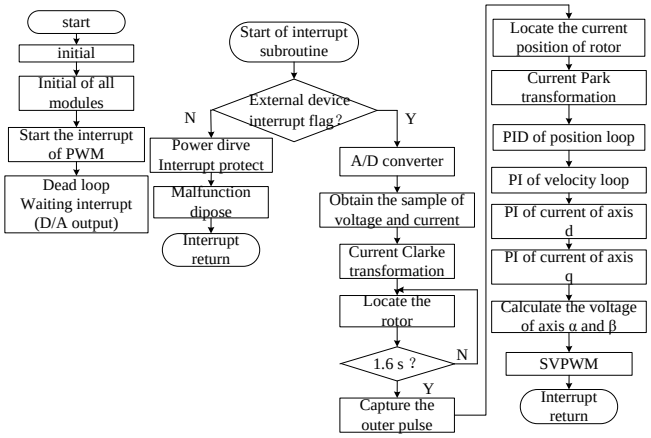

Figure 3. The main flow chart of software

Control period of system is 40μs. A/D conversion is triggered under the PWM even, and then program enter into periodic interrupt. After the sample signal was disposed, the new control signal of PWM is made by the program.

The result of experiment is also shows that the position loop is stable.

V. CONCLUSIONS

(1) The program of vector control algorithm is running on the MC9S12XS128 stability. Therefore MC9S12XS128 can replace TMS320LF2407 as the core of patrol robot.

(2) The current loop can maintain the proper functioning. Therefore, BTS7960B can replace the drive circuit built by independent components, and the right signal can be feed back by BTS7960B precisely.

(3) The time of velocity response and position response is short. Therefore, using PMSM as the drive motor, the drive abilities and mobile abilities of patrol robot are enhanced and power consume is reduced.

REFERENCES

[1] He Zhaoyu, Han Dan, “Fire Fighting of Multi Storied Factory Building Warehouse,” science and technology of firefighting, vol. 32, 2013, pp.81-83.

[2] Chen Rong, Kou Baoquan and Cheng Shukang, “AC servo motor and control,” Beijing: China Machine Press, 2008, pp.67-69.

The design of Hemodynamic Parameters Automatic Detecting Instrument with Function of Wireless Transmission

Yufeng Gao
Dept. of Institute of Electric & Information Engineering, Beihua University
Jilin, China
164085443@qq.com

Xiping Ma
Dept. of Institute of Electric & Information Engineering, Beihua University
Jilin, China
476036346@qq.com

***Abstract*—To design a hemodynamic parameters automatic detecting instrument to get the hemodynamic parameters from people through analyzing and calculating pulse wave from fingertip, then the instrument can send the detecting result to doctor and receive the reply message from doctor with the network of GSM. Making use of the reflective photoelectric sensor to get the pulse wave from fingertip, and the pulse wave can be analyzed and calculated automatically by the MCU of C8051F020, the detecting result of hemodynamic parameters can be sent to doctor through the TC35i module. The instrument realizes the function of collecting and calculating pulse wave, and the goal of sending and receiving message is also achieved. With the network of GSM, the instrument makes it easy to detect hemodynamic parameters without geographic restrictions, and it is very suitable for home health care.**

Keywords— hemodynamic parameter; pulse wave; TC35i; C8051F020

Ⅰ. INTRODUCTION

Currently, cardiovascular diseases have become one of the major diseases that threaten human health, and clinical studies have found that pulse wave from fingertip and cardiovascular diseases have a close relationship. The characteristic of pulse wave from fingertip can reflect many physiological and pathological features of cardiovascular system, and the hemodynamic parameters can be got through collecting and analyzing the pulse wave from fingertip. But the automatic measurement of the hemodynamic parameters is still a blind spot for these instruments. In this paper, the design of hemodynamic parameters automatic detecting instrument can achieve the goal of automatic measurement of hemodynamic parameters, and the hemodynamic parameters can be sent to a doctor by the GSM network through short message, and the user from a doctor can receive the reply short message, which has detection diagnosis. The instrument makes it easy to detect hemodynamic parameters without geographic restrictions [1].

Ⅱ. Overall design

The overall design of the instrument is shown in Figure 1.

The MCU of C8051F020 is the core of this instrument, it can save the value of personal information, such as, age, height, weight, systolic and diastolic blood pressure that are inputted through 4*4 keyboard .The MCU can also control the LCD module to display the pulse wave and the result of hemodynamic parameters, and control the TC35i module to send the result to the doctor through the GSM network and receive the reply message, which is from the doctor.

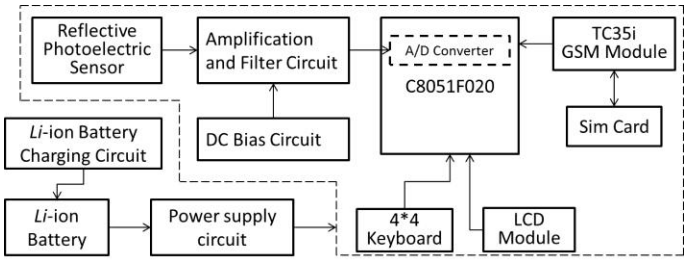

Figure 1. The overall design of the instrument

LCD module uses a resolution of 320 × 240 TFT-LCD screen, and it has 2.4 inch screen size.

In addition, the 4*4 keyboard as input devices can collect user's personal information and the doctor's cell phone number.

The instrument uses lithium battery to supply power for the entire system. The CN3068 lithium battery charging chip is the core of the lithium battery charging circuit, the chip only requires fewer external components, and meets the technical specifications of the USB bus.

Siemens makes TC35i GSM module, and we use it to complete the wireless transmission capabilities of this instrument by GSM network.

Ⅲ. THE DESIGN OF HARDWARE CIRCUIT

A. The principle of reflective photoelectric sensor

The instrument uses reflective photo plethysmo graphy (PPG) to collect pulse wave from fingertip. When a certain wavelength light beams to the surface of fingertip skin, the reflected light will be transmitted to the optical receiver. In this process, the light will be absorbed by the muscle tissue and blood, and the intensity of light which is received by optical receiver will be weakened, because the blood vascular volume is pulsatile changes under the action of the heart which is systolic and diastolic, the intensity of light which is received by optical receiver is also pulsatile changes as followed. This light signal is converted into

electrical signal, and then the changes of blood vascular volume can be obtained [2].

B. Amplification and Filter Circuit

The pulse wave from fingertip is weak physiological signal of human body, and the signal amplitude is in the millivolt level, so the amplification and filter circuit must be built to increase the signal amplitude and facilitate the acquisition of ADC. The pulse wave from fingertip is vulnerable to environmental light and the surrounding electromagnetic signal interference. Because the human pulse wave frequency is primarily between 0.1Hz and 8Hz, the first-order low-pass filter circuit whose cutoff frequency is 30Hz is used to filter the pulse wave signal.

C. The interface circuit of LCD module and MCU

The instrument uses a TFT-LCD module that is called XT240374P13, and the function of the LCD module is that, it can show the human–computer interaction and the pulse waveform of fingertip, and also the reply short message that is from the doctor.

D. GSM module of TC35i

TC35i module has both RF and baseband, and it supplies the standard AT command interface. TC35i module is equipped with a 40-pin 0.5mm pitch ZIF connector that connects to the cellular application platform. Special attention in the design is that, the TC35i module has a serial interface that is CMOS level, while serial port of C8051F020 is TTL level. Therefore, the circuit requires the NAND gate to achieve the purpose of level conversion.

The instrument only uses the function of sending and receiving short message, so the AT command about SMS is important for this design.

There are two commonly used modes for receiving and sending short message, the Text mode and PDU mode. Text mode is easy to use, but it does not support the Chinese short message. In this paper, the PDU mode is chosen, because it supports Chinese short message very well.

Ⅳ. THE DESIGN OF SOFTWARE

A. The extraction of a single pulse wave and calculation of hemodynamic parameters

The hemodynamic parameters need to be extracted from a single cycle of the pulse wave, so the first step is that, obtain a single wave from a set of pulse wave. It is the key point to realize the function of analyzing and processing the pulse wave automatically. The purpose is to extract the suitable pulse wave without human intervention.

In 600-waveform data point as a data source of extracting a single tilde, looking for pulse wave start and end points of a single tilde key is to find the minimal value in the data source[3].

Looking for the start and end point of single wave is to find out the minimum value from the data source which has 600 wave points. In order to achieve the purpose, the data source should be operated by the five-point differentiator. The differential equation is as follows:

$$y(nT) = \frac{1}{8}\left[2x(nT) + x(nT - T) - x(nT - 3T) - 2x(nT - 4T)\right] \quad (1)$$

B. The software design of TC35i module

To control the TC35i module, the main work is to write AT command to the module, and each AT command has a specific function. The detail software design of TC35i module is shown in the figure 5.

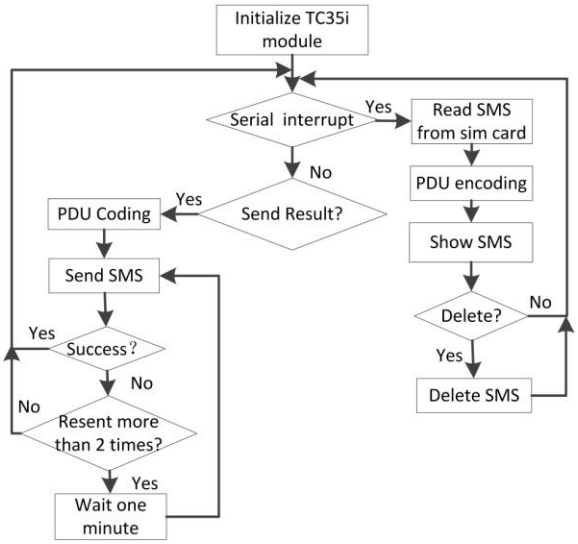

Figure 2. The diagram of software design of TC35i module

Ⅴ. CONCLUSION

The common method to diagnose cardiovascular disease is to calculate the hemodynamic parameters. However, most hospitals use invasive method to obtain these parameters. The invasive method can obtain these parameters accurately, but it also has a lot of disadvantage such as, costliness, danger and not suitable for people daily care. Clinical studies have shown that, pulse wave contains a large number of pathological and physiological information, so the hemodynamic parameters can be obtained through calculating and analyzing the pulse wave. The best advantage is that, the method is non-invasive.

This instrument uses pulse wave from fingertip to obtain the hemodynamic parameters of body, and the result of these parameters can be sent to the doctor through the short message with GSM network. The instrument is compact, easy to carry, and it can complete the detection in less than two minutes.

REFERENCES

[1] B.S. Kim and S.K. Yoo, *Motion artifact reduction in photoplethysmography usering independent component analysis*, IEEE Trans. Biomed. Eng., vol. 53, 2006, pp. 566-568.

[2] L. Sommo, *Time-varying filter for removal of baseline wander in exercise ECG*, in Computers in Cardiology, IEEE Computer Society Press,1991, pp. 145-148.

[3] R.E. De Meersman, A.S. Zion, S. Teitelbaum, J.P. Weir, J. Lieberman and J. Downey, *Deriving respiration from pulse wave: a new signal-processing technique,* Am. J. Physiol., vol. 39, 1996, pp.H1672-H1675.

Artificial Bee Colony and Neural Networks Optimization Test Generation Algorithm for Multiple Faults of Digital Circuits

ZHAO Ying
Electrical & information Engineering College
Beihua University
Jilin, China
e-mail zhaoying_jl@126.com

LIU Baisheng
Electrical & information Engineering College
Beihua University
Jilin, China
e-mail 731856651@qq.com

***Abstract*—A multiple stuck-at faults test generation algorithm based on artificial bee colony and neural networks for circuits is proposed in this paper because the test generation efficiency for multiple stuck-at faults in digital circuits is low. The algorithm converts multiple stuck-at faults to single stuck-at fault firstly and constructs the constraint circuit of the single stuck-at fault circuit using Hopfield neural networks. The test vectors for multiple stuck-at faults in the original circuit can be obtained by solving the zero value of energy function of the constraint network's interface circuit with artificial bee colony optimization algorithm. The experimental results on ISCAS'85 international standard test circuits show the feasibility and superiority of the algorithm.**

Keywords- artificial bee colony; neural networks; constraint circuit; energy function

I. INTRODUCTION

The rapid development of microelectronics technology makes the integration and complexity of digital integrated circuit higher and higher, which makes digital circuit test generation more and more difficult. In recent years, many scholars at home and abroad carry out a wide range of research and have some achievements, but the research has the disadvantage of long test generation time and low fault coverage, and most of the research model is for single stuck-at fault [1], the study of multiple stuck-at faults' test generation is very little. In order to guarantee the reliability of electronic system, it is usually necessary to have full test for some components[2], so test generation for multiple stuck-at faults of the digital circuit has very important significance. The multiple stuck-at faults are changed to equivalent single stuck-at fault in this paper, so the test generation of multiple stuck-at faults is changed to the test generation of single stuck-at fault. This paper adopted Hopfield neural network model in the single fault test generation, and construct the constraint circuit of the single stuck-at fault circuit, finally the test vectors for multiple stuck-at faults circuit can be obtained by applying artificial colony algorithm to solve the zero value of energy function of the constraint circuit' interface circuit. Experimental results on ISCAS'85 circuits show that the algorithm can quickly obtain multiple stuck-at faults' test generation vector, comparing with other literature, the test generation efficiency is improved obviously.

II. THE EQUIVALENT TRANSFORMATION OF MULTIPLE STUCK-AT FAULTS AND SINGLE STUCK-AT FAULT

Figure1(a) shows four lines with inputs V1, V2, V3, V4 ,and the respective outputs V5, V6, V7, V8. The multiple stuck-at faults here consists of the two stuck-at-0(s-a-0) faults on V1, V3 and the two stuck-at-1(s-a-1) faults on V2, V4.In order to transform the multiple stuck-at faults to single stuck-at fault,two additional gates should be inserted, one is in-line gate and the other is fault gate[3].

A. In-line gates: A two-input gate is inserted in each faulty line. The controlling input signal state for this gate is the same as the value at which the line is stuck. Thus, an AND(OR) gate is inserted in a line that is stuck-at-0(1) fault.

B. Fault gate: This is an n input AND gate that feeds all in-line gates either directly if the in-line gate is OR gate, or though an inverter if it is AND gate. The inputs to the fault gate are derived directly from all s-a-1 lines and via inverters from all s-a-0 lines. A single s-a-1 fault at the output of the fault gate is equivalent to the multiple stuck-at faults, so the multiple stuck-at faults are changed into equivalent single stuck-at fault. The s-a-1 fault at f in Figure1(b) is equivalent to the multiple stuck-at faults in Figure1(a).

To prove the method produced by the above is correct ,we examine the example of fig.1.We must prove two conditions:

Condition 1: Circuit equivalence. For Figure1(b),the functions can be obtained using Boolean algebra.

$$V_5 = V_1 \cdot (\overline{\overline{V_1}V_2\overline{V_3}V_4}) = V_1 \cdot (V_1 + \overline{V_2} + V_3 + \overline{V_4}) = V_1$$

$$V_6 = V_2 + \overline{V_1}V_2\overline{V_3}V_4 = V_2$$

$$V_7 = V_3 \cdot (\overline{\overline{V_1}V_2\overline{V_3}V_4}) = V_3 \cdot (V_1 + \overline{V_2} + V_3 + \overline{V_4}) = V_3$$

$$V_8 = V_4 + \overline{V_1}V_2\overline{V_3}V_4 = V_4$$

The results are identical to the original circuit.

Corresponding author:LIU Bai-sheng

Condition 2: Fault equivalence. The single stick-at fault after changing is identical to the multiple stuck-at faults of original circuit. For Figure1(a),the outputs are:

V_5=0; V_6=1; V_7=0; V_8=1

For Figure1(b),the outputs are:

$$V_5=0\cdot V_1=0; V_6=1+V_2=1$$

$$V_7=0\cdot V_3=0; V_8=1+V_4=1$$

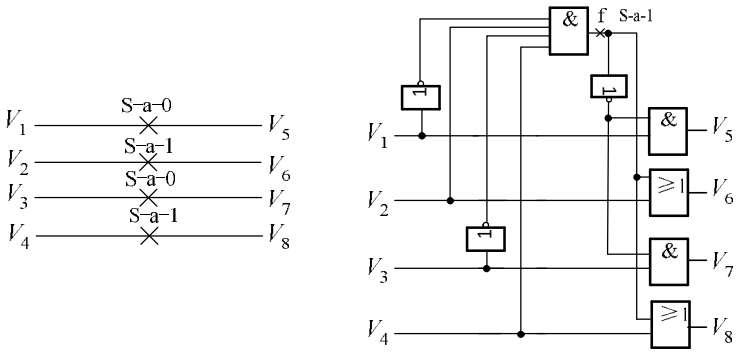

(a) The circuit of multiple stuck-at faults (b) The circuit after changing

Figure1. Change multiple faults into single fault

III. NEURAL NETWORK MODEL FOR SINGLE STUCK-AT FAULT

Hopfield two value neural network is applied to construct the model for single stuck-at fault. Hopfield two value neural network's energy function is defined by the formula:

$$E=-1/2\sum_{i=1}^{N}\sum_{j=1}^{N}T_{ij}V_iV_j-\sum_{i=1}^{N}I_iV_i+K \qquad (1)$$

Here V_i and V_j are state values(0 or 1) of neuron i and j, N is the number of neurons , I_i is threshold value of neuron i,T_{ij} is the weight value between neurons i and j, K is a constant. T_{ij}=T_{ji} and T_{ii}= 0.

The digital circuits are composed of basic gates circuits, so neural network model of digital circuits can be obtained by merging neurons of basic gates circuits and adding neurons' state values and weight values[4-5]. The energy function of digital circuits are the sum of energy function of basic gates circuits. For example, figure 2 is a simple digital circuit, the neural network model of OR gate and AND gate are shown in (a),(b),(c) of figure 3. The neural network model of figure 2 is shown in (d) of figure 3 by using the method, so the energy function of neural network for figure 2 is following:

$$E=-4V_4(V_1+V_2)-4V_5(V_2+V_4)-4V_6(V_3+V_5)$$
$$+2V_1V_2+2V_2V_4+2V_3V_5+2V_1+2V_2+2V_4+6V_5+6V_6 \qquad (2)$$

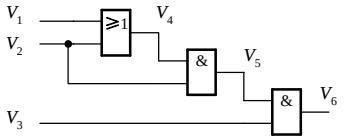

Figure2. A simple digital circuit

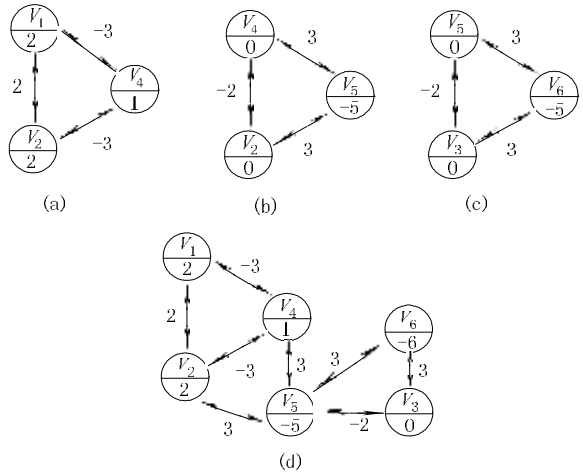

Figure3.Hopfield neural networks model of Figure2

Consistent states are the states that satisfy the circuit's function, other states that don't satisfy the circuit's function are called inconsistent states. When the neuron states are consistent with the function of the circuit[6], the energy function has global minimum value. In this paper, the energy function's value is 0 for all consistent states and energy function's value >0 for all inconsistent states.

In order to make the circuit be in consistent states, the constraint circuit should be constructed. The constraint circuits for single-output circuit and m outputs circuit are shown in Figure4 and Figure5[7].

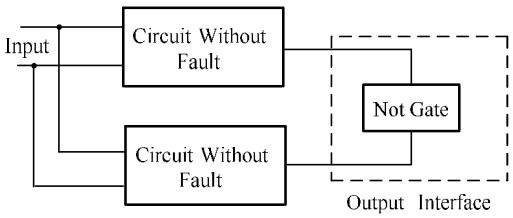

Figure4. Constraint networks for single-output circuit

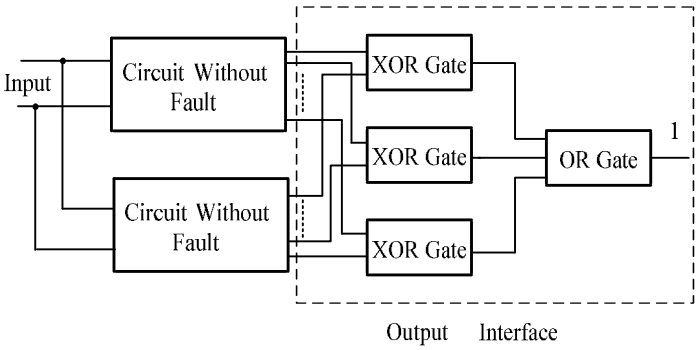

Figure5. Constraint networks for m-output circuit

Development of a sensing module for standing and moving human body using a shutter and PIR sensor

Won-Ho Lee, Ronnnie O.Serfa Juan, Hi-Seok Kim, and Hyeong-Woo Cha
Department of Electronics Eng., Cheongju University
298 Deaseong-ro Sangdang-gu, Chongju-city, Chungbuk, 360-764,
Cheongju, Republic of Korea
aultra@nate.com, ronnie71@naver.com, khs8391@cju.ac.kr, hwcha@cju.ac.kr

***Abstract*—Sensing module of standing and moving human body using shutter and pyroelectric infrared (PIR) sensor was developed. The module consists of Fresnel lens, PIR sensor, interface circuit of the PIR, micro control unit (MCU), and alarm light emitting diode (LED). The principle for standing human body is to chop the thermal heat of human body utilizing camera shutter. The human sensing signal in control part of this algorithm, detects the interrupt function. By unifying an apparatus and print circuit board (PCB), the developed product of the proposed sensing module can be replaced the commercially available detector. Experiment results show that sensing distance is about 7.0m and sensing angles is around 110° at room temperature. In these conditions, sending ratio is 100% and the power dissipation of the module rated as 100mW.**

Keywords-pyroelectric infrared sensor; sensor interface; chopping using shutter; standing body detector

I. INTRODUCTION

The pyroelectric infrared (PIR) sensor has high performance for IR detection at room temperature, and it does not need to use special and expensive cooling equipment like a photon-type detector [1]. Nowadays, pyroelectric devices are being implemented in human's daily life such as intrusion detection and smart usage of power consumption. Several studies were conducted in various applications, such as light sensing for buildings, traffic flow monitoring system, people's information collection [1]-[2]. However, in this case, detectors can be sensed only from moving human body because the PIR sensor has a differential reaction. Therefore, the conventional detector using PIR sensor cannot detect standing human body and its application is limited [3]-[4].

In general, to detect standing human body there are two methods, namely rotating PIR sensor like radar (rotation of PIR sensor) and chopping of infrared [5]. The former has a maximum detection distance of 6m and the sensing angle ranges between 0 to 180 degrees. However, the circuit implementation is complex and picked up large noise because of mixed circuit [5].

In this paper, we developed sensing module for standing and moving human body using chopping method which of consists of the following: a shutter, a Fresnel lens and PIR sensor [6]. We designed the circuits and the control algorithm, which makes up the prototype.

II. OPERATION PRINCIPLE AND MODULE CONFIGURATION

A. *Circuit design of sensing module*

Figure 1 shows the circuit diagram of the proposed sensing module for standing and moving human body using a shutter. The circuit consists of PIR sensor interface IC chip (BD 9251FV), MCU (MC97FI104), ISP (in-system programing), and RC network. BD9251FV act as amplifier and band-pass

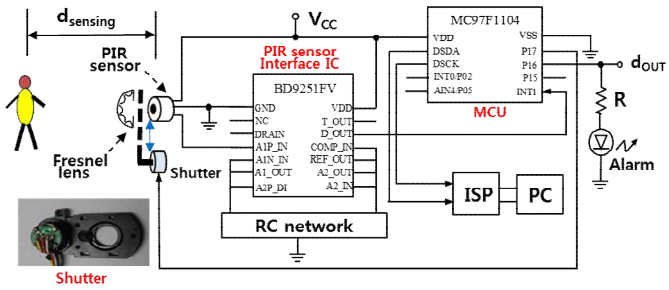

Figure 1. Circuit diagram of the sensing module

filttering for output signal of PIR sensor. The MCU act as controller of shutter motor, alarm, and algorithm. RC network made up of resistors and capacitors in order to operate amplification and the filteration. The shutter is a commercial product used in CCTV system. The shutter size is 3.4cm X 2.0 and the thickness and window diameter is 2.5mm and 10mm, respectively. This shutter operates on on-state at 3~5V_{DC} and at off-state 0V_{DC}.

The detecting principle of moving human body is same as the convention method. However, the detecting principle of standing human body has two steps; First, the shutter always open, PIR sensor detect a temperature of moving human body. If the PIR sensor detects human body's temperature, the MCU outputs alarms, otherwise the shutter is always on opened-state and MCU do not sounds the alarm. While, the next step is the standing state: occurs after detection of moving human body. This case, the MCU controls the algorithm of the shutter on opened-closed state alternately. This sensing operation is analogous to the differential action characteristics of PIR sensor like moving human.

This work was supported by the Industrial Core Technology Development Program (10049192, Development of a smart automotive ADAS SW-SoC for a self-driving car) funded By the Ministry of Trade, industry & Energy

B. *Mechanical design of the module*

Instrument for the sensing pipe size and prototype shown in Figure 2. To widen the detection angle, the distance between Fresnel lens and PIR sensor is 7.5mm, while the distance for edge of sensing pipe from shutter is 5mm.

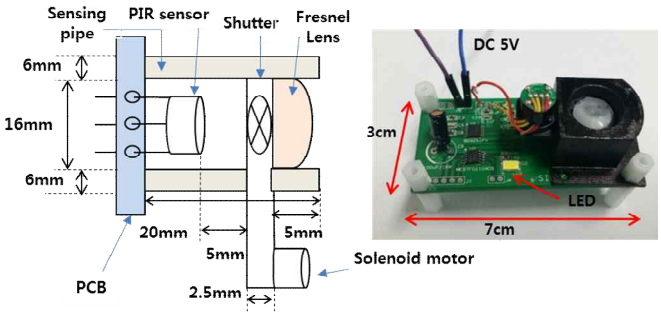

(a) pipe size (b) prototype

Figure 2. Design of instrument for sensing pipe size and prototype.

III. EXPERIMENT RESULTS AND DISCUSSION

We experimented with final prototype in order to detect distance and angle shown in figure 2(b). The devices in prototype were interface IC chip of BD9251FV [7], MCU of MC97FI104 [8], PIR sensor of RE431B [8], Fresnel lens of PF08-10W [9], a solenoid shutter. The resistor and capacitor value of RC network were same as data sheet of BD9251FV. The supply voltage was only DC 5V. The firmware was developed OCD2 emulator, a debugger, and standard 8051 compiler [8].

Figure 3 shows the characteristic for sensing distance versus sensing result at front side. The detection distance was measured by following the standing and movement of student. The output voltage is D_{OUT} or the power that supplies the LED during alarm state of MCU. It notes that the proposed sensing module can be detected with a distance of 7.5m for human body of standing and moving body. In this distance the detection ratio was 100%.

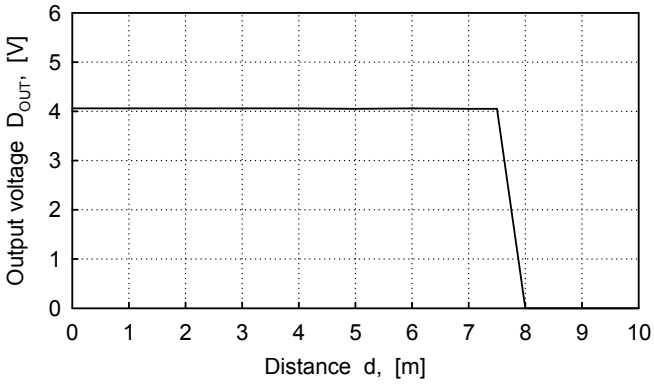

Figure 3. Measurement graph of sensing distance at front side .

Figure 4 shows characteristic for sensing degree of an angle from -60° to 60° at the front side. Detection angle follow a standing and moving of the student was measured. The distance was fixed a 7.0m. The output voltage was output D_{OUT} or LED alarm of MCU. It notes that the proposed sensing module can be detected angle from -55° to 55° at the front side for human body of standing and moving body. In this distance and angle the detection ratio was 100%.

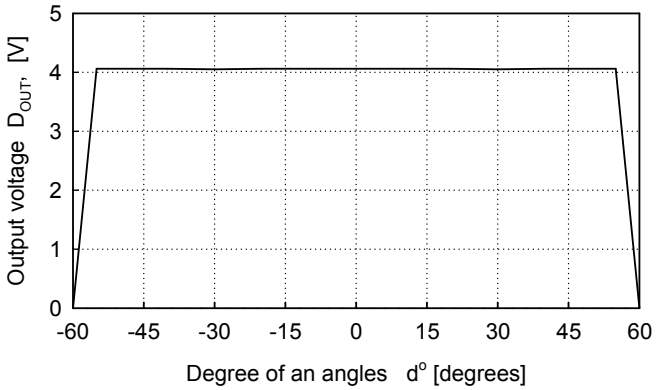

Figure 4. Measurement graph of sensing angle.

The final prototype is shown in figure 2(b) that has a power dissipation of 100mW with a supply voltage of 5V.

IV. CONCLUSION

Sensing module of standing and moving human body using shutter and PIR sensor was developed. The principle for standing human body is chopped utilizes the human body's thermal heat by the use of shutter. Experiment results show that sensing distance is about 7.0m and sensing angles is around 110° at room temperature. In these conditions, sending ratio was 100% and the power dissipation of the module rated at 100mW. By unifying an apparatus and PCB, the developed product of proposed sensing module can be replaced the commercially available detector for moving human body.

REFERENCES

[1] Josepth J. CARR, Sensors and circuits - sensor, transducers, supporting circuits for electronic instrumentation, measurement, and control, PTR, 1993.

[2] C. F. Tsai, M. S. Young, "Pyroelectric infrared sensor-based thermometer for monitoring indoor objects", Review of scientific instruments, Vol 74, No. 12, Dec. 2003

[3] Ying-Wen Bai and Yi-Te Ku, "Automatic room light intensity detection and control using a microprocessor and light sensors," Consumer Electronics, vol. 54, pp. 1173-1176, Aug. 2008.

[4] Mr. S.P Vijayaragavan and, Hardeep Pal Sharma,Guna sekar.C.H, S.Adithya Kumar, "Live Human Detecting Robot for Earthquake Rescue Operation," International Journal of Business Intelligents. vol. 2, pp. 83-87, June 2013.

[5] H.-W. Cha, Y.-S. Kim, S.-H. Park, P.-S. Hyun, S.-H. Yoon, 'Standing and moving human detector system using PIR sensor", Proc. of the 6th KIIT Summer Converence, vol. I, pp. 57-62, Jule 2007.

[6] H-W. Cha, W-H. Lee, H-S. Yun, "Development of standing and moving human body sensing module using shutter method," IEIE summer conference, vol. 37, no. 1, pp. 1005-1008, June 2014.

[7] Datasheet of BD9251FV, ROHM

[8] Datasheet of MC97F1104, ABOV Semiconductor.

[9] http://www.nicera.co.jp/pro/ip/ip-01.html#ip01

[10] http://www.diypro.co.kr/bbs/board.php?bo_table

Thursday, Feb. 25

Session IV : (Poster) Convergence IV

I/O Structure Design to improve the MicroGrid Gateway Hardware Interoperability

GabKeun Choi, GiUng Song, ByeongKeun Song, YongSuk Park, SsangSuk Oh, Hak Jang
Nexchal Co., Ltd.
SeongNam, Korea

***Abstract*—The research for the interoperability on gateway for micro grid has been performed mainly for the software such as Common Information Model (CIM) or OPC-UA. However, gateway for micro grid should satisfy electric requests for modbus communication with RS-232, 422, 485 to transfer the data or commands from various legacy devices not support IEC 61850 to Energy Management System (EMS), and should connect IEC 61850 based system and network. But, due to the features of existing legacy devices, there is inconvenience on system connection operation sometimes. In this paper, suggesting micro grid gateway design method to increase the interoperability of gateway for micro grid suggesting common I/O bus to maximize the interoperability by integrated management of I/O features of legacy devices.**

Keywords - Microgrid, Gateway, common I/O bus

I. INTRODUCTION

One way electricity transmission to the customer produced by existing electric power system has changed to the micro grid, independent dispersed local electric power supply system to maximize total network's energy using the electric power generated and supplied by prosumers, is having the limelight recently. [1] Accordingly, the devices to connect the new renewable energy such as wind power generation and sunlight generation to electrical power system is necessary. These devices need gateway to operate with Energy Management System (EMS).

Serial communication socket is used on micro grid to bring or transmit the data with the devices do not support IEC 61850, and the network gateway supporting Ethernet connection with EMS on IEC 61850 base has important role on interoperability of micro grid.

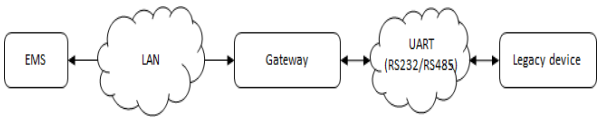

Figure 1 micro grid gateway

As [Figure 1], micro grid needs gateway to mutually operate different protocols of different manufacturer's legacy devices to connect with EMS. Also, below items should be fulfilled for ease of execution and site demands.

◯ UART(RS-232, 485, 422) and TCP/IP is mainly used as the protocol providing data, RS-232 and 485 do not used at the same time, however, it should be supplied at the same time on practical point of view.

◯ Gateway for micro grid needs robustness on the environment such as temperature and humidity and convenience in setting up because the install site condition is poor. [2]

II. GATEWAY I/O DESIGN FOR MICROGRID

As stated, micro grid is electric power supply system using distributed power and it is mainly formed with new renewable energy. Based on it, each control device installation site are mostly poor condition, so, especially, robust design for temperature, humidity, and service environment. Also, for legacy devices supplying data collected, but do not standardization, the protocols are different and each power supply system is different, so there are lots of restriction on installation and operation. To design gateway reflecting various requests from site, in this paper, designed optimized gateway for micro grid coincide with requests of site by design I/O common bus for integrated operation of different protocols.

A. Common I/O Bus

Generally used communication protocols in electric power device are RS485, RS422, RS232, and TCP/IP. RS232 is relatively simple and convenient communication type, but the communication distance is short, data transmission speed is slow and one-to-one communication. Also, it is single ended type, so weak to noise. RS422 and RS485 are differential, so strong to noise and data transmission speed is fast. Also, it can connect 1:10 and 1:32 for the devices, widely used in electric power devices. However, the connecting quantity of RS422 is smaller than RS485 as stated, so generally RS485 communication is commonly used. [3]

Meanwhile, in electrical power device, only one protocol among stated serial communication type is supplied, so it is difficult to operate each other. Using converter to overcome it, but sometimes communication error occurs because the electric feature is not matched. In this paper, suggested common bus for micro grid gateway to solve this problem. Designed converter for each protocol to accommodate various protocols stated and designed common I/O bus using Universal Serial Bus (USB). USB bus can corresponding low speed and high speed communication and used serial to USB driver offered as Linux open source. It is composed with 1:N having USB one port to several serial I/O structure to use several I/O. [4] Accordingly, each I/O device has unique ID, so when call the serial communication through USB, call it using ID. Also, by including L1 layer (physical layer) of protocol which has

different electrical feature on one board, improve signal feature to overcome potential difference error occurs when commercial converter.

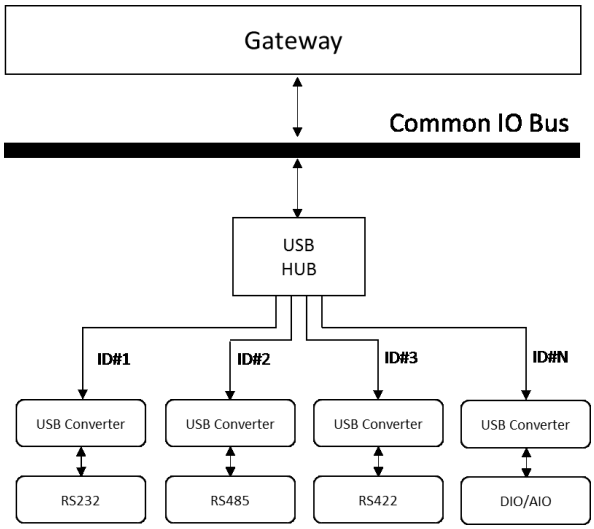

Figure 2 Common I/O bus

B. Specification design of gateway for microgrid

Most important function of gateway connecting different networks is connecting protocol for each network function. Especially, on gateway for micro grid, approaching on software for connection interoperability in upper level is also important, but connecting different physical features of different devices in low level is very important function.

In this paper, designed hardware specification standard as [Table 1] to fulfill the basics of gateway for micro grid stated, and especially, designed using 64-bit operation system for application software development convenience, also designed main memory as 8GB for smooth support for current programming language demands lots of memory.

Table 1 Microgrid gateway specification

Item		Standard
Basic data	OS	Linux
	CPU	Intel Baytrail (E3800)
	Main memory	8GB
	Debug terminal	2 Port
	SD card	1 slot
	Power button	1 ea.
LCD		8 inch
UART	RS232	2 Port
	RS485	2 Port
LAN Port	RJ45	2 Port
External I/O	AIO (5V)	16 Port
	DIO (5V)	32 Port
High power control (Relay:250V/15A)		2 Port

[Table 1] is the gateway designed based on the suggested standard and reflecting common I/O bus function stated.

Figure 3 Gateway for Microgrid

III. CONCLUSION

Communication feature of different devices and network connection are important on gateway for micro grid. In this paper, to reflect the features of gateway, not only approached in software, also designed suggesting common I/O bus type to improve hardware interoperability and improved hardware feature connection between gateway and device. Also, stably correspond Java based software development environment by supplying 64-bit processor and 8GB RAM.

REFERENCES

[1] https://ko.wikipedia.org/wiki/microgrid

[2] GK. Choi, GU. Song, SS. Oh, H. Jang, "I/O Structure Design for Microgrid gateway" in reading the book of 2015 KIEE Power Engineering Soceity Workshop, pp.191–192.

[3] https://ko.wikipedia.org/wiki/UART

[4] http://www.linux-usb.org/USB-guide/x356.html

A Bio-inspired Algorithm Based Time Synchronization Strategy in Infrastructure Wireless Mesh Networks

Seung Hyun Jeon
School of Electrical Engineering
KAIST
Daejeon, Korea
creemur@kaist.ac.kr

Jun Kyun Choi
School of Electrical Engineering
KAIST
Daejeon, Korea
jkchoi59@kaist.edu

***Abstract*—Wireless mesh networks (WMNs) have severe synchronization problem due to propagation delay. However, using the concept of bio-inspired algorithm has recently considered as synchronization solution. This paper proposes a bio-inspired algorithm based time synchronization strategy in infrastructure WMNs, which adaptively steers the beacon interval per mesh router (MR) or station (STA) for the delayed beacon due to a traffic overrun.**

Keywords-Infrastructure wireless mesh networks (WMNs); synchronization; bio-inspired algorithm; beacon interval

I. INTRODUCTION

In wireless mesh networks (WMNs), synchronization problem has still remained due to propagation delay [1]. Moreover, the conventional popular time synchronization protocol like network time protocol (NTP) is not proper for WMNs [2]. Recently, the researches on bio-inspired algorithm in WMNs have studied to solve time synchronization in distributed networks [1]. However, pulse coupled oscillators (PCO) based model fails synchronization due to transmission delay [3]. Besides, Kuramoto oscillator model is only synchronized on homogeneous delay [4]. In nature, for example, populations of flashing fireflies make the synchronization [3] and flocks converge as all birds fly with the same velocity [5].

In IEEE 802.11, an access point (AP) wakes up stations (STAs) with power saving mode as sending beacon frames periodically [7]. The beacon frame has timestamp, which can update local time for synchronization. However, IEEE 802.11 based WMNs still cannot guarantee synchronization due to deafness problem [8].

In this paper, we adapt flocking behavior to synchronization solution for WMNs like [6]. In detail, we propose a bio-inspired algorithm based time synchronization strategy in infrastructure WMNs. By a mesh router (MR) with gateway (G/W), time delay between the initial and the next synchronization can be reduced.

This work was supported by Institute for Information & communications Technology Promotion(IITP) grant funded by the Korea government(MSIP) (B0101-15-1270, Research on Communication Technology using Bio-Inspired Algorithm)

II. PROPOSED BIO-INSPIRED ALGORITHM BASED TIME SYNCHRONIZATION STRATEGY

A. Deployment, Spectrum Selection, and Channel Configuration

In our work, we consider infrastructure WMNs, which can be used for campus or office in small areas. Sometimes, infrastructure WMNs can be used to reducing outage in dense buildings. Here, we consider the distance among MRs is almost the same (i.e., uniform deployment) to reduce propagation delay for time synchronization and improve the effect on bio-inspired algorithm. In addition, throughput of WMNs is dramatically dropped by multi-hop routing (e.g., over three hops) [9]. Thus, we allow the only 2-hop routing like Fig. 1.

As presented in [10], we consider 5 GHz spectrum though the future Wi-Fi trend since wide, many channel bandwidths with low interference compared to 2.4 GHz can provide to WMNs. Finally, even though channels within 5 GHz spectrum have low interference, the MR with G/W and other MRs are configured with somewhat separate channels.

B. Proposed Time Synchronization Strategy

Fig. 1 shows the concept on a bio-inspired algorithm based time synchronization strategy. Beacon based time synchronization is described as virtual pulse. Default beacon interval is set as 100 msec [7]. The goal is to fit timestamps of other MRs and STAs into that of the MR with G/W in fast and repeatedly manner. First, before any transmission from the MR with G/W, the initial synchronization occurs. In Fig. 1, time delay about data transmission happens for 1-hop MR 1, STA 1 and *n*. Since the beacon late arrives at a receiver, ACK of the beacon including current time of reception is returned as feedback. Accordingly, the MR with G/W can adaptively steer beacon interval sent to each channel.

In order to control the adaptive beacon interval per MR or STA, a daemon within a peer-to-peer (P2P) application or a separate program can be required. For late arrival of the beacon, the interval at less than 100 msec can be set. Here, we can define threshold (Δ) for time shift. If Δ is small, re-

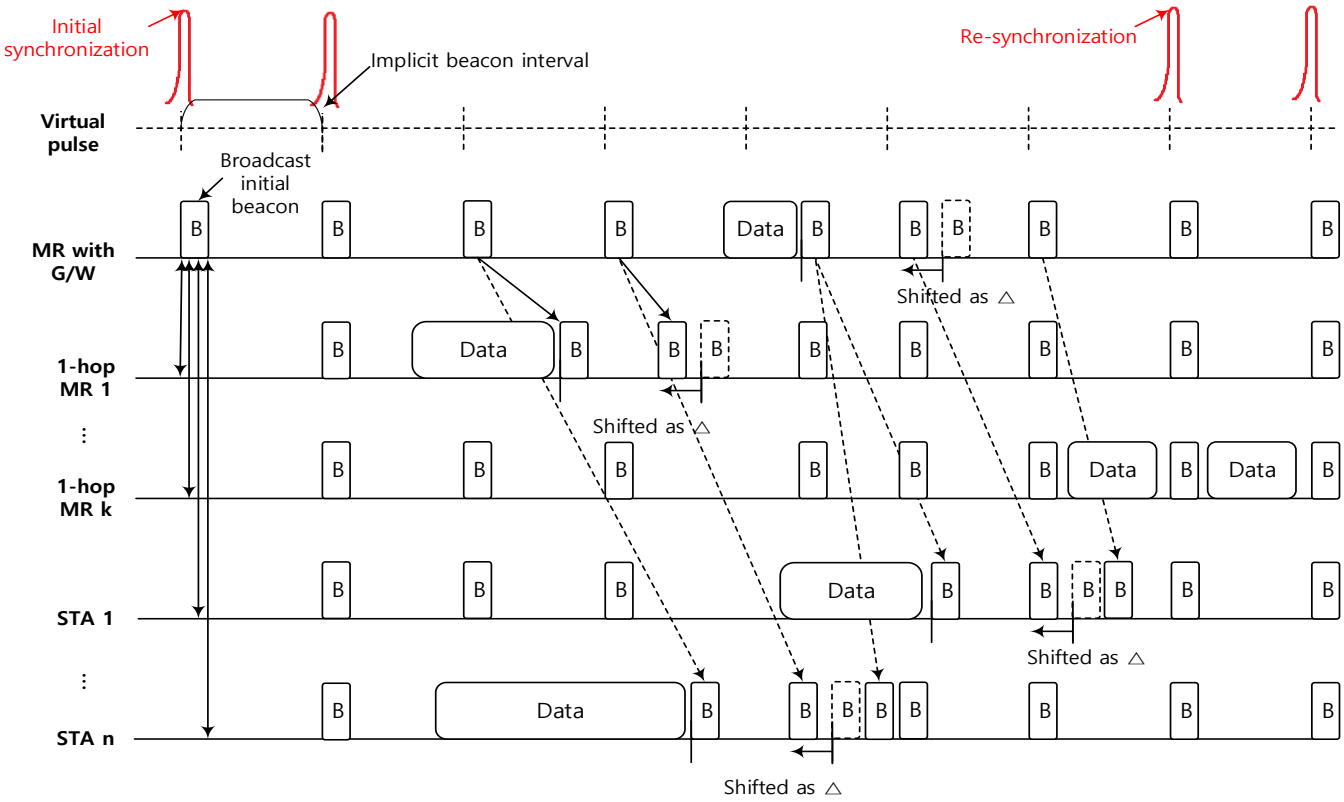

Figure 1. Concept on a bio-inspired algorithm based time synchronization strategy.

synchronization is slow. However, Δ is big, time shift may fail frequently. According to the number of STAs and data volume, an administrator for infrastructure WMNs can decide Δ.

C. *Discussion*

In Fig. 1, delayed beacon by data transmission are only considered. However, synchronization problem for large scale traffic as live streaming service may still happen. In our work, we consider 1-level based synchronization (without hierarchy). Because 1-hop MRs in Fig.1 should be synchronized their own STAs in 2-level. Thus, STAs over 2-level required to synchronized the beacon from 1-hop MRs. The timestamp of the beacon may not be accurate completely, compared to that of the beacon from the MR with G/W. For much synchronization in infrastructure WMNs, there may have the limit on the number of STAs. Finally, synchronization problem is required to select a proper bio-inspired algorithm as well as consider deployment, spectrum selection, and channel configuration for infrastructure WMNs comprehensively.

III. CONCLUSION

We proposed a bio-inspired algorithm based time synchronization strategy in infrastructure WMNs. The beacon interval sent to 1-hop MRs and STAs was adaptively steered and synchronization interval can be fast reduced. In addition, time synchronization for increasing STAs of 1-hop MRs may be considered as future work.

REFERENCES

[1] A. Tyrrell, G. Auer, and C. Bettstetter, "Synchronization inspired from nature for wireless meshed networks," *Proc. of the IEEE Conference on Wireless Communications, Networking and Mobile Computing (WiCOM)*, Wuhan, Sept. 22-24, 2006, pp. 1–4.

[2] http://www.ntp.org.

[3] U. Ernst, K. Pawelzik, and T. Geisel, "Synchronization induced by temporal delays in pulse-coupled oscillators," *Phys. Rev. Lett.*, vol. 74, no. 9, pp. 1570–1573, Feb. 1995.

[4] A. Papachristodoulou and A. Jadbabaie, "Synchronization in oscillator networks: switching topologies and non-homogeneous delays," *in IEEE Conf. Decision and Control and Eur. Control Conf. (CDC-ECC'05)*, pp. 5692–5697, Dec. 2005.

[5] F. Cucker, and S. Smale, "Emergent behavior in flocks," *IEEE Transactions on Automatic Control*, vol. 52, no. 5, pp. 852–960, May 2007.

[6] H.-H. Choi and J.-R. Lee, "A bio-Inspired transmit power control algorithm for linear multi-hop wireless networks," *IARIA International Conference on Networks (ICN)*, Feb. 2014.

[7] http://www.wi-fiplanet.com/tutorials/print.php/1492071.

[8] F. Dressler, O. B. Akan, "A survey on bio-inspired networking," *Computer Networks Journal (Elsevier)*, vol. 54, no. 6, pp. 881-900, April 2010.

[9] R. Sheshadri and D. Koutsonikolas, "Comparison of routing metrics in 802.11n wireless mesh networks," *in Proc. IEEE Inforcom'04*, Turin, Apr. 2013, pp. 14–19.

[10] W. Sun et al., "Wi-Fi could be much more," *IEEE Communications Magazine*, vol. 52, no. 11, pp. 22-29, Nov. 2014.

A Case Study of FDA Adverse Events on Depression

Hoon JIN
Dept. of Computer Science
Kyonggi University
Suwon, Korea
bioagent@gmail.com

So-Young Rho
Wol-Song Publishing Company
editgarden@naver.com

Chi-Bong Song
Wavus Company
cbsong@wavus.co.kr

Yong-Gyu Jung†
Dept. of Medical IT Marketing
Eulji University
Sungnam, Korea
ygjung@eulji.ac.kr

***Abstract*—Our study describes an analysis of taxon-specific characteristics after extraction and classification of samples involving drugs that cause side effects of depression (Depressive disorder, Depression) in the FAERS (FDA Adverse Events Reporting System) database. After filtering the drug attributes causing side effects, we tried to analyze the conditional dependent relationships between attributes using a Bayesian network.**

Keywords: Adverse event; Drug; FDA; FAERS; Depression; Side Effect.

I. INTRODUCTION

In 2010, the Korean Food and Drug Department received 64,143 reports of spontaneous adverse drug events; the total number was expected to exceed 10 million by 2014. Now these trends are increasing because in the aftermath of distribution accidents involving Aspirin used to treat hypertension, diabetes drugs, and Tylenol products used as an antipyretic and analgesic for children, concerns about drug side effects are on the increase. Drug safety assessment is the main research topic in most clinical trial processes, and the first step in detecting drug side effects is access to data on suspected adverse events. This study has surveyed and analyzed the cases involving certain drugs which caused depression as a side effect and extracted from the data collected by FAERS. Efforts were made to find hidden connections between the various attributes by building a Bayesian network.

II. BACKGROUND

A. Related research

[1] described mainly the structure and processing of the FDA adverse events database and presented a graph of the reliable reporting odds ratio (ROR) using an example of exenatide, a treatment for extreme pancreatitis, which showed a 95% classification rate when the Bayesian network was used. The FDA has conducted several of its own studies on drug side effects based on its data registered in the AERS. [2] analyzed data extracted for patients with two renal disease symptoms, retention and urinary retardation, using WebVDME 5.2. It examined the side effects that a drug used for these symptoms might cause by selecting PT (Prefer Term), where Prefer Term is a name of the side effects of interest, as a main experimental data attribute.

B. Bayesian networks

The Bayesian network offers great advantages for problem solving by expressing as a probability how each node is affected by the parent node as well as enabling prediction using dependency relationships with each of the variables. A number of useful machine learning algorithms have been suggested for disease prediction in experimental studies [3]. Of these, multi-layer perceptrons have shown the best performance for heart disease prediction, but the multi-layer perceptrons is deficient in showing hidden relationships among factors.

III. FAERS DATABASE

In the present study, about 1,800 million data points from the overall database for adverse drug effects from 2004 to 2012 were downloaded from the FAERS database created to track adverse drug effects for the FDA. These data were provided by doctors, pharmacists, healthcare professionals, and consumers and were collected from more than 140 countries.

A. Data Preprocessing

Table I shows the converted data attributes for experiments; the class value of interest is the outcome status code (Outcome_code) for each patient. PT (the preferred term for patient reactions) should be reported as diagnoses or symptom names, but the data collected from FAERS are recorded unclearly or include diagnostic opinions in many cases. Therefore, each PT from all the samples was converted into ICD-10 codes by manual checking [4].

Table I. Data Attributes.

Patient ID	Numeric
Drug name	Nominal
Role_cod	PS: Primary Suspect Drug SS: Secondary Suspect Drug
Duration_code	1dy: 1 day Over_1dy: more than one day Over_1wk: more than one week Over_2wk: more than two weeks Over_1mon: more than one month

† Corresponding author is Prof. Yong-Gyu Jung

	Over_6mon: more than six months Over_1yr: more than one year Over_3yr: more than three years
PT (ICD-10)	A, C, D, F, G, H, I, J, K, L, M, N, O, R, T, Unknown
De-challenge or Re-challenge	Y: Positive De(Re)challenge N: Negative De(Re)challenge U: Unknown D: Does not apply
Outcome_code	DE: Death HO: Hospitalization LT: Life-Threatening DS: Disability CA: Congenital Anomaly RI: Required Intervention to Prevent Permanent Impairment/Damage OT: Other Serious
Age	Numeric (year)
Sex	UNK: Unknown M: Male F: Female NS: Not specified
Weight	Numeric (kg)

IV. EXPERIMENTS

A. Drug classification and case studies

The 33 drugs related to depression in the data can be classified into five types: psychiatric drugs (some mainly used for depression and others for panic disorder, convulsions, and schizophrenia), chronic inflammation drugs (used for multiple sclerosis, arthritis, and spondylitis), a small number of non-smoking aids and contraceptives, and other drugs (Table II). Resuming and stopping the dosage are known to be main factors in decisions on drug administration by determining whether the reaction to natural drug treatment is positive.

Table II. Drug Products per Group.

Drug group	Products
Psychiatric	Bupropion; Celexa; Citalopram; Cymbalta; Effexor; Fluoxetine; Lexapro; Pristiq; Prozac; Seroquel; Zoloft; Zyprexa; Mirapex, Neurontin
Chronic inflammation	Avonex; Betaferon; Enbre; Forteo, Fosamax; Humira; Rebif; Tysabri; Vioxx
Non-smoking aids	Chantix; Wellbutin
Contraceptives	Depo-Phovera; Yasmin; Yaz
Other drugs	Accutane; Lariam; Oxycontin; Riba; Singulair

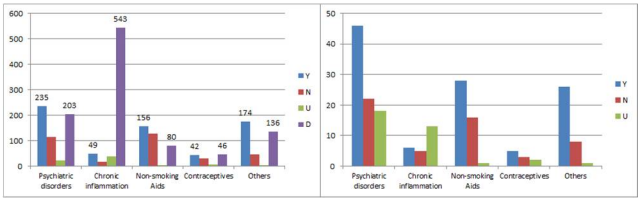

Fig. 1. Frequency of Drug Administration per Group (Left: De-challenge, Right: Re-challenge).

In Figure 2, the D code (does not apply) appears at high frequency in the chronic inflammation drug group. The Y code (positive de-challenge) was high for psychiatric drugs, non-smoking aids, and other drugs, and the N (negative de-challenge) was high for psychiatric drugs and non-smoking aids, but low for other drugs. The frequencies of the D code were not shown on the right side of the re-challenge graph, but the numbers were shown to be 489, 623, 319, 116 and 371 in order, and they accounted for the major portion of the re-challenge graph. This means that when a re-challenge was not performed, the possibility of side-effect occurrence was shown to be higher.

After data preprocessing, the final number of filtered attributes was 10, and the number of samples was 2,120 (Table I). The relationships between each of the items were analyzed using cleaned samples to determine which items affected the result state of the patient for each measured item. Figure 3 shows, in the form of a graph drawn using a Bayesian network learning algorithm, a model produced by 10-folds cross-validation of the entire data set. As shown in Figure 3, the final state of the patient was affected by weight, therapy period, indication of preferred term, re-challenge, and de-challenge. In addition, the therapy period was related with patient age, and the indication of preferred term was dependent on the drug and on the presence of de-challenge. Moreover, the choice of drug was affected by the patient's age and sex.

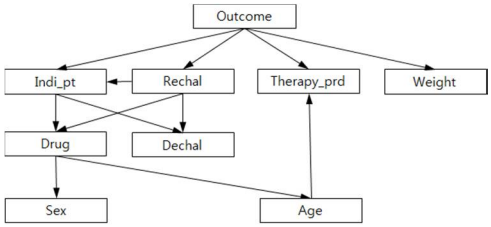

Fig. 3. Inferred Result from Bayesian Network.

V. DISSCUSSION

This study analyzed data regarding various patients who experienced depression as an adverse event when prescribed certain drugs. It was confirmed that although the experimental analysis targeted only a limited sample of the drugs causing depression as a side effect from the extensive database compiled by the FDA, the drugs belonged to the filtered samples included relatively large number of medications for mental disorders and chronic inflammation.

REFERENCES

[1] Poluzzi, E., et al., "Data mining techniques in pharmacovigilance: analysis of the publicly accessible FDA adverse event reporting system (AERS)", Data Mining Applications in Engineering and Medicine, Croatia: InTech, 2012, pp. 267-301.

[2] Division of Drug Risk Evaluation (DDRE), "Urinary Retention and Urinary Hesitation: NME Review Follow-Up", FDA Report, July 2007.

[3] Jung, Y. G and Jin, H., "Experimental comparisons of neural networks and logistic regres-sion models for heart disease prediction", Information: An International Interdisciplinary Journal, Vol. 16, No. 2(B), 2013, pp. 1295–1300.

[4] WHO, ICD 10 Codes, http://www.who.int/classifications/icd/en/.

Performance Enhancement of Column Indexing for Compressed Databases

Siwoo Byun
Dept. of Digital Media, Anyang University
Anyang, Korea
swbyun@anyang.ac.kr

***Abstract*—The memory-based column repository has become an attractive architecture for big database storage because of its compression performance and cheap flash drive has become a popular storage for high-performance servers because of its outstanding I/O performance, non-volatile, and power-economic nature. First, we introduce popular raw-oriented storage model and new column-oriented model. Second, we propose a dual-index model using flash memory to improve the effective performance of the high-speed column-oriented database system. Our index management scheme achieves superior search performance by index segmentation and compact indexing. In terms of the search performance, our scheme outperforms the traditional index management schemes.**

Keywords-component; Compressed database; Column-oriented index management; Compact index; Index Performance;

I. INTRODUCTION

Datawarehouses represent one well-known class of read-optimized system, in which periodically a bulk load of new data is performed, followed by a relatively long period of ad-hoc queries. In such environments, a column store architecture, in which the values for each single column are stored contiguously, should be more efficient [1]. This efficiency has been demonstrated in data warehouse marketplace by products like Sybase IQ [2]. With column store architecture, a DBMS need only read the values of columns required for processing a given query, and can avoid bringing into memory irrelevant attributes. In data warehouse environments where typical queries involve aggregates performed over large numbers of data items, a column store has a sizeable performance advantage [1, 3]. Recent flash memory storage has become a critical component in building high-performance servers. Especially, its storage density has been improved to a level at which it can be used not only as a main storage for portable computers but also as a mass storage for large-volume column databases [4].

II. COMPACT INDEX MANAGEMENT MODEL FOR COMPRESSED DATAWAREHOUSES

The B^+-Tree is an enhanced index of B-Tree and is considered to be more suitable than B-Tree for flash memory. In this respect, we proposed a new index management structure called *CptSeg-Index* (Compact and Segmented index), which is based on B^+-Tree and is able to efficiently handle the characteristics of flash memories and column-oriented database. The main idea behind the CptSeg scheme is based on dual index management and index segmentation.

Unlike the general row-oriented databases, column-oriented databases exploit data compression to save memory and to accelerate data access. Since column-oriented database handles mostly read-intensive datawarehouses, column-oriented database should manage big data accesses and frequent decompressing processes. Thus, the longer the data is, the more time it consumes in decompressing processes. In order to reduce this decompressing overhead and achieve fast data access, our CptSeg scheme exploits embedded segment indexing in leaf node. Unlike the general index scheme such as B-Tree, embedded segment indexing splits large data into small data units called embedded segment. The compression and decompressing overhead of the small segment is naturally lessened as compared to original large data.

In order to improve the performance of read operations in a column-oriented database system, we also exploit dual indexes. We classify the pointer of top node into two categories depending on their access type: *compact index* in case of read operation, *master index* in case of write operation. Since datawarehouses are modified infrequently, most transactions have a high possibility of remaining valid for a long time. In this case, top node select compact index which is very fast due to the space packing effect. In case of update operation, the top node selects master index and related nodes of the compact index are modified. This separation technique contributes to lessen index search overhead because the tree depth becomes shorter than that of master index. The basic architecture of our system is illustrated in Figure 1.

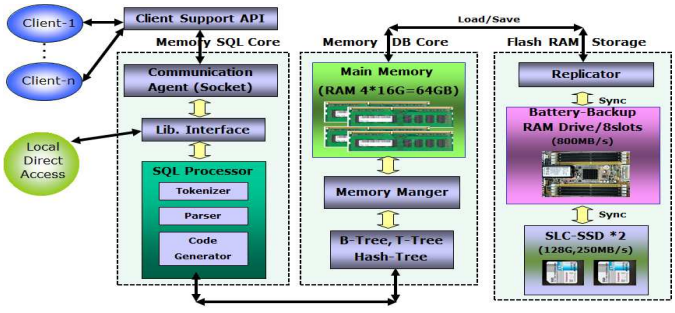

Figure 1. Architecture of Column-Memory Database System

Our index management algorithms performed by Index Manager (IM), which is responsible for handling search, insert, and delete operations associated with a database transaction issued by user applications.

Three types of index operations, CptSeg-Tree search, CptSeg-Tree insert, and CptSeg-Tree delete are transferred from IM. In order to read and write index nodes in flash memory, we devised two types of I/O operations, flash memory read and flash memory write, denoted by FM_Read() and FM_Write(), respectively. In order to compress the leaf or internal nodes efficiently, FM_Write() separates the node entries into a key array and a pointer array and then calculates the key offset and the pointer offset, after which it compresses the array of differences between the original value and the offset. The function of index manager can be shown in a diagram form as Figure 2.

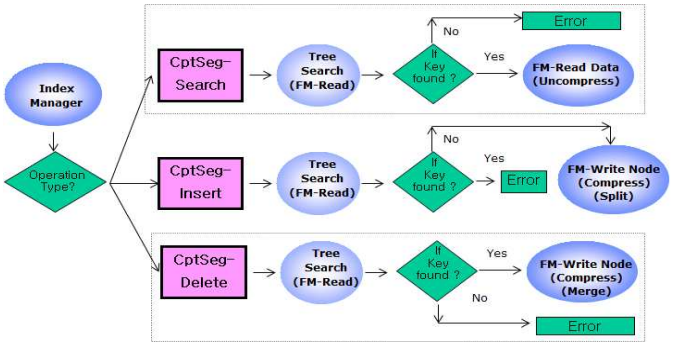

Figure 2. Index Operation Management Diagram

III. PERFORMANCE EVALUATION

We compared the performance of three types of modified tree to the well-known index, B^+-Tree. The average fill factor of the B^+-Tree was fixed to 70%, which is a basic value for the best performance [5]. We denote this basic B^+-trees as BTR-Org, shortly in our test. Our CptSeg scheme exploits empty space packing in internal and leaf nodes for space-efficiency. We denote this type of CptSeg tree as BTR-Pack. Our CptSeg scheme also exploits embedded segment compression in leaf nodes for search-efficiency. We denote this type of CptSeg tree as BTR-Seg. Finally, we also denote the type of CptSeg tree which exploits both embedded segmentation and compact index for best performance, as BTR-CptSeg. Our system consists of four distinct components: the user operation generator (UOG), the index operation manager (IOM), the index manager (IM), and the data manager (DM), as shown in Figure 3. The UOG is responsible for generating user operation, modelled as a sequence of read and write operations in a memory database.

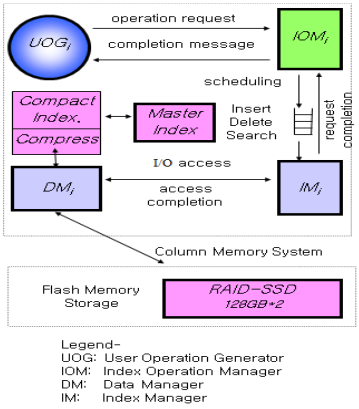

Figure 3. System Model for Performance Evaluation

The overall search throughput is presented in Figure 4. We show that the performance of each scheme levels off or begins to be degraded beyond 150. This fact implies that adding more search operations beyond that range simply contributes to increasing the search I/O contention. From this observation, we can claim that the performances are limited by the factor of I/O contention such as decompressing and read operations.

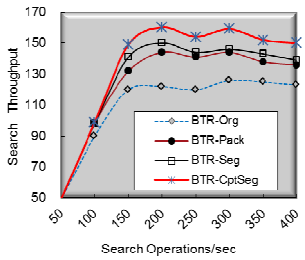

Figure 4. Update-Operation

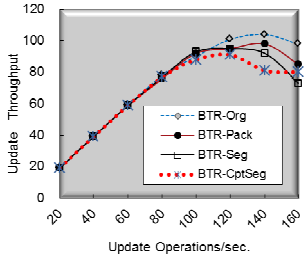

Figure 5. Search-Operation

The performance difference implies that a large portion of performance gain in BTR-CptSeg over BTR-Org comes from the implementation of column-aware indexing to minimize search I/O overhead. However, BTR-Org scheme meaninglessly fetches the empty area of 30% of flash memory space and this leads to require more I/O access to find the key and data in the B^+-tree. This is because B^+-tree maintains the average fill factor of 70% which was designed to reduce the number of frequent tree rebalancing in slow disk environment.

We also investigate the performance differences of four schemes in terms of column update operations. The update operation throughput as a function of num_CURs(number of column update requests per second) is depicted in Figure 5. We observed that the highest throughput is exhibited by BTR-CptSeg, followed by BTR-Seg, BTR-Pack, and BTR-Org.

IV. CONCLUSIONS

The compressed memory-based databases are being adopted in the high-speed data warehouses due to their I/O efficiency on read-mostly transactions. In order to improve the performance of search operation, we proposed compact index segmentation and dual index management in column-oriented database systems. Our scheme improves column search performance by compact search tree and space compression in internal and leaf nodes to shorten the index traverse range of column data. In terms of the search performance, our scheme outperforms the traditional index management scheme.

REFERENCES

[1] D. J. Abadi, P. A. Boncz, P. Alto “Column-oriented Database Systems. In VLDB”, Lyon, France, August 24-28, 2009.

[2] MacNicol R. and French B. “Sybase IQ multiplex - designed for analytics”, In VLDB, pp. 1227-1230, 2004.

[3] S. Ahn, K. Kim., “A Join Technique to Improve the Performance of Star Schema Queries in Column-Oriented Databases", Journal of Korean Institute of Information Scientist and Engineers, vol. 40, No.3, pp. 209-218, 2013

[4] S. Byun, “Column-aware Polarization Scheme for High-Speed Database Systems, Journal of Korean Society Internet Information vol. 13, No.3, pp. 83-91, 2012

[5] R. Elmasri and S. Navathe, Fundamentals of Database System, Addison-Wesley, 2010.

An Oriental Health Diagnosis System Based on WEB

You-Sik Hong
Dept. Computer Science of Sang-ji Univ.
Korea
yshong@sangji.ac.kr

Hyunsik Ahn
Dept. of Robot System Engineering
Tongmyong University, Korea
hsahn@tu.ac.kr

*Chun Kwan Park
Mokpo Maritime National University,
Mokpo, Korea
ckpark@mmu.ac.kr

***Abstract*—The pulse wave decision system is considered as very important point in the oriental medicine treatment because person's health and disease are grasped through measuring the pulse wave. Also the tongue diagnosis system become the main index that can decide the patient's health and digestive organ state. if the state of patient's pulse waveform were actual or false proof, the doctor has to examine the patient's state exactly. In this paper, we develop the smart electronics acupuncture treatment system which can treat the patient's diseases simply in any time, anywhere based on telemedicine technology.**

Keywords- *Fuzzy Rules, U Health, Acupuncture*

I. INTRODUCTION

In the oriental hospital, both feeling the pulse and tongue diagnosis are used as the main method to decide the disease state of patients by examining the wave state of pulse and the state of tongue and coated tongue. Therefore, they become the main index to decide the patient's health condition digestive organ state. In this paper, we develop the electronics acupuncture treatment system which can treat the patient's diseases in remote. First of all, This system decides the patient's condition through feeling the pulse and the tongue diagnosis based on Smart Phone. These days the research for the intelligent herbal medicine diagnostic system, which receives the patient's pulse wave in real time from the remote in any time and any place, and decide the health state of this patient in real time, and then can store the decision results and his/her pulse wave, has been done. The herbal treatment has more advantages than the western one, but it has the problem that has not proven its effects scientifically. So the research that gives the new medical treatment through the co-work treatment using the advantage of both herbal and western treatments, has been done. Especially as the oriental doctor decides the magnetic needle time, there are few objective data for acupuncturing. The patients living in the places where there are not the medical facilities, and the soldiers fighting in the battle field cannot receive the medical services easily. So in this paper, we have performed the simulation that can receive the doctor's treatment from the remote by transferring the patient's herbal medical data using the mobile phone.

* Corresponding Author : Chun Kwan Park

II. REASONING THE PATIENT'S DISEASE USING THE TONGUE DIAGNOSIS

In the oriental medicine, the tongue diagnosis has been used as the main method that the doctors can decide the state of patient's disease by examining the color and coated state of tongue from 3,000years ago. So the tongue diagnosis is the main index that can decide the state of patient's health and digestive organ. But when diagnosing the tongue, the color of coated tongue varies according to the color of foods that the patient ate, So these problems have to be considerated before deciding through the color of coated tongue.These days, to improve these problems, the study to analyze the volume and color of coated tongue exactly using the methof of infrared and ultraviolet ray has been done. Doctor can examine the function of heart and spleen through the tongue. The coated tongue of white color indicates the early stages of disease or the mild illnesses. So the doctors can figure out the relative seriousness, ongoing state, and convalescence of an illness. They also figure out the strength and weakness of the resisting power in the body. Like these, the tongue diagnosis can be used to actively figure out the raised part, reason, and symptom of illness. Figure 1 shows the basic theory of multipad electronic-acupuncture using pulse wave detection system based on Arduino sensor.

Fig. 1. Multipad with a built in electronic acupuncture

Figure 2 shows the system to decide the tongue diagnosis based on Smart Phone. In this system, we considered the stress and average number of patient's pulse. And we use these data

to reason the health state of patient.

The strength of the blood pressure indicating the strong and the weak of the blood spouted from the heart of signals that the human body generates, uses the method to measure by mostly attaching the sensor pad to the heart, But in oriental medicine, the method to measure the radial artery part of the wrist through some kind of sensors is used. Fuzzy rule generally have the IF-THAN form and is a series of process that analogizes the new relationship and fact from the certain given rule like fuzzy inference and used max-min inference. But Fuzzy extraction rule conclusion has two or more different belief values. To receive the digital value of signals generated from the sensor node in Embedded controller, WiFi module built in Embedded controller is set in AP mode. IP address of this module set as Gateway, and assigns IP address to the modules in DHCP or static that want to connect this AP.

Fig. 2. The system to decide the tongue diagnosis based on Smart Phone.

Figure 3 illustrates the Pulse wave decision system using fuzzy rules which depending on the patient's physical condition. In this paper, it is tried to classify the difference in physical characteristics such as thickness of skin and blood vessel, skin impedance, glandular nature of skin in order to come up with an accurate pulse analysis. In this matrix every element is the result of a pair wise comparison denoting the dominance of element i relative to element j. A comparison is also being made of the jth element with the ith element. The fuzzification membership functions in a fuzzy rule base are triangular typed ones. The fuzzy rule base composes of MISO (Multi Input Single Output) typed rule base. Each fuzzy membership function in a fuzzy rule base has a membership value area, and should be normalized in this area.

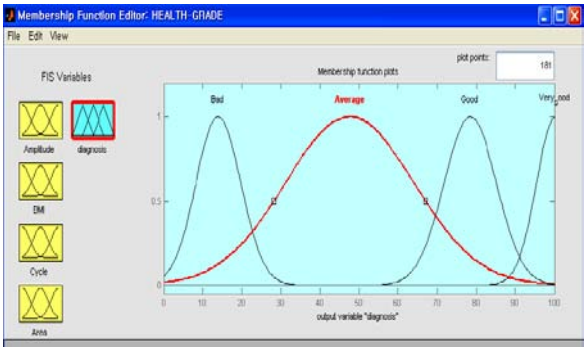

Fig. 3 Simulation of intelligent electronic acupuncture

III. CONCLUSION

The existing electronic acupuncture was given the medical treatment to the patient according to the oriental doctor's diagnosis for the wire environment, or the patients give the medical treatment to their own meridian system through the hand acupuncture by themselves. In this paper, we develop the system to reason the patient's diseases just by clicking the tongue diagnosis or feeling the pulse on the menu based on Internet or Smartphone. Moreover, In this paper we simulates the process that reasons the patient's disease exactly to solve these problems by considering the pulse wave and tongue diagnosis through Fuzzy logic and Fuzzy reasoning theory.

REFERENCES

[1] Y. J. Lee, J. Lee, H. J. Lee, H. H. Yoo, E. J. Choi, J. Y. Kim, "Study on the characteristics of blood vessel pulse area using ultrasonic," Korea Institute of Oriental Medicine researches, 13(3), pp111 -119, 2007.

[2] J. Lee, Y. J. Lee, H. J. Lee, E. J. Choi, J. Y. Kim, "Designing a stabilized process of pulse analyzing method using sigma 6" Korea Institute of Oriental Medicine researches, 12(2) pp 85 – 92, 2006.

[3] Y. G. Lee, "Diagnostic atlas 2 analyzing pulse" Chungdam books, pp 11 -14, 2003

[4] Gunal, S.; Edizkan, R. Subspace based feature selection for pattern recognition. *Information Sciences* 2008.

[5] http://www.etnews.co.kr/etnews/word.

[6]https://www.hurom.co.kr/community/health/health02_view.html?cate2=45&idx=108

[7] http://cafe.naver.com/doumdoll/82

[8] Hong You Sik, "Web-based smart electronic acupuncture system," The journal of the Institute of Webcasting, Internet and Telecommunication, v.13 no.4, pp.209 - 214, 2013

A Precise Multi-Stage Amplifier Circuits Module for Active Dry EEG Electrodes

Young Chang Jo, Hyuck Ki Hong, Yeon Shik Choi and Suk Won Jung
Human Care System Research Center, Korea Electronics technology Institute(KETI)
SeongNam-Si, GyeongGi-Do, South Korea
ycjo@keti.re.kr

Abstract— **Recently, active dry electrodes are to be widely used in many applications such as games, sports, wearable healthcare and military, etc. because dry electrodes do not use conductive wet gel which is inconvenient. Thus active dry EEG electrode is very useful to many people and the market grows rapidly. In this paper, a precise multi-stage amplifier circuits module for dry EEG electrodes have been proposed and tested. The size of dry electrode is about 20 mm diameter and frequency range is 0.1 ~ 40Hz. The supply voltage is single 5V. The test results shows the proposed circuit module has very precise EEG measuring performance.**

Keywords-component; multi-stage, amplifier circuit, dry, EEG, electrode

I. INTRODUCTION

Electroencephalography(EEG) is an electrophysiological monitoring method to record electrical activity of the brain. It is typically noninvasive, with the electrodes placed along the scalp, although invasive electrodes are sometimes used in specific applications. EEG measures voltage fluctuations resulting from ionic current within the neurons of the brain. In clinical contexts, EEG refers to the recording of the brain's spontaneous electrical activity over a period of time, as recorded from multiple electrodes placed on the scalp. Diagnostic applications generally focus on the spectral content of EEG, that is, the type of neural oscillations (popularly called "brain waves") that can be observed in EEG signals [1].

EEG is most often used to diagnose epilepsy, which causes abnormalities in EEG readings [2]. It is also used to diagnose sleep disorders, coma, encephalopathies, and brain death. EEG used to be a first-line method of diagnosis for tumors, stroke and other focal brain disorders [3], but this use has decreased with the advent of high-resolution anatomical imaging techniques such as magnetic resonance imaging (MRI) and computed tomography (CT). Despite limited spatial resolution, EEG continues to be a valuable tool for research and diagnosis, especially when millisecond-range temporal resolution (not possible with CT or MRI) is required. Derivatives of the EEG technique include evoked potentials (EP), which involves averaging the EEG activity time-locked to the presentation of a stimulus of some sort (visual, somatosensory, or auditory). Event-related potentials (ERPs) refer to averaged EEG responses that are time-locked to more complex processing of stimuli; this technique is used in cognitive science, cognitive psychology, and psychophysiological research [4].

There are two kinds of electrodes to measure EEG signals. One is wet electrode and the other is dry electrode. Wet EEG electrodes are more accurate but dry EEG electrodes are to be popular recently because dry electrode s don't use conductive wet gel which is inconvenient. In this paper, we introduced newly designed multi-stage amplifier circuits prototype module for active dry EEG electrodes.

II. CIRCUIT DESIGN

The simplified block diagram of the designed multi-stage amplifier circuits for dry EEG electrodes is shown in Figure 1. The main block of the circuits consists of high impedance, high gain input amplifier stage, differential amplifier stage, active high pass filter stage, active notch filter, 4 stage active low pass filter circuits and analog to digital converter circuits.

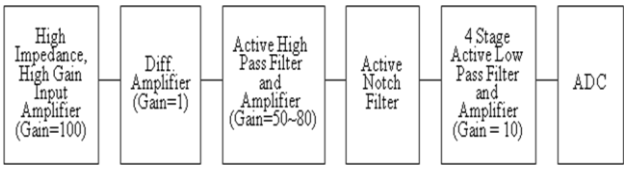

Figure 1. Circuit block diagram of dry EEG electrodes

High impedance and high gain amplifier stage consists of a high impedance, zero-drift buffer amplifier and a high gain(x100) amplifier circuits. Figure 2 shows the differential amplifier circuits with AD623 IC have three electrodes. Two differential electrodes(CH+, CH-) are used for complete suppression of common mode noise in EEG signals. The other one is for active reference electrode(REF_COM). In many biomedical signal measurement applications, reference electrode should be properly driven to improve ac common mode noise rejection by bootstrapping the capacitances of electrode, thus minimizing the capacitance mismatch between the inputs. Because the AD623 output voltage is developed with respect to the potential on the reference terminal, many grounding

problems can be solved by simply tying the REF_COM pin to the appropriate local ground. The REF_CMO pin should, however, be tied to a low impedance point for optimal common mode rejection. Active high pass filter and amplifier stage consists of an active HPF with 0.1 Hz cutoff frequency and an amplifier

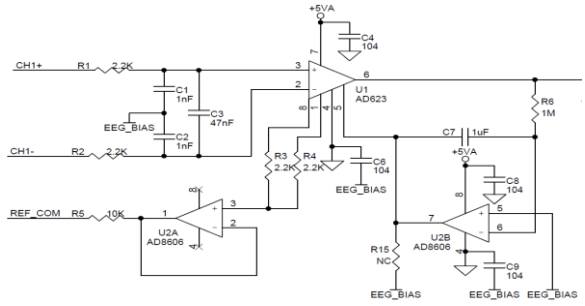

Figure 2. Schematic diagram of differential amplifier circuits

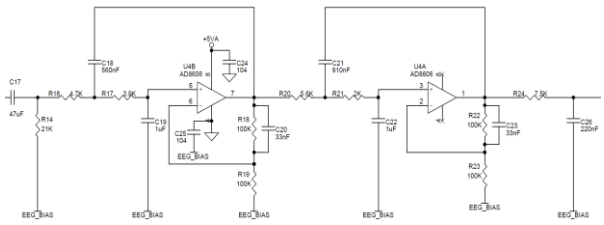

Figure 3. Schematic diagram of 4-stage active low pass filter and amplifier circuits with low gain(x10)

circuit with medium gain(x50~80). Active notch filter used for 60Hz AC power noise suppression. As shown in Figure 3, 4-stage low pass filter and amplifier stage consist of 4 multi stage LPF circuits with 40Hz cutoff frequency and low gain(x10) amplifier circuits. 4 stage LFP circuits have two simple RC filters and two active 2nd order LPF circuits. Overall curoff frequency is designed by about 40Hz.

III. Circuit Implementation and Test Results

The proposed EEG amplifier circuits have been implemented in PCB. Figure 4(a) shows the prototype module of high impedance and high gain amplifier stage with 20mm diameter size of PCB. The implemented 3 channel multi-stage amplifier circuits for dry EEG electrodes are shown in Figure 4(b).

(a) (b)

Figure 4. The photograph of implemented PCB module of proposed EEG sensing circuits : (a) high impedance and high gain amplifier stage (b) 3 channel multi-stage amplifier circuits for dry EEG electrodes

Figure 5 shows the measured results of output analog EEG signals. Figure 5(a) shows measured EEG signals on prefrontal cortex during relaxed mode when the low frequency alpha waves(8~13Hz) are dominant. Figure 5(b) shows measured EEG signals on prefrontal cortex during working mode when the high frequency beta waves(13~40Hz) are dominant.

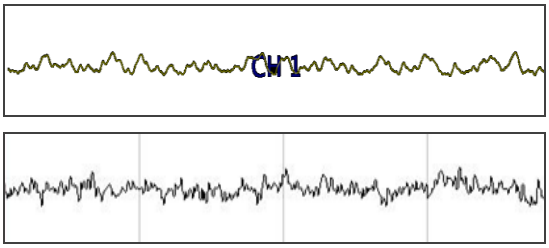

Figure 5. The measured EEG signals with the proposed circuits module : (a) during relaxed mode when the low frequency alpha waves are dominant (b) during working mode when the high frequency beta waves are dominant

IV. Conclusions

Recently, active dry electrodes are to be widely used in many applications such as games, sports, wearable healthcare and military, etc. because dry electrodes do not use conductive wet gel which is inconvenient. Thus active dry EEG electrode is very useful to many people and the market grows rapidly. In this paper, a precise multi-stage amplifier circuits module for dry EEG electrodes have been proposed and tested. The size of dry electrode is about 20 mm diameter and frequency range is 0.1 ~ 40Hz. The supply voltage is single 5V. The test results shows the proposed circuit module has very precise EEG measuring performance.

Acknowledgment

This work was supported by the Korean Ministry of Trade, Industry & Energy and KEIT under project contract No. 10053091[Development of human-body-friend smart patch and home-based healthcare service solution for monitoring acute/chronic brain/cardiovascular diseases]

References

[1] [1] E. Niedermeyer and F.L. da Silva, Electroencephalography: Basic Principles, Clinical Applications, and Related Fields. Lippincot Williams & Wilkins.2004

[2] B. Abou-Khalil and K.E. Musilus, Atlas of EEG & Seizure Semiology. Elsevier. 2006.

[3] M. A. Lopez-Gordo, D. Sanchez-Morillo and F. Pelayo Valle, Dry EEG Electrodes. Sensors, Vol. 14, pp.12847-12870; , 2014.

W.Y. Huang, Y.W. Cheng and K.T. Tang, A 0.5-V Multi-Channel Low-Noise Readout Front-End for Portable EEG Acquisition, Proceeding of IEEE EMBC 2015, pp. 837–840, August 2015.

A Study of Distance measure apparatus using IMU and Camera

Seungwhan Lee
School of Electrical Engineering
University of Ulsan
Ulsan, South Korea
yisikyong@naver.com

Hansil Kim
School of Electrical Engineering
University of Ulsan
Ulsan, South Korea
hskim@ulsan.ac.kr

Abstract - **This paper proposes accurate measurement method using IMU and camera to compensate the existing measuring system problem. The Kalman filter and HDR, HSR filter is used with IMU and camera. The performance is analyzed using sensor fusion and is made up for weakness**

Keywords-IMU; Kalman filter;HDR; HSR;sensor fusion

I. INTRODUCTION

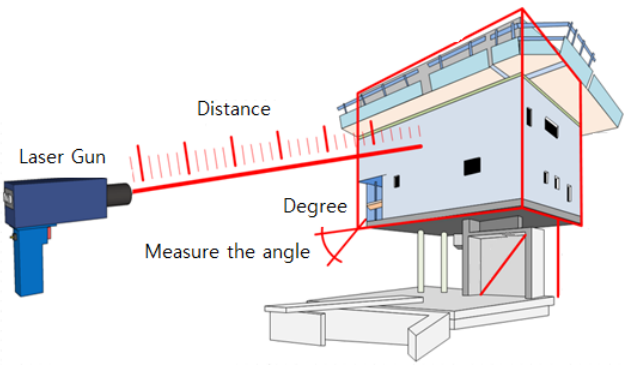

There are several method to measure the distance. One of those is lase sensor. It is possible to measure quickly and accurately using laser beam. Above all things it is contactless processing and is applicable for moving particle regardless of environment.

The existing industry uses a yard tape, but it needs another helper when the distance is too long. Sometimes it rewinds automatically by the elastic force. To remedy shortcomings, the laser measurement system will be useful.

Identify applicable sponsor/s here. If no sponsors, delete this text box. (sponsors)

II. EASE OF USE

A. *Sensor fusion Algorithm*

The goal of sensor fusion is easy to measure the distance when the object moves at the same speed.

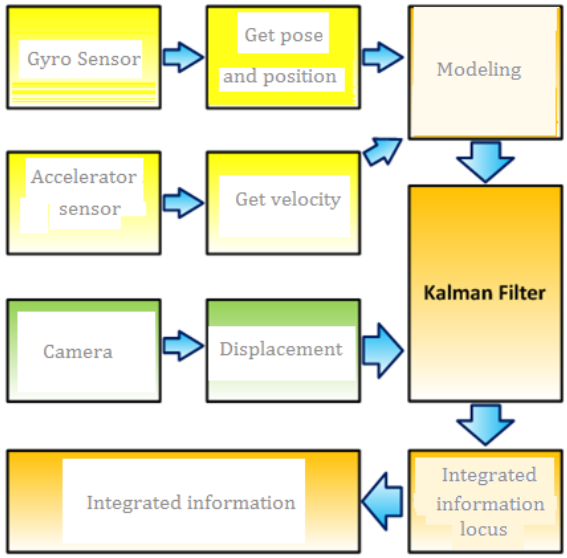

B. *The proposed system*

The data from IMU and camera is fused to moving displacement data by the information of position and acceleration information. IMU only has a limit to get the precise measurement. This paper gives an idea to combine IMU with camera.

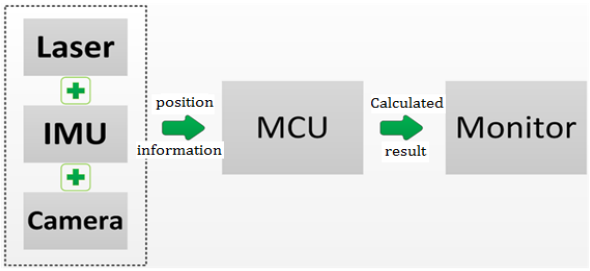

III. FUSION WITH KALMAN-FILTER AND IMUG

The angular velocity and acceleration is integrated and the position and velocity of moving object is calculated from initial position. The quaternion is used for getting pose.

Finally, complete position is predicted and is initialized for next stage.

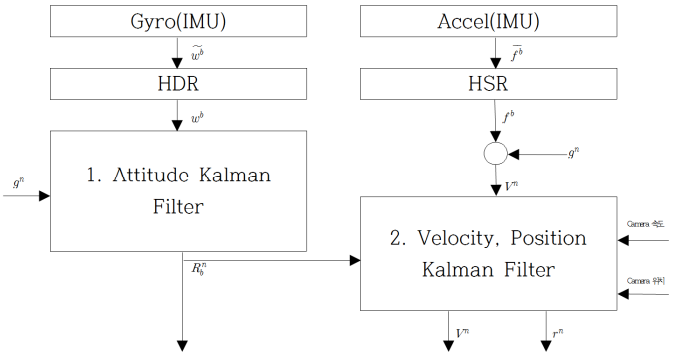

IV. FEATURE DETECTION

Feature detection techniques extract edges, the vertices, and contours from image. We compare Herris corner detection algorithm with Trajkovic algorithm. Harris corner detection method is widely used, but is sensitive to noise and there is a lot computational drawbacks. But in order to reduce the noise, it is needed a larger window. There are still big problems like lots of calucation and loss of important information. Therefore, it is not suitable for real-time processing. In this paper, the feature points extracted by the Trajkovic 8-neighbors method.

V. EXPERIMENTS

The experiment is executed in the yard and confirmed by the proposed system.

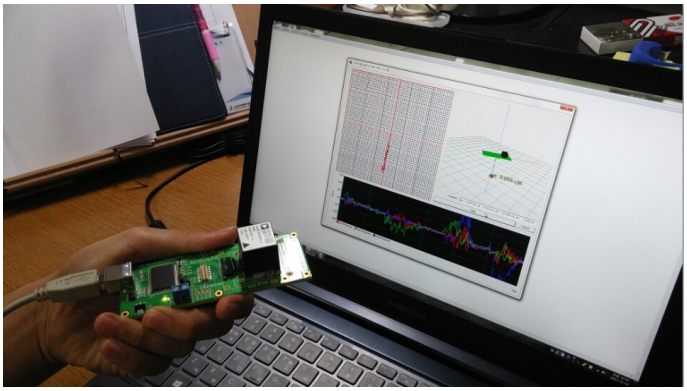

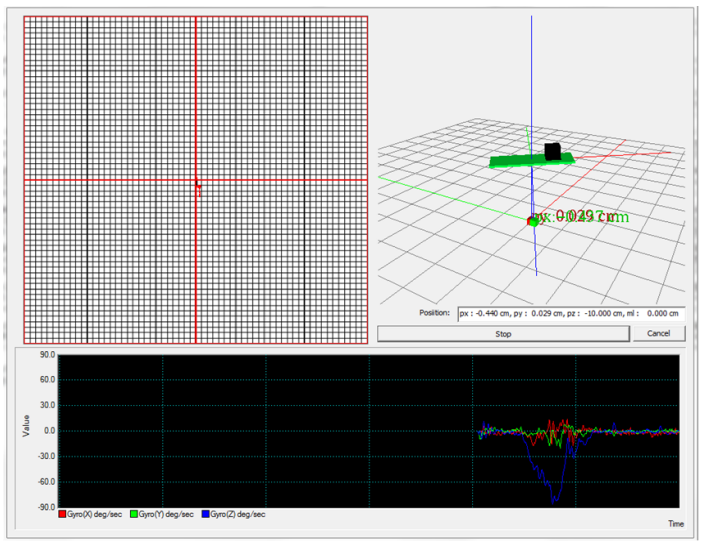

[1] Zhi Shen, "Low cost two dimension navigation using an augmented Kalman filter/Fast Orthogonal Search module for the integration of reduced inertial sensor system and Global Positioning System", Transportation Research Part C 19 (2011) 1111-1132.

[2] Kido Lee, Yunsoo Choi, Impyeong Lee and Seokjae Sa "Experimental Comparison of Software for Real-time GPS Precision Position," GIS/RS spring conference, pp. 399-304, May 2005.

[3]] NMEA data, Table of Contents http://www.gpsinformation.org/dale/nmea.htm

[4] National Marine Electronics Association, http://www.nmea.org/

[5] B. Hofmann-Wellenhof, H. Lichtenegger, J.Collins, "GPS Theory and Practice, 5/e",Sigmapress, pp1-419, March 2009

[6]] P. D. Groves, Principles of GNSS, Inertial, and Multisensor Intergrated Navigation System, Artech house, 2007..

Development of a MSP Prototype for Novel Biometric Technology based on Skin Tissue Optics

Young Chang Jo, Hyuck Ki Hong and Yeon Shik Choi
Human Care System Research Center
Korea Electronics technology Institute(KETI)
SeongNam-Si, GyeongGi-Do, South Korea
ycjo@keti.re.kr

Hae Na Kim and Dong Hyun Kim
School of Electrical & Electronic Engineering
Yonsei University
Seoul-Si, South Korea
hnkim@yonsei.ac.kr

***Abstract*—This paper investigates the possibility of MSP(Multi-spectral Skin Photometrics) as a novel biometric technology to facilitate automatic identification of individuals. MSP using transmission and diffuse reflection difference with variable wavelength provides information about both the surface and subsurface characteristics of the human skin tissue. It is found in this paper that 8 people have their unique characteristics each other under the same wavelength. Personal difference of skin tissue components concentration and anatomical characteristics measured by multi spectral light offers possibility of MSP as more enhanced biometric technology**

Keywords-MSP; multispectral; skin; photometrics; biometric; identification

I. INTRODUCTION

Biometrics refers to metrics related to human characteristics. Biometrics authentication is used in computer science as a form of identification and access control [1]. It is also used to identify individuals in groups that are under surveillance. Biometric identifiers are the distinctive, measurable characteristics used to label and describe individuals [2]. Biometric identifiers are often categorized as physiological versus behavioral characteristics [3]. Physiological characteristics are related to the shape of the body. Examples include, but are not limited to fingerprint, palm veins, face recognition, DNA, palm print, hand geometry, iris recognition, retina and odour/scent. Behavioral characteristics are related to the pattern of behavior of a person, including but not limited to typing rhythm, gait, and voice. Some researchers have coined the term behaviometrics to describe the latter class of biometrics [4].

Conventional biometric technology, such as fingerprint, veins etc. could be replicated by identity theft. So, it is necessary to develop personal identification technology based on biomedical signals to avoid identity theft. In this paper, we introduce novel skin tissue optics based MSP(Multispectral Skin Photometrics) biometric technology and show feasibility as an new personal identification devices.

II. MSP MODULE DESIGN

Dermis have several layers, stratum corneum, epidermis, dermis, subcutaneous layer, etc. Diffuse reflected light shows the effects of thickness of skin layers, morphology of skin interfaces, scattering properties due to collagen mix, density, orientation, capillary density, etc. and each of these vary by individual. Figure 1 shows light penetration depth into skin with different wavelength. Red light could penetrate deeply than blue light. The simplified functional block diagram of proposed MSP module is shown in Figure 2. Proposed MSP module consists of LED array, photodiode array, low pass filter, photocurrent amplifier circuits, MCU and PC interface control circuits.

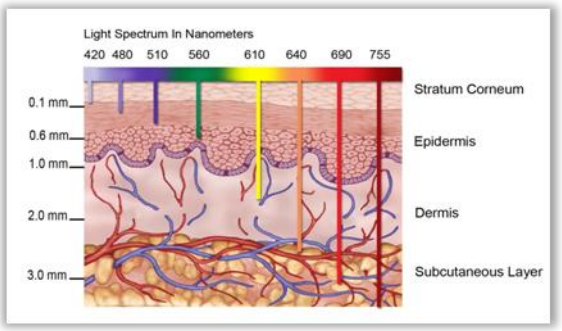

Figure 1. Light penetration depth into skin tissue with different wavelength

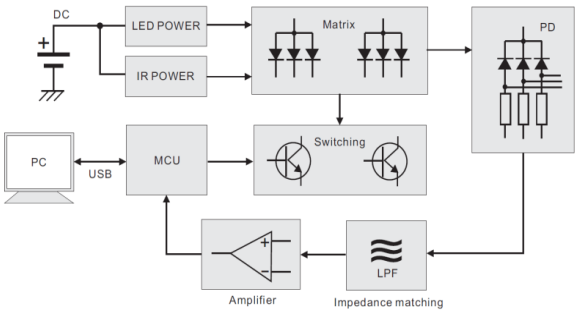

Figure 2. Simplified functional block diagram of proposed MSP module

III. EXPERIMENTAL RESULTS

The implemented prototype MSP module was shown in Figure 3. MSP sensor consists of LED matrix and 7 photodiode array. MSP sensor is attached in human wrist and the photocurrent are measured by each photodiode. In this experiment, we only use 2 IR LED as a input light source. Figure 4 shows the output signals of 7 channel photodiode of MSP module with 2 IR LED. This viewer program is implemented inPC and also serve as a user interface control software. Figure 5 shows comparison test results of individual photocurrent value of 8 people at different photodiode channel. Figure 6 shows comparison of individual photocurrent pattern of 8 people at different photodiode channel. From this experimental results, we can see that individuals have his own photocurrent and this characteristics could be used as a novel personal identification device.

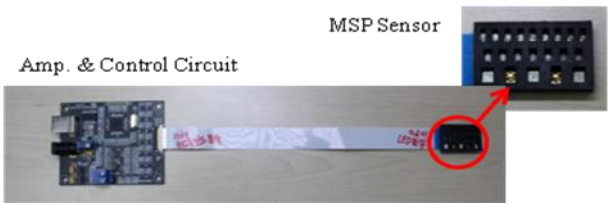

Figure 3. Implemented prototype of the proposed MSP module

Figure 4. The output MSP signals shown by control software

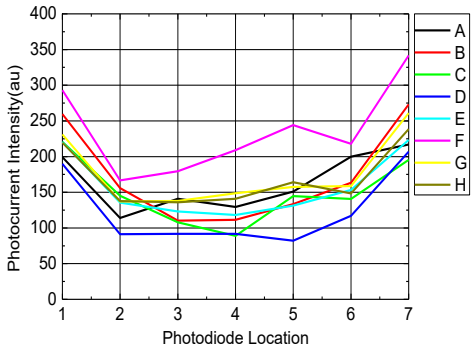

Figure 5. Comparison of individual photocurrent value of 8 people at different photodiode channel

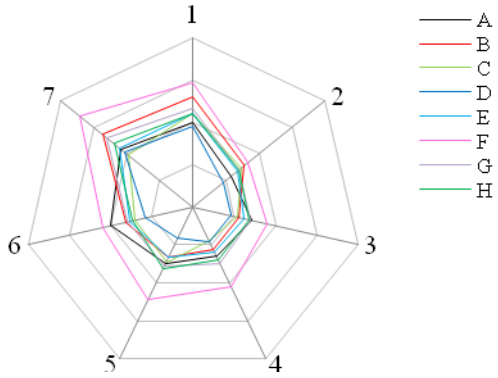

Figure 6. Comparison of individual photocurrent pattern of 8 people

IV. CONCLUSIONS

This paper investigates the possibility of MSP(Multi-spectral Skin Photometrics) as a novel biometric technology to facilitate automatic identification of individuals. MSP using transmission and diffuse reflection difference with variable wavelength provides information about both the surface and subsurface characteristics of the human skin tissue. It is found in this paper that 8 people have their unique characteristics each other under the same wavelength. Personal difference of skin tissue components concentration and anatomical characteristics measured by multi spectral light offers possibility of MSP as more enhanced biometric technology.

ACKNOWLEDGMENT

This work was supported by Institute for Information & communications Technology Promotion(IITP) grant funded by the Korea government(MSIP) (No. R0190-15-2054, Development of Personal Identification Technology based on Biomedical Signals to Avoid Identity Theft)

REFERENCES

[1] A.K. Jain, L. Hong and S. Pankanti, Biometric Identification. Communications of the ACM, vol. 43, No. 2, pp. 91–98, 2000.

[2] *A.K. Jain, A. Ross, A* Handbook of Biometrics. *Springer. pp. 1–22. 2008.*.

[3] R. K. Rowe, K. A. Nixon, P. W. Butler, multi-spec fingerprint acquisition, Advances in Biometrics, Springer, 2008.

[4] P.V. Reddy, A New Antispoofing Approach for Biometric Devices, IEEE Trans. on Biomedical Circuits and Systems, vol. 2, Iss. 4, pp. 328 – 337, 2008

Requirements of the Smart Patch for Cardiac Arrhythmia and Congestive Heart Failure Disease

Ein Jeong Hwang, So Hyun Kim, Hyo Seon Kim, Do hoon Oh
Institute for IT Convergence
Myongji Hospital
Goyang-si, Gyeonggi-do, Korea
einjeong@gmail.com, sohyunkim99@gmail.com, khs26195131@gmail.com, dohoon5@yahoo.co.kr

***Abstract*— This paper is requirements of the smart patch. The purpose of the smart patch is for patients with cardiac arrhythmia and congestive heart failure. The smart patch is sent to the smartphone by measuring the ECG, body temperature, physical activity, fluid assessment. Smart patch is required communication protocols standard terms, authentication and security features.**

Keywords – cardiac arrhythmia, congestive heart failure, electrocardiogram(ECG), smart patch, holter

I. INTRODUCTION

This paper study is about the smart patch (personal medical device and platform). The smart patch measure ECG, body temperature, physical activity and fluid assessment in real life. So, the ECG signal is very important. This study describes the ECG signal and the smart patch requirements.

II. ECG SIGNAL

The ECG is measured 12 signals in a stable state and the measurement time is about 1-2 minutes.[1][2][3] Figure 1 shows are ECG signals. [4]

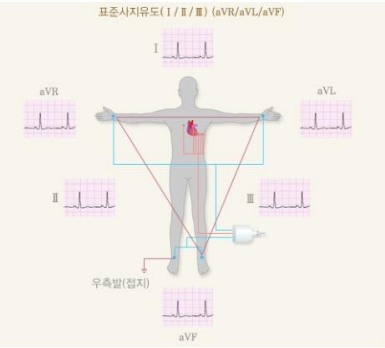

Figure 1. Three leads of ECG

A. *Standard limb leads, Bipolar limb leads*

LEAD1: The potential difference between the left and right hands
LEAD2: The potential difference between the right and left foot
LEAD3: The potential difference between the left foot and left hand

B. *Unipolar limb leads*

aVR: The potential difference between the right wrist (RA) to the center of the heart

aVL: The potential difference between the left wrist (LA) to the center of the heart
aVF: The heart and the left ankle, the potential difference between the center (LF)

C. *Precordial leads, Chest leads*

V1: The right edge of the sternum between the fourth rib
V2: The left edge of the sternum between the fourth rib
V3: The middle part of the V2 and V4
V4: The fifth intercostal space left clavicle and the center line intersects site
V5: The fifth intercostal space left clavicle and the center line intersects site
V6: The horizontal central armpit area and V4

D. *Holter test*

The holter measures ECG for 24 hours ECG signals are V1, V5(chest lead) and lead 2(Standard limb leads). The Holter measures the three of the twelve ECG for arrhythmia patients. Figure 2 shows location of the Holter patch. The patient is recorded in the note or touching holter when an event occurs. The event is recorded hours and behavior or condition. Events are behavior (walk, lunch) and symptoms (dizziness, chest pain).

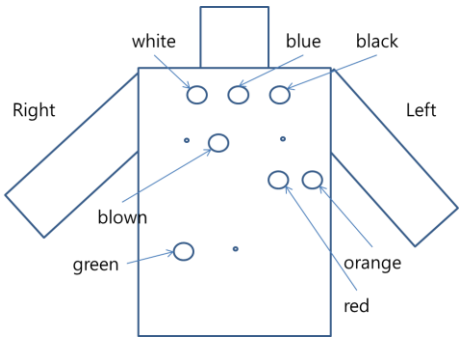

Figure 2 Locations of holter and color of patch

After 24 hours, filtered and the noise are removed clinical pathologist is the holter ECG signal. It is sent to the doctor. Holter signal is analyzed by the experts.

III. SMART PATCH

Smart patch is connected to the smartphone and healthcare service platform. This is a personal care device that it is measure and analyze ECG signal in daily life. Therefore, accurate and signal analysis of an ECG is very important. This study summarized the requirements of the smart patch. Requirements are ECG, design, functional model and standards, etc.

A. Signal analysis

Smart patch should have a function similar to holter. It is measured 3 signals (V1.V5, lead 2) for 24 hours. The input signal is analyzed by normal or risk. The algorithm is needed for the signal analysis. The algorithm are tachycardia, bradycardia, heart rate and so on. Also, this algorithm requires the integration of the guidelines ECG, activity and body temperature.

The smart patch design model should be considered for signal accuracy. The existing patches are mainly triangular model. But this study design should also consider the wrists and left chest measurement signal.

B. Standards

[Communication protocol]

ISO/IEEE11073 Device Specializations standards

- IEEE Std 11073-10406 TM Dev specialization –Basic ECG(Heart Rate Profile)
- IEEE Std 11073-10406 TM Dev specialization –Basic ECG (Simple ECG Profile)
- IEEE Std 11073-10408 TM Dev specialization-Thermometer

[Privacy and Security]

- HIPAA((The Health Insurance Portability and Accountability Act)
- ISO/IEC27001 ISMS Series
- ISO 27799

[Medical device Certification]

- IEC60601-1 3rd
- IEC62304 (Medical device software life cycle processes) [5]

C. Requirements

- Data standards : Clinical cord and terminology
- Document standard (Template)
- Examples of scenario
- Design of smart patch
- Guideline of ECG event
- Functional model of healthcare platform (Interoperability)
- Clinical Algorithms
- Method of fluid assessment measurement

IV. CONCULSION

This study is has shown that smart patch requirements. There are EKG signal, holter, standards, certification, and etc…The smart patch is being designed. So, it remains to be seen whether correct. This study lays the foundation for future work on smart patch.

ACKNOWLEDGMENT

The research and writing of this article were made possible by funding from the "Development of human-body-friend smart patch and home-based healthcare service solution for monitoring acute/chronic brain/cardiovascular diseases (No, 10053091)"

REFERENCES

[1] Ji je Gun,et al."Medical Terminology Illustrated in Color", Academya Publishing Company, 2015. ISBN 978-89-5938-304-7

[2] Kim Dae Sik, Kim Beong Won, Choi Suk Chul, et al. "Clinical Physilolgy", Korea Medical Book Publishing Company, 2012, ISBN 978-89-7043-875-7

[3] "Korea Heart Rhythm Society Symposium 2015", Korean Heart Rhythm Society

[4] http://www.kams.or.kr/ , Korean Academy of Medical Sciences(KAMS)

[5] https://www.iso.org/obp/ui/#iso:std:iec:62304:ed-1:v1:en IEC62304:2006

3 Dimensional Segmentation of Depth Images for Cognitive Robots

Hyunsik Ahn
Department of Robot System Engineering
Tongmyong University
Busan, Korea
hsahn@tu.ac.kr

Jun-Ho Moon
Department of Robot System Engineering
Tongmyong University
Busan, Korea
mjho629@nate.com

***Abstract*— In this paper, a 3D segmentation algorithm for object recognition with noise reduction of normal vector of depth data is presented. In 3D data acquired from RGB-D camera, normal vectors of all points are computed and a 3D Median filtering algorithm with neighbor points is applied. For 3D segmentation, a region growing in 3D points with a dot product of normal vectors of neighbor points is computed and similar points are selected by a threshold value. An example shows the proposed noise reduction and segmentation algorithms can be applied to 3D object recognition of robots.**

Keywords- 3D noise filtering, 3D segmentation, cognitive robot, 3D region growing, cognitive system, human–robot interaction

I. INTRODUCTION

For advanced human-robot interaction in the situation of robot companions, robots need to have the capability of sharing the cognition of objects with human and handling them according to the commands of users [1]. These robots should have the ability of the cognition, therefore the quantitative recognition of objects with 3D data as well as color data is essential [2]. For 3D cognition of objects, 3D segmentation is essential [4, 5], but the performance is not enough when it applied to home appliance objects like books, cups, cans, etc. In this paper, a 3D object segmentation algorithm for object recognition to be applied to the vision module of a cognitive robot is proposed. First, depth images are acquired from RGB-D camera, and a 3D median filtering algorithm by selecting median value among neighboring normal vectors is applied. For 3D segmentation, inner products of neighboring normal vectors are computed and same regions of 3D data are determined by a threshold value.

II. 3D FILTGERING AND SEGMENTATION USING NORMAL VENCTOR

The acquisition of depth image is very important because the raw data acquisition is directly related the result of 3D segmentation. In this paper, a Kinect sensor made by Microsoft is used as an RGB-D sensor. Since the sensor can provide 1mm depth resolution with the range of 40cm to 4m with low price, it is adopted in many robot vision applications. The acquired depth data of the sensor has the format of (u, v, *depth*) with perspective coordinate system. For the 3D image processing, first the data is transformed to (u, v, x, y, z) from perspective to Cartesian coordinate systems. In the 3D data, each point of (x, y, z) can be connected to neighbor points and construct a 3D mesh image graphically. A point has two neighboring points that produce a normal vector of the point as shown in Fig. 1. A 3D point p_0 has 8 neighbor points and the normal vector $\mathbf{n}_0$ can obtained by cross product of p_4 and p_6.

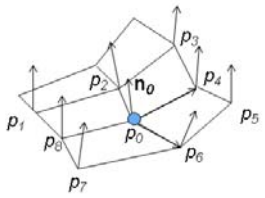

Fig. 1 Neighboring points and normal vector of 3D data

The depth image acquired from RGB-D camera may have noises stemmed from the depth resolution and accuracy of the sensor itself. These noises could distort the normal data and influence 3D segmentation negatively. In this paper, for reducing the noises, we propose a 3D median filter. First, the normal vectors of all the points of the 3D data are computed and 8 neighbor points and their normal vectors are defined. Then the median valued vectors of the points are computed by selecting X, Y, Z axes components of the median values respectively as shown in (1).

$$\begin{aligned} x'_m &= \mathrm{Med}\,(x_{n0}, x_{n1,\ldots,}x_{n9}) \\ y'_m &= \mathrm{Med}\,(y_{n0}, y_{n1,\ldots,}y_{n9}) \\ z'_m &= \mathrm{Med}\,(z_{n0}, z_{n1,\ldots,}z_{n9}) \end{aligned} \qquad (1)$$

The median of normal vectors $\mathbf{n}_{m0}$ are accomplished by computing distance between the normal vectors $\mathbf{n}_i$ and the median valued vector $\mathbf{m}(x'_m, y'_m, z'_m)$, and selecting one of $\mathbf{n}_i$ that has minimum in the distance like (2). Therefore, 3D median filter selects the median of normal vectors exist in a local neighboring points. The filter produces a noise reduction effect of normal vectors and the function of enhanced pre processing for 3D segmentation.

$$\mathbf{n}_{m0} = \{\, \mathbf{n}_i \mid \mathrm{Min}(\mathrm{Dist}(\mathbf{m}(x'_m, y'_m, z'_m), \mathbf{n}_i))\} \; i = 0.1.\ldots.8 \qquad (2)$$

Secondly, a 3D segmentation algorithm is applied to the filtered 3D data. It is a 3D region growing that is comparing the normal vectors with the neighboring points and expanding the points which have same characteristics with a seed point. In this approach, for determining the similarity, it uses dot product of normal vectors and Euclidian distance between center point and neighboring points. First, the center point p_i and 4 neighboring points p_j and their normal vectors are defined. As the dot product of the normal vectors of p_i and p_j, Ip_{ij} is computed. That means the similarity of the orientation of the vectors. And Euclidian distances of neighboring points Dp_{ij} are computed. To discriminate the same characteristics of neighboring points, the threshold value of the difference of orientation T_o, and that of the distance T_d are predetermined empirically. The same regions are determined finally with (3).

$$\begin{aligned} &\text{If } Ip_{ij} \le T_o \,\&\, Dp_{ij} \le T_d \\ &\quad \text{then } p_i \text{ is same region with } p_i \\ &\quad \text{else } p_j \text{ is same region to } p_i \end{aligned} \qquad (3)$$

III. Experimental Results

The experimentation of the proposed 3D segmentation algorithm was tested on a vision module of a cognitive robot, TUBO. The vision module of the cognitive system of the robot used a RGB-D camera, Kinect of Microsoft, for 3D recognition of objects. Fig. 2 shows the cognitive robot, and the color and depth images acquired from the sensor embodied at the front of the head. Fig. 3 shows a mesh typed 3D data transformed from the depth image and expressed graphically, the image of original normal vectors, and the result of 3D median noise filtering. The result shows the noise reduction using the proposed 3D median filtering was successful. Fig. 4 shows the normal vector graphically depicted with the color according to the orientation of normal vectors, and the result of the segmentation. The result of 3D segmentation shows the region of the cup of the image was segmented well.

(a)

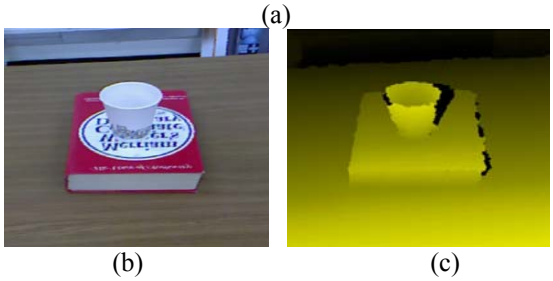

(b) (c)

Fig. 2. (a) A cognitive robot as a test bed, (b) a color image of Kinect and (b) a depth image

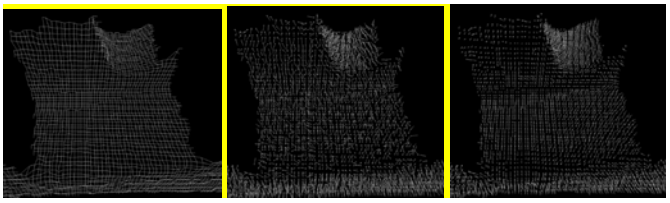

(a) (b) (c)

Fig. 3. (a) A mesh typed 3D data, (b) a normal vector image, and (c) the result of 3D median noise reduction

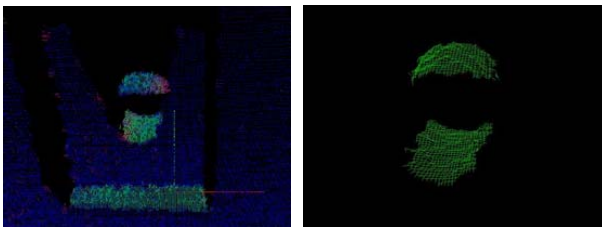

(a) (b)

Fig. 4. (a) The normal vector and (b) the result of 3D segmentation

IV. Conclusion

In this paper, a 3D object segmentation algorithm for object recognition to be applied to cognitive robots was proposed. Depth images were acquired from RGB-D camera, and a 3D median filtering algorithm by selecting the median value of neighboring normal vectors was applied. For 3D segmentation, dot products of neighboring normal vectors are computed and same regions of 3D data are determined by a threshold value. For being applied to a real work of robots, the algorithm should be tested and enhanced on the more complicate environments.

Acknowledgment

This research was supported by Basic Science Research Program through the National Research Foundation of Korea (NRF) funded by the Ministry of Education, Science and Technology(2012-0003116).

References

[1] Deb Roy, "Semiotic Schemas: A Framework for Grounding Language in Action and Perception," *Artificial Intelligence*, vol. 167, pp. 170–205, 2005.

[2] H. Ahn, H-B Go, "Natural-Language-Based Robot Action Control Using a Hierarchical Behavior Model", IEEK Transactions on Smart Processing and Computing, Vol. 1, No. 3, December 2012.

[3] Li Guan Ting Yu Peter Tu and Ser-Nam Lim, "Simultaneous Image Segmentation and 3D Plane Fitting for RGB-D Sensors", Robotics and Autonomous Systems, IEEE Computer Society Conference on Computer Vision and Pattern Recognition Workshops Vol. 1, pp. 49–56, 2012.

[4] K. Khoshelham and S. O. Elberink, "Accuracy and resolution of kinect depth data for indoor mapping applications", Sensor, Vol. 12, pp.1437 1454, 2012.

A CaaS Model Based on Cloud/IoT Service for Cognitive Robots

Hyunsik Ahn
Department of Robot System Engineering
Tongmyong University
Busan, Korea
hsahn@tu.ac.kr

***Abstract*— In this paper, a CaaS (Cognition-as-a-Service) model based on cloud/IoT service for cognitive robot is proposed. To be able to serve general service robots, the model is devised according to modules of a cognitive system, computing power distribution, and real-time requirement. This model can make cloud robots more efficient and practical with the proper distribution of the computing work of sensory-motor and cognition of the cognitive system.**

Keywords- Cognition as a Service, cognitive robots, sentence-based cognitive system, cloude service, internet of things, human–robot interaction

I. INTRODUCTION

For humans interacting with robots as daily life companions, robots need to represent experienced cognitive information, store it in a proper form, and retrieve it with a reasoning procedure. There have been multiple studies linking cognitive information to symbols or language in the area of grounding and anchoring topics [1, 2]. However, these kinds of robots need lots of computing power for advanced intelligent functions. To overcome this problem, the research on cloud robot has been growing interest with the increasing concerns on cloud computing. The cloud robot service provides robots to connect to cloud environment, to use huge computing infrastructure, and to get the results from the server to apply to the robot. RoboEarth, one of the achievements, realizes the concept of cloud robot service that multiple robots having various shapes and functions form and share recognized information to serve human in a same environment [3]. The cloud robots share data about environments, actions, and objects, and offload heavy computation to a cloud server. However, since these services are framed in their own service models, it is difficult to serve cognitive robots properly. One of the reasons seems to stem from that the characteristics of cognitive structure was not fully considered on the cloud server model.

In this paper, a CaaS (Cognition-as-a-Service) model based on cloud/IoT service for cognitive robot is proposed. To be able to serve cognitive robots, the model is devised according to cognitive modules, real-time requirement, information sharing, and computing power distribution based on a sentential cognitive system [3]. This model can make cognitive robots more efficient with the proper distribution of the computing power, sharing of information, and covering environmental IoT.

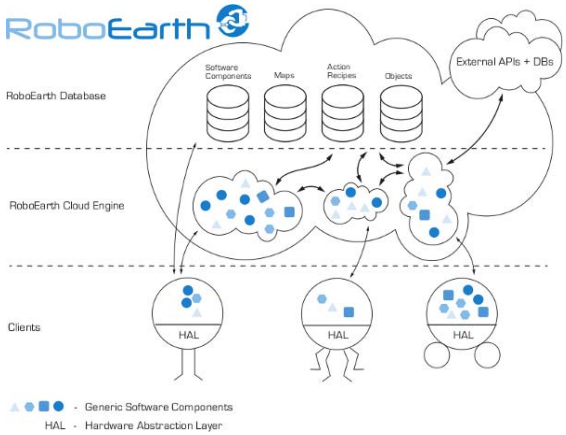

Fig. 1. RoboEarth service concept

II. CAAS MODELING FOR COGNITIVE ROBOT

Cloud robot services applying the technology of cloud computing and internet service to robots utilize computing power, storage and communication through internet infrastructure. For instance, as shown in Fig 1, RoboEarth supports the service of storing software component, mapping information, behavior information, and object information with a DB, and utilizing a cloud engine for services by the virtualization of the information.

In this paper, to apply the cloud robot service to a sentential cognitive system (SCS), a CaaS model is proposed. The main function of SCS is recognizing events and producing sentences expressing the cognitive information of the events. The basic idea of CaaS model is scrutinizing the cognitive structure of the robot and supporting the cloud service with the unit of cognition. Moreover, by distributing computation power properly from the service and the robot itself, the perception and behavior of the robot work more efficiently. Fig. 2 shows the model of robot cloud service based on CaaS for cognitive robots. The cognitive system is embodied in a robot, the parts needed cloud services are marked with dotted

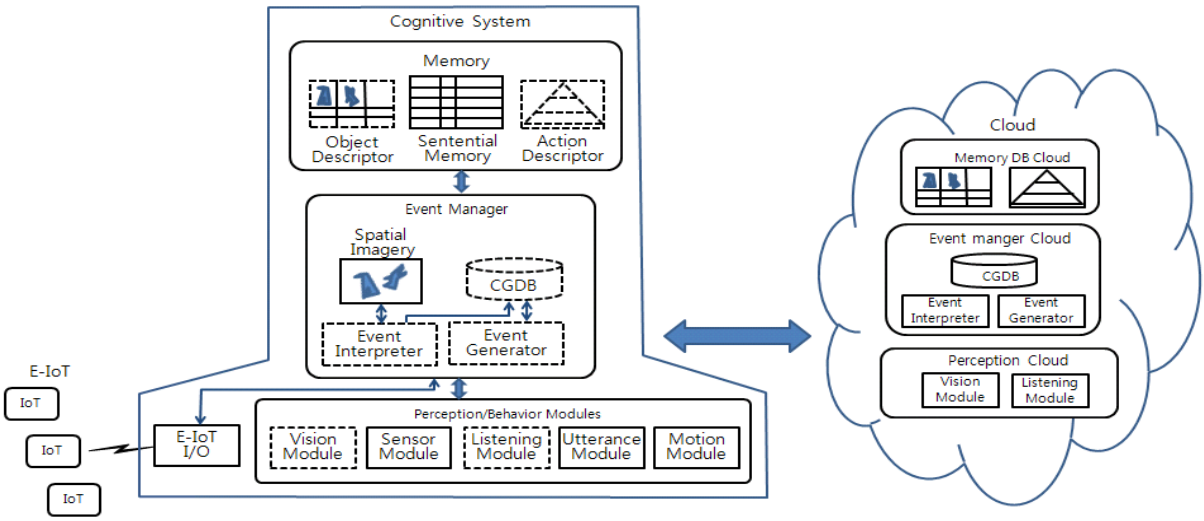

Fig. 2. The block diagram of robot cloud service based on CaaS

boxes and the ones that are essential to the robot are marked with solid boxes. The dotted box related to cloud service is connected virtually with the cloud server, shares information, and offloads computing burdens.

The SCS has a multimodal scheme, each module has its own distinctive function. In the lower part of the cognitive system, there are perception and behavior modules linked to the external world. The vision module is to recognize visual events by capturing scenes by a camera and recognizing objects. The listening module analyzes the acquired sentences captured from the speech of humans via a natural language processor. These two modules depend on the cloud service because they need high computing power but not real time processing. A sensor module covers all sensing including touching, sound, and temperature. An utterance module generates sentences by constructing a sentence and using TTS (text-to-speech) for uttering it. An action module controls the action of the robot. These 3 modules are not proper for the cloud service because they don't need much computing power but real time processing is very important.

In the event manager, the event interpreter needs the cloud service because it links cognitive information to sentences, which demands computing power. The event interpreter acquires the information of environmental IoT and interpreted it. The event generator also requires the cloud service because it needs computing power for making sentences and actions. The Cognitive Grammar DB (CGDB) needs the cloud service because it analyzes sentences with the grammar DB. The spatial imagery doesn't need the cloud service because it is a mental model of the robot and essential to the robot.

In the memory, the object descriptor expressing the shape and pose of the objects uses the cloud service for sharing the object information except for the essential to the robot. In the case of the action descriptor, since the command of human as an episode should be shared, it needs cloud service. Episodes and primitive actions are needed the service but the atomic actions are not needed because it depends on the kinematic characteristics of the robot. The sentential memory of the SCS is essential to the robot as a long-term memory, then it is not needed the cloud service.

III. Conclusion

In this paper, a CaaS model based on cloud/IoT service for cognitive robot was proposed. To be able to serve cognitive robots, the model was devised according to cognitive modules, computing power, information sharing, and real-time requirement. This model can make cloud robots work more efficiently with low price for the computing work of sensory-motor of the cognitive system.

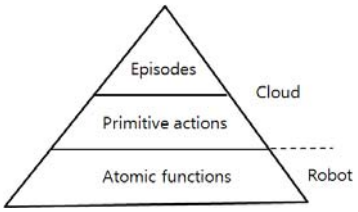

Fig. 3. The distribution of the cloud service and the robot for the action descriptor.

Acknowledgment

This work was supported by Institute for Information & communications Technology Promotion(IITP) grant funded by the Korea government(MSIP) (B0126-15-1078).

References

[1] Deb Roy, "Semiotic Schemas: A Framework for Grounding Language in Action and Perception," *Artificial Intelligence*, vol. 167, pp. 170–205, 2005.

[2] Silvia Coradeschi and Alessandro Saffiotti, "An introduction to the anchoring problem," *Robotics and Autonomous Systems*, vol. 43, pp. 85–96, 2003.

[3] http://roboearth.org.

[4] Hyunsik Ahn and Hyun-Bum Ko, "Natural-Language-Based Robot Action Control Using a Hierarchical Behavior Model," IEIE Transactions on Smart Processing & Computing, Vol. 1, No. 3, pp.192-200. 2012.

Reduced Complexity of QRD-M Detection Scheme in MIMO-OFDM Systems

Jong-Kwang Kim
uT Communication Research Institute
Sejong University
Seoul, Korea
jongkwang91@naver.com

Jae-Hyun Ro
uT Communication Research Institute
Sejong University
Seoul, Korea
ilovebisu@nate.com

Hyoung-Kyu Song [1]
uT Communication Research Institute
Sejong University
Seoul, Korea
songhk0514@gmail.com

***Abstract*— In multiple input multiple output-orthogonal frequency division multiplexing (MIMO-OFDM) systems, several detection schemes have been developed for high error performance and low complexity. In several detection schemes, maximum likelihood (ML) and QRD-*M* have optimal error performance. However, these detection schemes have very high complexity. Thus, this paper proposes reduced complexity of QRD-*M* detection scheme in MIMO-OFDM systems. The proposed detection scheme has two stages, i.e. partial zero-forcing (ZF) and conventional QRD-*M*. The proposed detection scheme has higher error performance and lower complexity than the decision feedback equalizer (DFE).**

Keywords-component; MIMO-OFDM; partial ZF; QRD-M

I. INTRODUCTION

In wireless communication systems, multiple input multiple output-orthogonal frequency division multiplexing (MIMO-OFDM) system offers high data rate without additional bandwidth. However, MIMO-OFDM system has difficulty in accurate detection of each transmission signal. For accurate detection in MIMO-OFDM systems, several detection schemes have been developed. Maximum likelihood (ML) detection has optimal error performance. However, the complexity of ML detection increases exponentially when the number of transmission antennas and modulation set increase. And QR decomposition-*M* algorithm (QRD-*M*) has optimal error performance with lower complexity than the ML detection [1]. However, the complexity of the QRD-*M* also increases exponentially when the number of candidates *M*, transmission antennas and modulation set increase due to tree structure. Also, zero-forcing (ZF) is attractive for simple linear implementation. However, the error performance of the ZF is often not acceptable for other systems [2].

The performance indicators of detection schemes in MIMO-OFDM systems are error performance and complexity. However, in general, these two indicators have trade-off relationship. Thus, for seeking a compromise between the error performance and the complexity, this paper proposes very low complex QRD-*M* detection scheme which is inferior to conventional QRD-*M* in terms of the error performance.

II. SYSTEM MODEL

The MIMO-OFDM system model which has $M = 2^L$ transmission antennas and receive antennas is considered where L is integer which is larger than 1. So, M OFDM symbols are denoted as $\mathbf{X} = \begin{bmatrix} X_1 & X_2 & \cdots & X_M \end{bmatrix}^T$ where $(\cdot)^T$ means transpose operator. For simple notation, subcarrier index k is dropped. And all OFDM symbols from M transmission antennas are sent through rich scattering complex Rayleigh fading channel as follows,

$$\mathbf{H} = \begin{bmatrix} H_{11} & H_{12} & \cdots & H_{1M} \\ H_{21} & H_{22} & \cdots & H_{2M} \\ \vdots & \vdots & \ddots & \vdots \\ H_{M1} & H_{M2} & \cdots & H_{MM} \end{bmatrix}, \quad (1)$$

where H_{ij}, $i, j = 1, 2, \cdots, M$ means channel coefficient from the j-th transmission antenna to the i-th receive antenna. Then, at the receiver, M received symbols $\mathbf{Y} = \begin{bmatrix} Y_1 & Y_2 & \cdots & Y_M \end{bmatrix}^T$ after the process of fast Fourier transform (FFT) are denoted as

$$\mathbf{Y} = \mathbf{HX} + \mathbf{N}, \quad (2)$$

where $\mathbf{N} = \begin{bmatrix} N_1 & N_2 & \cdots & N_M \end{bmatrix}^T$ is a complex additive white Gaussian noise (AWGN) vector which has zero mean and covariance matrix $E\left[\mathbf{N}\mathbf{N}^H\right] = \sigma^2\mathbf{I}$ where $(\cdot)^H$ means transpose operator and $\mathbf{I}$ is identity matrix.

III. PROPOSED DETECTION SCHEME

The proposed detection scheme has two stages. At first, partial ZF (slightly different to conventional ZF) stage is used to divide large matrix into multiple small matrix for low complexity. Then, conventional QRD-*M* (full *M*) is used to each small matrix for high error performance. For easy understanding, the proposed detection scheme is described in 4×4 MIMO-OFDM system without noise components.

1) Corresponding author

A. *Partial ZF*

Unlike the conventional ZF, partial ZF nulls not all interference signals. So, the partial ZF does not have to calculate the pseudo-inverse of channel matrix. The purpose of the partial ZF is to simply divide the 4×4 MIMO-OFDM system into two 2×2 MIMO-OFDM system for low complexity. So, one matrix contains X_1 and X_2. And another matrix contains X_3 and X_4. For the partial ZF, cancelling is used as follows,

$$\begin{bmatrix} Y_{1,c} \\ Y_{2,c} \end{bmatrix} = \begin{bmatrix} Y_1 \\ Y_2 \end{bmatrix} - \mathbf{K} \begin{bmatrix} Y_3 \\ Y_4 \end{bmatrix}, \tag{3}$$

where $\mathbf{K} = \begin{bmatrix} k_{31} & k_{41} \\ k_{32} & k_{42} \end{bmatrix}$ is a weight matrix for cancelling which is satisfied with equation as follows,

$$\begin{bmatrix} H_{33} & H_{34} \\ H_{43} & H_{44} \end{bmatrix}^T \begin{bmatrix} k_{31} & k_{32} \\ k_{41} & k_{42} \end{bmatrix} = \begin{bmatrix} H_{13} & H_{23} \\ H_{14} & H_{24} \end{bmatrix}^T. \tag{4}$$

So, after the cancelling, the received signals $\mathbf{Y}_{c1} = \begin{bmatrix} Y_{1,c} & Y_{2,c} \end{bmatrix}^T$ in (3) are as follows,

$$\mathbf{Y}_{c1} = \begin{bmatrix} Y_{1,c} \\ Y_{2,c} \end{bmatrix} = \begin{bmatrix} \hat{H}_{11} & \hat{H}_{12} \\ \hat{H}_{21} & \hat{H}_{22} \end{bmatrix} \begin{bmatrix} X_1 \\ X_2 \end{bmatrix}, \tag{5}$$

where $\hat{H}_{ij}$, $i, j = 1,2$ is a new channel component. For clarity, the new channel components are denoted as follows,

$$\begin{bmatrix} \hat{H}_{11} & \hat{H}_{12} \\ \hat{H}_{21} & \hat{H}_{22} \end{bmatrix} = \begin{bmatrix} H_{11} & H_{12} \\ H_{21} & H_{22} \end{bmatrix} - \mathbf{K} \begin{bmatrix} H_{31} & H_{32} \\ H_{41} & H_{42} \end{bmatrix}, \tag{6}$$

In the result of **(**5**)**, the modified received signals contain only X_1 and X_2. Likewise, the same cancelling process is applied to the $\begin{bmatrix} Y_3 & Y_4 \end{bmatrix}^T$ and existing 4×4 MIMO-OFDM system is divided into two 2×2 MIMO-OFDM systems. Another 2×2 MIMO-OFDM system $\mathbf{Y}_{c2} = \begin{bmatrix} Y_{3,c} & Y_{4,c} \end{bmatrix}^T$ is as follows,

$$\mathbf{Y}_{c2} = \begin{bmatrix} Y_{3,c} \\ Y_{4,c} \end{bmatrix} = \begin{bmatrix} \hat{H}_{33} & \hat{H}_{34} \\ \hat{H}_{43} & \hat{H}_{44} \end{bmatrix} \begin{bmatrix} X_3 \\ X_4 \end{bmatrix}. \tag{7}$$

B. *QRD-*M *in* 2×2 *MIMO-OFDM*

After the partial ZF, two 2×2 MIMO-OFDM systems are generated in (5) and (7). And then, all transmission symbols $\hat{X}_1, \hat{X}_2, \cdots, \hat{X}_4$ are estimated by applying conventional QRD-*M* with $M = |S|$ to the (5) and (7). The complexity of the proposed detection scheme is very lower than the conventional QRD-*M* which is applied to original MIMO-OFDM system in (2) because the QRD-*M* in the proposed detection scheme is applied to only 2×2 MIMO-OFDM system.

IV. Simulation Results

In this section, the simulation result for bit error rate (BER) performance is shown. The used simulation parameters are explained in Table 2. Fig. 3 shows the BER performance of the proposed detection scheme and ZF-DFE for comparison. At low signal-to-noise ratio (SNR), the BER performance of the proposed detection scheme is lower than the ZF-DFE because the partial ZF stage in the proposed detection scheme amplifies the noise components. So, due to these amplified noise components, the conventional QRD-*M* stage in the proposed detection scheme may detect wrong transmission symbol no matter how it has great error performance. However, at high SNR, the error performance of the proposed detection scheme is higher than the ZF-DFE because the partial ZF stage amplifies the noise components with lower scale than that of low SNR. So, the conventional QRD-*M* stage detects the transmission symbol well.

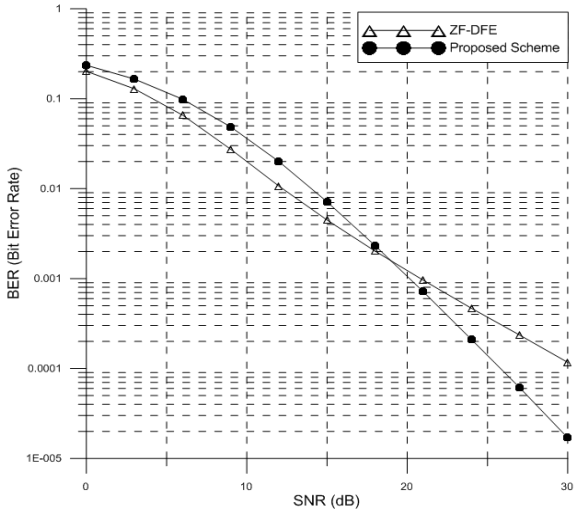

Figure 1. The BER performance of the proposed detection scheme in 4×4 MIMO-OFDM system.

I. Conclusion

This paper proposes the low complex QRD-*M* detection scheme in MIMO-OFDM systems. The proposed detection scheme has higher error performance than the ZF-DFE at high SNR and has low complexity.

Acknowledgment

This research was supported by Basic Science Research Program through the National Research Foundation of Korea(NRF) funded by the Ministry of Science, ICT and future Planning(No. 2013R1A2A2A01067708) and by ICT R&D program of MSIP/IITP. [R0101-14-0189, Development of the next generation convergence broadcasting and monitoring systems combined with the networks].

References

[1] H.J.Choi, and H.K.Song, "Advanced QRD-*M* Detection with Iterative Scheme in the MIMO-OFDM System," IEICE Trans. Inf. & Syst., vol. E97-D, no. 2, pp. 340–343, Feb., 2014.

[2] J.K.Ahn, H.W.Jang, and H.K.Song, "An Improved Low Complexity Detection Scheme in MIMO-OFDM Systems," IEICE Trans. Inf. & Syst., vol. E97-D, no. 5, pp. 1336–1339, May, 2014.

Cooperative Spectrum Sensing Based Routing Protocol in Mobile Cognitive Radio Ad-hoc Networks

Le The Dung, Nhu Tri Do
Dept. of Electronics & Computer Engineering in
Graduate School, Hongik University, Republic of Korea
dungtle@ieee.org, dotrinhu@gmail.com

Beongku An
Dept. of Computer & Information Communications
Engineering, Hongik University, Republic of Korea
beongku@hongik.ac.kr

Abstract— **In this paper, we propose a cooperative spectrum sensing based routing protocol in mobile cognitive radio ad-hoc networks (CRAHNs) to improve the correctness of sensing decision at each secondary user, resulting more users are allowed to participate in forming routing path in the networks. In our proposed protocol, all secondary users exchange the information of local spectrum sensing decision and use majority rule to obtain the final spectrum sensing decision. To evaluate the performance of our proposed cooperative spectrum sensing based routing protocol, we compare the performance of our protocol in terms of packet delivery radio and path establishing delay with those of local spectrum sensing DSR routing protocol. Simulation results show that our protocol outperforms local spectrum sensing DSR and has better scalability as network size increases.**

Keywords- cognitive radio ad-hoc networks; cooperative spectrum sensing; performance evaluation

I. INTRODUCTION

Cognitive Radio Ad-hoc Networks (CRAHNs) is a key paradigm that has attracted much attention of researchers recent years. In CRAHNs, Secondary User (SUs) can utilize spectrum access opportunities for transmission when Primary Users (PUs) do not use the licensed spectrum.

Spectrum sensing is the key function of cognitive radio to prevent the harmful interference with licensed users and to improve the spectrum's utilization. To further enhance the sensing performance, cooperative spectrum sensing which exploits the spatial diversity of SUs is used [2]. By cooperation, SUs can share their local sensing information for making a combined decision more accurate than individual decisions. Based on how cooperating SUs share the sensing data in the networks, cooperative spectrum sensing can be classified into three categories: centralized [3], distributed [4], and relay-assisted [5]. In this paper, we employ distributed cooperative spectrum sensing because it is the most suitable sensing scheme in cognitive radio ad-hoc networks where no infrastructure FC exists.

The rest of this paper is organized as follows. Section II describes the system model including network model and wireless link used in this paper. Section III presents the architecture including packet format and routing algorithm used in our proposed cooperative spectrum sensing based routing protocol. The performance of our routing protocol is presented and discussed in Section IV. Finally, the paper is concluded in Section V.

II. SYSTEM MODEL

A. Network Model

In this paper, we assume that all PU and SUs share one licensed spectrum band. There is one PU locating at the center of network area of $a \times a$ while N_S SUs and are randomly distributed in the network area according to uniform distribution. The operation of PU on licensed spectrum band is associated with ON-OFF state where the number of times, x, that PU occupies licensed spectrum in a time unit follows Poisson distribution with active rate λ_P.

$$P_X(x) = \frac{\lambda_P^x}{x!} e^{-\lambda_P} \tag{1}$$

B. Wireless Link Model

The wireless link is characterized by log normal shadow fading, i.e. a node i transmits signal with power P_t which is received at node j with power given by

$$P_r = P_t G_t G_r \left(\frac{\lambda}{4\pi d_0} \right)^2 \times \left(\frac{d_0}{d} \right)^\alpha \times 10^{\frac{X_0}{10}} \tag{2}$$

where d_0 is the reference distance, d is the distance between two nodes, α is path loss exponent, and X_0 is a Gaussian random variable with zero mean and a variance in dB.

Then, the SNR γ at the receiver j is calculated as

$$\gamma = \frac{P_{r0}}{P_r + N_0} \tag{3}$$

where P_{r0} is the received power at node j from node i. P_r is the aggregate signal power received at node j from other transmitters.

Consequently, the wireless link between transmitter i and receiver j can be established if the SNR at j is greater or equal to a specific threshold γ_{th}, i.e. $\gamma \geq \gamma_{th}$.

This research was supported by the MSIP (Ministry of Science, ICT and Future Planning), Korea, under the ICT/SW Creative Research program (IITP-2015-R2212150026) supervised by the IITP (Institute for Information & communication Technology Promotion).

III. THE COOPERATIVE SPECTRUM SENSING BASED IN MOBILE COGNITIVE RADIO AD-HOC NETWORKS

The architecture including packet format and routing algorithm of our proposed cooperative spectrum based routing protocol will be presented below.

A. Packet Format

To implement cooperative spectrum sensing based routing protocol, we use Route Request (RREQ), Route Reply (RREP), and DATA packet with format shown in Fig. 1.

RREQ

Src. ID (8 bits)	**Dst. ID** (8 bits)	**Route Record**	**Sequence Number** (8 bits)	**TTL** (8 bits)

RREP

Src. ID (8 bits)	**Dst. ID** (8 bits)	**Route Record**

DATA

Route Record	**Data payload** (512 bytes)

Figure 1. The format of RREQ packet, RREP packet, and DATA packet used in our proposed cooperative spectrum sensing based routing protocol.

Using the above control packets, we now present the routing algorithm of our proposed cooperative spectrum sensing based routing protocol as follows.

B. Routing Algorithm

The idea behind our proposed routing protocol is to take the advantage of cooperative spectrum sensing to correct local sensing results of SUs so that more SUs are allowed to communicate in the networks. Consequently, path establishment among arbitrary source SU and destination SU is improved.

IV. PERFORMANCE EVALUATION

Fig. 2 plots path establishing delay corresponding to local spectrum sensing based routing protocol and our proposed cooperative spectrum sensing based routing protocol. As observed in Fig. 2, the time needed to establish a routing path increases as network size (i.e. number of SUs and corresponding network area) is bigger. The reason is that the control packets, i.e. RREQ and RREP may have to go through longer paths before reaching destination SU and source SU,

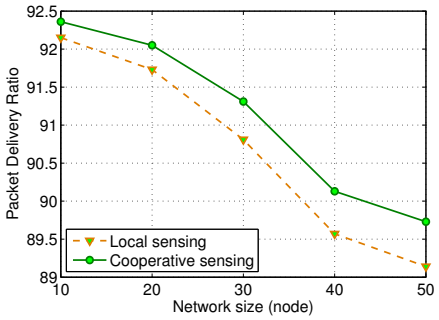

Figure 2. Packet delivery ratio corresponding to local spectrum sensing based DSR routing protocol and our proposed cooperative spectrum sensing based roting protocol as a function of network size; $N_S = 10 \sim 50$, $N_P = 1$, $v =$ 20 km/h, $\lambda_P = 0.1$, $\alpha = 2$, $\gamma_{th} = 30$ dB.

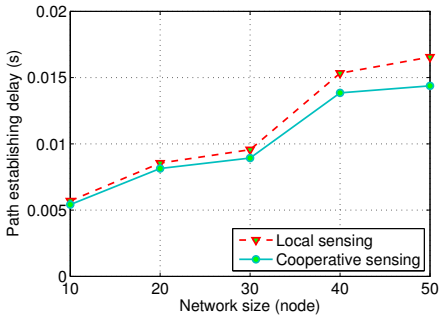

Figure 3. Path establishing delay corresponding to local spectrum sensing based DSR routing protocol and our proposed cooperative spectrum sensing based roting protocol as a function of network size; $N_S = 10 \sim 50$, $N_P = 1$, $v =$ 20 km/h, $\lambda_P = 0.1$, $\alpha = 2$, $\gamma_{th} = 30$ dB.

respectively. However, our proposed routing protocol has lower path establishing delay compared with that of local spectrum sensing DSR.

Fig. 3 depicts average hop count of the path between arbitrary source SU and destination SU corresponding to local spectrum DSR and our proposed cooperative spectrum sensing based routing protocol. As shown in Fig. 3, when the number of SUs and correlating network area increase, the average hop count of routing path is higher because the distance between source SU and destination SU is longer. However, our proposed routing protocol employs cooperative spectrum sensing to increase the number of SUs allowed to communicate in the networks. Therefore, the hop count of multi-hop path is shorter compared with local spectrum sensing DSR. The difference in average hop count is not noticeable as network size is small but is significant when network size is bigger.

V. CONCLUSION

In this paper, we propose a routing protocol which employs cooperative spectrum sensing to improve the sensing decision at every SU. As confirmed from simulation results, we can see that our proposed cooperative spectrum based routing protocol outperforms local spectrum sensing DSR protocol in terms of packet delivery ratio, path establishing delay, and average hop count and has better scalability as network size increases.

REFERENCES

[1] I. F. Akyildiz, W. Y. Lee, and K. R. Chowdhury, "CRAHNs: Cognitive radio ad hoc networks," Ad Hoc Networks, vol. 7, no. 5, pp. 810-836, July 2009.

[2] I. F. Akyildiz, B. F. Lo, and R. Balakrishnan, "Cooperative spectrum sensing in cognitive radio networks: A survey," Journal of Physical Commmunication, vol. 4, no. 1, pp. 40-62, March 2011.

[3] J. Unnikrishnan and V. V. Veeravalli, "Cooperative Spectrum Sensing for Primary Detection in Cognitive Radio," IEEE Journal of Selected Topics in Signal Processing, vol. 2, no. 1, pp. 18-27, February 2008.

[4] Z. Li, F. Yu, and M. Huang, "A Cooperative Spectrum Sensing Consensus Scheme in Cognitive Radios," in Proc. of IEEE INFOCOM'09, pp. 2546-2550, April 2009.

[5] N. T. Do and B. An, "Cooperative Spectrum Sensing with the Interference Constraint in Cognitive Radio Networks," Sensors, vol. 14, no. 5, pp. 8037-8056, May 2014.

Characteristics of Horizontally Polarized ESPAR Antenna using Stacked Structure

Jae Sung Park
Dankook University
Youngin-si, South Korea
lacjae@naver.com

Kyu Tae Lee
Kongju University
Choenan-si, South Korea
ktlee@kongji.ac.kr

Jung-hun Oh
Electronics and Telecommunications
Research Institute
Daejeon-si, South Korea
jhoh70@etri.re.kr

Young Jun Lee
Dankook University
Youngin-si, South Korea
ljsidkr@naver.com

Hak Keun Choi
Dankook University
Youngin-si, South Korea
hkchoi@dankook.ac.kr

***Abstract*—In this paper, a horizontally polarized Electrically Steerable Parasitic Array Radiator (ESPAR) antenna is proposed. The active element of the proposed antenna uses an antenna that has similar characteristics to those of a loop antenna. In addition, four parasitic elements are positioned above and below the active element, which enables size reduction. The reactance values applied to the parasitic element are also separated into two values, allowing the adjustment of various values. Polarization diversity can also be applied by using it together with a vertically polarized antenna.**

Keywords—ESPAR, Loop antenna, Beamforming antenna, polarization diversity

I. INTRODUCTION

The development of a variety of communication services is making communication systems very complex. To address this problem, many communication services need to be integrated into one system. As a result, antennas and systems that can simultaneously use multiple bandwidths are being commercialized [1]. A beamforming antenna can solve problems that are difficult to solve in the system by adjusting the direction of the pattern radiated from the antenna. In addition, the communication performance is improved by avoiding interference from multiple paths or by reinforcing the directivity in one direction [2].

The beamforming antenna changes the direction of the radiation pattern by changing the phases delivered to multiple radiation elements, using a phase shifter or digital signal processing. This antenna has a complex structure and is very large [3]. Therefore, many studies are being conducted on the Electrically Steerable Passive Array Radiator (ESPAR) antenna using a single active element with a PIN diode or varactor diode. The ESPAR antenna using a single active element enables the change of the radiation pattern by using mutual coupling between one active element and multiple parasitic elements [4].

Many studies have been conducted on vertically polarized ESPAR antennas such as the Cross CPW ESPAR antenna, which facilitates impedance matching over a distance or line thickness by using a cross CPW transmission line for the active element structure or an ESPAR antenna that achieves broadband using a fractal structure [5, 6].

In this paper, an active element that has similar characteristics to those of a horizontally polarized Alford loop antenna is stacked with the same parasitic elements above and below the active element. Then the radiation pattern can be varied by changing the reactance value applied to the parasitic elements. The stacked structure can be implemented at a low height, and because this acts as a horizontally polarized antenna, it can be applied to polarization diversity together with a vertically polarized antenna for improved communication efficiency [7].

II. STRUCTURE

Figure 1 shows a horizontally polarized ESPAR antenna. As shown here, the active element is composed of curved lines in 0°, 90°, 180°, and 270° directions on the top and bottom surfaces of one substrate. For the parasitic elements, one circular plate is divided into 12 pieces, and each group of three pieces is bundled together to form one parasitic element. The reactance value can be varied by separating the capacitor from one parasitic element. This was designed to enable more detailed changes of reactance by controlling the reactance with separate parasitic elements. Unlike the ESPAR antenna, where the capacitance value of the parasitic element has a vertical polarization, the two parasitic elements of the proposed antenna have the same capacitance value, while the other two parasitic elements have different capacitance values. The structure

where the active element and parasitic elements are all arranged on one substrate needs a large area, but the proposed antenna can use a smaller area by applying a stacked structure. Fig1 shows the active element's length was L1=28mm and the parasitic element's radius was R1=48.2mm and the distance between active element and parasitic elements was H=2.4mm. The proposed antenna uses the RF-4 substrate (specific inductive capacity: 4.5).

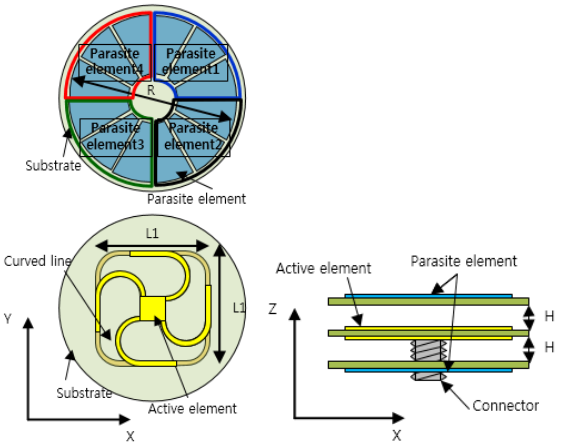

Fig 1. The structure of horizontally polarized ESPAR antenna

III. Antenna Characteristics

Figure 2 shows the voltage standing wave ratio (VSWR) of the proposed antenna. As shown here, it is 3:1 or lower at 2.41–2.48 GHz. A loop antenna has difficulty in impedance matching due to low radiation resistance and high reactance, but the active element of the proposed antenna can achieve a low VSWR at 2.45 GHz by crossing curved lines on the top and bottom surfaces of one substrate and by adjusting the distance between the active element and the parasitic element.

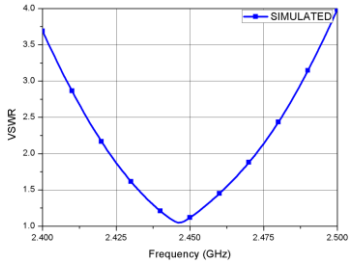

Fig 2. VSWR of proposed antenna

Figure 3 shows the radiation pattern of the proposed antenna. The pattern changes case by case according to the changing reactance. The 2.4 GHz, 2.45 GHz, and 2.5 GHz patterns all show the same directivity.

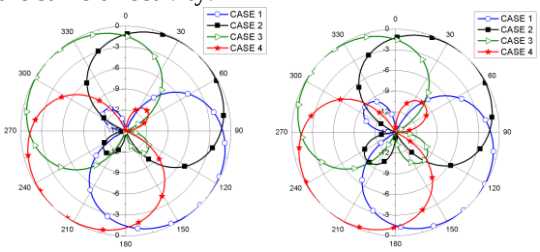

(a) (b)

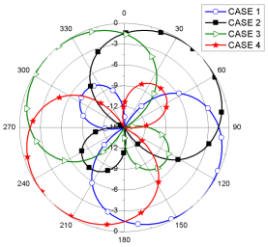

(c)

Fig 3. Radiation patterns of proposed antenna (a) 2.4 GHz (b) 2.45 GHz (c) 2.5 GHz

IV. Conclusion

This paper proposed an ESPAR antenna that consists of a horizontally polarized loop antenna applied as an active element and proposed stacked parasitic elements. The proposed structure is a small structure with a low profile, unlike the ESPAR antenna formed on a single substrate that uses a large area. Polarization diversity was enabled in a small space by using it together with a vertically polarized ESPAR antenna.

Acknowledgment

This work was supported by an Institute for Information & Communications Technology Promotion (IITP) grant funded by the Korean government (MSIP) [No. R0101-15-244, Development of 5G Mobile Communication Technologies for Hyper-connected smart services].

References

[1] C. L. Hu, W. F. Lee, Y. E. Wu, C. F. Yang and S. T. Lin, "A compact multiband inverted-F antenna for LTE/WWAN/GPS/WiMAX/WLAN operations in the laptop computer," IEEE Antennas Wireless Propagation Letters, vol. 9, pp. 1169–1173, 2010

[2] Chryssomallis. M., "Smart antenna," IEEE Antennas and Propagation Magazine, vol. 42, no. 3, pp. 129–136, June, 2000

[3] T. Ohira and K. Gyoda, "Electrically steerable passive array radiator antennas for low-cost analog adaptive beamforming," Proc. IEEE Int. Conf. Phased array Syst. Technol., pp. 101–104, 2000

[4] H. Kawakami and T. Ohira, "Electrically Steerable Passive Array Radiator Antennas," IEEE Antennas and Propagation Magazine, vol. 47, no. 2, pp. 43–49, April, 2005

[5] Kyu-Bo Kim Seung-Hwan Lee and Hak-Keun Choi, "The characteristics of a wideband ESPAR antenna using Koch fractal shaped elements," Microwave And Optical Technology Letters, vol. 57, no. 9, pp. 2108–2112, Sep. 2015

[6] Jae-Sung Park Seung-Hwan Lee and Hak-Keun Choi, "The characteristics of the dipole ESPAR antenna using the cross coplanar waveguide feed," Microwave And Optical Technology Letters, vol. 57, no. 10, pp. 2238–2242, Oct. 2015

[7] R. G. Vaughan, "Polarization Diversity in Mobile Communications," IEEE Trans. Veh. Technol., vol. 39, no. 3, pp. 177–186, Aug. 1990

Distributed Multi-Channel Scheduling for Ad-Hoc Cognitive Radio Networks

Young-Min Kwon
School of Electrical, Electronics & Communication Engineering
KOREATECH
Cheonan, Republic of Korea
kym9102@koreatech.ac.kr

Hyung-Kun Park
School of Electrical, Electronics & Communication Engineering
KOREATECH
Cheonan, Republic of Korea
hkpark@koreatech.ac.kr

***Abstract* — In a multi-channel ad-hoc cognitive radio network, there is no central station and requires distributed packet and channel scheduling. An important requirement of the cognitive radio network is to avoid interference to primary networks. In this paper, we propose distributed packet scheduling scheme for ad-hoc multi-channel cognitive radio networks. Each node calculates independently its own priority with probabilistic manner and selects one of multi channels considering the primary user's traffic pattern to minimize interference to the primary networks.**

Keywords-component; Cognitive Radio network; Ad-hoc Network; Medium access control; propotional fair

I. INTRODUCTION

Recently, the demand of wireless spectrum is rapidly increased due to the increase of various wireless services and applications. To cope with the shortage of the spectrum and improve spectrum usage efficiency, Cognitive Radio (CR) has been proposed [1].

In a multi-channel CR network, spectrum allocation is one of the most important issues[2]. Proportional Fair (PF) scheduling algorithm [3] which is designed to guarantee performance of entire system as well as fairness among users is one of the widely deployed schemes for resource allocation in conventional wireless networks. However, conventional PF is for the centralized networks. For the ad-hoc CR networks, distributed scheduling scheme is required and it considers the dynamic nature of CR networks due to the primary traffic[4].

In this paper, we propose a distributed packet scheduling protocol for the multi-channel CR networks. Using the backoff time set by priority, each secondary user can access the channel in the distributed network. The proposed scheduling considers the primary user's traffic pattern and predicts the spectrum hole to minimize interference to the primary users.

II. PRIORITY OF SECONDRY USERS

In the ad-hoc CR networks, each SU should decide its own priority. Each SU calculates its proportional fairness factor. When the *i*-th node try to transmit data to *j*-th node with data rate $R_{i,j}$, the proportional fairness priority $PF_{i,j}$ is defined by (1) and we will call it as proportional farness factor.

$$PF_{i,j}(t) = \frac{R_{i,j}(t)}{T_i(t)} \tag{1}$$

where T_i is average transmission rate of *i*-th node. Average data rates of candidate nodes are included in the beacon message in the reporting phase. At every transmission of data packet, each node update average data rate. Average data rate T_i of i -th node is updated according to the following equation.

$$T_i(t+1) = (1-1/T_c(t))T_i(t) + \left(1/T_c(t)\right) R_i(t) \tag{2}$$

In ad-hoc CR networks, each node can calculate its own priority, but does not know the other nodes' fairness factor. To figure out other node's priority, we get the following probability that *i*-th node has the highest priority than others.

$$\gamma_i(t) = \prod_{j=1, j\neq i}^{N} \Pr(PF_i(t) > PF_j(t)) \tag{3}$$

with the probability $\gamma_i(t)$, the node i can guess its priority among the nodes. To calculate the probability $\gamma_i(t)$, we should know the probability density function of data rate. We use the fact that transmission rate is inversely proportional to the distance. The probability that the proportional fairness factor of *i*-th receiver is greater than that of j-th node can be calculated by

$$\Pr\left(PF_i > PF_j\right) = \Pr\left(\frac{T_j}{T_i} R_i > R_j\right) = P_{R_j}\left(0 < d < \frac{T_j}{T_i} R_i\right) \tag{4}$$

Each node can get its own priority, *PO,* with threshold, β [5].

$$PO_i(t) = \begin{cases} 1 & if \ \ \beta_{M-1} \le \gamma_i(t) \\ 2 & if \ \ \beta_{M-2} \le \gamma_i(t) < \beta_{M-1} \\ & \cdots \\ M & if \ \ \gamma_i(t) < \beta_1 \end{cases} \tag{5}$$

III. CHANNEL SELECTION AND DISTRIBUTED ACCESS SCHEME

In the multi-channel CR networks, we should select a channel to minimize the interference to the primary users. To find the channel with minimum interference, we predict spectrum hole using the PU's traffic pattern. We assumed the Poisson distribution model. To estimate the spectrum hole, The probability that there is no PU traffic during spectrum hole T'_{free} is should be greater than certain threshold α.

$$\alpha \le e^{-\lambda_i T'_{free}} \tag{6}$$

where λ_i is the PU's packet arrival rate in channel i.

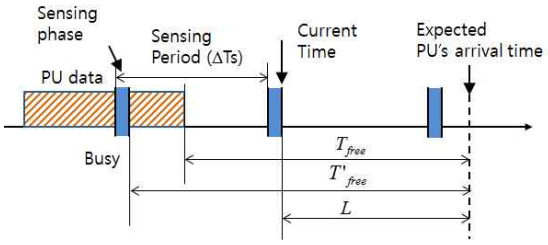

Figure 1. Prediction of spectrum hole

As shown Fig.1, after calculate the T'_{free} value, we can get the remaining spectrum hole L.

Fig.2 shows the example of medium access procedure when four different candidate nodes have different or same priority. Each node calculates its own backoff time using the PO parameter.

$$Backoff_i = SIFS + (PO_i - 1)Time\_slot \tag{7}$$

The nodes try to access the channel with highest spectrum hole L value at first, and if the channel is already occupied, then the nodes try to access the channel with the next highest L value.

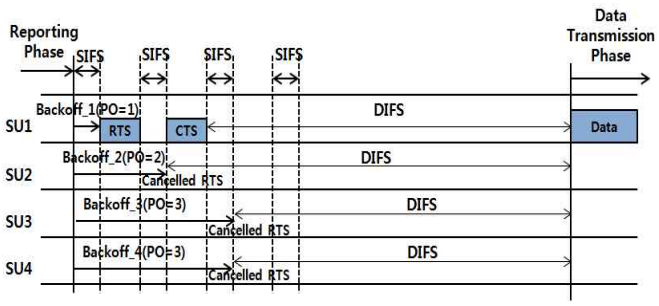

Figure 2. Illustration of channel access scheme

IV. SIMULATION AND RESULTS

To evaluate the performance for the proposed scheduling sheme, computer simulation was performed. We consider multi-rate transmission according to the standard of IEEE 802.11g. Fig 3 and 4 shows the collision probability and system throughput. Throughput of conventional method is more or less than the proposed one, but the collision probability is much higher than the proposed one. In CR network, interference to the primary user is most important problem and the conventional scheme is not proper for the CR networks. The proposed scheme can control the collison rate and throughput using the parameter α.

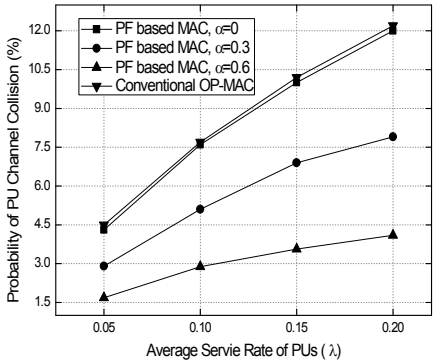

Figure 3. Probability of Collision with PU's packet

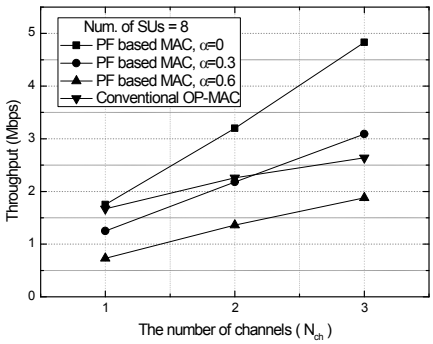

Figure 4. Throughpu according to the number of channels

ACKNOWLEDGMENT

This research was supported by Basic Science Research Program through the National Research Foundation of Korea(NRF) funded by the Ministry of Education, Science and Technology(2011-0021164)

REFERENCES

[1] J. Mitola and G.Q. Maguire Jr., "Cognitive radio: Making software radios more personal," IEEE Pers. Commun., vol. 6, no. 4, pp. 13–18, Aug. 1999.

[2] H. You, E. Ekici, H. Kremo, and O Altintas, "Throughput-efficient channel allocation in multi-channel cognitive vehicular networks," Proc. INFOCOM, April 2014

[3] A. Jalali, R. Padovani, R. Pankaj, "Data throughput of CDMA-HDR a High efficiency-high data rate personal communication wireless system," Proc. VTC-2000-Spring, May 2000.

[4] J. Lee, and H. Park, "Channel Prediction-Based Channel Allocation Scheme for Multichannel Coginitive Radio Networks," Journal of Communications and Networks, Vol. 16, NO. 2, April 2014.

[5] H. Park "Distributed Proportional Fair Scheduling for IEEE802.11 Wireless LANs" Springer, Wireless Personal Communications, Vol.54, No. 4, pp.719-727, Sept. 2010

Physical Layer Security of Wireless Networks under Hardware Impairments

Kyusung Shim*, Nhu Tri Do†, Beongku An‡
*Information System Graduate School of Smart City Science Management Hongik University, Republic of Korea
†Dept. of Electronic and Computer Engineering in Graduate School, Hongik University, Republic of Korea
‡Dept. of Computer and Information Communications Engineering, Hongik University, Republic of Korea
Emails: *kyusung@hongik.ac.kr, †dotrinhu@gmail.com, ‡beongku@hongik.ac.kr

***Abstract*—In this paper, we study physical layer security of wireless networks in presence of one eavesdropper. Assume that the channel state information of the eavesdropper cannot be obtained at the transmitter, it is estimated through the channel state information of a torch node. In addition, considering the impact of hardware impairments at the transmitter, we analyze system performance in terms of secrecy outage probability over Rayleigh fading channels. The closed-form expression of the system secrecy outage probability is derived. Analytical results are validated by Monte-Carlo simulation results. The numerical results reveal the effects of the hardware impairment and the use of the torch node on physical layer security of the wireless system.**

***Index Terms*—physical layer security, hardware impairment, torch node, channel state information, secrecy outage probability**

I. Introduction

According to information-theoretic perspective, physical layer security (PLS) secures the wireless communications by evaluating the physical characteristics of the wireless channels. In related works [1], authors assumed that the eavesdropper also sends its channel state information(CSI) to transmitter. However, in this paper, we consider the scenario in which eavesdropper does not send its CSI to transmitters. In order to obtain the CSI of the eavesdropper, we deploy one torch node which is located near the eavesdropper and the torch node reports its CSI to the source [2]. Through the torch node's CSI, we estimated the eavesdropper channel by using the model of imperfect CSI channel.

On the other hand, Hardware impairment refers to the distortions caused by both transmitters and receivers. In [3], and the referenced therein, the impact of hardware impairments on relay communications was investigated in detail.

The main contributions in this paper are as follows. First, we try to resolve practical issues of wireless communications that we did not receive the CSI of the eavesdropper and the hardware impairment at the transmitter. Second, we obtain the closed-form expression of the secrecy outage probability(SOP) of the considered system.

The rest of this paper is organized as follows. Section II describes the system model. Section III presents outage performance analysis with closed-formexpression. The performance evaluation with numerical results is presented in Section IV. Finally, the paper is concluded in Section V.

II. System Model

Let us consider a direct communication from a source S to a destination D as depicted in Fig. 1. In addition, the transmission is observed by one eavesdropper E. There is a torch node T is that deployed to help evaluating the CSI of the eavesdropper. Considering hardware impairment at the

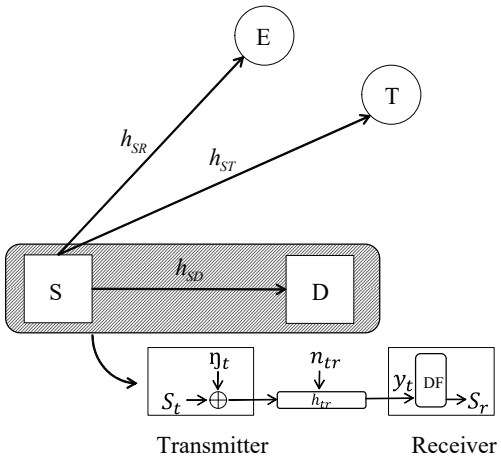

Fig. 1. The source-destination transmission is overheard by one eavesdropper. In addition, the hardware impairment effect is taken into account at the source and the destination.

transmitter, the received signal from S to D is given by [3]

$$y_{SD} = \sqrt{\mathcal{P}} h_{\mathrm{SD}}(x_S + \eta_S) + \omega_D, \tag{1}$$

where $\eta_S \sim \mathcal{CN}(0, \mathcal{P}\kappa^2)$ represents distortion noise. The role of the T is to provide its CSI to the S. We can represent the channel coefficient h_{SE} by using h_{ST} that is given by

$$h_{\mathrm{SE}} = \rho h_{\mathrm{ST}} + \epsilon\sqrt{1-\rho^2}, (0 < \rho \leq 1), \tag{2}$$

where ρ denotes the correlation coefficient that indicates the accuracy of channel estimate over channel state of h_{ST}. the received signal at the eavesdropper y_{SE} is given by

$$y_{SE} = \sqrt{\mathcal{P}}(\rho h_{\mathrm{ST}} + \epsilon\sqrt{1-\rho^2})(x_S + \eta_S) + \omega_E. \tag{3}$$

The signal-to-noise-plus-distortion ratio(SNDR) of main and eavesdropper channel are given by [3]

$$\gamma_{SD} = \frac{\mathcal{P} g_{SD}}{\mathcal{P} g_{SD}\kappa^2 + N_0}, \tag{4}$$

$$\gamma_{SE} = \frac{\mathcal{P}\rho^2 g_{ST} + \mathcal{P}(1-\rho^2)N_0}{\mathcal{P}\rho^2 g_{ST}\kappa^2 + \mathcal{P}(1-\rho^2)N_0\kappa^2 + N_0}, \quad (5)$$

where g_{SD}, g_{ST} are channel gains of main and eavesdropper, respectively. The secrecy capacity is determined by the difference between the capacity of the main channel and that of the eavesdropper channel [1]. Thus the secrecy capacity is given by

$$C_S = \max\left(\log_2\left(\frac{1+\frac{\mathcal{P}g_{SD}}{\mathcal{P}g_{SD}\kappa^2+N_0}}{1+\frac{\mathcal{P}g_{SE}}{\mathcal{P}g_{SE}\kappa^2+N_0}}\right), 0\right). \quad (6)$$

III. Outage Performance Analysis

The P_{sop} is the probability of the event that the secrecy capacity drops below a predefined target secrecy rate [4]. For predefined target secrecy rate $\mathcal{R}$, the P_{sop} in our system is given by

$$\begin{aligned} P_{\text{sop}} &= \Pr(C_S < \mathcal{R}) \\ &= \Pr\left(\frac{\mathcal{P}g_{SD}}{\mathcal{P}g_{SD}\kappa^2 + N_0}\right. \\ &\left. < (2^{\mathcal{R}}-1) + \frac{2^{\mathcal{R}}\mathcal{P}\rho^2 g_{ST} + 2^{\mathcal{R}}\mathcal{P}(1-\rho^2)N_0}{\mathcal{P}\rho^2 g_{ST}\kappa^2 + \mathcal{P}(1-\rho^2)N_0\kappa^2 + N_0}\right). \end{aligned} \quad (7)$$

Let $a_1 = \mathcal{P}, a_2 = \mathcal{P}\kappa^2, a_3 = N_0$; and $b_0 = 2^{\mathcal{R}} - 1$, $b_1 = 2^{\mathcal{R}}\mathcal{P}\rho$, $b_2 = 2^{\mathcal{R}}\mathcal{P}(1-\rho^2)N_0$, $b_3 = \mathcal{P}\rho\kappa^2$, $b_4 = \mathcal{P}(1-\rho^2)\kappa^2 N_0 + N_0)$; $\Omega = \frac{a_1 x}{a_2 x + a_3}$; (7) is re-written as follows:

$$\begin{aligned} P_{\text{sop}} &= \Pr\left(\frac{a_1 x}{a_2 x + a_3} < b_0 + \frac{b_1 y + b_2}{b_3 y + b_4}\right) \\ &= \Pr\left(\Omega < b_0 + \frac{b_1 y + b_2}{b_3 y + b_4}\right), \end{aligned} \quad (8)$$

where $z_1 = b_0 + \frac{b_2}{b_4}$, $z_2 = b_0 + \frac{b_1}{b_3}$, $c_1 = a_1 b_0 b_3 + a_1 b_0$, $c_2 = a_1 b_0 b_4 + a_1 b_2$, $c_3 = a_2 b_3 - a_3 b_0 b_3 + a_3 b_1$ and $c_4 = a_2 b_4 - a_3 b_0 b_4 + a_3 b_2$.

After some algebraic manipulations, the closed-form expression of P_{sop} is given by

$$\begin{aligned} P_{\text{sop}} = & \exp\left(-\frac{1}{\lambda_Y} z_1\right) \\ & + \frac{1}{\lambda_Y}\left[\frac{d_4^2 z_2^2 + 2d_2 d_5 z_2 + d_5^2}{d_1 d_4 z_2^2 + 2d_2 d_5 z_2 + (d_2 d_5 - d_3 d_4)}\right. \\ & \left. \times \exp\left(-\frac{d_1 z_2^2 + d_2 z_2 + d_3}{d_4 z_2 + d_5}\right)\right] \\ & - \frac{1}{\lambda_Y}\frac{d_4^2 z_1^2 + 2d_2 d_5 z_1 + d_5^2}{d_1 d_4 z_1^2 + 2d_2 d_5 z_1 + (d_2 d_5 - d_3 d_4)} \\ & \times \exp\left(-\frac{d_1 z_1^2 + d_2 z_1 + d_3}{d_4 z_1 + d_5}\right), \end{aligned} \quad (9)$$

where $d_1 = \lambda_X c_3$, $d_2 = \lambda_X c_4 + \lambda_Y c_1$, $d_3 = \lambda_Y c_2$, $d_4 = \lambda_X \lambda_Y c_1$ and $d_5 = \lambda_X \lambda_Y c_4$.

IV. Numerical Results

In this section, we present simulation results obtained by carrying out the Monte-Carlo simulations. Fig. 2 shows the P_{sop} of the our system model as a function of transmit power $\mathcal{P}$ where κ is a different value. From Fig. 2, we can observe that the P_{sop} decrease as the transmit power increased at transmit power from -10dB to 10dB. However, the P_{sop} increases as the transmit power increased at transmit power from 10dB to 30dB. As κ increased, the P_{sop} is increased. The patterns of simulation result curve and analysis result curve are similar.

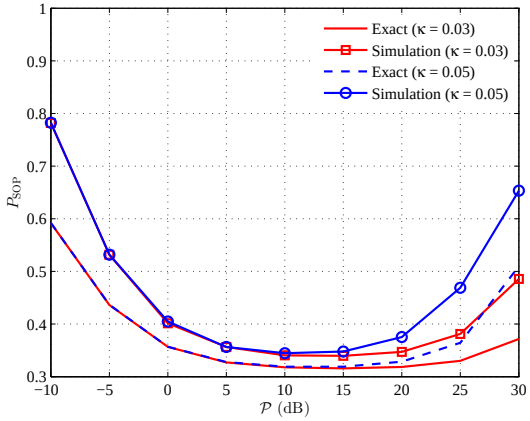

Fig. 2. System secrecy outage probability P_{sop} as a function of transmit power $\mathcal{P}$ with $N_0 = 1$, $\lambda_X = 3.7$, $\lambda_Y = 1.3$, $\kappa = 0.03$ and $\mathcal{R} = 0.5$ $bit/s/Hz$.

V. Conclusions

In this paper, we study the physical layer security of wireless networks under the effects of hardware impairments. More specifically, we assume that the eavesdropper did not send its channel state information at the transmitter. Thus, a torch node is deployed to the eavesdropper in order to estimate the channel state information of the eavesdropper channel. In addition, hardware impairment is considered at the transmitter. The closed-form expression of secrecy outage probability is obtained and derived. The numerical results show that distortion noise effects on the secrecy outage probability.

Acknowledgment

This research was supported by the MSIP(Ministry of Science, ICT and Future Planning), Korea, under the ICT/SW Creative Research program (IITP-2015-R2212150026) supervised by the IITP(Institute for Information & communication Technology Promotion).

References

[1] Y. Zou, X. Li, and Y. chang Liang, "Secrecy outage and diversity analysis of cognitive radio systems," *IEEE Journal on Selected Areas in Communications*, vol. 32, no. 11, pp. 2222–2236, November 2014.

[2] Y. Choi and D. Kim, "Performance analysis with and without torch node in secure communications," *2015 International Conference on Advanced Technologies for Communications (ATC)*, October 2015.

[3] E. Bjornson, M. Matthaiou, and M. Debbah, "A new look at dual-hop relaying: Performance limits with hardware impairments," *IEEE Transactions on Communications*, vol. 61, no. 11, pp. 4512–4525, November 2013.

[4] V. N. Q. Bao, N. Linh-Trung, and M. Debbah, "Relay selection schemes for dual-hop networks under security constraints with multiple eavesdroppers," *IEEE Transactions on Wireless Communications*, vol. 12, no. 12, pp. 6076–6085, December 2013.

Ageriga Smart Phone Keyboard Structure and SNS

Byoungmin Im
Agerigna co.LTD
4F, Howon B/D, 1363-7, Secho Gu,
Seocho Dong, Seoul, Republic of Korea
imubiqutious@gmail.com

Beongku An
Dept. of Computer and Information
Communications Engineering,
Hongik University, Republic of Korea
beongku@hongik.ac.kr

***Abstract*—**Nowdays, stereotypes about QWERTY keyboard of smart phone are disappearing. We made breakthrough in existing input method by using a digital IT technology. For example, Anyone can freely design a keyboard by adding horizontal lines or vertical lines so that it is easier to use. Following this trend, many linguists have developed their own original keyboard designs. However, it's actually rare to receive fervent response from a market. In this paper, we propose a method that can provide optimally smart phone keyboard input service of Agerigna to users using smart phone keyboard.

Keywords— Agerigna , Keyboard , vowel and consonant

I. INTRODUCTION.

Ethiopians use their own letter, Amharic. Amharic has about 280 letters which consist of 238 letters combined into 7 vowels and 34 consonants and diphthongs. Fig.1 presents the vowel and consonant of Amharic letters. There are initial sounds and input value of computer keyboard in the left row from 1 to 34 while there are vowel pronounce and input value in the right line. This is similar with Japanese which has about 50 letters combined into 5 vowel and 10 consonant.

U:up D:down		1	2	3	4	5	6	7	8	9	10	11	12
new keyboard		U	UU	UUU	D	DD	null	DDD	DUU	UD	UDD	UDDD	DU
hard keyboard		e	u	i	a	ie	null	o	ue	u'	ua	uie	ui
1	h'	ሀ	ሁ	ሂ	ሃ	ሄ	ህ	ሆ					
2	h.	ሐ	ሑ	ሒ	ሓ	ሔ	ሕ	ሖ					
3	hh'	ኀ	ኁ	ኂ	ኃ	ኄ	ኅ	ኆ	ኈ	ኍ	ኋ	ኌ	ኈ
4	l'	ለ	ሉ	ሊ	ላ	ሌ	ል	ሎ		ሏ			
5	m'	መ	ሙ	ሚ	ማ	ሜ	ም	ሞ		ሟ			nja
6	ss'	ሠ	ሡ	ሢ	ሣ	ሤ	ሥ	ሦ					
7	s'	ሰ	ሱ	ሲ	ሳ	ሴ	ስ	ሶ		ሷ			
8	r'	ረ	ሩ	ሪ	ራ	ሬ	ር	ሮ		ሯ			rja
9	x'	ሸ	ሹ	ሺ	ሻ	ሼ	ሽ	ሾ		ሿ			
10	q'	ቀ	ቁ	ቂ	ቃ	ቄ	ቅ	ቆ	ቈ	ቍ	ቋ	ቌ	ቊ
11	b'	በ	ቡ	ቢ	ባ	ቤ	ብ	ቦ		ቧ			
12	t'	ተ	ቱ	ቲ	ታ	ቴ	ት	ቶ		ቷ			
13	c'	ቸ	ቹ	ቺ	ቻ	ቼ	ች	ቾ		ቿ			
14	h'	ኀ	ኁ	ኂ	ኃ	ኄ	ኅ	ኆ		ኇ			
15	ny'	ኘ	ኙ	ኚ	ኛ	ኜ	ኝ	ኞ		ኟ			
16	e'	አ	ኡ	ኢ	ኣ	ኤ	እ	ኦ		ኧ			
17	ee'	ዐ	ዑ	ዒ	ዓ	ዔ	ዕ	ዖ					
18	k'	ከ	ኩ	ኪ	ካ	ኬ	ክ	ኮ	ኰ	ኵ	ኳ	ኴ	ኲ
19	kh'	ኸ	ኹ	ኺ	ኻ	ኼ	ኽ	ኾ					
20	w'	ወ	ዉ	ዊ	ዋ	ዌ	ው	ዎ					
21	z'	ዘ	ዙ	ዚ	ዛ	ዜ	ዝ	ዞ		ዟ			
22	zh'	ዠ		ዢ	ዣ	ዤ	ዥ	ዦ		ዧ			
23	y'	የ	ዩ	ዪ	ያ	ዬ	ይ	ዮ					
24	d'	ደ	ዱ	ዲ	ዳ	ዴ	ድ	ዶ		ዷ			
25	j'	ጀ	ጁ	ጂ	ጃ	ጄ	ጅ	ጆ		ጇ			
26	g'	ገ	ጉ	ጊ	ጋ	ጌ	ግ	ጎ	ጐ	ጓ	ጓ	ጋ	ጐ
27	t.	ጠ	ጡ	ጢ	ጣ	ጤ	ጥ	ጦ		ጧ			
28	c.	ጨ	ጩ	ጪ	ጫ	ጬ	ጭ	ጮ		ጯ			
29	p.	ጰ	ጱ	ጲ	ጳ	ጴ	ጵ	ጶ		ጷ			
30	ts'	ጸ	ጹ	ጺ	ጻ	ጼ	ጽ	ጾ		ጿ			
31	tz'	ፀ	ፁ	ፂ	ፃ	ፄ	ፅ	ፆ					
32	f'	ፈ	ፉ	ፊ	ፋ	ፌ	ፍ	ፎ		ፏ			
33	p'	ፐ	ፑ	ፒ	ፓ	ፔ	ፕ	ፖ					
34	v'	ቨ	ቩ	ቪ	ቫ	ቬ	ቭ	ቮ					

Fig.1. Ethiopian literal symbol system

Ethiopians download and use Amharic letter input software instead of using a basic input method due to complex structure, and hard keyboard is replaced with touch screen soft keyboard with dissemination of smart phone. In this paper, we study and propose smart phone keyboard structure of Agerigna to solve these problems. In the first, It has a significant advantage to use by the keyboard feature. We can use a wider keyboard on a small screen of mobile device because we reduced existing columns from 10 to 8 while keeping the existing 21 initial consonants. In the second, we can easily enter consonant and vowel by turns for vowel keys located in the right side. At last, anyone can use it because it is very simple to enter vowel for shift key. This paper consists of as follows. Section II explains proposed system structure and algorithm, and section III presents the performance evaluation of the proposed system. Finally, the conclusion of the paper is given in section IV.

II. AGERIGNA SMART PHONE KEYBOARD STRUCTURE USING SOFRWARE

Fig. 2 and Fig.3 explain the basic concepts and algorithm of the proposed system, respectively. System corresponds to each key put in a form of 8X3 on the touch screen. Main consonants and shift consonants of Amharic letters are located in the left side, and there are 2 keys changing vowels in the right side. If a main consonant has been entered on the key pad with one or more function keys, system will recognize it as Amharic letter combined into the consonant and a basic vowel. It is a system that has a controller converting it to Amharic letter combined into the predefined vowel by repetition of vowel shift key. Considerations for the proposed system in this paper are as follow:

- Inconveniences of a mobile keyboard as compared with a PC keyboard
- Inconvenience in input of Amharic by smart phone
- Inconveniences of a mobile keyboard as compared with a PC keyboard
- Frequency in use of vowel(the rate of use%) and combination of vowel and consonant
- Utilization of English(%) in input of Amharic

- The rate of use of letter, number and special character in input of Amharic
- The rate of use of voice or writing recognition

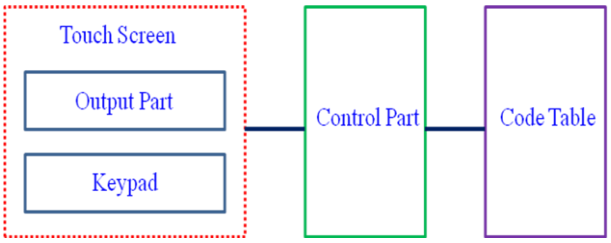

Fig. 2. A basic concept of the system

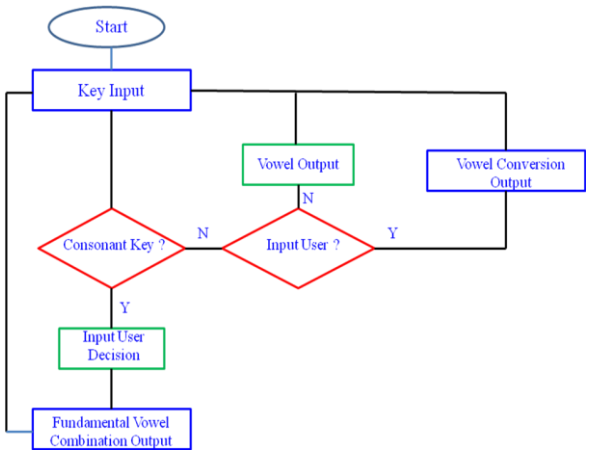

Fig. 3. System algorithm

Fig. 4 shows the structure of the proposed key board while Fig. 5 presents the structure of the Agerigna keyboard developed by multiring company, respectively.

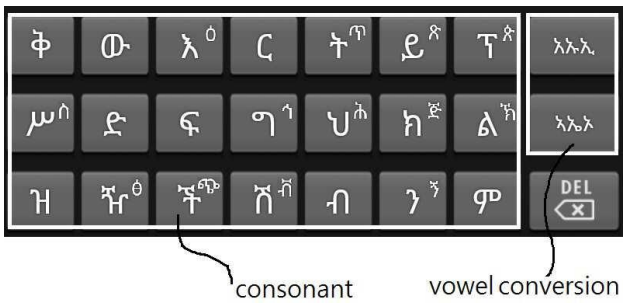

Fig. 4. The structure of the proposed key board

Fig. 5. Structure of Agerigna keyboard developed by multiring company

III. PERFORMANCE EVALUATION AND DISCUSSION

The main features of the proposed Key board in this paper are as below. First, we can use it on the mobile without any change of 21 existing initial sounds. Second, it is easier to enter in vowel and consonant shifts by vowel keys located in the right side. Third, it is simple for user to learn it. Therefore, the proposed system can solve the problem in use of English key board and touch screen keyboard of multiring company.

IV. CONCLUSION

We can develop and use many kinds of Smart Phone Keyboard by king stereotypes in the digital age. In this paper, we propose and evaluate the smart phone keyboard of Agerigna that can provide user an innovative way to enter Amharic by using digital IT technology. We expect technology development of SNS keyboard through the way proposed in the paper.

REFERENCES

[1]Taekyoung Kwon, Sarang Na, Sang-ho Park, "Drag-and Type: A New Method for Typing with Virtual Keyboards on Small Touch screens," IEEE Transactions on Consumer Electronics, Vol.60, Issue 1 , pp. 99 –106, February 2014.

[2]Chanwoo Chun, "A Systematic Technique of Smart Phone Keyboard Layout Design for Optimal Text-Messaging," Proc. of IEEE ICCE 2015, pp.603-605, January 2015.

[3] https://en.wikipedia.org/wiki/Amharic

[4] http://www.cld-korea.org/diversity/diversity2_1.php

[5] https://developers.**google**.com/**open-source**

[6]http://www.aau.edu.et/?s=amharic

[7]http://amharic.com/contents/en-us/d33.html

[8]https://code.**facebook**.com/**projects**

An Energy Harvesting Aware Routing Protocol in Mobile Ad-hoc Wireless Sensor Network

Kyuhyun Shim
Dept. of Information System in
Graduate School of Smart City Science Management
Hongik University, Republic of Korea
lread714 @naver.com

Beongku An
Dept. of Computer and Information
Communications Engineering,
Hongik University, Republic of Korea
beongku@hongik.ac.kr

***Abstract*—In this paper, we propose an energy harvesting aware routing protocol in mobile ad-hoc wireless sensor networks. Our proposed routing protocol is based on AODV protocol and takes into account the amount of remainder energy, the charging rate of each node, and the hop count of routing path. We evaluate the performance of our proposed protocol by conducting simulation on OPNET. The results show that packet delivery ratio is similar to our previous study. However, network lifetime is longer compared with our previous study.**

Keywords - mobile ad-hoc wireless sensor network; energy harvesting; AODV; routing protocol;

I. INTRODUCTION

In recent years, wireless ad-hoc network technology has been developed and applied to many fields. One kind of wireless ad-hoc networks is wireless sensor networks (WSN). In WSNs, the size of sensor node is often small and nodes freely move in the networks. Due to the limited battery capacity in WSN, node lifetime is an important parameter. The reason is that setting nodes are not easy to fix and changed node in WSN. In recent years, many studies focus on how to increase network lifetime in WSN.

DEHAR is a new adaptive and distributed routing algorithm for finding energy optimized routes in WSN with energy harvesting [1]. Commonly used on-demand routing protocol in the WSNs is Ad-hoc On-demand Distance Vector (AODV)[2] protocol which selects the shortest path. However, ADOV did not consider the fact of energy. In [3], they proposed incorporating the path accumulation feature in AODV. In [4], they use the concept of energy distance introduced by [1]. They applied AODV routing protocol but do not consider hop count to select routing path.

In this paper, we propose a routing protocol, called AODV-EH, which is based on AODV routing and takes the effect of energy harvesting and efficiency into consideration. We evaluate the performance of AODV-EH by using OPNET simulator and compare with other routing protocols.

The rest of this paper is organized as follows. In Section II, we give the overview of AODV and our proposed routing protocol. In Section III, we present our simulation environment and experiment results of the AODV-EH. Finally, conclusion and future work are given in Section IV.

II. PROPOSED ENERGY HARVESTING AWARE ROUTING PROTOCOL

A. Overview of AODV routing protocol

In AODV a route is selected from the following processes. The network that adopts AODV is silent until a connection is requested. When a sender node (or source node) needs a connection between the sender node and a destination node, the sender node broadcasts a Route Request (or RREQ for short) for connection. Other nodes in the network forward this message, and record the node that they heard it form, creating a temporary routes back to the sender node. When a node receives such a message and already has a route to the desired receiver node (or destination), it sends a Route Reply (RREP) backwards through a temporary route to the requesting node. The sender node then adopts the route with least hops through other nodes [2].

B. An energy harvesting aware routing: AODV-EH

A route selecting algorithm is proposed by the following equation

$$E_{average} = \frac{1}{H}\sum_{i=0}^{H}[pE_i + k(1-p)C_i] \quad (1)$$

In Eq.(1), $E_{average}$ means average energy of nodes over each route. H is hop-count between a source and a destination. E_i is remainder of node energy. C_i is energy of charge rate per unit. p is portion of between E_i and C_i. For example, if E_i is more important than C_i. Then p is larger than 0.5 and k make balance between E_i and C_i. We choose route of the largest result of Eq.(1). If the average energy of each route equals, then we consider stability of route by using Eq.(2).

$$E_{stability} = \frac{1}{H}\prod_{i=0}^{H}[pE_i + k(1-p)C_i] \quad (2)$$

In Eq.(2), $E_{stability}$ means stability of each route, and the information(E_i , C_i) of each node over each route is multiplied. The larger result of Eq.(2) means that this route is more stability. Therefore, we choose the route with the largest result of Eq.(2) as the selected route.

Fig.1 shows the system model used in this paper. In our model, there are two paths having different node remaining energy between a source and a destination. According to

algorithm of AODV-EH which is presented in previous part, a routing path is selected.

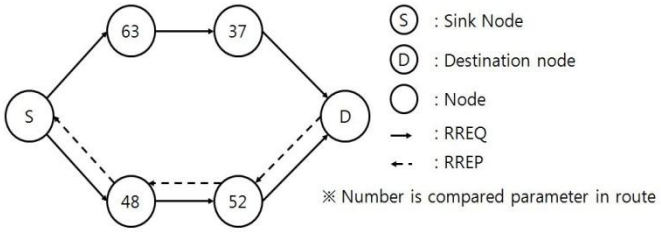

Figure 1. System mode for proposed AODV-EH.

III. PERFORMANCE EVALUATION

In this section, the performance of AODV-EH is evaluated by using OPNET. The considered WSN in this paper consists of 50 sensor nodes in sensing field. There are one sink (gateway) and one monitor center. The simulation parameters are summarized as follows.

TABLE 1. SIMULATION SET UP

Parameter	Descriptions
Simulation area	1,000m × 1,000m
Number of mobile node	50
Random way-point Mobility	0~40*km/h*, 0-360°
Radio range	250m
Capacitor	100mW
Charge rate of node	1~ 5mW

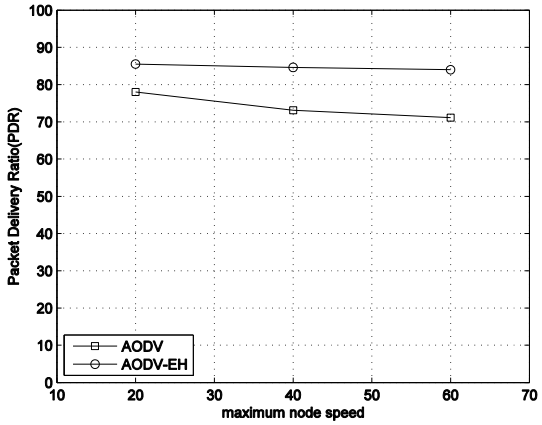

Figure 2. PDR as a function of node speed

Fig.2 shows the comparison results of PDR for AODV-EH and AODV as a function of node speed. Node speed means maximum node speed that is randomly changed from 0 km/h to V_{max}. As we can see Fig.2, AODV and AODV-EH have similar patterns of PDR while PDR decreases as speed is increased. PDR of AODV-EH is better than PDR of AODV. AODV-EH considers energy level and reminder. However, AODV considers hop count to select route.

Fig.3 shows that average energy of selecting route as a function of simulation time of interval. As we can see in Fig.3, when node speed increases, consumption of energy increases. In the high speed, the control signal to find the route between a source node to a destination node consumes a lot of energy comparing to low speed. From Fig.3, we can observe that node of high speed needs to many control signals to find route path. In general node case of AODV, average energy of node tends to continue to decrease while AODV-EH tends to repeat increasing and decreasing. The reason is that AODV-EH considers energy charging at each nodes.

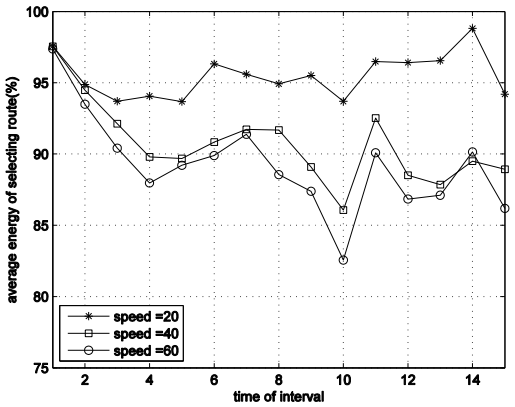

Figure 3. Average energy of selecting route as a function of node speed

IV. CONCLUSION

In this paper, we propose an energy harvesting aware routing protocol, called AODV-EH. The main feature of the proposed AODV-EH is to consider together the remaining energy and energy harvesting of each node, number of hop-count of a route, route stability based on average energy together. The performance evaluation shows the proposed energy harvesting aware routing method can be applied for mobile wireless ad-hoc and sensor networks.

ACKNOWLEDGMENT

This research was supported by the MSIP (Ministry of Science, ICT and Future Planning), Korea, under the ICT/SW Creative Research program (IITP-2015-R2212150026) supervised by the IITP(Institute for Information & communication Technology

REFERENCES

[1] Jakobsen. M.K., Madsen. J., Hansen. M.R., "DEHAR: A distributed energy harvesting aware routing algorithm for ad-hoc multi-hop wireless sensor networks," *2010 IEEE International Symposium on World of Wireless Mobile and Multimedia Networks (WoWMoM)*, pp.1-9, June 2010.

[2] C.perkins, E. Beling-Royer, S. Das, "Ad hoc on-demand distans vector(aodv) routing," RFC 3561, 2003.

[3] Gwalani. S., Belding-Royer. E.M., Perkins. C.E., "AODV-PA: AODV with path accumulation," *IEEE International Conference* in *Communications, 2003. ICC '03.* , pp.527-531, May 2003.

[4] Pu Gong, Quan Xu, Chen, T.M., "Energy Harvesting Aware routing protocol for wireless sensor networks," *2014 9th International Symposium* in *Communication Systems, Networks & Digital Signal Processing (CSNDSP)*, pp.171-176, July 2014.

The Improved Performance of the Shadow Area User by Using the Relay in the Wireless Communication System

Ji-Hun Gill
uT Communication Research Institute
Sejong University
Seoul, Korea
qqbqnutnut@gmail.com

Young-Min Ko
uT Communication Research Institute
Sejong University
Seoul, Korea
cruz22@naver.com

Hyoung-Kyu Song [1]
uT Communication Research Institute
Sejong University
Seoul, Korea
songhk0514@gmail.com

***Abstract*— Nowadays, wireless communication system is actively used in everyday life. The most important thing is the performance improvement. In the MIMO-OFDM system can provide multiplexing gain or diversity gain. These gains are obtained in proportion to the increase of the number of antennas. However, the use of the multiple antennas has the problems. Therefore, this paper proposes a cooperative system for improving of performance in the bad communication environment area.**

Keywords-component; MIMO-OFDM, OSIC, relay, V-BLAST

I. INTRODUCTION

Transmission systems based on orthogonal frequency division multiplexing (OFDM) can be extended to a multiple input multiple output (MIMO) systems in order to obtain high performance [1]. The MIMO-OFDM system obtains the high data rate or the high reliability without the use of additional bandwidth and power consumption in wireless communication [2]. However, the use of the multiple antennas has the problems for the limited size, high cost and hardware limitations. In order to overcome these problems, the cooperative communication has recently been researched. The cooperative communication has been considered as an alternative way to achieve spatial diversity in case the terminals can't use the multiple antennas. The cooperative communication can provide the high performance by using only the minimum antennas in wireless communication. The vertical Bell laboratories layered space time (V-BLAST) is an effective MIMO-OFDM system which provides spatial multiplexing gain and reception diversity gain. For this reason, a lot of detection algorithms have been proposed for the MIMO-OFDM systems. One of the typical MIMO multiplexing schemes is vertical Bell laboratories layered space time (V-BLAST). The V-BLAST is an effective MIMO-OFDM system which provides spatial multiplexing and reception diversity gain. For this reason, a lot of detection algorithms compared with V-BLAST have been proposed for the MIMO-OFDM systems. Among those detection algorithms for V-BLAST, the linear detection schemes are popular way to detect the received signals with low complexity. However, linear detection schemes have the worse performance among MIMO detection schemes for noise enhancement. The ordered successive interference cancellation (OSIC) detection scheme has better performance than linear detection. In order to overcome the problems for using the multiple antennas, this paper proposes a cooperative MIMO-OFDM system as Fig. 1. The communication takes place only over cooperative communication for performance improvement to the user in the cell boundary. The source and destination only communicate through the relay. Also, the source, the relays and the destination have two antennas. As a result, the source can overcome the problems of the multiple antennas.

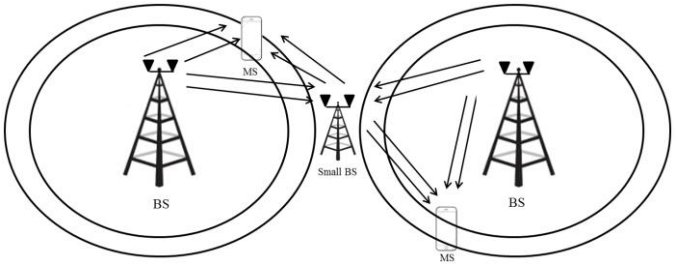

Figure 1. Proposed cooperative system model

II. PROPOSED SHCEME

This paper proposes the cooperative communication system using small base station in order to obtain high performance. The base station transmits the signals to the MS which is located in cell boundary. And the small base station which is received the signals from the base station retransmits the same signals to the MS. The small base station plays a role as relay in the proposed scheme. The transmission signals are presented in Table 1. The proposed configuration of transmission signals uses the CDD shceme in order to obtain the improved diversity gain.

1) Corresponding author

TABLE I. THE CONFIGURATION OF TRANSMISSION SIGNALS

Time slot	BS		Small BS	
	Tx_1	Tx_2	Tx_1	Tx_2
$T=1$	S_1	$S_{1\delta_1}$	–	–
$T=2$	S_2	$S_{2\delta_1}$	S_1	$S_{1\delta_1}$
$T=3$	S_3	$S_{3\delta_1}$	S_2	$S_{2\delta_1}$
⋮	⋮	⋮	⋮	⋮
$T=n$	S_n	S_{n,δ_1}	S_{n-1}	S_{n-1,δ_1}

The proposed configuration of transmission signals applying the CDD scheme is presented in Table 1. In each time slot, the two signals are transmitted by BS. Also, small BS which receives the signals from BS retransmits the signals to MS which is in the cell edge shadow area. The received signals at the MS are expressed as follows,

$$Y_{n,i} = S_{2n-3} G_{1,i} + S_{2n-2,\delta_1} G_{2,i} + r$$
$$S_{2n-2,} H_{1,i} + S_{2n-2,\delta_1} H_{2,i} + N_{n,i} \quad (1)$$

*G*1,I and *G*2,i are channels that connect the signals from BS to the *i*-th antenna of the MS. Also, *H*1,*i* and *H*2,*i* denote the channels that connect the signals from the Small BS to the *i*th antenna of the MS. The noise at the *i*-th antenna of the destination at time *n* is represented by *Nn*,*i*. The cyclically delayed symbols give only an effect on the destination as multi-path. Therefore, the Eq. (1) can be expressed as follows,

$$Y_{n,i} = S_{2n-3} G_i + S_{2n-2,} H_i + N_{n,i} \quad (2)$$

In this system, the received signals are detected by OSIC detection scheme. The accurate detection of the first signal affects the overall system performance. The proposed scheme is intended to strengthen the DFE properties by using CDD scheme. The system obtains diversity gain and multiplexing gain at the same time by using the proposed scheme. As a result, the proposed scheme provides a reliable communication in the cell edge shadow area.

III. SIMULATION RESULTS

In this section, the proposed scheme is evaluated in comparison with the conventional scheme. In this simulation, the simulation parameters are as follows: the number of carriers is 256, the cyclic prefix (CP) length is 64 and the modulation is BPSK modulation. The channel model is a Rayleigh fading channel model and the number of channel paths is 7. The cyclic delay length is considered that δ 1 is 128. The convolutional coding is applied with the constraint length of 3 and the code rate of 1/2. The proposed scheme has the simulation result in case of cooperative scheme using cooperation of small base stations. And the comparison subject is the conventional system which communicates only between BS and MS. In Fig.2, The proposed cooperation scheme has high performance than the conventional scheme.

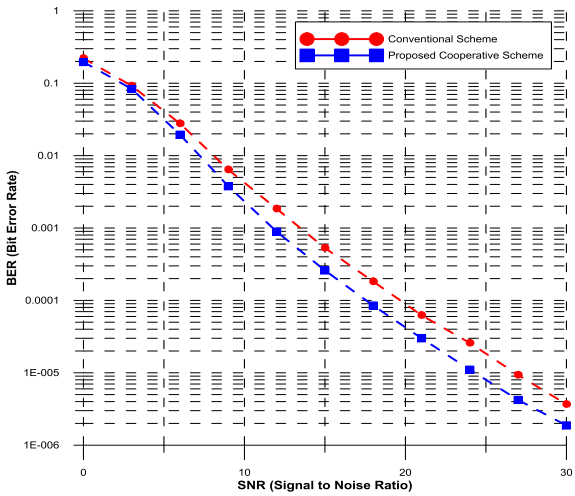

Figure 2. BER performance of the proposed scheme compared to the conventional shcme

The proposed cooperation scheme obtains a high performance by strengthening the OSIC properties through CDD scheme. According to the simulation results, the proposed scheme can obtain the improved BER performance effectively.

IV. CONCLUSION

In this paper, the cooperation scheme using the cooperation of small BS is proposed in order to improve the communication performance in the cell edge shadow area. In the BS transmits the signal by using Tx1. The other antenna transmits the cyclically delayed signals in order to provide diversity gain. The configuration of cooperative transmission signals reinforces the OSIC properties. Therefore, the proposed cooperative scheme can achieves a high performance. As a result, the proposed cooperative scheme ensures a sufficient communication environment by using the cooperation of the small BS when the MS is located in cell edge shadow area.

ACKNOWLEDGMENT

This research was supported by Basic Science Research Program through the National Research Foundation of Korea(NRF) funded by the Ministry of Science, ICT and future Planning(No. 2013R1A2A2A01067708) and was supported by the IT R&D program of MOTIE/KEIT [10054819, Development of modular wearable platform technology for the disaster and industrial site].

REFERENCES

[1] E. H. Lee and H. K. Song, "An improved transmission rate in cooperative communication based on OFDMA system", *IEICE Trans. Fundamentals.*, vol. E96-A, no.7, pp.1677-1670, July 2013

[2] M. S. Baek, S. Y. Yeo, Y. H. You and H. K. Song, "Combined QRD-M and DFE detection technique for simple and efficient signal detection in MIMO-OFDM systems", *IEICE Trans. Commun.*, vol. E90-B, no.5, pp.1261-1265, May 2007

Enhanced Performance Using Selective Subcarrier in the Wireless Fidelity Backscatter

Sang-Young Kim
uT Communication Research Institute
Sejong University
Seoul, Korea
12ksy12@naver.com

Yong-Jun Kim
uT Communication Research Institute
Sejong University
Seoul, Korea
kyjgood88@naver.com

Hyoung-Kyu Song [1]
uT Communication Research Institute
Sejong University
Seoul, Korea
songhk0514@gmail.com

***Abstract*—This paper proposes the signals detection scheme using selective subcarrier for enhanced communications coverage in the wireless fidelity backscatter system. The conventional system uses every subcarriers of good channel condition in order to enhanced performance. Especially, when signal to noise ratio is increased , the proposed scheme has efficient performance. From the simulation results, the proposed scheme has good bit error rate performance compared to the conventional scheme.**

Keywords-component; subcarrier; wireless fidelity Backscatter; wireless fidelity Reader; wireless fidelity Tag

I. INTRODUCTION

Recently, internet of things (IoT) sensor technique is expected to rapidly increase in the wireless communication system. Now, main system of IoT such as near field communication (NFC), Bluetooth and wireless fidelity (Wi-Fi) system do not support special sensors combination of tag and device to device communication (D2D) at the same time [1]. But, batteryless system such as Wi-Fi backscatter system can solve these problems. And Wi-Fi backscatter system is one of the schemes developing radio frequency identification (RFID) sensor networks because it can provide the connection of the internet of RFID devices by the ambient Wi-Fi signals [2][3].

When the technical problem is solved, Wi-Fi backscatter system uses existing communication infrastructure without extra reader and battery compared to the conventional system. And Wi-Fi backscatter system may overcome limitation of existing technology using smart tag is exploited. But the Wi-Fi backscatter system has the disadvantages of the limited communication distance and the low data rate by the limited. Thus, paper proposes the signal detection scheme using selective subcarrier of good channel condition for enhanced data rate and communication distance

This paper is composed as follows. Section 2 shows the system model of the Wi-Fi backscatter system which harvests the energy from the Wi-Fi signals. Section 3 describes the conventional scheme and the proposed scheme of signal detection using selective subcarrier in the Wi-Fi backscatter system. Section 4 shows the enhanced performance of bit error rate (BER) and section 5 draws a conclusion.

II. WI-FI BACKSCATTER SYSTEM MODEL

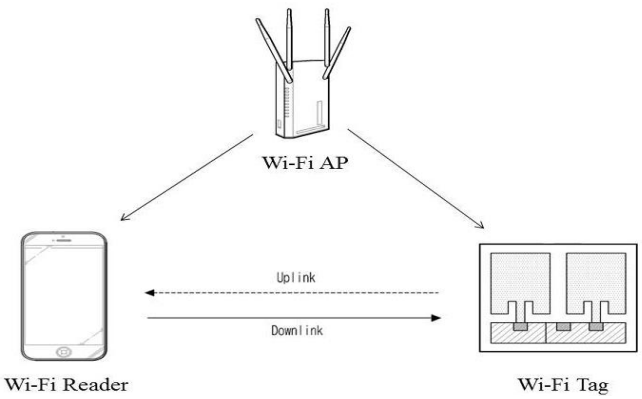

Figure 1. System model of Wi-Fi Backscatter

The Wi-Fi backscatter system is composed of the three devices as Wi-Fi access point (AP), Wi-Fi Reader and Wi-Fi Tag. The Wi-Fi AP transmits the Wi-Fi packets to the Wi-Fi Reader and Wi-Fi Tag. The Wi-Fi Tag that is a radio frequency (RF) powered device harvests the energy using ambient RF signals.

The Wi-Fi backscatter communication is as follows, The Wi-Fi Reader transmits clear to send (CTS) to self for prevent transmission of other Wi-Fi devices. The Wi-Fi Reader sends preamble to Wi-Fi Tag in order to confirm the identification (ID). If Wi-Fi Tag ID and Wi-Fi Reader ID are same, Wi-Fi Tag transmits channel state information (CSI) or received signal strength indicator (RSSI) to Wi-Fi Reader. Then, the Wi-Fi Reader transmits the payload to Wi-Fi Tag by the presence or absence of the Wi-Fi packet. The Wi-Fi Tag can know the presence of the Wi-Fi packet as '1' or the absence of

1) Corresponding author

the Wi-Fi packet as '0'. Then the Wi-Fi Tag reflects the received signals from the Wi-Fi Reader.

III. PROPOSED SHCEME

This section explains the proposed scheme of signal detection using selective subcarrier in the Wi-Fi backscatter system. The Wi-Fi Reader must detect the signals from Wi-Fi Tag. The Wi-Fi Reader uses average power of subcarrier of Wi-Fi packet in order to signal is detected. But, if channel condition is bad, power of subcarrier is attenuated. Thus, performance of received signals is poor because every subcarrier with the attenuated power is used.

The proposed scheme determines reference value of '1' or '0' using fixed preamble packet. Next, the presence of the Wi-Fi packet as '1' of payload chooses subcarriers of good channel condition that passes reference value. The absence of the Wi-Fi packet as '0' chooses subcarriers of good channel condition that not passes reference value. The fig. 2 shows detection scheme using selective subcarrier.

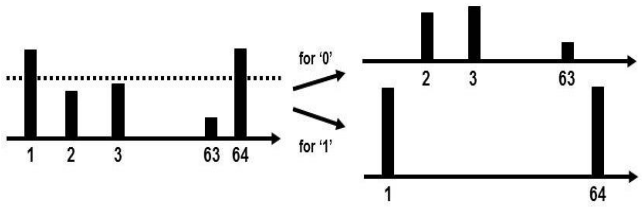

Figure 2. Detection scheme using selective subcarrier

IV. SIMULATION RESULTS

TABLE I. USING PARAMETERS OF PROPOSED SCHEME

Parameters	Value
Packet	IEEE802.11n
The number of total packets	58
The number of total preamble	8
The fast Fourier transform	64
Bandwidth of channel	20MHz
Modulation scheme	QPSK
Channel model	UWB1m, 3m, 5m

The simulation results show the BER performance of the conventional scheme and the proposed scheme in the Wi-Fi backscatter system.

Table 1 describes the simulation parameters. The proposed scheme uses the 30 subcarriers of 64 subcarriers because the channel condition of 30 subcarriers is good. Figure 3 shows BER performance according to distance such as 1m, 3m and 5m. The conventional scheme has the better performance in the additional white Gaussian noise (AWGN) channel because the conventional scheme has a lot of samples of subcarriers. But the proposed scheme has the better performance in the ultra-wideband (UWB) channel. The proposed scheme may have BER performance of 10^{-2} in the 60dB. However, the conventional scheme has not good BER performance with high SNR gain.

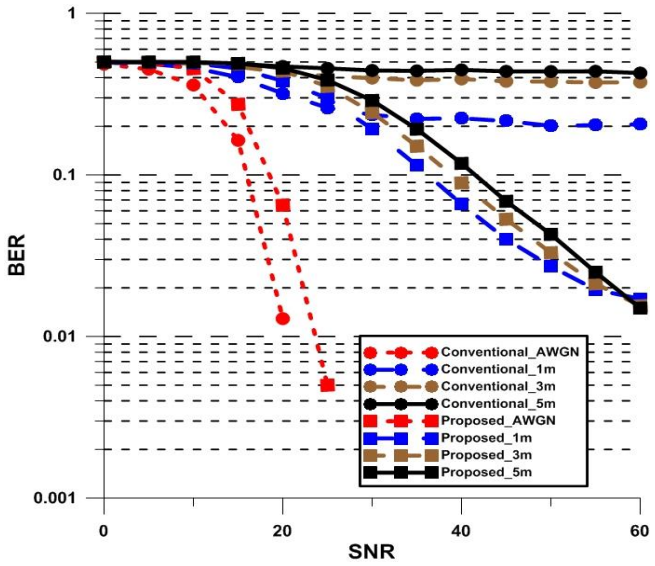

Figure 3. BER performance of the conventional scheme and the proposed scheme using selective subcarrier

V. CONCLUSION

This paper proposes the signal detection scheme of selective subcarrier. This scheme has advantage of BER performance compared to the conventional scheme using every subcarrier. Especially, when SNR is increased, the proposed scheme has efficient performance. The Wi-Fi backscatter system can use existing infrastructure with Wi-Fi packet and energy harvesting with ambient Wi-Fi signals. But, the conventional Wi-Fi backscatter system has a short communication coverage and low performance. Thus, the proposed scheme solves these problems.

ACKNOWLEDGMENT

This research was supported by Basic Science Research Program through the National Research Foundation of Korea(NRF) funded by the Ministry of Science, ICT and future Planning(No. 2013R1A2A2A01067708) and Institute for Information & communications Technology Promotion(IITP) grant funded by the Korea government(MSIP) (No.B0126-15-1076, Development of non-powered technology combined with ambient RF energy harvesting and Backscatter data transfer)

REFERENCES

[1] Kallogg B., Aaron P. and Shyamnath G. , "David W.Wi-Fi Backscatter: Internet Connectivity for RF-Powered Devices." SIG-COMM' 14, Chicago 2014

[2] Gollakota S. Reynolds M.S., Smith J.R., Wetherall D.J. "The emergence of RF-powered compution." IEEE Computer Society, vol. 47, no.1, pp.345—357, 2014

[3] Olgun U., Chen C.C. and Volakis J.L. "Design of an efficient ambient Wi-Fi energy harvesting system," IET Microwaves Antennas & Propagation, vol. 6, no. 11, pp.1200--1206, 2012

Trends and Requirements of data management platform in IoT environment

Hwashin Moon, Yongho Kim
Mobile Security Research Section
Electronics and Telecommunications Research Institute
Daejeon, Rep. of Korea
hsmoon@etri.re.kr, wtowto@etri.re.kr

Jeongnyeo Kim
Cyber Security System Research Department
Electronics and Telecommunications Research Institute
Daejeon, Rep. of Korea
jnkim@etri.re.kr

***Abstract*—The data sharing is one of essential factors which make IoT service smart. This characteristic has led to the interest in data management platform in IoT. In this paper, we describe two representative data management approach based on cloud and distributed storage respectively. Based on the closer analysis of each data system, we also present the requirements which data management platforms have to consider. In particular, we introduce the requirement for reliable IoT service.**

Keywords-IoT; data management; cloud centric architecture; distributed storage infrastructure; IoTservice security

I. INTRODUCTION

IoT means the global infrastructure for the information society, enabling advanced services by interconnecting physical and virtual things based on existing and evolving interoperable information and communication technologies (ICT) [1]. In making IoT services smart and advanced, data sharing plays an essential role. For this reason, IoT technology has been evolving to share and exploit more and more data based on the increasing number of interconnected devices. Recently, data management system for more efficient and secure data sharing has begun to attract attention.

Currently, most of data management platforms have used the cloud as their storage [2]. This results from the widely deployed cloud infrastructure and easy to use interface. Similar to how web services access to the cloud, IoT devices in the cloud based approaches also directly communicate with the cloud. This direct connection has seemed to be a natural way for IoT. However, through closer inspection of IoT applications, [3] showed that this approach has the following limitations at large scale: privacy, security, scalability, latency, bandwidth, availability, and durability control. To mitigate these limitations, [3] proposed the distributed storage architecture using not only cloud but also various local devices or systems as its storage.

Although cloud based approach has some limitations at large scale, it is expected for cloud based approach to be still utilized at the some part of IoT environment. Thus, for efficient data management service in IoT, it is necessary to examine closely how each approach should be improved. As the step toward this, in this paper, we describe the recent data management system about each approach. Through the analysis of each data system, we also introduce what to be considered for successful data management service in IoT. In particular, from a reliable IoT service point of view, we present the necessity about device integrity which existing data management systems have not considered yet, to the best of our knowledge.

II. EXISTING DATA MANAGEMETN SYSTEMS IN IOT

A. Bolt (Cloud centric architecture)

Bolt using the cloud as the storage is the data management system for connected homes. Its main purpose is efficiently to store the data generated from a lot of devices in connected homes and to provide the data to the various applications within and outside home. It abstracts the data as a stream identified by the three tuple, <Home ID, App ID, Stream ID>, where Home ID and App ID indicate the application that generates the data stream. To support data query based on the time and application specific value, it adds the tag to each record in data stream. For more efficient query, it manages the index that says the stored location of the records related to each tag and so helps the applications to find out the interested data in the large storage. In addition, for scalability and performance, it also proposes the several techniques such as data chunking and segmentation [2].

One of main characteristics of bolt is data sharing between applications running on the different homes. For this sharing, it selects the cloud as its storage. However, this sharing raises the following security issues: the reliability of the cloud storage servers and the access control. To tackle these issues, it uses a trusted key server which manages the private-public key pairs for each application and distributes the secret keys. With the trusted key server, bolt mediates these security issues by supporting the data confidentiality, integrity, and access control. For example, to ensure the data confidentiality on untrusted storage server, the data owner in bolt creates a secret key, encrypts each data record with the secret key, and stores the encrypted data in the untrusted server. The secret key is shared between applications through the key server. The shared secret key helps to prevent unauthorized applications from reading data. In addition, by using the hash-based key regression and lazy revocation techniques [4], bolt reinforces the efficiency of

This work was supported by ETRI R&D program of MSIP (Ministry of Science, ICT and Future Planning) Korea [R0110-15-1001]

access control based on the shared secret key. Lastly, bolt uses the data signature to verify data integrity.

B. Global Data Plane (Distributed storage infrastructure)

In IoT applications, most of data are generated from the edge of network [3]. Most data acquired by IoT devices can or should be processed locally and immediately discarded [3]. Some data is ephemeral, while other data should be durable [3]. These data can contain extremely privacy-sensitive information [3]. Some IoT applications such as control system may require the low latency and high Quality of Service [3]. These features of IoT applications reveal some limitations about cloud centric approach. Firstly, the data management in the cloud can incur a significant amount of upstream traffic. As the current network has focused on more downstream bandwidth, the continuously increasing IoT data can saturate the upstream link. Secondly, it is unnecessary to move the data which are locally used. This unnecessary upstream can lead the poor scalability and latency. Thirdly, because the cloud is out of user's control, the privacy, security, and durability of data are also out of user's control. For these reasons, the authors of [3] argued that cloud is not enough to cover the increasing and evolving IoT applications.

To solve these limitations, [3] proposed a distributed storage platform, called Global Data Plane (GDP). GDP uses various types of storage from heterogeneous computing platforms such as cloud [2], fog [5] and gateway to local storages such as SSD and flash RAM on the device or sensors. Above network layer, GDP constructs a distributed storage platform similar to peer-to-peer storage systems. To optimally manage the data, called logs, within this overlay platform, GDP utilizes location-independent routing based on Distributed Hash Table (DHT) and a variety of placement and replication policies. By placing, migrating and replicating data dynamically and optimally, these techniques help to guarantee the scalability, latency, bandwidth, QoS, durability, and privacy. Like bolt, GDP also utilizes encryption and signing based on the cryptographic keys to support integrity, confidentiality, and access control. In addition, GDP additionally proposes the Common Access APIs (CAAPIs) on the top of storage layer. The CAAPI layer helps to make applications by providing the useful functions such as query, key-value store, and database operations to the applications.

III. DATA PLATFORM REQUIREMENTS IN IOT

IoT is expected to consist of billions of heterogeneous devices beyond the scale of web-based and Internet-based platform. It is also expected that the considerable number of IoT devices operate under the limited resource and the network with high packet loss and low throughput. Due to these characteristics, data management service for storing, querying, and sharing IoT data have to consider not only performance but also the following requirements in developing its architecture.

- **Scalability**: Platform has to be able to cover the continuously increasing IoT applications, devices and data generated by them.
- **Lightness**: The resource constrained devices also have to use the data management service.
- **Interoperability**: Data service has to provide the common and flexible API to support the heterogeneous devices. Platform, consisted of various systems and networks, also has to try to provide reliable service.
- **Quality of Service**: Over the dynamically changed environment, platform has to try to satisfy the requirement of IoT applications such as latency.

In addition, the privacy sensitive information generated by IoT devices demands the following security requirement.

- **Confidentiality, authentication, and access control**: Data stored in the untrusted servers must to be protected from unauthorized access.
- **Privacy control by user**: User can want to control or check the durability of his own data. User can also want to regulate the security policy. It can give "the control by user" more trust to separate the policy from mechanism. Of course, this function has to be simple and easy to use.

Lastly, some of IoT services, which particularly make a decision based on the data, need to check the reliability of data. Considerations to support this requirement are as follows:

- **Data integrity**: Before using data, applications must check whether the data is changed or not maliciously.
- **Device integrity**: Malicious or infected applications (or devices) can generate and deploy the false data. The fake data, particularly in service such as e-health, can result in severe impact. Thus, data platforms need at least to manage the integrity information about devices which afford to check integrity. However, existing data management platforms have not considered device integrity yet.

ACKNOWLEDGMENT

This work was supported by Institute for Information & communications Technology Promotion (IITP) grant funded by the Korea government (MSIP) (NO. R0110-15-1001, Secure hardware containers technology to protect IoT devices from Denial of Service attack)

REFERENCES

[1] Recommendation ITU-T Y.2060, "Overview of Internet of Things", ITU-T, 2012

[2] T. Gupta, R. P. Singh, A. Phanishayee, J. Jung, and R. Mahajan, "Bolt: data management for connected homes", In Proceedings of the 11th USENIX Symposium on Networked Systems Design and Implementation (NSDI 14), 2014

[3] B. Zhang, N. Mor, J. Kolb, et al., "The cloud is not enough: saving IoT from the cloud", 7th USENIX Workshop on Hot Topics in Cloud Computing (HotCloud 15), 2015

[4] K. Fu, S. Kamara, and T. Kohno, "Key regression: enabling efficient key distribution for secure distributed storage", Computer Science Department Faculty Publication Series, 2006

[5] F. Bonomi, R. Milito, J. Zhu, and S. Addepalli, "Fog computing and its role in the internet of things", In Proceedings of the first edition of the MCC workshop on Mobile cloud computing, 2012, ACM

Security Performance Score and Economic Investment

Quan Tran Hai[1], Trang Hoang Thi Huyen[1], Seong Oun Hwang[1], Young Yung Shin[2], Myungchul Kim[2], Chaeho Lim[2]

[1]Hongik University, [2]KAIST

Abstract

Cost effective cyber security is usually done at the governance level. The aim of capital investment of cyber security defense by government policy is to increase cyber security level or security score of each organization. Level A score cyber security can be achieved by effective and efficient security control with legal compliance. In this paper, we investigate the US agency cost effective model and show that the model allows us to spend money efficiently in security.

1. Overview

For a long time, Republic of Korea has received a number of cyber attacks from China and North Korea attackers. Chinese hackers are mostly targeting economic values and North Korean hackers are doing for political terror as well as financing issue. Meanwhile, to respond to cyber attacks, the United States has a risk management strategy called "Risk can never be eliminated and so it must be MANAGED".

2. Related Study

2.1 Risk Management Framework

The United States federal government defines the definition of the necessary security controls to their computer assets by Federal Information Security Modernization Act (FISMA) [1]. FISMA legislation in 2002 is now the fundamental governance of cyber security of the US with budget control by OMB. Risk management process should take the following four steps: (1) Framing Risk, (2) Assessing Risk, (3) Responding to Risk, and 4) Monitoring Risk. Risk management process is mainly in stages by the monitoring risk that shows the quantitative analysis of the status of various items such as risk and security controls, security capabilities, and scored level.

2.2 The Stages of Security Capabilities of Organization

The security level of the organization is known as the competence of the security control of the security risks. It checks whether security controls are effective and efficient, and legal compliance is carried out by analyzing the actual operating data. For example, in the case of vulnerability management, the score is driven by the number of effectively operated assets among total assets. Finally, the security score can be calculated by the sum of all security control risk as follows:

$$RISK^{VULNERABILITY} = (Asset^{Effect} / Asset^{TOTAL}) \times 100$$

$$RISK^{ORGANIZATION} = SUM (RISK^{SC1}, RISK^{SC2,} .... RISK^{SCn}) / n$$

* SC : Security Control

2.3 OMB Security Management Control

The United States Office of Management and Budget (OMB) has instituted a number of laws, regulations, and directives that govern establishment and implementation of federal information security practices. These laws, regulations, and directives establish federal and agency level responsibilities for security management control, define key information security roles and responsibilities, identify minimum information security controls, specify compliance reporting rules and procedures, and provide other essential requirements and guidance. They also provide an infrastructure for developing and promulgating detailed standards and implementation guidance to federal agencies and overseeing implementation of required practices through NIST (National Institute of Standards and Technology) and the Government Accountability Office (GAO), respectively.

2.4 Capital Planning and Investment Control Process

This model is offered by the GAO [2]. It is used for facilitating effective implementation of OMB capital planning and NIST security requirements. This model is comprised of 3 phases such as Select (activities involved with assessing and prioritizing current and proposed IT projects), Control (activities designated to monitor the investment) and Evaluate (determining the efficacy of the investment).

2.5 FISMA Score

Security performance is measured by the FISMA score, which is established by the following criteria [3]: (1) A score: Item was fully implemented and is considered by the larger cyber community as an improvement over previous practices or fills a previous void; now requires only routine maintenance. (2) B score: Item was significantly implemented and represents an improvement, but still requires some additional action to achieve fully-implemented status. (3) C score: Item was implemented but has received mixed or negative reviews from the larger cyber community; or implementation has proven to have gaps or flaws in application. (4) D score: Item still in work; or item's implementation was delayed to the point that it suggests a lack of leadership or decisiveness in assigning priorities, or compounding delay in other areas. (5) F score: No progress shown against the item or item has received universal criticism for having no value to enhancing cybersecurity.

3. Security Cost Analysis

We obtained the data in Table 1 by compiling FISMA reports [4,5,6] over recent fiscal years and then combining cost and security score for all agencies. At first, we collected the score of all agencies in term of all attributes as well as the spending of agencies and put them side by side. We also translated the score in numeric into letter score for easy visibility. Finally, in order to have insights in the trends, we added marker in the table to indicate the status of agencies in score and money by comparing with the previous year. As can be seen from Table 1, most of the FISMA scores in all the

agencies increase, which means that the agencies are spending money efficiently in security. However, there are some agencies whose score is decreasing, but still in high score. For instance, the scores of Department of Homeland Security and Nuclear Regulatory Commission agencies are decreasing in 2014 (98 and 96).

Table 1. FISMA score and budget

Agency	FY 2014			FY 2013			FY 2012		
	Score (In %)	Score (In letter)	Spending (In Million $)	Score (In %)	Score (In letter)	Spending (In Million $)	Score (In %)	Score (In letter)	Spending (In Million $)
General Services Administration	99	A+	53	98	A+	46	99	A+	19
Department of Justice	99	A+	579	98	A+	446	94	A	216
Department of Homeland Security	98	A+	1343	99	A+	1109	99	A+	615
Nuclear Regulatory Commission	96	A	19	98	A+	17	99	A+	12
Social Security Administration	96	A	59	96	A	40	98	A+	167
National Aeronautics and Space Administration	95	A	102	91	A-	150	92	A-	65
Department of the Interior	92	A-	48	79	C+	38	92	A-	50
Department of Education	91	A-	32	89	B+	22	79	C+	19
National Science Foundation	87	B+	163	88	B+	86	90	A-	13
United States Agency for International Development	86	B	16	83	B-	22	66	D	2
Environmental Protection Agency	84	B	7	77	C+	20	77	C+	26
Department of Labor	82	B-	17	76	C	23	82	B-	34
Department of Veterans Affairs	80	B-	153	81	B-	121	81	B-	111
Department of Energy	78	C+	257	75	C	218	72	C-	214
Office of Personnel Management	74	C	7	83	B-	7	77	C+	13
Department of the Treasury	67	D+	200	76	C	268	76	C	403
Department of Transportation	63	D-	91	61	D-	96	53	F	116
Small Business Administration	58	F	5	55	F	5	57	F	4
Department of Agriculture	53	F	88	37	F	63	34	F	61
Department of State	42	F	114	51	F	86	53	F	28
Department of Health and Human Services	35	F	170	43	F	181	50	F	191
Department of Housing and Urban Development	19	F	14	29	F	12	66	D	14
Department of Defense	NA	NA	8955	NA	NA	7106	NA	NA	12056
Department of Commerce	NA	NA	213	87	B+	163	61	D-	155

Because FISMA score is the sum of all the agencies' score, if an organization is said to be A level of security, it means that most of the agencies in that organization have score A, or their score are increasing to reduce the gap with A level.

In order to achieve cost-effectiveness in security, most of the agencies should have increasing scores while the costs are decreasing. For example, we look at some of the agencies: Environment Protection Agency is considered cost-effective. In Fig. 1, we can see that the score of this agency is increasing through the years: 77 in 2012, 77 in 2013 and 84 in 2014, respectively, equivalent to rank B. But the money spent for this agency is decreasing dramatically: 26 million dollars in 2012, 20 million dollars in 2013 and 7 million dollars in 2014, respectively. This is an example of cost effective organization in security. The less money is spent while maintaining/increasing its score, the more cost-effective the agency is.

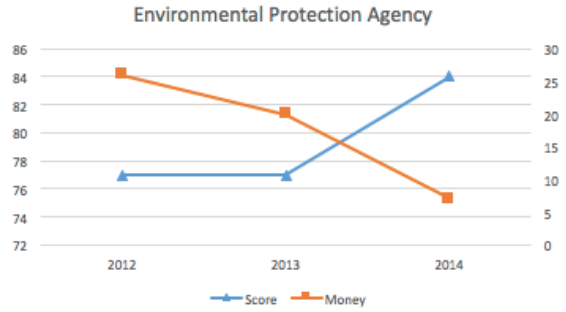

Figure 1. Environmental Protection Agency

4. Conclusion

In the paper, we studied from cyber security risk management system by the FISMA legislation, through verification of security level of each agency and budget control by OMB, which comprises the US agency cost effective model. The analysis result confirms that the model allows us to spend money efficiently in security. That is, each federal government agency can achieve a higher level of security with the reduced security budget.

Republic of Korea has also operated the ISMS (Information Security Management System) [7] for critical infrastructure security management, which is similar to FISMA. However, it lacks budget control, so it does not play a substantial role in increasing the security level. Therefore, we suggest that Republic of Korea needs to consider increasing the practical security level by adopting models like the US agency cost effective model.

5. References

[1] FISMA - http://www.dhs.gov/fisma.

[2] SP 800-100 – Guide for Managers.

[3] Federal Government Cybersecurity Progress: Obama Administration Report Card 2009-Present.

[4] Fiscal Year 2012: Report to Congress on the Implementation of The Federal Information Security Management Act of 2002, March 2013.

[5] Annual report to congress: Federal information security management act; office of management and budget, May 1, 2014.

[6] Annual report to congress: Federal information security management act; office of management and budget, February 27, 2015.

[7] ISMS, http://isms.kisa.or.kr/kor/intro/pimsIntro02.jsp.

Acknowledgement

It was supported by the MSIP (Ministry of Science, ICT and Future Planning), Korea, under the Global IT Talent support program (NIPA-2014-H0905-14-1004) supervised by the NIPA (National IT Industry Promotion Agency) and by Institute for Information & communications Technology Promotion(IITP) grant funded by the Korea government(MSIP) (No.R2213-15-0002, Electronic receipt processing, analysis system). It was also supported by Basic Science Research Program through the National Research Foundation of Korea (NRF) funded by the Ministry of Education (2014R1A1A2054174).

Design of Intelligence System for Detecting New Malware

Insung Yeo[1], Vu Duc Ly[1], Seong Oun Hwang[1], Chaeho Lim[2]

[1]Hongik University, [2]KAIST

Abstract - New malwares normally operate 30 minutes prior existing security systems react. Previous security products such as AntiVirus and Intrusion Detection System (IDS) known as signature-based system fail to detect new malware. In order to detect a new malicious code, sufficient time to collect and analyze the target is required. In this paper, we consider these limitations and suggest an intelligence system design to analyze and respond as soon as possible when a new malware penetrates the system.

Key words: APT, Web Drive by Download, IDS, AntiVirus, Profiling, Signature

I. Introduction

Recently, the APT (Advanced Persistent Threat) [1] attacks targeting governments and companies have occurred frequently. APT refers to a constant type of whole offensive manner attacks which have been performed for a long time using social engineering, zero-day vulnerabilities and latest techniques. Despite the considerable expenditure on current security products, attackers have bypassed these defenses and spread malicious code without any interruption.

A. Limitations of traditional security products

Traditional security products cannot counteract attacks such as zero-day and APT until they identify the malware and make the corresponding malware signatures. Even if they manage to do them, they usually miss due golden time (it may range from a couple of minutes to a number of minutes; but we set 30 minutes on average as golden time) and the information from the user's PC was leaked.

As shown in Fig. 1 which was released in 2012 from Verizon [2], the time for a malicious code to proceed from the initial infringement to the final operation phases is within a few minutes. On the other hand, it takes from a day to even a week for malware analysists to identify and respond appropriately to the malware.

Therefore, firewall, IDS/IPS (Intrusion Prevention System) and AntiVirus are not sufficient to defend against modern threats that leverage a combination of technologies such as various attack vectors and vulnerabilities.

Figure 1. Malware infringement and response time

B. The needs and goals of intelligence system

As we mentioned above, the existing approaches are not appropriate in dealing with the current situation because new malwares are created and distributed massively in a very short time everyday and most of them cannot be checked practically.

Therefore, the need for intelligence system to detect such malware and threats in advance is required rather than the existing after-the-fact analysis to detect malware that have already been propagated. Intelligence system can be defined as a system that collects, manages and processes the data which will be used to determine security actions. Through the intelligence system, we can analyze strategies, technologies and pattern information of attackers. In addition to this, we can achieve critical goals such as prior detection of attacks, reduction of fatal actions, and provision of important insights into security threats.

II. Design of intelligence system

A. System design

To overcome the limitations of traditional security products, we offer our system as shown in Fig. 2. At the time of writing this paper, the components in the system are partially developed.

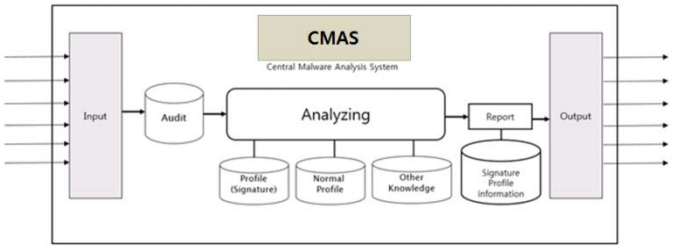

Figure 2. Central malware analysis system

B. Component description

a. Input part

This system is fed with suspicious files which are collected through malicious URL, e-mail and honeypot. These input files are not determined to be malicious or not yet, and will be under further testing at the next step.

b. Audit part

It extracts some basic information such as name, size and source from the suspicious files received from the Input part and then stores them in the database.

c. Analyzing part

In the Analyzing phase, it checks if a suspicious file matches any of existing detection information in Signature DB, Profiling DB and Other Knowledge DB. If the file does not match, the system analyzes it further by using malware analysis module.

d. Report part

Report module provides information on the suspicious file to the security administrator and stores the analysis result in Signature Profile information DB.

e. Output

It provides detection systems such as AntiVirus and IDS with signature information of the malware. It can also provide the information in the form of OpenIOC [3] to security organizations or vendors.

III. PCS (Payload Chase System)

We finished the overall design of the proposed intelligence system whose component modules are being developed now. In parallel with this development, we also developed a system called PCS (Payload Chase System) to complement and verify the intelligence system. PCS collects new malware downloadable at the distribution page by Drive-by-Download [4] attacks in advance, records the AntiVirus detection rate of malware, and monitors the change of them as time passes by.

As you look at the results of the VirusTotal [5] query in Fig. 3, most of AntiVirus vaccines cannot detect new malware at the initial stage. They begin to detect after a period of time, which reflects that AntiViruses take time to analyze and block new malware. However, if we combine the proposed intelligence system with PCS together by allowing PCS to feed the analysis result to the intelligence system, we can quickly cut off the new malware in advance.

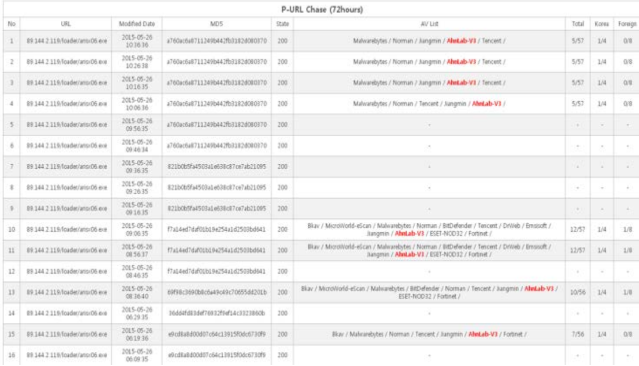

P-URL Chase (72hours)

No	URL	Modified Date	MD5	State	AV List	Total	Korea	Foreign
1	89.144.2.119/loader/ans06.exe	2015-05-26 10:36:36	a760ac6a8711249b442fb3182d080370	200	Malwarebytes / Norman / Jiangmin / AhnLab-V3 / Tencent /	5/57	1/4	0/8
2	89.144.2.119/loader/ans06.exe	2015-05-26 10:26:38	a760ac6a8711249b442fb3182d080370	200	Malwarebytes / Norman / Jiangmin / AhnLab-V3 / Tencent /	5/57	1/4	0/8
3	89.144.2.119/loader/ans06.exe	2015-05-26 10:16:35	a760ac6a8711249b442fb3182d080370	200	Malwarebytes / Norman / Jiangmin / AhnLab-V3 / Tencent /	5/57	1/4	0/8
4	89.144.2.119/loader/ans06.exe	2015-05-26 10:06:36	a760ac6a8711249b442fb3182d080370	200	Malwarebytes / Norman / Tencent / Jiangmin / AhnLab-V3 /	5/57	1/4	0/8
5	89.144.2.119/loader/ans06.exe	2015-05-26 09:56:35	a760ac6a8711249b442fb3182d080370	200	-	-	-	-
6	89.144.2.119/loader/ans06.exe	2015-05-26 09:46:34	a760ac6a8711249b442fb3182d080370	200	-	-	-	-
7	89.144.2.119/loader/ans06.exe	2015-05-26 09:36:35	821b0b5fa4503a1e638c87ce7ab21095	200	-	-	-	-
8	89.144.2.119/loader/ans06.exe	2015-05-26 09:26:35	821b0b5fa4503a1e638c87ce7ab21095	200	-	-	-	-
9	89.144.2.119/loader/ans06.exe	2015-05-26 09:16:35	821b0b5fa4503a1e638c87ce7ab21095	200	-	-	-	-
10	89.144.2.119/loader/ans06.exe	2015-05-26 09:06:35	f7a14ed7daf01b19e254a1d2503bd641	200	Bkav / MicroWorld-eScan / Malwarebytes / Norman / BitDefender / Tencent / DrWeb / Emsisoft / Jiangmin / AhnLab-V3 / ESET-NOD32 / Fortinet /	12/57	1/4	1/8
11	89.144.2.119/loader/ans06.exe	2015-05-26 08:56:37	f7a14ed7daf01b19e254a1d2503bd641	200	Bkav / MicroWorld-eScan / Malwarebytes / Norman / BitDefender / Tencent / DrWeb / Emsisoft / Jiangmin / AhnLab-V3 / ESET-NOD32 / Fortinet /	12/57	1/4	1/8
12	89.144.2.119/loader/ans06.exe	2015-05-26 08:46:35	f7a14ed7daf01b19e254a1d2503bd641	200	-	-	-	-
13	89.144.2.119/loader/ans06.exe	2015-05-26 08:36:40	69f98c3690b8c6a49c49c70655dd201b	200	Bkav / MicroWorld-eScan / Malwarebytes / BitDefender / Norman / Tencent / Jiangmin / AhnLab-V3 / ESET-NOD32 / Fortinet /	10/56	1/4	1/8
14	89.144.2.119/loader/ans06.exe	2015-05-26 06:29:35	36dd4fd83def76932f9ef14c3323860b	200	-	-	-	-
15	89.144.2.119/loader/ans06.exe	2015-05-26 06:19:36	e9cd8a8d00d07c64c13915f0dc6730f9	200	Bkav / Malwarebytes / Norman / Tencent / Jiangmin / AhnLab-V3 / Fortinet /	7/56	1/4	0/8
16	89.144.2.119/loader/ans06.exe	2015-05-26 06:09:35	e9cd8a8d00d07c64c13915f0dc6730f9	200	-	-	-	-

Figure 3. PCS malware detection inquiry

IV. Conclusion

In the paper, we raised the need to take prior measures to cope with the massive distribution of new malware within a short time. As a systematic approach to meet the need, we defined a concept of intelligence system and proposed our own intelligence system. We also showed how the system can operate efficiently and effectively by detecting and preventing new malware in advance. Our future work is to completely develop the component modules of the system and extract intelligence and insights by operating the entire system.

Acknowledgement

It was supported by the MSIP (Ministry of Science, ICT and Future Planning), Korea, under the Global IT Talent support program (NIPA-2014-H0905-14-1004) supervised by the NIPA (National IT Industry Promotion Agency) and by Institute for Information & communications Technology Promotion(IITP) grant funded by the Korea government(MSIP) (No.R2213-15-0002, Electronic receipt processing, analysis system). It was also supported by Basic Science Research Program through the National Research Foundation of Korea (NRF) funded by the Ministry of Education (2014R1A1A2054174).

Reference

[1] ROMAN JASEK, MARTIN KOLARIK and TOMAS VYMOLA, “APT detection system using honeypots”, The Faculty of Applied Informatics Tomas Bata University in Zlín, pp. 25-29, August, 2013.

[2] http://www.wired.com/images_blogs/threatlevel/2012/03/Verizon-Data-Breach-Report-2012.pdf.

[3] http://openioc.org/.

[4] Marco Cova, Christopher Kruegel and Giovanni Vigna, “Detection and analysis of drive-by-download attacks and malicious JavaScript code”, University of California in USA, pp. 281-290, April, 2010.

[5] https://www.virustotal.com/.

Malware Classification based on Big Data Processing

Seong Oun Hwang, Vu Duc Ly, Insung Yeo

Hongik University

Abstract –There are a lot of malware in the wild. Some of them belong to known malware families. Yet variants of malware families unknown pose a serious threat to cyber security. Traditional signature-based approaches cannot appropriately address these unknown malware until the corresponding signatures are available. In this paper, we propose a method for classifying these unknown malware families using machine learning techniques on big data processing platform.

Key words: malware classification, machine learning, big data processing

I. Introduction

A. Limitations of traditional malware detection

Traditional anti-virus vendors's approaches based on signature are largely ineffective against sophisticated malware such as metamorphic malware, for example. It takes time from analyzing advanced malware to obtaining its signature which can be easily bypassed by metamorphic malware.

Antivirus companies receive up to several thousands of new malware samples on a daily basis. From a practical viewpoint, the analysis of these malware samples cannot be performed in a timely manner.

B. The needs and goals of malware classification based on big data processing

The important insight behind these malware is that they may share typical static/dynamic patterns. Therefore we aim to exploit these shared patterns for classification of malware. In order to classify malware including unknown families efficiently, we need to apply machine learning techniques [1] based on big data platform [2] to time-intensive tasks such as: extracting features (static and dynamic) from malware samples, training classifier how to distinguish the characteristics of different malware families.

II. Design of malware analysis system based on big data processing

A. System design

To overcome the limitations of traditional anti-virus approaches, we offer our malware classification system as shown in Fig. 1, which will be operated on our big data processing platform as shown in Fig. 2. At the time of writing this paper, some components in the system are partially being developed.

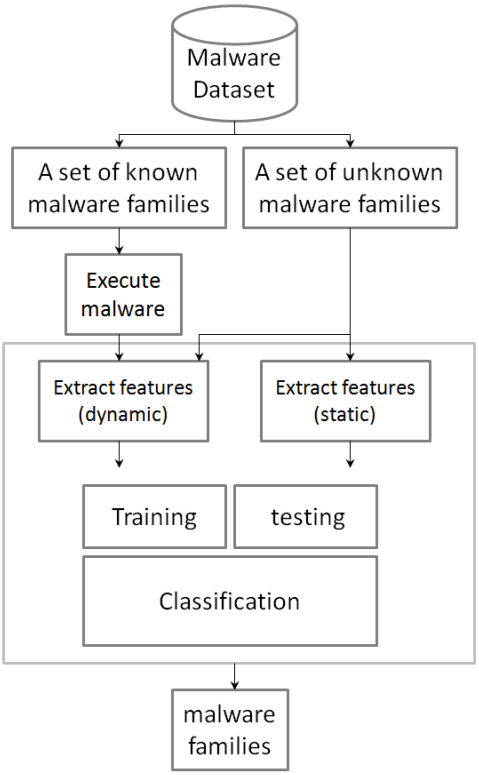

Figure 1. Malware classification system

B. Component description of malware classification system

a. Malware dataset
This system is fed with suspicious files which are collected through malware sandboxes [3,4,5,6], e-mail and honeypot. These input files are not determined to be malicious or not yet, and will be under further testing at the next step.

b. A set of known malware families
The collection of malware that identified by some anti-virus vendors.

c. A set of unknown malware families
The collection of malware which have not been identified by anti-virus vendors.

d. Execute malware

This module executes malware in a sandbox environment and stores the behavior-based analysis result (malware report) to a database.

e. Extract features (dynamic)

This module extracts dynamic features reflecting behavioral patterns, such as file, registry, and network activities.

f. Extract features (static)

This module extracts static features including hexadecimal byte sequences, instruction sequences and API/system call sequences of an executable program.

g. Training and classification

In the training phase, the algorithm gets the malware from the database, uses the extracted features to make the training set, and finally pass the training set to the classifier. Machine learning techniques are applied for identifying the shared pattern of each malware family and the shared N-grams (a sequence of bytes of fixed or variable length, extracted from the hexadecimal dump of an executable program). The classifier will learn from the training set to increase the knowledge of itself. Classification models that we currently consider in our system include Support Vector Machine [8] and Logistic Regression [9].

C. Architecture of big data platform

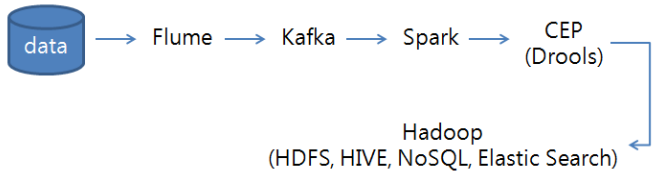

Figure 2. Big data platform architecture

Figure 2 shows our big data platform architecture. Data includes the malware dataset described above. When setting a big data environment, Flume is used to transfer collected data to Kafka, which forwards the data to Spark. Spark is a real-time batch processing engine. We use Drools as a CEP (Complex Event Processing) engine. Next we use additional systems and tools such as file system (HDFS), data query and analysis (HIVE), NoSQL DB (MongoDB), and Search Engine (Elastic Search).

III. Experiment

In parallel with the development of the above components, we collected 100,000 malware samples from [3] by using our automated collection program. We are also being labeling the samples by using VirusTotal API [6] and partitioning them into common families defined by Semantic [7].

Based on the analysis described above, our system automatically extracts a set of attributes as in Table 1.

Table 1. List of major feature set

Dynamic/ Static	Feature name
Dynamic	create_mutex_1(name=”virus1”)
	enum_process_1(apifunction=”Process32First”)
	query_value_2(“HKEY_LOCAL…\Run”, value = “virus1”)
Static	DLL Injection Sequence Call (OpenProcess, VirtualAllocEx, WireProcessMemory, CreateRemoteThread)
	Anti Debugging Sequence Call (IsDebuggerPresent, CheckRemoteDebuggerPresent, NtQueryInformationProcess, OutputDebugString, GetTickCount, QueryPerformaceCounter)
	HTTP Connection (InternetReadFile, InternetCloseHandle, InternetOpenUrl!)
	Embedded shellcode (NOP, XOR, rep movsb)

IV. Conclusion

In the paper, we raised the need to take proactive measures to cope with unknown malware efficiently. As a systematic approach to meet the need, we defined a methodology of machine-learning based on big data processing platform and proposed its architecture. Our future work is to completely develop the component modules of the malware classification system and operate it on a big data processing platform.

Acknowledgement

It was supported by the MSIP (Ministry of Science, ICT and Future Planning), Korea, under the Global IT Talent support program (NIPA-2014-H0905-14-1004) supervised by the NIPA (National IT Industry Promotion Agency) and by Institute for Information & communications Technology Promotion(IITP) grant funded by the Korea government(MSIP) (No.R2213-15-0002, Electronic receipt processing, analysis system). It was also supported by Basic Science Research Program through the National Research Foundation of Korea (NRF) funded by the Ministry of Education (2014R1A1A2054174).

Reference

[1]C. M. Bishop. Pattern Recognition and Machine Learning, Springer Publishing Company, New York, NY, 2006.
[2]Apache Hadoop. https://hadoop.apache.org, 2015.
[3] Malwr. https://malwr.com, 2010.
[4] Anubis. http://anubis.iseclab.org, 2009.
[5] ThreatExpert. http://www.threatexpert.com, 2010.
[6] VirusTotal. http://www.virustotal.com, 2012.
[7] Semantic. http://www.semantic.com, 2015.
[8] B. Schölkopf and A. J. Smola. Learning with Kernels: Support Vector Machines, Regularization, Optimization, and Beyond. MIT Press, Cambridge, MA, 2002.
[9] T. Hastie, R. Tibshirani, and J. Friedman. The Elements of Statistical Learning: Data Mining, Inference, and Prediction. Springer Publishing Company, New York, NY, 2001.

Implementation of a Testbed for Testing Cyber Attack Countermeasures of the IEC 61850 Based Electric Power Control System

Inhoe Kim, Kyutae Lee
Dept. of Radio Science Engineering, Kongju National University, Chonan, Korea.
{ihkim, ktlee}@kongju.ac.kr

Seokhong Min, Jaedouk Choi
R&D Center, SystemBank, Inc., Daejeon, Korea.
{shmin, jdchoi}@system2000.kr

***Abstract*—In this paper, we implement a testbed for testing cyber attack countermeasures of the IEC(International Electrical Committee) 61850-based next generation substation automation networks using an open source-based SDN(Software Defined Networks) platform. The proposed SDN-based networks using the OpenFlow protocol contains a software-based system controller and hardware-based traffic forwarding systems. The system controller manages all forwarding policy as a control center that decides all actions on the each forwarding system. And the traffic forwarding systems perform forwarding the traffic through the forwarding policy using the FPGA(Field Programmable Gate Array). The proposed systems can support line-rate and exactly performs DPI(Deep Packet Inspection) for unauthorized traffic flows with low latency in heavy loaded networks such as data centers.**

Keywords: IEC 61850, Cyber Attack, Countermeasures, Testbed, SDN

I. INTRODUCTION

The substation is one of the core element in the power grid and offers interconnection between the generating units, the power transmission units and the electric supplies. The IEC 61850[1]-based substation automation systems use the ethernet frame for exchanging real-time data, and the system performs control using the data. This can make maximizing capacity, effectiveness, reliability, safety and data integration. However, any countermeasure solutions for filtering the cyber attacks was not ready for that.

This paper propose a testbed for testing cyber attack countermeasures of the IEC 61850-based substation automation networks such as APT(Advanced Persistent Threat) attack. The our testbed uses the open source-based SDN platform that contains a software-based system controller and hardware-based traffic forwarding systems. The system controller manages all forwarding policy as a control center that decides all actions on the forwarding systems. And the traffic forwarding systems perform forwarding the traffic using the forwarding policy of the system controller. The forwarding policy of the each traffic forwarding system is prepared by network administrator. The proposed systems can control all data of the IEC 61850-based next generation substation automation networks using the ethernet frame. We can make easily this solution by using the OpenFlow protocol.

This paper consists of three sections. In section II, we describe the proposed systems including the log system. The experimental results in an implemented testbed of the proposed systems are shown in section III. Finally, section IV comes to a conclusion and further study areas.

II. THE TESTBED FOR TESTING APT ATTACK COUNTERMEASURES

The proposed systems can be implemented as shown in Fig. 1.

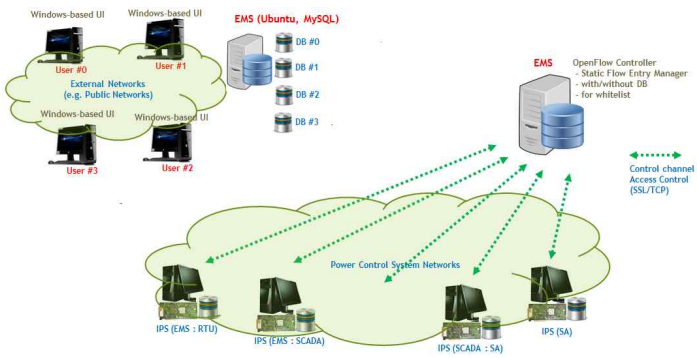

Figure 1. The Implemented Testbed

The implemented testbed consists of two functions. One is a part for testing the cyber attack countermeasures. The other is a function for logging the information of filtered traffics by the forwarding policy in the traffic forwarding systems. Although the testbed has two functions largely, it has an extra function. The extra function is an EMS(Element Management System) that controls the testbed remotely. The system administrator configures experiments and gathering the experimental results by using the EMS software as shown in Fig. 2.

For testing the cyber attack countermeasures and logging the information of the filtered traffics, we firstly update the predefined whitelist as the forwarding policy from the EMS to

Korea Institute of Energy Technology Evaluation and Planning (KETEP), the Ministry of Trade, Industry and Energy, Republic of Korea.

each forwarding system using a control channel as shown in Fig. 1. There is some information to handle the traffics in the forwarding tables. After this, the forwarding systems receive the whitelist and adopt the whitelist to its forwarding tables. The cyber attack traffics are filtered by the whitelist in the forwarding systems. And information of filtered traffics by filtering are logged in its local log system. Finally, the information in the each forwarding system is integrated and managed by the EMS as shown in Fig. 2.

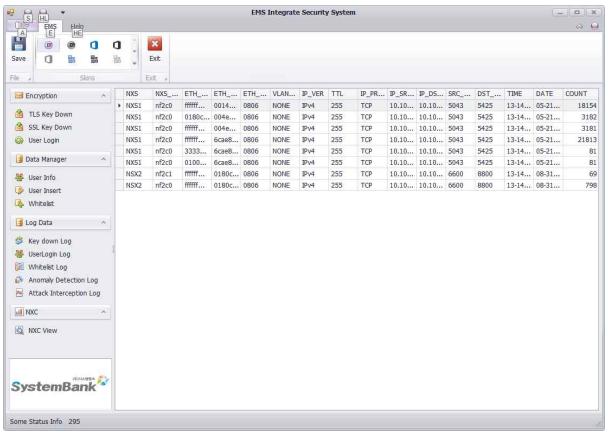

Figure 2. Whitelist log of the EMS Software for controlling the testbed

III. IMPLEMENTATION

The implemented testbed use the OpenFlow protocol basically, and the testbed consists of two systems. One is the OpenFlow controller as the system controller, the other is the OpenFlow switches as the traffic forwarding systems. The OpenFlow system has a variety of usage models to adopt traffic engineering of networks as followings[2]. We apply a function of network access control as a usage model to our implemented system for testing cyber attack countermeasures.

- user-defined routing protocols
- admission control
- network access control
- network management
- energy management and VoIP mobility and hand off

The implemented system consists of four systems as followings.

- EMS (user, log, whitelist, NXC and NXS management)
- EMS client with EMS software (user as administrator)
- NXC (network access controll)
- NXS (whitelist-based network traffic forwarding system)

In the system, the EMS client is an administrator's system for configuring and monitoring the testbed by using the EMS software. The whitelist for each NXS is defined by the EMS software. The NXC distributes the pre-defined whitelist in the EMS to each NXS and the NXS updates its forwarding tables by using the whitelist. The NXS performs filtering the non pre-defined traffic by using its forwarding tables. The each NXS's whitelist is not the same, because the forwarding policy is not the same in each NXS. Fig. 3 shows the implemented testbed.

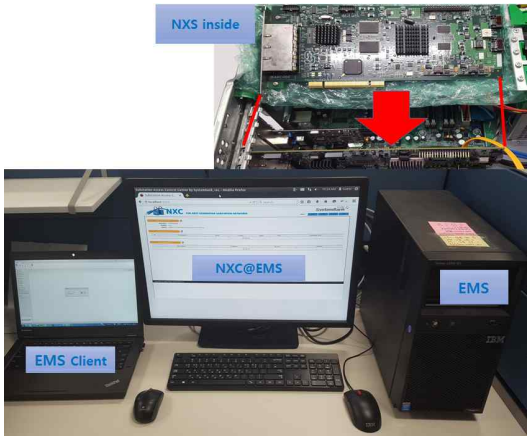

Figure 3. The implemented system for testing cyber attack countermeasures

If non pre-defined traffic flows come into the NXS, the NXS will perform filtering the flows after DPI of the flows. And the information of the filtered flows is logged in its local log system. The NXS's decisions for filtering perform using the FPGA. So, the implemented system can support line rate with low latency, and without any load to processor. Fig.4 shows NXS's filtering results for the non pre-defined traffic flows.

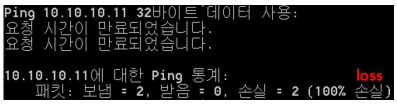

Figure 4. Filtered ICMP messages.

IV. CONCLUSION AND FUTURE WORKS

In this paper, we proposed a countermeasure system for cyber attack and implemented a testbed. The proposed system does not need any switches or routers when you construct IEC 61850-based electric power control system. The proposed system can support line rate with low latency, and without any load to processor. Because forwarding decisions for real-time traffics in the IEC 61850-based networks are performed by the hardware.

For future studies, we plan to produce a experimental product for the NXS and we plan to implement a new testbed with the new NXS.

ACKNOWLEDGMENT

This work was supported by the Power Generation and Electricity Delivery Core Technology Program of Korea Institute of Energy Technology Evaluation and Planning (KETEP) granted financial resource from the Ministry of Trade, Industry and Energy, Republic of Korea (no. 20131020402090).

REFERENCES

[1] www.iec.ch

[2] www.openflow.org

IoT Relationship between Korea and Philippine

(to make our nations sustainable with fusion of literature, art, science and technology)

Seung Chang Park
Department of IT-ethic and POSEN experts
KITELA Institute
Daejeon, South Korea
scpark39@naver.com

Jong Hyun Park
Department of Public Administration
Han Nam University & KITELA Institute
Daejeon, South Korea
jhpark092001@naver.com

***Abstract*—This paper studies for IoT relationship between Korea and Philippine to make our nations sustainable with fusion of literature, art, science and technology. IoT(Internet-of-Things) is a part of long-term evolution which is improving the human-lives and contents related to the green energy harvesting, the food and clothes and houses, the earth climates and environments, the solar system including galaxy. So this paper is the first pilot study for creation of the IoT value-chain of industry, economy, and trade between Korean ICT and Philippine ICT businesses.**

Keywords - IoT, Relationship, Korean ICT, Philippines ICT, Fusion, IT-ethics, Literature, Art, Science, Technology

I. INTRODUCTION

Nowadays in our earth, our human has many bad and evil contact points for survive. Suddenly many peoples are dead or injured due to 1) the earth troubles of earthquake, volcano explosion, typhoon, drought, tornado, fire, heat wave, magnetic storm, water-shortage, food-shortage, clothes-shortage and ultra-violet. 2) the nature troubles of viruses(ex: zika, ebola), venomous insect, toxin-animal and plants, monstrous animal and plants, body-cancer and disease. 3) the machine troubles of disorder, robot-revolt, bio-chip error, electronic bomb, and computer-virus. 4) the law troubles of corruption, political death, imprisonment, betray and persecution. 5) the politics troubles of war, terror, military collision and dispute. 6) the internet troubles of shut-down, mal-disconnect, phone-tapping, file-cracking, computer/smart phone-disorder, voice-phishing, smishing, pharming, DDoS attack and evil-codes.

All governments are focused to solve these six troubles including problems and evil-phenomenon with national budget-payment or investment but our goodness efforts are limited to protect our good lives against these bad things. As an example, IoT(Internet-of-Things) is going to open the new market of almost nations except the poor nation or the digital shortage area in this global world but everything is not connected to all internets. Many styles of internets are the national internet, the social internet, the private internet and the special-purpose internet like some military or some environmental wire/ wireless communication networks. All enterprises providing network switching, antennas and cables are developing the new markets related to IoT services and contents. So, two nations of Korea and Philippine must go to make our nations sustainable with fusion of Literature, Art, Science and Technology(LAST).

II. ANALYSIS

1. Infra-technologies to solve these six troubles

On two sides of Big Data and IoT services, there are many economic and social damages and losses due to the six troubles. Including personal trauma, our global troubles or problems are in a personal life, a family life or a society life from birth to death. So our ancestor and we have focused so many efforts to solving them from the Renaissance. And from 21st century, the various styles of Internets such as super-high speed internet, middle-speed internet, low-speed internet, internet portal services, web services and identification recognized internet are consumed by our human in our Korea-ASEAN FTA(Free Trade Agreement) system and world-wide networks. So, this paper forecasts enterprises' green-growth to make their marketing products and services innovative during at least the next 20~50 years with these six troubles and needs of its solutions. Therefore human can reduce the cost and period of solutions which Infra-technologies are mobile LTE(Long-Term-Evolution) devices, smart IoT sensors, high-definition CCTV(Closed Circuit TV), Q-R Code, RFID(Radio Frequency IDentification) tag, multiple modems of optic, microwave or low-frequency radio links, internet protocol processors, big data analyzers and automatic translated web-services.

2. IoT-ethics to solve these six troubles

Among them, internet portal and SNS(Social Networking Services) are cyber ethics-tools. After IPv6 address system was started, the number of machine connected to internet is increasing from thousands to billions and the real-time presentation or displayed scenes are almost consumed via social media. So those peoples become users of smart devices operating on platform and networks. Those devices are transferring or playing those contents such as broadcasting, image, moving picture, e-book, 2D/3D animation, recorded sound files. Nowadays, in a country there are DMB(Digital Multimedia Broadcasting), Cable TV, Satellite TV and Radio, Internet TV and Radio, SMB(Social Media Broadcasting), personal broadcasting, etc.

So after 10 years, the amount of knowledge, wisdom and technology can be over Yota(1024)Byte to solve our six troubles but the basic shortages of Water, Food, Energy cannot be solved in this earth. Just the unique solution is to control the

population level under the provision level of them. On the other hand, for our survival and sustainability, our government and UN(United Nations) and peoples must develop a new ethics applicable to a personal life, a public life and a national life. IoT-ethics are configured of kindness, regard, humor, contribution and donation operating on various internets and smart contents. Our goodness is true in our world because our human has a smart brain in each body of a man or a woman.

For our sustainability in this earth from 21th to 51th century, our expert system and AI(Artificial Intelligence) are operating for human safety, health and environmental purification. So the high-speed IoT network and social networking services are necessary for our ubiquitous computing lives. Nowadays, Big Data and IoT technology is enhanced to solve the specific big problems such as DDoS attack, Voice-phishing, Smishing, Pharming, Computer-virus, Evil-code, Hacking and Personal Information Protection, etc. The laws of information protection and security are effective for future lives. As shown as this (Fig. 1), So we can create our new ubitopia(Ubiquitous Utopia) era with IoT relationship and trade system between Korea and Philippine in which peoples can develop our literature, art, science and technology.

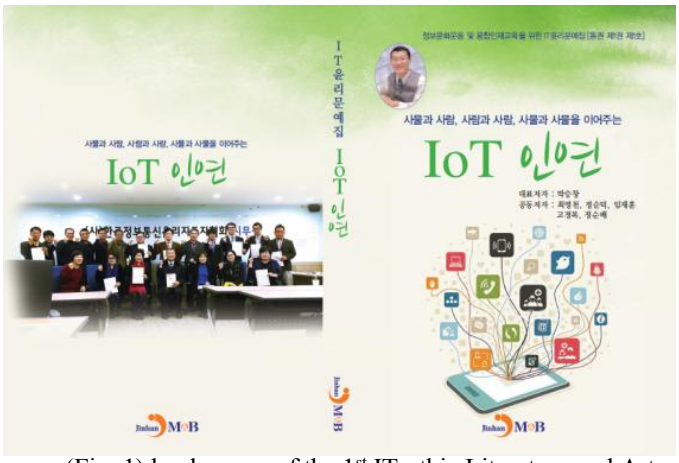

(Fig. 1) book cover of the 1st IT-ethic Literature and Art

III. CONCLUSION

In this paper, we study some effective direction and smart lives with IoT evolution. For smart civilization and human sustainability the new lawful direction of IoT-ethics is to make the existed law modified or a new IoT law. And the new social direction of it is to make some periodic movements and some informative broadcasting programs. And the new technical direction of it is to make the system smart and optimized for reliability, stability, safety, fidelity and economy. So Korean government, industries, universities, research institutes, army and KITELA can give Philippine each of poems and literatures, arts, knowledges, technologies and experiences through some transfer contracts whenever Philippine wants to receive them.

IoT relationship is needed for our ICGHIT and the added programs such as meeting, seminar, workshop, symposium, forum, education, exercise, concert, exhibition, publication, press, broadcasting, movie, drama, music album, gallery, etc. So our Korean and Philippine can make the delightful future of people for smart cultures and ethic lives based on IoT technology. From July 2016 year to June 2025 year(Fully 10 years) as our 1st action step of ubitopia consensus, this paper proposes that we open the fusion event having a brand-new KP-LAST(Korea Philippine – Literature, Art, Science and Technology) concert in Manila.

Biography Data

Dr. Seung Chang Park is the BoB (Best of Best) leader of KITELA(Korean IT-Ethics Leaders' Association) and a professor of Chungwoon University. From November 19 in 2015 year, He is the 7th ICT (Broadcasting) industry-professor appointed by Korean Ministry of Labor. He has a majority of electric electronic ICT engineering, Broadcasting engineering, Software, IT-Ethics lecture and his professional Poem-Novel-Essay-Column-Scenario-Music-Art contents. He has received multiple awards for his research, development, creating of art and poem, teaching and auditing for installation and operation of electric and electronic system, ICT system, Broadcasting, IoT Instrument and LED lighting-system, LED/OLED/Display clustering-system. He is the current commissioner of the IEIE computer society.

REFERENCES

[1] Seung Chang Park, Ubiquitous Mobile Computing, Jinhanbook, October 2003.
[2] Seung Chang Park, Ubitopia, ETNews, July 2004
[3] Seung Chang Park and 8 Authors, Ubiquitous Life Ethis, Jinhanbook, July 2009.
[4] Seung Chang Park, "A Report on the Telecommunications Advisory Mission Project : Consultation of NGN Technology Policy in the Philippines", Philippine CICT and Korea KISDI&KAIST-IPPSO, October 2009.
[5] Seung Chang Park, "A study about the new technology and industry-policy direction of contents-ethics for CDN of the future OneWeb", SKT Review, Vol.22 No.5, pp.630~640, October 2012.
[6] Seung Chang Park, "A pilot study for IT-ethical Literature Art based on u-Computing", the 2014 IEIE Summer proceedings, June 2014.
[7] Seung Chang park and Nojeong Heo, The Analysis of IoT technology commercialization strategy, Jinhanbook, September 2014.
[8] Seung Chang Park, The analysis of Big Data/IoT technology commerccialization strategy, Jinhanbook, August 2015.
[9] Seung Chang Park and 5 Authors, The 1st IT-ethics Literature and Art : "IoT relationship", Jinhanbook and KITELA, December 2015.

Analysis of 5G Mobile Communications Industry Environment

Se-Hwan Park
Korea Institute of Science and Technology Information(KISTI): ReSEAT Program
Seoul, Korea
World00117@reseat.re.kr

Jong-Yun Kim
Kyungdong University: Dept of Computer Engineering
Kosung, Korea
kjyuni@kduniv.ac.kr

***Abstract*—** With the rapid popularization of explosive smart terminal due to the increase in broadband, high speed transfer rate can realize the need for mobile technology 5G. Future mobile service technology can accommodate mobile cloud and low-cost media realize energy efficiency improved mobile communication environment. In addition to a variety of high-tech components technology development and the convergence of fixed and mobile network/based on the service side of the CPND technical characteristics are required. In addition, the networking and wireless Internet 5G mobile communication system-related key technologies can be combined in a variety of technical characteristics and 5G of technology convergence in the system should be developed that can combine. 5G mobile communication system is the rate of transmission of holographic 3D 100Gbps can transmit images to a mobile network.

Keywords-5G mobile service, mobile cloud, energy efficiency, CPND, wireless Internet, convergence, realistic 3D/4D/Hologram, Giga KOREA, lifestyle change

Ⅰ. INTRODUCTION

Smart media devices with the introduction of the explosive growth in data traffic, and popularize fast(35ZB in 2020, M2M Terminal penetration increases within 10 years and 500 per traffic increases 20~120, etc.) due to the high speed/high capacity/high quality media raises new demand needs. This is a broadband, high speed transfer rate can realize the need for 5G mobile technology. The development of the ICT industry in the first half as 5G system innovation is the key to the breakthrough of wireless communication technology in transformation for the infrastructure and technological development worldwide, while the competition is intensifying. 5G mobile communication network through detection, storage, processing, USN, the ubiquitous information environment, an integrated things aims to build. Increase exponentially in the next mobile services technology, smart media devices and M2M terminals, such as mobile cloud and popularized in the media realized that due to the number of mobile services is changing rapidly diversified aspects yoni live a low-energy efficiency with enhanced mobile communications environment. Korea by the end of 2015 Pre-5G by the end of 2017, 5G mobile technology demonstrations, trial implementation, completion of the development of the technology by 2018, 2018 Pyeongchang Winter Olympics unfold, a pilot project in December 2020 aims to technology development and commercial services on standardization. 5G mobile communication system, the implementation of Korea's world-class ICT infrastructure and technical skills in graft of 5G through the surrounding industry to enable big ramifications.

Ⅱ. 5G Mobile Communication System Driving Issue

May 2015 present, wired & wireless telecommunication service subscribers may summarize briefly the current situation as follows[1]:

- mobile phone subscribers of Korea is total 57,765,248 persons, the number of smart-phones total subscribers 41,669,694 peoples(72.1%). the total number of 4G-LTE(A) subscribers 37,921,456 people(91.9% : SK Telecom 17,716,090, KT 11,373,698, LGU+ 8,831,668)
- mobile communication technology by type the number of subscribers, CDMA 5,019,000, WCDMA 9,652,686, LTE 37,921,456 persons
- wireless internet subscribers in total 52,472,590 persons(SK Telecom 26,213,045, KT 16,159,107, LGU+ 10,100,438)
- subscribers of Tablet PC 564,617 persons(SK Telecom 225,378, KT 321,252, LGU+ 17,987)

As the world's highest mobile environment surrounding user-based infrastructure. In particular, 4G-LTE(A) in the case of services, the entire Smart-phone subscribers 63.5%, enough to take broad and holds a large number of users.(For the second quarter of 2014, the current world level 112 countries, about 2 million 8 thousand subscribers in the introduction stage level)

In 5G mobile system, the definition of wireless internet is wireless and mobility equipped through a mobile phone. 5G would like to implement in wireless mobile communication system, the scope of the Internet industry coverage and the app market rated classification system, expert opinion, in-depth analysis of a professional database, including all 4 categories(networks, system & terminals, solutions & platforms, contents), 24 of which were classified as category, 100 classification[2][3][4].

Ⅲ. Global Trends of Mobile Services

Within the next 10 years ago the world smart media device penetration rate is 3.5 times, M2M devices is expected to increase to 500 times as much, to the extent that the data traffic 20~120 times per terminal, explosive growth is expected. The growth rate is a smart media devices spread around the world, 22% in 2010 and in 2020, an increase of 76% and is expected to record an ongoing. M2M terminal growth rate of spread is 90 million in 2010 and in 2020, as 45 billion is expected to increase rapidly. In addition, the sensor-based things information(traffic/weather control, etc.), media-centric services(CCTV, video transmission inter vehicles, etc.), and gradually expanding broadband is expected to be a high-volume M2M services[5][6]. (See figure 1).

Figure 1. Trend of the Global Penetration of Smart Media Devices and M2M Devices

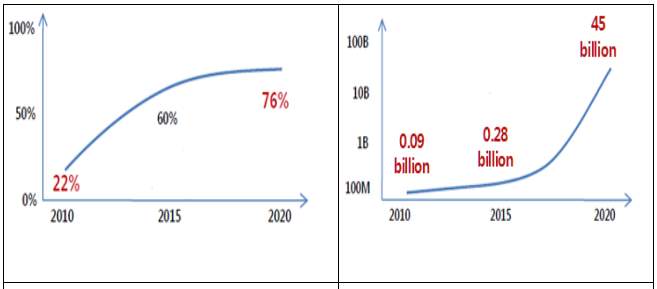

smart media devices | M2M terminals

* source : Jewon Cho(2014. 6),
UMTS/IDATE/Cisco/Gartner(2014) data overall.

Mobile video data of continuous growth(in 2010 52.8%, in 2015 66.4%) and UCC(User Created Contents), Full-HD-level 12 million PIXEL high quality of multimedia data, such as a-grade Smart-phone camera and was about 25 times due to increased [5][7][8].

Ⅳ. Environment Change of Mobile Communications

Wireless network management costs and increase demand, while small cell base station installation continues to increase as a result, the base station's wireless backhaul is being built. Globally, the number of small-cell base stations and wireless backhaul 34,316 units in 2011, 1,306,297 units in 2014, 3,553,282 units in 2016 are expected big market. In 2011~2016 small cell base stations sales an average of 120%, the average annual sales of wireless backhaul, 304% is expected to continue to grow its broadband[5][9]. During the 2011~2016 'build trend of small-cell base stations & wireless backhaul' to indicate to Table 1.

<Table 1> Build Trend of Small-cell Base Stations & Wireless Backhaul

	2014	2015	2016	Total	CAGR [%]
small-ell [100unit]	601.8	1,073.3	1,671.1	601,82	120
wireless backhaul [100unit]	704.5	1,192.4	1,882.1	704.5	304
Total	1,306.3	2,265.7	3,553.2	60,886	212.00 (ave.)

* source : Jewon Cho(2014. 6), Mobile Export(2012. 10)\

Ⅴ. CONCLUSION

5G mobile communication system is macro cell, micro cell, small cell and relay etc. various cell and communication mode will used. In addition, incorporating a wide variety of convergence technology and it can be very complicated situation mixed frequencies may be deployed. In such an environment, such as high-capacity MIMO femto-cell system and move to more efficiently utilize the frequency can be a very good way. In particular, the frequency efficiency are the most important resources in the mobile communication problems, because even in the high-speed data transmission technology, a universal cellular networks can be applied to the continuous technological research is needed to improve performance.

ACKNOWLEDGEMENT

This research was supported by the ReSEAT Program funded by the Korean Ministry of Science ICT & Future Planning through, the National Research Foundation of Korea and the Korea Lottery Commission grants.

REFERENCES

[1] “Wire/Wireless Telecommunication Service Subscribers Statistics_2015. 5”, Korean Ministry of Science ICT & Future Planning, 2015. 7.
[2] “2013 Mobile Internet Industry Trend of Korea”, MOIBA, 2014. 12.
[3] “Broadcasting & Communication Sector Statistical Classification System Research”, korea communications commission, 2014. 12.
[4] “Wireless Internet Ecosystem to build the Good Circulation Structure Plan”, KISDI, 2014. 12.
[5] Jewon Cho, “5G Mobile Communication”, 2014. 6.
[6] UMTS/IDATE/Cisco/Gartner(2014) data overall.
[7] “The New Mobile World Order Perspectives on the Future of the Mobile Industry”, Cisco, 2012. 9.
[8] ABI Research/Cisco(2014) data overall.

Friday, Feb. 26

Session V : (Poster) Multimedia and Signal Processing

Simulator implementation research for the rangefinder production

Kyun Park
Department of Computer Science
Sangmyung University
Seoul. Rep. of Korea
Dreamhigh_k@naver.com

Sang-ug Kang
Department of Computer Science
Sangmyung University
Seoul. Rep. of Korea
sukang@smu.ac.kr

***Abstract*—Precise focal length is needed to take more clear image. As we all know, camera could check surface of the subject by its self focusing function. However, it couldn't work so accurately that all image could have clear picture. To solve this problem, we incorporate a simulator helping to get clear image, using laser and image sensor device. It could provide the information expected to be helpful for making a rangefinder.**

Keywords :laser; rangefinder; simulatoer; displacement sensor;

I. INTRODUCTION

Contact and Non-contact displacement measurement techniques are broadly applicated due to industry development. ; grasp location data of products, data of robots used in welding processing, trace axis of weld, machining meteorological measurements. Contact techinique uses touch trigger probe or scanning probe when non-contact uses light, sound and magnetic field, etc. Contact techinique spends too much time and has difficulty in correction though it could measure broad area more accurately than non-contact. In the contrary, non-contract techinique which is not incisive, has more rapid measuring speed and remote measuring system. This is the reason why research about non-contact sensor is lively progressed[1][2][3][4][5]. We incorporate the simulator which could be useful for producing a rangefinder, by using principle of non-contact displacement sensor. Here is the method.

- Laser measuring system is necessary. - For clear image test, the height of subject and camera should be same. However, camera moves to check images, and it induces alteration of subject's height and slope. We could solve this by using hyperspeed method ; laser.
- Project laser at a certain angle on subject.
- Sensing reflection image of laser
- Find the coordinate of the most bright site.
- Figure out exact distance between the subject and the camera.

II. COMPOSITION OF FECOMETER

The rangefinder used in this paper consists of laser, image sensor, and camera.(Figure 1) After setting up the accuracy and incidence angle of laser, it projects beam on subject. Nature of light makes the beam reflected to the direction of image sensor, and image is produced on the sensor. We observe phase of the image and figure out the distance.

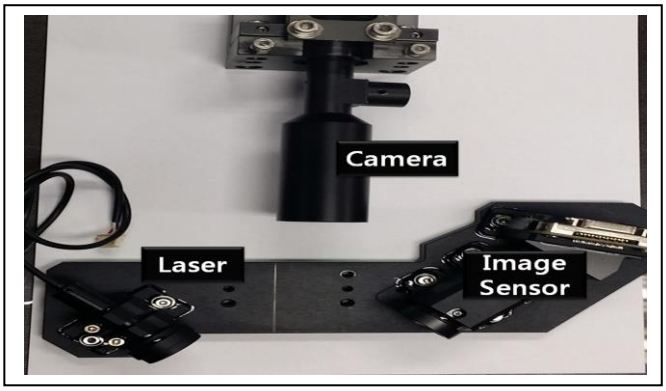

Figure1. Composition of fecometer

If the slope on the surface if the object is not a change in the height level in the ideal, may scan only a specified position at a high speed, but without a test to know the distance to obtain the clearest image, Since the actual situation, has a bumpy surface, most of the object is fine, test the surface of all objects at high speed must be provided a way to obtain a clear image of an object surface of interest.

In this paper, improving the accuracy of the laser beam, the incident point of the algorithm, then finally implemented by applying the reflecting point of the algorithm in the simulator to implement by observing the appearance of rimed reflection image on the image sensor to obtain the clearest image.

III. SIMULATOR FOR THE IMAGE INFORMATION OBTAINED

A. Input environment setting

At first, set start and end point of sensor for efficient image acquisition because image sensor could only get images in its own range. Set width of lasers at both ends to present 2-dimensional laser beam. In addition, users could input shape of targets and laser's angle as they want..

B. Algorithm and image acquisition

- Save coordinates of input objectives

This paper is sponsored by the fund of Employment contract SW master's program from National IT industry Promotion Agency.

- Set coordinates of laser's start point and set equations of each laser.
- Find crossing points between objectives and equations of lasers and define them as incident points.
- Represent every lines in laser beam heading direction of image sensor as linearized equation using incidents points and gradient of objectives.
- Solve simultaneous equation(2,4) to find reflection points on image sensor which are reflected in objectives.
- Suppose each reflection point has own brightness and apply them.
- Set x-coordinate of sensor as x-axis and brightness of reflection point as y-axis to draw graphs.
- Acquire image of laser using graphs(7)..

C. *User interface*

For effective user interface design, there are some requirements. When using the first method is used it must be straightforward and can be clearly understood by the consistent applicaton across multiple parts. It must also be able to use effectively in the future[6]. Supposed simulator provides GUI(Graphic User Interface) considering this. Figure 2 is the GUI of this simulator. Here is the instructions.

- Several configurations like controlling accuracy of laser is handled by setting.
- Input of subject : press draw button and draw the shape you want using mouse drag on SurfaceInOut screen(Right Top) or press Load button and read text file already defined.
- Laser beam on Monitor screen(Left Top) is activated by pressing Simulator button and operate through Continue, Step, Stop button.
- Shape of image on image sensor is expressed on ImageSensorLook screen as bidimentinal graph.(Right Bottom)

The distance for the most clear image is expressed as constant on Height screen.

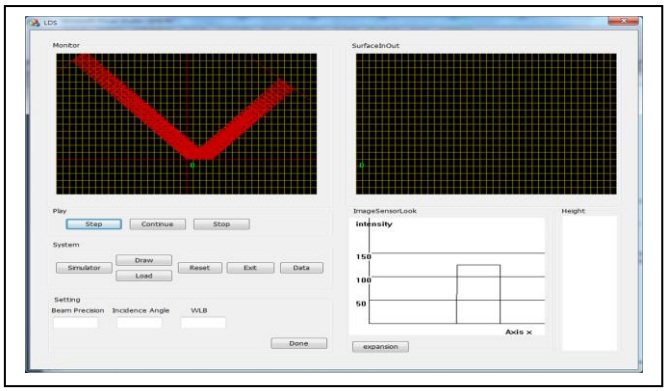

Figure2. Simulator GUI

D. *Program operation*

Using algorithm of improving accuracy of laser, point of incidence and point of reflection, handle the operation of laser and image sensor. Get data of the most clear image by simulating the image brightness. Incorporate simulator which is similar to real world delivering distance to camera with optical triangulation method.

IV. CONCLUSION

Conventional study about non-contact devices have difficulty in user acquiring whole image which laser projects because most of them use slit beam projection at a single aspect[7][8]. Developing the simulator acquiring entire images could make users recognize entire photos and extract the portion they want. Though this proposal could improve usability, we should study new algorithm about filtering method for accurate image acquisition and verify integrated algorithms by using 3D-conversion..

REFERENCES

[1] Hyun-Zic Lee, Tae-Jo Ko, Hee-Sool Kim, "Reverse Engineering by effect ivedigitizing with Sensor Fusion," Collection of Korea Society of Precision Engineering, pp.419~422, 1999

[2] Jae-Yoon Lee, Seung-Woo Kim, "Design of a Non-contact Type Displacement Measurement System Based on Optical Triangulation Method," Collection of the Korean Society of Mechanical Engineers, vol.16, no.6, pp.1030~1035, 1992.

[3] C.W.Lee, S.J.Na, "A Study on the Influence of the Objects's Reflectance on the Active Range Finder," Collection of the Korean Society of Mechanical Engineers, vol.18 , no.11, pp.2944~2953, 1994.

[4] Jong Sung Park, Kyuwon Jeong, "Characteristics of the Laser Displacement Sensor Using Optical Triangulation Method," Korea Society of Precision Engineering, vol.16, no.7, pp.40~50, 1999.

[5] H.I.Oh, H.S.Kim, "Development of a Sensor System to Measure Real Time Vibro Displacement of Civil Structure," Information and Control Conference, pp.823~825, 2003.

[6] S. Krug, Don't Make Me Think! A Common Sense Approach to Web Usability, 3rd ed. San Francisco, Ca:New Riders, 2004.

[7] S.K.Hong, Y.S.Kim, H.K.Lee, H.C.Kim, G.E.Yang, "A Study on Reducing Errors in Scanning Object and Registration using a Laser Scanner", Journal of the Korean Society for Precision Engineering, vol.20, no.9, pp.197~204, 2003

[8] Y.J.Lee, J.K.Sung, D.H.Kim, Y.B.Lee, "Measuremensts of 3-Dimension Position of Object Using CCD Camera and Line Laser(Part1)", Proceedings of the KSMPE Conference, pp.64-72, 2006

A Study on Performances in Banknote Recognition and Counterfeit Banknote Detection Based on Log Analysis for Banknote Slot of Banknote Counter

I Il-Hong Kim
Dept. of Computer Science,
Graduate School, Sangmyung University,
Seoul, Republic of Korea
E-mail: kih205@gmail.com

Sang-ug Kang
Corresponding author,
Dept. of Computer Science, Sangmyung University,
Seoul, Republic of Korea of Korea
E-mail: sukang@smu.ac.kr

Dae-sik Jeong
Kisan Electronics,
Seoul, Republic of Korea
E-mail: jeong.daesik@kisane.com

***Abstract*— This study proposes a research in banknote recognition and counterfeit banknote detection performances according to conditions of banknote slots by comparing data on the banknote slots and banknote image processing recognition through banknote recognition data log of banknote counter. Using data mining techniques, this study verified and analyze the performances of banknote counters by comparing the data on the result value of algorithm which recognize banknotes when the banknotes are inserted into banknote counters in order to investigate which characteristics of result values detect a forgery and recognize normally banknotes. Through the results of experiment, it was ascertained how capabilities for banknote recognition vary according to the conditions of banknote slots when banknotes are inserted. This study classified the degree of influences by numerically categorizing and definition how banknote recognition data discriminate counterfeit bills from genuine money.**

Keywords - Datamining, Banknote counter, Log analysis, Statistics

I. INTRODUCTION

Banknote counter banknotes counting of office automation is very important and is tendency of increase. in particular, financial industry of banknote counters the banknote counting, recognized , damaged banknote, country banknote classify is on the increase [1].

Multinational banknote recognition is available, the need for basis functionality and banknote clustering are emphasized. Features of the bank bill counter banknote recognition and classification performance can significantly affect the reliability in the entire system. banknote recognition algorithm is should be clearly aware of the characteristics or data pattern contained in the banknote [1].

Therefore by reducing the margin of error of the algorithm that understanding the characteristics of the banknote recognition performance averaged and accuracy that is required for system problem and it is important to explore the effects of the different recognition data pattern.

When banknotes are inserted into banknote counters, it sometimes happens that genuine money is miss recognized as counterfeit banknotes or the opposite happens. With regard to this point, this study proposes to analysis how capabilities for banknote recognition vary according to the conditions of banknote slot(H/W) through log analysis of banknote counter system. Finally, it is also necessary to investigate how specific data on recognition algorithm have impacts on distinguishing data on counterfeit banknotes from genuine ones.

II. METHOD

In the system log collection stage, data information is acquired through log management program until banknotes are inserted into banknote counter slot and information about the banknotes is calculated.

In the data preprocessing stage, machining data process proceeds. It is performed that collected original data are processed and converted to analysis data format.

In the system log analysis stage, two categories are clustered, using EM Clustering algorithm to classify the processed log data as genuine banknote and counterfeit ones. In order to investigate how recognition algorithm data vary according to the insert slot data skew, center value of the clustered data. Using Native Bayesian classifier, this study analyses the results which are shown as class or target is changed as various attributes “Fig 1” [2][3][4].

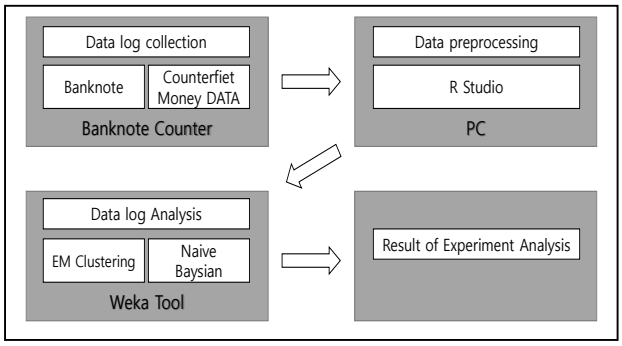

Figure 1. Banknote Log Analysis Progress

This paper is sponsored by the fund of Employment contract SW master’s program from National IT industry Promotion Agency.

A. Data preprocessing

The data processing proceeded in order to convert the collected original log data into suitable format for an experiment. Using R program which is statistical analysis tool, pre-processing is carried out. Each record in the pre-processing is complete, first sheet of banknote recognition table data and is composed of 54 feature.

TABLE I. DSCRIPTION OF FEATURES

Name	*Feature*	*Description*	*Value*
Error	O	Banknote Error Code	0x00****
Size	S	Bankenote Size	3**x1**
Skew	A_1	Banknote Skew Angle	-25 ~ 25
ST	A_2	ST Banknote Recognition	0 ~ 255
IR1~12	$A_3 \cdots A_{14}$	Infrared Ray	0 ~ 255
IRR_F1~F5	$A_{15} \cdots A_{19}$	lnfrared Ray	0 ~ 255
IRR_B1~B5	$A_{20} \cdots A_{24}$	lnfrared Ray	0 ~ 255
UV-T,R,F	$A_{24} \cdots A_{26}$	Ultraviolet Ray	0 ~ 255
STF1~5	$A_{27} \cdots A_{31}$	ST Front Banknote Recognition	0 ~ 255
STB1~5	$A_{32} \cdots A_{36}$	ST back Banknote Recognition	0 ~ 255
DEF1~3	$A_{37} \cdots A_{39}$	DE Front Banknote Recognition	0 ~ 255
DEB1~3	$A_{40} \cdots A_{42}$	DE Bacnk Banknote Recognition	0 ~ 255
MG1~20	$A_{43} \cdots A_{52}$	Banknote Magnetic Recognition	0 ~ 255

B. Data log analysis

R programs is used to compare data statistics and Weka Tool, EM(Expectation maximization) Algorithm, Naive Baysian.

C. EM (Expectation maximization) Clustering

An initial value for estimating a number of parameters begins. Using the parameters to calculate the probability of each of the data belongs to a community. It is estimated to hold the parameters, and then repeat the process using the computed probabilities.

- Parameter Initialization

$$\mu_A^0, \sigma_A^0, p_A^0 \epsilon; \quad (1)$$

- At iteration j : compute the probabilities

$$\Pr(A|x) = \frac{Pr^j(x|a)P_A^j}{Pr^j(x)} \quad (2)$$

- Update the new mixture parameters

$$P_A^{j+1} = \frac{1}{n}\sum Pr\,(A|x) \quad (3)$$

$$u_A^{j+1} = \frac{\sum_x xPr(A|x)}{\sum_x Pr(A|x)} \quad (4)$$

$$a_A^{j+1} = \frac{\sum_x P(A|x)(x-u_A^{j+1})^2}{\sum_x P(A|x)} \quad (5)$$

- Compute the log estimate $E_j = \sum_x \log\left(Pr^j(x)\right)$
- Stop if $(E_j - E_{j+1}) \leq \epsilon$; Otherwise set j=j+1 to (2)step

D. Naïve Baysian

$$DR = \frac{TP}{TP + FN}$$

$$\text{FPR} = \frac{FP}{FP + TN}$$

TP: True Positive TN: True Negative

FP: False Positive FN: False Negative

TP presents that H/W feature is not related to S/W feature and H/W feature has no impacts on recognition performance. TN indicates that other data influence recognition performance although H/W feature has nothing to do with S/W feature. It is examined that FP represents H/W feature is related to S/W feature but has no impacts on recognition performance. FF means that H/W feature is associated with S/W feature and other data influence recognition performance.

III. RESULT

Some of the feature analysis, was found singular point pattern. And analyzing each characterized by a statistical method. In order to investigate the impacts and accuracy which H/W feature and S/W feature have on banknote recognition DR (Detection Rate), FPR (False Positive Rate) is ascertained.

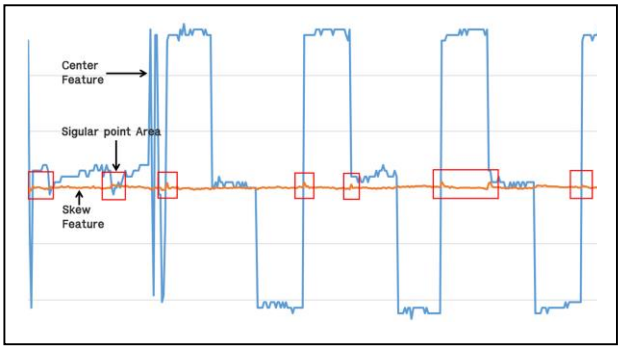

Figure 2. Comparison of Skew feature and Center feature

With log data analysis, this study proposes a research in banknote recognition and counterfeit banknote detection performances according to conditions of banknote slots by comparing data on the banknote slots and banknote image processing recognition through banknote recognition data log of banknote counter.

REFERENCES

[1] A. P. Dempster, N. M. Laird, and D. B. Rubin. “Maximum likelihood from incomplete data via the em algorithm” Journal of the Royal Statistical Society: Series B, 39(1):1–38, 1977.

[2] S. Y. OH, "Bayesian Method Recognition Rates Improvement using HMM Vocabulary Recognition Model Optimization," Journal of Digital Convergence, pp.273-278 1738-1916, 2014

[3] J. K. PARK, M. R. HAN, H. W. KIMA, “Study of Cheater Detection in FPS Game by using User Log Analysis”, Journal of Korea Game, 15(3), 177-188, 1598-4257, 2015

[4] H. K. KIM, H.W. YOON, E. K. LEE, “Estimation Methods for Population Pharmacokinetic Models using Stochastic Sampling Approach”, 28(2), 175–188, 205

Upscaling Detection of a Digital Image using the Pixel's Gradients

Kang Hyeon RHEE*
*Dept. of Electronics Eng. /School of Design and Creative Eng., Chosun University,
Gwangju 501-759, Korea
E-mail: khrhee@chosun.ac.kr

***Abstract*—For a design of the upscaling detection in the altered digital images, this paper presents a new feature vector that is formed from AR (Autoregressive) coefficients by AR model of the gradients of the horizontal and vertical lines in an image. In the proposed algorithm, AR coefficients are computed from the gradients of the lines. Subsequently, the defined 15 Dim. feature vector is trained in a SVM (Support Vector Machine) for the upscaling detection in the forged images.**

In the experiment, three kinds test items are AUC (Area Under Curve), a classification ratio and a minimal average decision error. The performance is excellent at median filtering (3×3), and less at JPEG (90) on the upscaling detection.

However, in the measured performances of all items, AUC by the sensitivity (TP: True Positive rate) and 1-specificity (FP: False Negative rate) is above 0.9. Thus, it is confirmed that the grade evaluation of the proposed algorithm is 'Excellent (A).'

Keywords— ***Forgery image; Upscaling Detection; Upscaling Image Forensic.***

I. INTRODUCTION

In the image alterations, the content-preserving manipulation is using scaling and so on, using the forgery method [1,2,9,13]. An upscaling image is especially preferred among some forgers because it used on a larger displayer. Furthermore, the upscaling detection could classify to the altered images. This state of the art is in [3-7]. Consequently, the upscaling detector becomes a significant forensic tool for the recovery of the processing history of a forgery image.

In this paper, a newly upscaling detection algorithm is proposed, in which the feature vector is formed from AR coefficients by AR model of the gradients of the horizontal and vertical lines in an image [9,14].

The rest of the paper is organized as follows. In Section 2, it briefly presents the theoretical background of the autoregressive (AR) modeling [7] and an image line's gradients. In Section 3, it describes the construction of the new feature vector, and the method to classify the upscaling of the proposed upscaling detection algorithm. The experimental results of the proposed algorithm are shown in Section 4. The performance evaluation is compared with the previous one and followed by some discussions. Finally, the conclusion is drawn, and the future work is presented in Section 5.

II. THEORETICAL BACKGROUND

In this section, an image pixel's gradients are shortly introduced.

A. Autoregressive Modeling

AR coefficients computed as

$$a_k^{(r)} = \mathrm{AR}(\mathrm{mean}(d^{(r)})) \tag{1}$$

$$a_k^{(c)} = \mathrm{AR}(\mathrm{mean}(d^{(c)})) \tag{2}$$

$$a_k = (a_k^{(r)} + a_k^{(c)})/2 \tag{3}$$

where r and c mean that row and column directions respectively in an image, and k is AR order number, $1 \le k \le p$, p is maximum order number. Again AR coefficients are to be the difference image by following

$$d(i,j) = -\sum_{q=1}^{p} a_k^{(r)} d(i,j-q) + \varepsilon^{(r)}(i,j) \tag{4}$$

$$d(i,j) = -\sum_{q=1}^{p} a_k^{(c)} d(i-q,j) + \varepsilon^{(c)}(i,j) \tag{5}$$

where $\varepsilon^{(r)}(i,j)$ and $\varepsilon^{(c)}(i,j)$ are the prediction errors [12] in the row direction and column direction respectively, and q is a surround range of (i,j), $q<3$.

B. Line's Gradients of Image

The gradients of the horizontal and vertical line in an image x are defined as G_r and G_c respectively as follows:

$$G_r(i,j) = x(i,j+1) - x(i,j) \tag{6}$$

$$G_c(i,j) = x(i+1,j) - x(i,j) \tag{7}$$

III. PROPOSED UPSCALING DETECTION ALGORITHM

For the proposed upscaling detection algorithm, AR coefficients are computed by AR model with (6) and (7) then to be as follows:

$$a_k^{(r)} = AR(mean(G_r)) \tag{8}$$

$$a_k^{(c)} = AR(mean(G_c)) \tag{9}$$

$$a_k = (a_k^{(r)} + a_k^{(c)})/2 \tag{10}$$

As like (3), a_k [1st : 15th] is formed to be 15 Dim. feature vector in this paper.

The upscaling detection method is described as following steps.

[Step 1] Computing line's gradients of an image.

[Step 2] Built AR model of Step 1's gradients.

[Step 3] Step 2's AR coefficients [1^{st} : 15^{th}] are formed to be 15 Dim. feature vector.

[Step 4] 15 Dim. feature vector is trained on SVM classifier.

[Step 5] The upscaling detector implemented by the trained SVM

IV. Performance Evaluation

The employed method uses an SVM classifier (11) with 15 Dim. feature vector.

$$K(x_i, x_j) = \exp(-\gamma \| x_i - x_j \|^2) \quad (11)$$

Moreover, the formed 15 Dim. feature vectors to a SVM classifier with trained fore-fold cross-validation in conjunction with a grid search.

$$(C, \gamma) \in \{(2^i, 2^j) | 4 \times i, 4 \times j \in Z\} \quad (12)$$

UCID 1,388 images DB [8] is used for the upscaling detection, and test image types are prepared UP1.1, Up1.5, Unaltered, JPEG (QF=90) and, MF3 respectively.

Subsequently, the trained classifier model is used to perform the classification on the testing set. Among UCID 1,388 images DB, randomly 1,000 images are selected in training, and the rest 388 images are testing.

In Fig. 1, ROC curves show each performance on (a) UP1.1 vs. Test images and, (b) UP1.5 vs. Test images respectively.

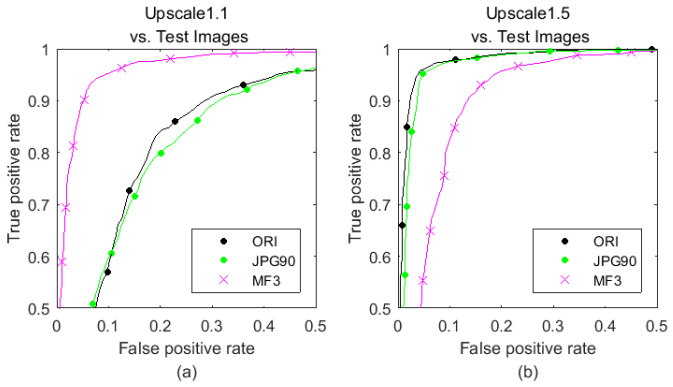

Fig. 1. ROC Curves of the employed upscaling detection method.

However, in the measured performances of all items, AUC (Area Under Curve) by the sensitivity (TP: True Positive rate) and 1-specificity (FP: False Negative rate) is above 0.9. Thus, it is confirmed that the grade evaluation of the proposed algorithm is '*Excellent* (*A*).'

In all the above experiments, the proposed upscaling detection considered only AR coefficients of the image line's gradients to form the feature vector.

V. Conclusion

In this paper, we have proposed a new robust upscaling detection method. We built AR model of an image pixel's gradients and used the AR coefficients as upscaling detection feature vectors.

AR model of the employed method will serve as the further research content to the upscaling detection.

To the best of our knowledge, this is the first complete solution of AR model of the variations of the horizontal and vertical lines in an image.

However, the proposed upscaling detection in spite of a short length of the feature vector, the performance results are excellent due to AUC and a classification ratio are upper 0.9.

Finally, the proposed approach can be applied also to solve different forensic problems, like the previous upscaling detection methods.

Acknowledgment

This research was supported by the Ministry of Trade, Industry and Energy (MOTIE), KOREA, through the Education Support program for Creative and Industrial Convergence. (Grant Number N0000717)

Notice

This paper is a partially rearranged version of [9,14]. The experiment is attempted to an upscaling 110% and 150%, but the used theoretical method is AR model only for the feature vector according to an image line's gradients.

References

[1] Kang Hyeon RHEE, "Median Filtering Detection using Latent Growth Modeling," *IEIE, Journal of IEIE*, Vol. 52, No. 1, pp. 61-68, 2015.1.

[2] Kang Hyeon RHEE "Image Forensic Decision Algorithm using Edge Energy Information of Forgery Image, " *IEIE, Journal of IEIE*, Vol. 51, No. 3, pp. 75-81, 2014.3.

[3] Chenglong Chen, Jiangqun Ni and Jiwu Huang, "Blind Detection of Median Filtering in Digital Images: A Difference Domain Based Approach," *Image Processing, IEEE Transactions on*, Vol. 22, pp. 4699-4710, 2013.

[4] H. Yuan, "Blind forensics of median filtering in digital images," *IEEE Trans. Inf. Forensics Security*, Vol. 6, no. 4, pp. 1335–1345, Dec. 2011.

[5] Tomáˇs Pevný, "Steganalysis by Subtractive Pixel Adjacency Matrix," *Information Forensics and Security, IEEE Transactions on*, Vol. 5, pp. 215-224, 2010.

[6] Yujin Zhang, Shenghong Li, Shilin Wang and Yun Qing Shi, "Revealing the Traces of Median Filtering Using High-Order Local Ternary Patterns," *Signal Processing Letters, IEEE*, Vol. 21, pp. 275-279, 2014.

[7] Xiangui Kang, Matthew C. Stamm, Anjie Peng, and K. J. Ray Liu, "Robust Median Filtering Forensics Using an Autoregressive Model," *IEEE Trans. on Information Forensics and Security*, vol. 8, no. 9, pp. 1456-1468, Sept. 2013.

[8] http://homepages.lboro.ac.uk/~cogs/datasets/ucid/ucid.html (2015.4.1)

[9] Kang Hyeon RHEE, "Forensic Decision of Median Filtering by Pixel Value's Gradients of Digital Image," *IEIE, Journal of IEIE*, Vol. 52, 2015.

[10] G. Cao, Y. Zhao, R. Ni, L. Yu, and H. Tian, "Forensic detection of median filtering in digital images," *in Multimedia and Expo (ICME)*, 2010, Jul. 2010, pp. 89–94. 2010.

[11] Stamm, M.C., Min Wu, K.J.R. Liu, "Information Forensics: An Overview of the First Decade," *Access IEEE*, pp. 167-200, 2013.

[12] S. M. Kay, Modern Spectral Estimation: Theory and Application. Englewood Cliffs, NJ, USA: Prentice-Hall, 1998

[13] Kang Hyeon RHEE, "Framework of multimedia forensic system," *Computing and Convergence Technology (ICCCT), 2012 7th International Conference on*, *IEEE Conf. Pub*., pp. 1084-1087, 2012.

[14] Kang Hyeon RHEE, "Median filtering detection of digital image using the pixel's gradients." ITC-CSCC 2015 Seoul Korea, 2015.

Eye Tracking System Using a Web Camera

Jae-Ik Lee, Shin Won Park
Department of Energy Convergence Engineering
Yeungnam University
Gyeongsan, Rep. of Korea
{jilee3,psw0085}@ynu.ac.kr

Chan-Su Lee
Department of Electronic Engineering
Yeungnam University
Gyeongsan, Rep. of Korea
chansu@ynu.ac.kr

***Abstract*—This paper presents an eye tracking system using a web camera. After detecting face and eye areas, the center of pupil is estimated from eye areas using convolution operation and circular Hough transform. The head motion is compensated based on eye corner's locations and their distance. The proposed eye tracking system is applied for the eye movement estimation for picking up an object situation in psychophysical experiments.**

Keywords-eye movemen tracking, circular hough transform

I. INTRODUCTION

Eye tracking is the process to estimate the gaze direction by pupil movement tracking and head rotation estimation. Eye tracking systems are used in many applications such as human visual interests and visual searching procedure evaluation while driving, cognitive study, and human computer interaction. There are several types of eye tracking systems: eye-attached tracking, optical tracking, and electric potential measurement.

In this paper, a web camera-based eye tracking system is developed. Recently optical eye tracking systems have been developed and widely used. However, most of the optical eye tracking systems are based on infrared/near-infrared cameras and require expensive equipment like infrared lights and cameras [1]. In addition, infrared based eye tracking system cannot be used in outdoor environment such as automotive driving. To solve such problems, a cheap web camera-based eye movement tracking system is developed. The proposed system is based on face detection and eye area detection using Adaboost algorithm [2]. After eye area detection, the center of pupil is estimated and tracked for eye movement estimation.

II. METHOD

Color image sequences from a web camera are used as input data. At first, face is detected from each input image. Similarly, eye area is also detected. Each pupil center and its size, eye corners are estimated. Eye movement is computed from the variation of pupil center after normalization of eye location using detected eye corners.

A. Face and eye detection

Each frame of image sequence is converted into grey image and histogram normalization is applied for contrast adjustment. Viola-Jones object detection algorithm [2] is applied for face detection and eye detection.

This work was supported by Human Resources Program in the Transportation Specialized Lighting Core Technology Development (No. N0001364) granted financial resource from the Ministry of Trade, Industry & Energy, Republic of Korea

B. Estimation of pupil center

Discrimination of iris and pupil is more difficult in Asian than in Eurpoean. We assume that pupil center is the same as iris center. Tsekeridou [3], Vezhnevets [4] estimated iris center by finding circular area center using convolution. Eye image is convolved with a function, emphasizing the circular regions of dark pixels:

$$W(x,y,c) = \frac{\sin((x^2+y^2)/c)}{(x^2+y^2)/c}$$

,where parameter c controls the radius of iris to have maximum weight. Mean position of 3% of darkest pixels are used to estimate iris center.

Iris center is refined more accurately and its radius is also estimated using circular hough transformation [5] from previously estimated iris center. Starting from estimated center, ±5pixel areas are used as a potential center, and find most highly supported circle with radius variation. The pixels ranging only from [-π/4, π/6] and [5 π/6, 5 π/4] are used since other areas are covered by eyelid and does not contribute to making circular pupil contour.

Figure 1. An example of estimated center of pupil and radius of the circle

C. Eye corner detection

A skin color segmentation algorithm is applied to detect eye corners. The color space is converted to YCbCr from RGB detected eye areas. Skin color threshold value in the YCbCr space with modification from the proposed parameter by Chai [6] provides good performance in segmentation of eye area from other face area. Figure 2 shows binary image when we set detected skin areas to 255 and other areas to 0.

Figure 2. Detected eye areas after binarization

Eye corners are detected after applying flood-fill algorithm for the binarized eye areas to remove noisy components. From the detected eye corners, the middle of eye corners and minimum distance between eye corners are computed. The middle of the eye corner is used to remove translation of eye location from head motion in different frames by aligning the eye location. The distance between eye corners are used to normalize zooming effects due to head movement toward/away from the camera.

Figure 3. Images after applying flood-fill algorithms

Human subject is requested to look at front object at the beginning of capturing sequence. In the following frames, the middle of eye center and the distance between eye corners are normalized to the initial frame location and its distance when we computer movement of pupil center. The location of pupil center is used for the estimation of eye movement.

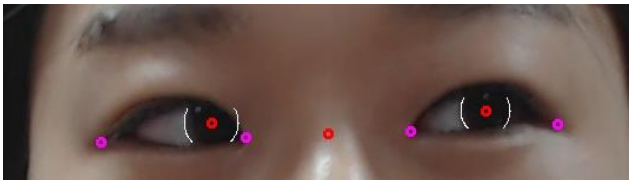

Figure 4. Detected eye corners and the middle of eye corners

III. EXPERIMENTAL RESULTS

In the preliminary experiment, a subject asked to move one step left and one step right. Here, one step means the movement of eye across one block of the test square block to search requested object.

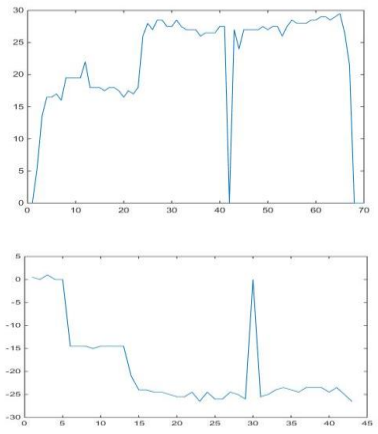

Figure 5. One step left/right eye movement

Figure 5 shows estimated eye movements, where X axis is frame number and Y axis is eye movement, variation of eye location in pixel unit. The mean eye movement of left eye movement and right eye movement is used. Dropping to zero at frame number 30 is from failure of eye center estimation due to eye blinking. We plan to interpolate such a missed eye location from eye locations of previous frames.

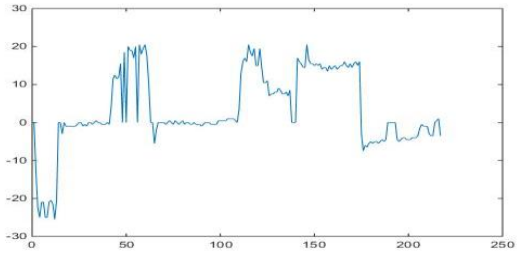

Figure 6. Eye movement tracking when searching for an object to pick up

Figure 6 shows tracking result of eye movement when a subject is asked to pick up an object from block segmented shelf, where several different objects are located in different place. Simple threshold of the eye movement can be used to find out which block in the self is searched.

IV. CONCLUSION

This paper presented an eye tracking system using a web camera. Tracking pupil center movement with normalization for head movement after face detection and eye detection can provide eye movement information in each frame with 30Hz frame rate.

For more accurate eye tracking, we need to improve pupil detection algorithms and to develop more accurate head motion compensation methods especially during head rotation.

REFERENCES

[1] Y. Ebisawa “Improved video-based eye-gaze detection mcthod”, IEEE Transactions on Instrumentation and Measurement, Vol. 47, No. 4, pp. 948 -955, Aug. 1998.

[2] P. Viola and M. Jones, “Robust Real-Time Face Detection,” International Journal of Computer Vision, Vol. 57, No. 2, pp 137-154, 2004

[3] S. Tsekeridou and P. Ioannis “Facial feature extraction in frontal views using biometric analogies,” In Proc. EUSIOCO. Vol. 98. 1998, pp. 315-318.

[4] V. Vezhnevets and A. Degtiareva, “Robust and accurate eye contour extraction,” in Proc. GraphiCon, pp. 81–84, 2003.

[5] A. Al-Rahayfeh, and M. Faezipour, “Enhanced Frame Rate for RealTime Eye Tracking Using Circular Hough Transform”, in Proc. IEEE Long Island Systems, Applications and Technology Conference, Long Island, USA, pp. 1-6, 2013.

[6] D. Chai and K. N. Ngan, “Locating facial region of a head-and shoulders color image,” in Proc. Of IEEE Automatic Face and Gesture Recongnition, pp. 124-129, 1998

Analysis of complex modulation with layered spatial light modulators

Sungjae Park, Jinyoung Roh, and Hwi Kim*
Department of Electronics and Information Engineering
Korea University, Sejong Campus
2511 Sejong-ro, Sejong City 339-700, South Korea
hwikim@korea.ac.kr

***Abstract*: The complex modulation hologram shows a very clear and accurate holographic image. The complex modulation which is composed of layered amplitude and phase only spatial light modulators is introduced. This structure allows us to improve the respective disadvantages of the amplitude only and phase only modulators. In this paper, we analysis and study the noise characteristics of the layered spatial light modulators depending on the interval and size of pixel.**

Keywords: Holographic display, Multilayers, Complex modulation.

I. INTRODUCTION

Recently, the research and development of holographic three-dimensional (3D) display technology have been very actively conducted. Stereoscopic display of 3D display used in movie theater causes confusion, because of vergence-accommodation mismatch. In principle, holographic 3D display is an ideal 3D display without any artificial defect [1]. Technology of the spatial light modulators (SLMs) to display hologram has been continuously developed. In particular, research on the complex modulation is an integral part [2, 3]. We usually use the amplitude only SLMs or phase only SLM to observe the holographic images. The problems occur in these devices when observing holographic image. DC noise and twin are occurred in amplitude SLM. Also unclean image is observed in phase only SLM and complicate the process for calculation computer generated hologram (CGH). By contrast, these problems do not occur in complex modulation. General CGH is represented by complex field. Thus, holographic images are most natural under the complex modulation. The complex modulation method using cascaded amplitude and phase only SLMs is analyzed. The ultimate objective of the proposed method overcomes the limitation of the amplitude and phase only modulated panels. It is expected to provide a clear hologram that improve the respective disadvantages of the two modulated panel previously used.

In this study, we address validity and effectiveness of complex modulation to reduce the respective noise of the amplitude and phase only modulated panels. Though there are many methods that can reduce noise in hologram [4], our approach would solve this problem by using multi-layered structure of amplitude and phase only modulated panels. Additionally, the analysis of the problem is caused by the distance between multilayers and size of pixel.

II. VALIDITY AND EFFECTIVENESS IN COMPLEX MODULATED PANEL

We propose complex modulated panel can be implemented as shown in Fig. 1. CGH pattern of amplitude and phase set on each of amplitude and phase panel with layered structure. Then, the system enters the hologram complex data into the eye through the lens of the plane wave transmitted through the amplitude only panel and phase only panel. This system overcomes the limitation of the amplitude and phase only modulated panel and provides a clear reconstructed holographic image that improve the respective disadvantages of the two modulated panel previously used because of we can observe complex data.

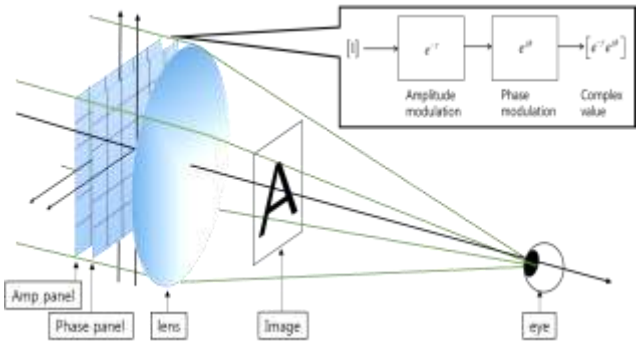

Figure 1. Complex modulated panel system schematic.

The reconstructed holographic image $F(x_2, y_2)$, is obtained by

$$F(x_2,y_2)=\frac{1}{(j\lambda d_1)(j\lambda d_2)}e^{j\frac{\pi}{\lambda d_2}(x_2^2+y_2^2)} \times\iint\left[e^{j\frac{\pi}{\lambda}\left(\frac{1}{d_1}+\frac{1}{d_2}-\frac{1}{f}\right)(u^2+v^2)}circ\left(\frac{u^2+v^2}{\rho^2}\right)\times A'\right]e^{-j\frac{2\pi}{\lambda d_2}(ux_2+vy_2)}dudv.$$
$$A'=\iint e^{j\frac{\pi}{\lambda}\left(\frac{1}{d_1}-\frac{1}{F}\right)(x_1^2+y_1^2)}G(x_1,y_1)e^{-j\frac{2\pi}{\lambda d_1}(x_1u+y_1v)}dx_1dy_1 \quad (1)$$

where $G(x_1, y_1)$ is the CGH pattern before passing through the field lens, $circ\left(\left(u^2+v^2\right)/\rho^2\right)$ is the size of the pupil, d_1 is the distance between the pupil and the CGH, d_2 is the distance between the pupil and the retina, f is a focal length

of the field lens and (u,v) is spatial domain in pupil. Here, $e^{j\frac{\pi}{\lambda}\left(\frac{1}{d_1}+\frac{1}{d_2}-\frac{1}{f}\right)(u^2+v^2)}$ is the key factor to make the accommodation effect in the system. Figure 2 illustrates reconstructed image of CGH by the function of Eq. (1). Because of DC and twin noise, reconstructed image of CGH by amplitude only modulation as shown in Fig. 2(b) has a lot of noise and brighter than other image. Result of phase only modulation in Fig. 2(c) is also difference from the original image as shown in Fig. 2(a). But complex modulation in Fig. 2(d) is almost similar to the original image and does not have the noise. Thus, we have confirmed the validity and effectiveness in complex modulation for improve the respective noise of the amplitude and phase only modulated panels.

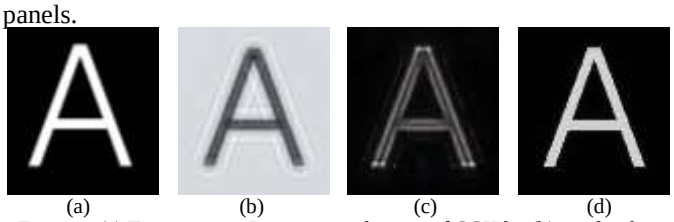

(a) (b) (c) (d)

Figure 2. (a) Target image. Reconstructed image of CGH by (b) amplitude only modulation. (c) phase only modulation. (d) complex modulation.

III. ANALYSIS OF RECONSTRUCTED IMAGE IN COMPLEX MODULATION

In this section, the phenomenon with the interval and the size of pixel of complex modulation with layered SLM is analyzed. Figure 3 shows the accommodation effect of complex modulation when focal plane are alphabet 'A' and 'B' respectively. For the simulation setup, the pixel size is 8.5um, focal length is 0.5m, and 'A' and 'B' are separated from 0.1m. In this result, unlabored accommodation effect appear and focused alphabet of reconstructed image seem clear with any aliasing.

(a) (b)

Figure 3. Accommodation effect of reconstructed image in complex modulation with focus on alphabet (a) 'A' and (b) 'B'.

In the next step, we observed the phenomenon in accordance with the interval of multilayers in the same pixel size. The reconstructed images in complex modulation are displayed according to distance difference between the multilayers illustrated in Fig. 4. When the distance between the multilayers is 0mm virtually as shown in Fig. 4(a), a uniform intensity and a clear image can be seen. However in actual case, we can see non-uniform intensity distribution of reconstructed image by increasing interval of the multilayers as shown in Fig. 4 (b) and (c). Because diffraction occurs in between the amplitude and phase panel. By increasing the interval of the multilayers, noise generates due to influence of different pixel other than a pixel.

(a) (b) (c)

Figure 4. Reconstructed image with interval of multilayers at (a) 0 mm. (b) 0.5 mm. (c) 1 mm.

Next, we analyzed the phenomenon of the pixel pitch in a fixed panel interval in the complex modulation. The reconstructed image according to the pixel size changes when the distance between the multilayers be the same do not show a significant difference. The set-up of Fig. 5 is the distance between the multilayers is 1 mm, a pixel size is 8.5 um, 11 um and 13.68 um. The smaller the pixel size occurs the noise at the periphery of the image and intensity of the alphabet 'A' image is different. This phenomenon is occurred because the pixel size becomes smaller the diffraction appear well. But the result was a finely largely unchanged. The image 'B' is observed a different common characteristic that the larger the pixel size is reduced accommodation effect.

(a) (b) (c)

Figure 5. Reconstructed image by size of pixel (a) 8 (b) 11(c) 13.68 um.

IV. CONCLUSION

In this paper, we addressed validity and effectiveness of complex modulation that is composed of the amplitude and phase only modulated panels. We found that little noise is generated with respect to the inter-layer distance. It is an interesting result. If more widely studied phenomenon in complex modulation and finding a solution, a very good modulation device will be able to emerge.

REFERENCES

[1] J. Hong, Y. Kim, H.-J. Choi, J. Hahn, J.-H. Park, H. Kim, S.-W. Min, N. Chen, and B. Lee, "Three-dimensional display technologies of recent interest: principles, status, and issues," Appl. Opt. **50**, H87–H115 (2011).

[2] J-P. Liu, W.-Y. Hsieh, T.-C. Poon, and P. Tsang, "Complex Fresnel Hologram Display using a Single SLM," Appl. Opt. 50, H128-H135 (2011).

[3] L. Gonçalves Neto, D. Roberge, and Y. Sheng, "Full-range, continuous, complex modulation by the use of two coupled-mode liquid-crystal television," Appl. Opt. 35, 4567-4576 (1996).

[4] E. Ulusoy, L. Onural, and H. M. Ozaktas, "Full-complex amplitude modulation with binary spatial light modulators," J. Opt. Soc. Am. A 28, 2310-2321 (2011).

Numerical analysis of dielectric guided-mode resonance reflective filter

Soobin Kim, Dajeong Im, Sungjae Park, Youngjin Jeon and Hwi Kim*
Department of Electronics and Information Engineering
Korea University, Sejong Campus
Sejong, Korea
hwikim@korea.ac.kr

***Abstract*— Structural color filter is researched actively since it can complement dye-based color filter. We solved the problem of monolithic dielectric guided-mode resonance (GMR) filters with narrow bandwidth by using refractive index of 1.8. Since the depth of binary grating and the thickness of substrate of RGB color filters are same respectively, process at one go is practicable. Also, the structural color structure having wide viewing angle is suggested and demonstrated.**

Keywords-Diffraction and gratings, Color filter

I. INTRODUCTION

Color filter is the key sector in the various electronic equipment for image display. Dye-based color filter has many physical limitations such as low effectiveness, imperfect color selectivity [1]. Therefore, structural color filter based on diverse optical properties is researched actively since it can complement dye-based color filter. Dielectric GMR reflective filters are generally known that it can have high efficiency with narrow bandwidth [2, 3].

In this paper, we propose RGB binary structural color filters using refractive index material of 1.8 for broadband viewing angle. Manufacturing process of RGB color filters in one pixel at a stroke is almost impossible in the previous studies because each structure has different depth. Since the proposed structure has same thickness, process at one go is possible. However, these colors are not observable in every direction due to the short period. We also propose the structure that compensates wide viewing angle even at short period.

II. CHARACTERISTIC OF DIELECTRIC BINARY GMR REFLECTION-TYPE FILTER

Figure 1(a) shows monolithic dielectric binary structure. Since we found that a high refractive index is the key point for broadband color filter in the previous research, we use refractive index of 1.8 in this structure. In Fig. 1(b)-(d), transmission and reflection spectrum of RGB color filters what we found through the parametric study are shown. We used Fourier modal method (FMM) which is a kind of rigorous coupled-wave analysis (RCWA) in this simulation [4]. What is important here is that the thickness of substrate and the height of RGB color filters are same. Thus, manufacturing process of RGB color filters is possible at a single stroke. Pitches of RGB color filters are 510nm, 400nm, and 360nm, and widths of those are 306nm, 280nm, and 144nm, respectively.

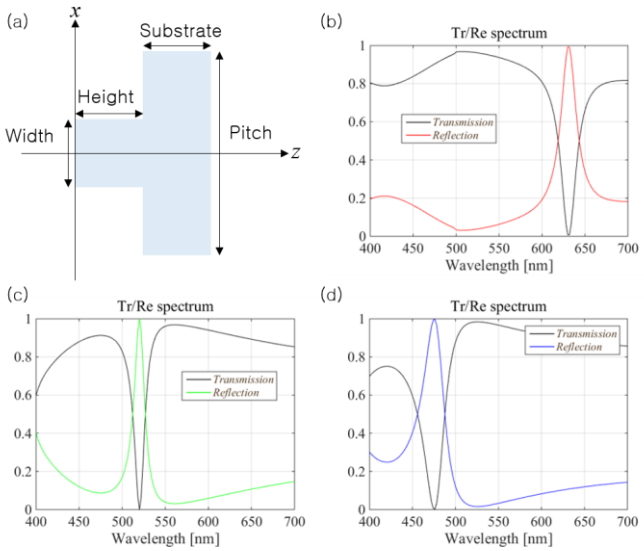

Figure 1. (a) Monolithic binary structure. (b) Transmission and reflection spectrum of RGB color filters.

As is well-documented in many previous studies, color filter using GMR has no tolerance for incidence angle as shown in Fig. 2(a)-(c). If an angle of incidence varies, the observed color is also changed. To prove this, white diffraction simulation passed off. In the conventional white diffraction simulation, plane wave was used. Because the structure is repeated infinitely in this simulation, interference is observed in the field visualization. Thus, Gaussian light source and geometric optical wave (GOW) are applied to our simulator for making clear field visualization without interference. In Fig. 2(d)-(f), the result of white diffraction is shown when incidence angle is 22.5 degree. Left region and right region are divided reflection field omitted input and transmission respectively on z=0 basis.

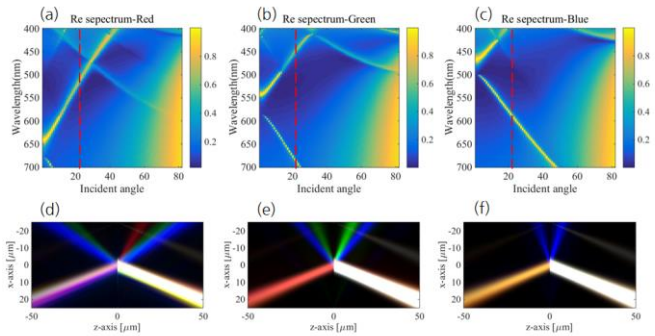

Figure 2. Spectrogram in accordance with the incident angle of (a) red, (b) green, and (c) blue. Field visualization of (a) red, (b) green, and (c) blue.

III. PROPOSED STRUCTURE TO COMPENSATE VIEWING ANGLE

Since pitches of RGB color filters are shorter than wavelengths, observable points are limited. To be exact, we can observe color at only -1st, 0th, and 1st positions. The ultimate goal of our research is to find a reflection-type color filter which has wide viewing angle. In this paper, we propose the structure that compensates wide observation angle even at short period.

Proposed structure is described in Fig. 3(a) and its field visualization is shown in Fig. 3(b). Compared to Fig. 2(d)-(f), structural colors are visible in every direction. However, the intensity of reflection light is low. We put aluminum (Al) in the last layer to improve intensity. According to our expectation, the brightness of reflective light is enhanced, as shown in Fig. 4.

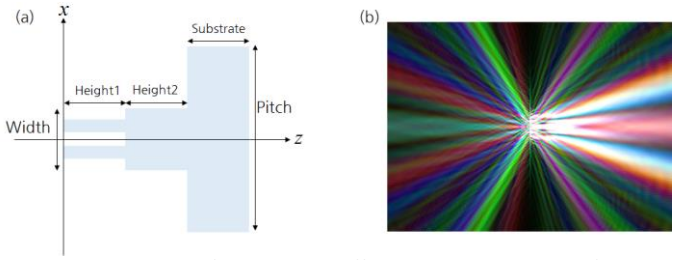

Figure 3. (a) Structure for high-order diffraction and (b) the result of white light diffraction.

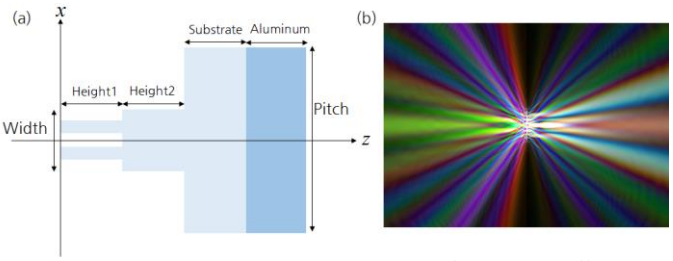

Figure 4. (a) Proposed structure and (b) the result of white light diffraction.

IV. CONCLUSION

We proposed monolithic dielectric refection-type RGB color filters using high refractive index material. It is notable that manufacturing process of RGB color filters is possible at a stroke. But observable points are limited because pitches of RGB color filters are shorter than wavelengths. To compensate viewing angle, the structure having wide observation angle even at short period is proposed. Hereafter, we have a desire to find structure that compensate the light more equally.

ACKNOWLEDGMENT

This work was supported by the Industrial Strategic technology development program (No.10042797, Development of master machining system and 10% energy saving molding system for 100nm~100 ㎛ nano hybrid structures) funded by the Ministry of Knowledge Economy(MKE, Korea).

REFERENCES

[1] M. J. Uddin and R. Magnusson, "Highly efficient color filter array using resonant Si3N4 gratings," *Optics Express*, vol. 21, pp. 12495-12506, 2013/05/20 2013.

[2] S. S. Wang and R. Magnusson, "Theory and applications of guided-mode resonance filters," *Applied Optics*, vol. 32, pp. 2606-2613, 1993/05/10 1993.

[3] R. Magnusson and Y. Ding, "MEMS tunable resonant leaky mode filters," *Photonics Technology Letters, IEEE*, vol. 18, pp. 1479-1481, 2006.

[4] H. Kim, J. Park, and B. Lee, *Fourier modal method and its applications in computational nanophotonics*: CRC Press, 2012.

An Area-Efficient 32x32 Pipeline 2-D FFT/DCT Processor

Jinkyu Kim and Juehyun Lee
Electronics and Telecommunications Research Institute
Daejeon, Korea
kimjk@etri.re.kr and juehyun@etri.re.kr

Kyoungrok Cho
Department of Information & Communication Engineering
Chung-buk National University, Korea
krcho@chungbuk.ac.kr

***Abstract*—This paper presents a pipeline 2-D fast Fourier transform (FFT) processor supporting computation 2-D discrete cosine transform (DCT) with 32×32 length. The proposed radix-2^5 processor has no complex multiplication except trivial multiplication and no requiring memory storing the twiddle factors. The synthesis results show that the architecture is capable to process a 32×32 2-D FFT/DCT in 2106 clock cycles at 122MHz. It costs 2845 lookup-tables (LUTs) and 6 block RAMs including reordering memory. The comparison results indicate that the proposed pipelined processor has the highest cost efficiency with compared to conventional method.**

Keywords—2-D discreate cosine transform, 2-D fast Fourier transform, FPGA

I. INTRODUCTION

Recently, the 2-D FFT and DCT have been widely applied in the area of image compression and video compression, such as JPEG, MPEG-2/4 and HEVC. And the design complexity is increasing due to image of higher resolution. Therefore a variety of designs have been proposed to satisfy requirements of system.

Many researchers have recently designed 2-D FFT or DCT in a number of ways to achieve a high processing rate, effective area and low power consumption. Tumeo et al. [1] presented a fast 8×8 2-D DCT hardware accelerator for a FPGA-based SoC which takes 80 clock cycles at 107MHz. Yuan-Chu et al. [2] presented the high efficiency reconfigurable pipeline processor supporting 128/256/512/1024/1536/2048-point 1D FFT/IFFT for Long Term Evolution (LTE) standard and 16×16 2-D DCT computation for the high image quality standard, namely High Efficiency Video Coding (HEVC). Lin et al. [3] presented the triple-mode reconfigurable pipeline 256-point FFT/IFFT and 8×8 2-D DCT processor.

In this paper, we propose an area-efficient 32×32 pipeline 2-D FFT processor supporting 32×32 2-D DCT. To reduce hardware complexity radix-2^5 algorithm is adopted. Also the design uses constant multiplication to remove the complexity of multiplication.

This paper organized as follows. In Section 2, we discuss the 2-D FFT/DCT algorithm to derive the architecture of hardware. And the pipeline architecture is described in Section 3. We will show the hardware cost and performance comparisons in Section 4. Finally, conclusions are drawn and the futures works are discussed in Section 5.

II. 2-D FFT/DCT ALGORITHM

The 2-D DFT with a length of N is defined as follows:

$$Y(k,l)=\sum_{m=0}^{N-1}\sum_{n=0}^{N-1}y(n,m)\cdot W_N^{nk}\cdot W_N^{ml},$$
$$where\ W_N^{nk}=\exp(-j2\pi\frac{nk}{N}),\ W_N^{ml}=\exp(-j2\pi\frac{ml}{N}) \quad (1)$$

Where W_N is the twiddle factor, n and m are the time index, k and l are the frequency index. To reduce computational complexity, N point 1-D DFT can be decomposed to five-dimensional small radix-2 processors with the linear index mapping method. Moreover, the relation between small radix-2 processors can be described as a common factor algorithm (CFA) [4].

The $N\times N$ 2-D DCT $C(k, l)$ of the input signal $x(n, m)$ is defined as follows :

$$C(k,l)=\sum_{m=0}^{N-1}\sum_{n=0}^{N-1}x(n,m)\cdot\cos\left(\frac{\pi(2n+1)k}{2N}\right)\cdot\cos\left(\frac{\pi(2m+1)l}{2M}\right)$$
$$where\ n,m,k,l=\{0,1,2,...,N-1\} \quad (2)$$

Where the post-scaling factor is omitted. To use 2-D FFT processor for 2-D DCT operation, the input data $x(n, m)$ could be reordered as bellow.

$$\begin{aligned}y(n,m)&=x(2n,2m)\\ y(n,N-1-m)&=x(2n,2m+1)\\ y(N-1-n,m)&=x(2n+1,2m)\\ y(N-n-1,N-m-1)&=x(2n+1,2m+1)\end{aligned} \quad (3)$$

After the applying of (3), (2) can be rewritten as

$$C(k,l)=\sum_{m=0}^{N-1}\sum_{n=0}^{N-1}y(n,m)\cdot\cos\left(\frac{\pi(4n+1)k}{2N}\right)\cdot\cos\left(\frac{\pi(4m+1)l}{2M}\right)$$
$$where\ n,m,k,l=\{0,1,2,...,N-1\} \quad (4)$$

Using the shifted 2-D FFT (SFFT) processor with the 1/4 sample shift in time domain, 2-D DCT in (4) can be calculated [5]. The 1/4 sample shifted FFT for $y(n, m)$ in (4) is defined as follow.

$$Y_S(k,l) = \sum_{m=0}^{N-1}\sum_{n=0}^{N-1} y(n,m)\cdot W_N^{(n+\frac{1}{4})k}\cdot W_N^{(m+\frac{1}{4})l} \quad (5)$$

If the reordering of time shifted 2-D FFT output with N, it can be defined as $Y_S(N-k, l)$. Finally, (4) is calculated by combing (5) as follow.

$$C(k,l) = \frac{1}{2}\left(\mathrm{Re}\{Y_S(k,l)\} - \mathrm{Im}\{Y_S(N-k,l)\}\right) \quad (6)$$

III. PIPELINE ARCHITECTURE

Fig. 1 represents the proposed architecture. Both 2-D FFT and 2-D DCT can be operated at the same time according to (6). The entire design is composed of an input buffer, 32x32 2-D FFT processor, a complex multiplier for time shift and an output buffer with LIFO.

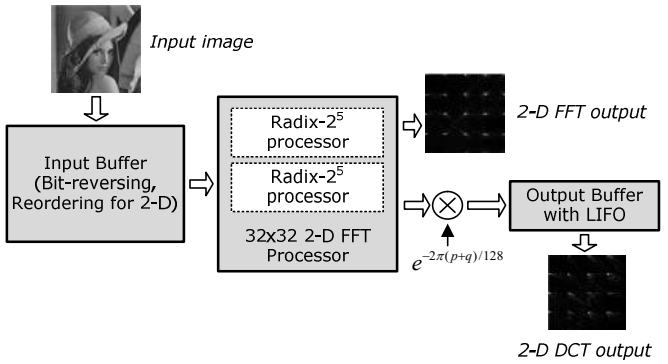

Fig. 1. The architecture of 2-D 32×32 DCT/FFT processor

Input buffer remaps the input sequence for bit-revered ordering operation and 2-D mapping according to (3). The reordered output is fed into the 2-D 32×32 FFT processor which is composed of two radix-2^5 processor. Finally, the output buffer has the FIFO for 32 sample delay of real part and the LIFO to reorder the imaginary part of the FFT. Also it has the adder to acquire the 2-D DCT data.

Two radix-2^5 processors operate the row and column of image respectively. Each processor has no complex multiplier except the trivial constant multiplication to reduce the area of design. The 2-D FFT results are multiplied by $e^{-2\pi(p+q)/128}$ to get the 1/4 sample time shifted 2-D FFT. The real part of 2-D FFT is fed into first-in-first-out (FIFO) to align the 32 clock cycles because of the delay of imaginary part. The imaginary part of 2-D FFT is inputted to the last-in-last-out (LIFO) buffer to reorder the output sequence according to (6). It exchanges the input and output ports per 32 clock cycles using the LIFO control signal to reduce the size of register files.

IV. EXPERIMENTAL RESULTS AND COMPARISON

We use Xilinx ZC702 evaluation board to verify the 2-D FFT/DCT processor and designed the floating/fixed modeling using Matlab/C++ programming. The hardware is descripted using System Verilog and synthesized using Synplify Pro 2014.03. And it is implemented using Xilinx Vivado 2014.2.

The total latency of the proposed design is 2106 clock cycles from the first input data to the first output data. The estimated maximum clock cycle is 122MHz. Table I presents the results of the proposed 2-D FFT/DCT processor. Conceicao [6] implemented the 2-D IDCT with low latency using Altera FPGA. But it has 28,311 LUTs due to 32 samples per clock cycle. Martuza [7] designed the 8×8 point 2-D DCT with 706 LUTs. The proposed 2-D FFT/DCT processor is integrated into AXI4 interface of ZYNQ processing system for real-time verification.

TABLE I. COMPARISON OF HARDWARE COMPLEXSITY

	Proposed	Conceicao [6]	Martuza [7]
Transform Type	2-D FFT/DCT	2-D IDCT	2-D DCT
Transform Size	32	32	8
Technology	Xilinx ZC7020	Altera Stratix IV	Xilinx Virtex 4
Hardware Size(LUTs)	2845	28,311	706
Frequency (MHz)	122	43.62	-
Latency (clock cycles)	2106	33	65
Samples per clock	1	32	1

V. CONCLUSION

In this paper, we presented the pipeline 2D FFT/DCT processor with effective area. The hardware with only trivial multiplication, which can process 32×32 size in dual mode. Therefore, it can be used in applications, such as image compression requiring high data throughput.

ACKNOWLEDGMENT

This work was supported by Institute for Information & communications Technology Promotion (IITP) grant funded by the Korea government (MSIP) (No.B0126-15-1024, 100 Gbps Coherent/OFDM DSP Development).

REFERENCES

[1] Tumeo, Antonino, et al. "A pipelined fast 2D-DCT accelerator for FPGA-based SoCs." VLSI, 2007. ISVLSI'07. IEEE Computer Society Annual Symposium on. IEEE, 2007.

[2] Yu, Yuan-Chu, and Yuan-Tse Yu. "Design of a high efficiency reconfigurable pipeline processor on next generation portable device." Digital Signal Processing and Signal Processing Education Meeting (DSP/SPE), 2013 IEEE. IEEE, 2013.

[3] Lin, Chin-Teng, Yuan-Chu Yu, and Lan-Da Van. "Cost-effective triple-mode reconfigurable pipeline FFT/IFFT/2-D DCT processor." Very Large Scale Integration (VLSI) Systems, IEEE Transactions on 16.8 (2008): 1058-1071.

[4] Burrus, C. Sidney. "Index mappings for multidimensional formulation of the DFT and convolution." Acoustics, Speech and Signal Processing, IEEE Transactions on 25.3 (1977): 239-242.

[5] Hsiao, Shen-Fu, et al. "Efficient VLSI implementations of fast multiplierless approximated DCT using parameterized hardware modules for silicon intellectual property design." Circuits and Systems I: Regular Papers, IEEE Transactions on 52.8 (2005): 1568-1579.

[6] Conceicao, Ruhan, et al. "Hardware design for the 32× 32 IDCT of the HEVC video coding standard." Integrated Circuits and Systems Design (SBCCI), 2013 26th Symposium on. IEEE, 2013.

[7] M. Martuza, et al."A cost effective implementation of 8×8 transform of HEVC from H.264/AVC" in Electrical & Computer Engineering (CCECE), 2012 25th IEEE Canadian Conference on, Montreal, Quebec, pp. 1-4.

A recommendation system based on object of the interest

Sung-Woo Byun, So-Min Lee, Seok-Pil Lee
Dept. Computer Science
Sangmyung University
Seoul, Korea
123234566@naver.com, somin4412@nate.com,
esprit@smu.ac.kr

Kwang-Yong Kim, Kee-Seong Cho
Dept. Intelligent Convergence Media Research Department
Electronics and Telecommunications Research Institute
(ETRI)
Daejeon
kwangyk@etri.re.kr, chokis@etri.re.kr

***Abstract*— Needs of contents recommendation technologies are increasing as the number of the media content on TV and Internet is increased. For the precise recommendation, researches on collaborative filtering recommendation system are increasing. But these researches have problems in scalability and cold-start. To solve these problems, this paper proposes the recommendation system based on user's content consumption according to watching time pattern and objects of interest. For this, we extract objects of interest from 259 media contents and 157 users and then calculate preference scores. To evaluate the performance of the proposed system comparison tests are done with the results of the existing collaborative filtering systems.**

Keywords-component; Collaborative filtering; Recommendation system; Consumption patterns; Objects of interest;

I. INTRODUCTION

Needs of contents recommendation technologies are increasing as the number of the media content on TV and Internet is increased. To reflect demands of users, a variety of customized broadcasting services have been researched. A typical service is personalized broadcasting service and it allows the users to watch the program or the desired part of programs they want at any time. Also it can provide the scenes with objects that the users are most interested in through utilization of multiple camera angles. For more precise recommendations in the personalized broadcasting service, collaborative filtering systems have been researched [1]. But these researches have problems in scalability and cold-start. To solve these problems, this paper proposes the recommendation system based on user's content consumption according to watching time pattern and objects of interest. For these, we analyze the objects while the users are watching contents, and extract the user-interested objects. Then we design and implement a recommendation service system with capability of recommendation of the contents with user-interested objects. The rest of this paper is organized as follows. Section 2 presents the overall structure and method of our recommendation system. Section 3 and 4 explain the experimental data set and the results, respectively. Section 5 presents summaries and conclusions.

II. PROPOSED METHOD

A. *Object-based media service metadata schema*

The object-based media service metadata schema was used to recommends contents with the object which users are interested in. The object-based media service metadata is a technology structure that can search and extract information about all of the objects while users are watching TV. The following figure 1 is a Credits Item structure, which stores information about that objects.

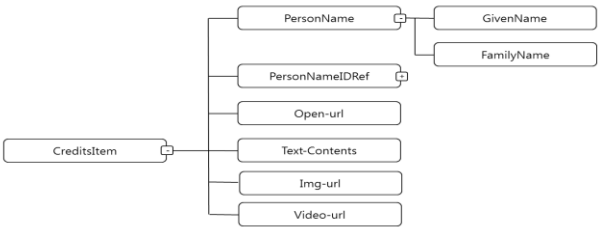

Figure 1. CreditsItem Type which stores information about the object

Object name, object id, and additional knowledge information were added to the original 'TV-Anytime Credits Item Type [2]. For the Program Information Table, which contains the information about the scenes, and the Segment Information Table, which composed of the segment information about the beginning and ending frames of an object in the scenes, the structure that has been suggested in previous research was used [3].

B. *Preference score calculation using watching time pattern*

Equation that calculates user's preference score is shown in (1). The time that the user has spent on a program was divided by the total time of program, and then reflected to the user's preference score.

$$PF_{score} = \frac{V_e - V_s}{PG} \quad (1)$$

C. *Proposed recommendation system with user-interested object*

First, contents are grouped by genre. And then segment information is extracted from the whole contents. When users are watching the contents, preference score of user-interested objects is calculated. Finally, the recommendation system shows the top-Nth contents to user using user's preference score.

D. *Evaluation Indicators*

Various evaluation methods have been proposed for evaluation to recommendation system performance. In this research, we use the precision rate and the recall rate method that are the basic measures used in evaluating search strategies. The precision rate is the ratio of the number of contents which user consumes to the total number of recommended contents. The precision rate is shown in (2).

$$Precision\ Rate = \frac{|T \cap R|}{|R|} \tag{2}$$

The recall rate is the ratio of the number of recommended contents to the total number of contents which user consumes the recall rate is shown in (3).

$$Recall\ Rate = \frac{|T \cap R|}{|T|} \tag{3}$$

From this, R is the number of contents recommended by system. T is the number of contents which user consumes.

III. EXPERIMENTAL DATA

TABLE I. CONTENTS INFORMATION OF GENRE

Genre	Number of contents
News	30
Documentary	31
Entertainment	64
Drama	42
Music	54
Animation	30

As shown in Table I, the experimental data is collected from a total of 259 contents subdivided into seven branches by genre like 34 for news, 31 for documentary, 64 for entertainment, 42 for drama, 54 for music, and 30 for animation.

IV. EXPERIMENT RESULT

Table II shows the result evaluating performance of the proposed recommendation system. We compared proposed recommendation method with user based collaborative filtering [4], clustering + user based collaborative filtering [5] using precision rate and recall rate while increasing recommended content.

Table II Performance evaluation

Top-Nth		Proposed recommendation result	User based collaborative filtering	Clustering + User based collaborative filtering
4	***Precision***	54.36508	13.095	32.539
	Recall	25.95139	7.8	16.613
6	***Precision***	48.67725	16.402	30.423
	Recall	30.34672	12.513	20.97
8	***Precision***	44.44444	16.468	27.182
	Recall	33.39001	15.312	24.14
10	***Precision***	42.69841	14.444	25.238
	Recall	37.22976	16.483	26.831

Average of precision rate of proposed recommendation method was 47.546295. It was better than average of precision rate of user based collaborative filtering (15.1022) and clustering + user based collaborative filtering (28.8455). Average of recall rate of proposed recommendation method was 31.72947. It was better than average of precision rate of user based collaborative filtering (12.977) and clustering + user based collaborative filtering (22.1385).

V. CONCULSION

For the precise recommendation, researches on collaborative filtering recommendation system are increasing. But these researches have problems in scalability and cold-start. To solve these problems, this paper proposes the recommendation system based on user's content consumption according to watching time pattern and objects of interest. For this, we extract objects of interest from 259 media contents and 157 users and then calculate preference scores. To evaluate the performance of the proposed system comparison tests are done with the results of the existing collaborative filtering systems.

ACKNOWLEDGMENT

This work was supported by Institute for Information & communications Technology Promotion(IITP) grant funded by the Korea government(MSIP) (No.R0101-15-293,Development of Object-based Knowledge Convergence Service Platform using Image Recognition in Broadcasting Contents)

REFERENCES

[1] Kwon Hyeong-Joon, Chung Dong-Keun, Hong Kwang-Seok, "A Multimedia Recommender System Using User Playback Time", Journal of Korean Society for Internet Information, Vol.10, No.1, pp.111-121, 2009, 02

[2] SP003v1.3 Part A:Metadata. TV-Anytime Forum(2002)

[3] Sung-Woo Byun, So-Min Lee, Soek-Pil Lee, "Metadata Management System Implementation for Object-oriented Personalized Media Service based on Multiple Camera" Journal of The Korea Society of Broadcast Engineers, Vol. 19, No. 5, 631-639, 2014.

[4] Michael D. Ekstrand, John T. Riedl, Joseph A. Konstan, "Collaborative Filtering Recommender Systems", Foundation and Trends in Human-Computer Interaction, Vol.4, No.2, pp.81-173, 2010

[5] Chul-Yong Sun, Yong-Jin Kang, Kyu-Sik Park, "A Study of IPTV-VOD Program Recommendation System using Collaborative Filtering", Journal of Korea Multimedia Society, Vol.13, No.10, pp.1453-1462, 2010, 10

Line-defect removal in the fast-Fourier transfrom based synthesis of polygon computer-generated hologram

Youngjin Jeon, Jaebeom Kwon, Dajeong Im and Hwi Kim
Department of Electronics and Information Engineering
Korea University, Sejong Campus
2511 Sejong-ro, Sejong 339-700, South Korea
hwikim@korea.ac.kr

***Abstract*—The line-defect problem is appeared because of the limited-period in the computation grid when we calculate the polygon computer-generated hologram (CGH) by the fast Fourier transform (FFT). To solve this problem, we propose the method that is accomplished by partially filtering the angular spectrum of the polygon consisting the 3D object. Through partially filtering the angular spectrum of intersection line, the line-defect removal optical reconstruction results of polygon CGH are presented.**

Keywords-componen: Holographic display, Polygon Computer Genarated Hologram, Fast-Fourier Transform.

I. INTRODUCTION

The holographic 3D display is considered as ultimate three-dimension (3D) display. The computer-generated hologram (CGH) synthesis is one of the most important technologies for the holographic 3D display. There are several ways to generate CGH, but we use the polygon CGH method that have the advantage of realistic and fast calculation time [1]. There are two calculation ways in the polygon CGH synthesis, the first way is analytic method and the second way is fast-Fourier transform method. The analytic method is that calculating polygon angular spectrum CGH by analytical Fourier transform formula in the angular spectrum domain. While, the FFT based method can be applied for textured polygon CGH, but the discrete calculation induces some numerical errors in the CGH calculation. As a consequence, when using the fast-Fourier transform method, we can see that line-defect problem occurs around the borders of adjacent triangular polygons [2]. In this paper, we analyze the cause of the line-defect defects and presents an effective filtering method for removing the line-defect.

II. ANALYSIS OF THE LINE-DEFECT PROBLEM.

Ideally, when we calculate the angular spectrum CGH of polygon by the analytic method, the exact angular spectrum of polygon facets can be obtained. However, in the FFT-based method, the discrete approximation of the continuous angular spectrum integral induces some numerical errors. A representative example is the line defect problem observed in the reconstructed holographic image as shown in Fig. 1(a). The angular spectrums of the sides of two adjacent polygons are overlapped in the shared border. Unlike the analytic method, the angular spectrum of normal direction that represents the border edges of polygon causes the line-defect since the phase mismatch of the angular spectrum s of two triangular facets. To resolve this problem, we propose a partial filtering method of the phase-mismatched angular spectrum components of the polygon object, where the phase-mismatched partial angular spectrum components of the borders of the two adjacent triangular facets is selectively filtered that should be removed when the two adjacent triangular is connected. Comparing Figs. 1(a)-1(c), we see that the proposed filtering method for the FFT-based CGH synthesis is effective in line defect removal and comparable to the analytic method. In Fig. 1(b), the line defect is clearly removed and all the line-defect is disappeared on the object surface.

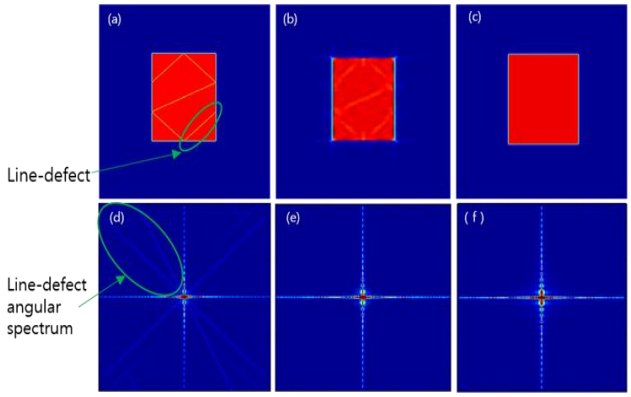

Figure 1. Reconstructed object by conventional method (a), its angular spectrum (d), reconstructed object by proposed method (b), its angular spectrum (e) and reconstructed object by analytic method (c), its angular spectrum (f).

III. PARTIAL LINE-DEFECT FILTERING METHOD

Generally, the reconstructed object by using the polygon CGH synthesis method is consisted of many light field elements of unit triangular facets. Each light field elements of unit triangular facets have own angular spectrum, and it has a particular shape that is consisted of three-lines along the perpendicular directions to all sides of the triangle as shown in Fig. 2.[3]

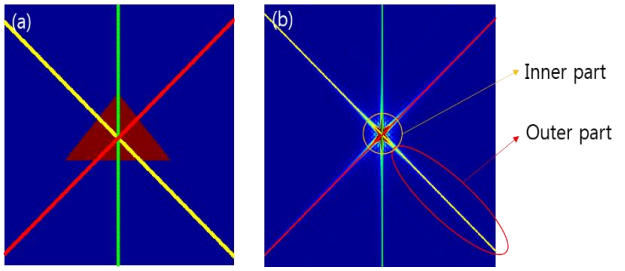

Figure 2. (a) A unit triangle facet in the local coordinate and (b) its angular spectrum profile

Angular spectrum of polygon can be divided into two parts, one is outer part and the other is inner part as shown in Fig. 2(b). The outer parts of angular spectrum have signal of each side of the triangle and inner parts that have low-frequency area have signal of inner facet of triangle.

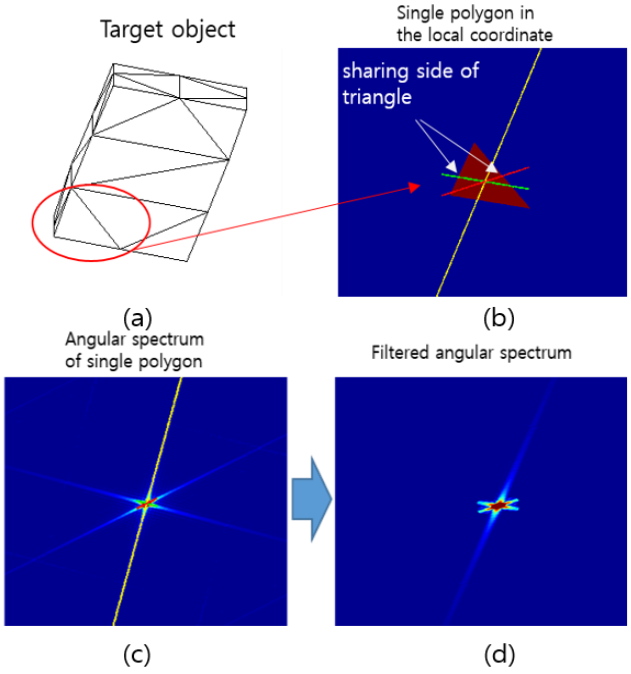

Figure 3. (a) The target object, (b) single polygon in the local coordinate, (c) angular spectrum of single polygon, (d) filtered angular spectrum

Our purpose is removing line defects, therefore, our region of interest (ROI) is an inner triangle facet except the shared edges of triangles while all outer angular spectrums (non-ROI) should be eliminated by filtering. The result of filtered angular spectrum is shown in Fig. 3. In Fig. 3(b), there are two shared edges of triangle. Thus, its angular spectrum is filtered along the direction of perpendicular of shared edges. In Fig. 3(d), we can observe filtered angular spectrum that only remain in the ROI.

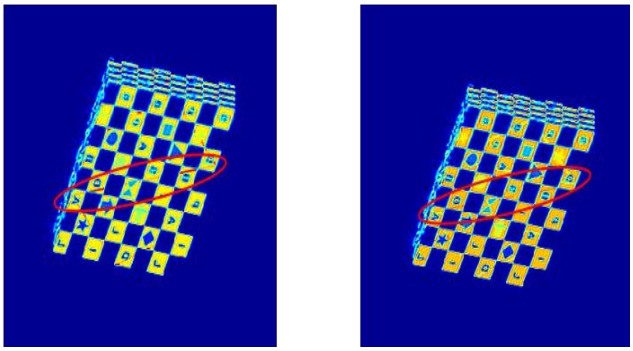

Figure 4. Reconstructed 3D object by (a) fast-Fourier transform and (b) the proposed method.

We observe the line-defect of the reconstructed image is removed clearly in Fig. 4. (b), but a little noise still is remained because of un-optimal filtering size. The size of remaining inner part of angular spectrum determines the quantity of signal of triangle inside facets. If we remain too much signal of low frequency, line-defect noise will be appeared. Therefore, suitable size of filtering is required. It is necessary to find the optimal size of filtering size.

IV. CONCLUSION

In this paper, we proposed a method to remove the line defect problem of the FFT-based polygon CGH synthesis by partially filtering the angular spectrum of the polygon units. When removing the non-ROI area of angular spectrum, the proper choice of size of remaining low-frequency area is important. If we remove the low-frequency area too much, that causes signal loss of inside of triangle facets. While, if we remain low-frequency area too much, that also cause remain noise of the sides of triangle. Finding optimal remaining area of low-frequency is our future work.

ACKNOWLEDGMENT

This work was supported by Samsung Future Technology Fund of Samsung Electronics Inc. under Grant Number SRFC-IT1301-07

REFERENCES

[1]] H. Kim, J. Hahn, and B. Lee, "Mathematical modeling of triangle-mesh-modeled three-dimensional surface objects for digital holography," Appl. Opt. 47, D117-D127 (2008).

[2] D. Im, J. Cho, J. Hahn, B. Lee, and H. Kim, "Accelerated synthesis algorithm of polygon computer-generated holograms," Opt. Exp. **23**, 2863-2871 (2015).

[3] D. Im, E. Moon, Y. Park, D. Lee, J. Hahn, and H. Kim, "Phase-regularized polygon computer-generated holograms," Opt. Lett. **39**, 3642-3645 (2014).

Kernel source verification on the embedded system

Wang Ye[1], Seungcheon Kim[2], KyuTae Lee[3] , Kee-young Kwon[4], Hyun-Bae Choi[5]
Dept. of Electronic and Information Engineering, Lishui University, Zhejiang province, China[1]
Dept. of Information and Communication Engineering, Hansung University, S.Korea[2]
Div. of Information & Communication Engineering, Kongju National University, S.Korea[3]
Dept. of Electrical, Electronic and Control Engineering, Kongju National University, S.Korea[4]
R&D team, Creative Lighting Technology, S.Korea[5]

wychina_2007@hotmail.com, kimsc@hansung.ac.kr , ktlee@kongju.ac.kr, kky@kongju.ac.kr, iltchoi@lycos.co.kr

Abstract – Embedded system device is a hardware system with a special processor and interface modules which has their own function and performance and software under operating system. For developing a new device, developer searches for new interface modules with a driver algorithm on the market to reduce times. In this case, the program kernel code interfaced with this module could be the same as others product one. Then it would be difficult to verify that which code is the original source program as for keeping the copyright. On property right verification, this kind of kernel code could make a problem as it is verified. In case of the open source code, each developer program could be the same on line by line as the code is released by an interface module vendor. In this paper we show a case study to keep the property right to owner as for the module interface and communication interface, peripheral interface whether it has open source or not. .

I. Introduction

As to IT device system, it is called the Embedded system now a days that is the same as a small personal computer with a tiny Operating system and special application software. The device function is similar to general operating system (OS) but it has a limited operating performance as conventional one. On fast developing trends, many useful handheld devices are now released in faster and in smaller with embedded systems. [1]

But as for the copyright and intelligent property claim, it is becoming the important new issues for keeping original developers to preserve their right. The conventional procedure to verify these copyright problems on the software is to extract comparison result as to each code by lines or function by function simply.

The embedded system with OS has more difficulties in the verification to extract the illegal use proof. They use a different language, different OS and especially different microprocessor on their systems even it has the same function and procedure. As each microprocessor has own binary code, verification procedure would be difficult.

In this paper, we studied case results on the comparison and extraction to their binary code on the embedded system. And also we discuss about open source code and market released module interface program comparison.

II. Embedded system basics

The handheld device as the navigation system in our car is a useful equipment in these days. The configuration is below figure 1.

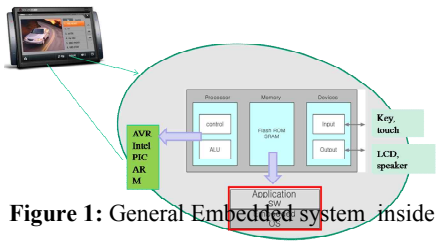

Figure 1: General Embedded system inside

It figures out with its special microprocessor such as AVR, PIC and ARM etc. and has input device and output device like touch LCD panel or keypad etc. as basics. Based on the processor, an operating system(OS) and application program is installed on the device.

Microprocessor has the architecture with CPU, FlashROM, SRAM, and peripheral interfaces as below Figure 2. For figuring out for embedded system the processor has a Flash memory and special interface blocks to support a mobile service.

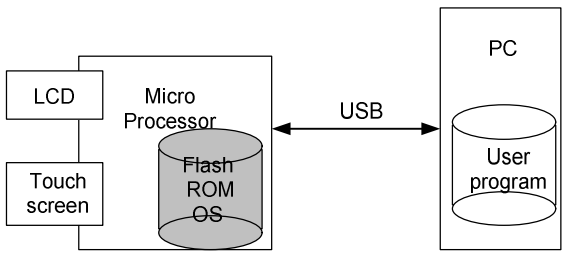

Figure 2: Embedded processor architecture

What we are interesting is in the FlashROM which has a system program and its application code on their special microprocessor. Generally the system program is a realtime operating system such as Linux or Windows and application code are running on its OS. Most applications are reserved on the FlashROM as a scattered image file constructed with Ramdisk memory area.

An verification procedure for seeking an illegal source code is focused on its image code on the memory. But their program code is depended on the special microprocessor chip. As we know, making a program code procedure is like as below.

At first, to assign a job procedure, a flowchart is figured out step by step. With this flowchart, a programmer make a source code with one's interesting program language for the special processor to the device. After all binary code is generated through compiling procedure, execution code is downloaded to their device. With this example we see that the binary code in the device inside is only fit

with a special processor. It is a different whenever the developer choose a different language or processor . Sometimes complier options could make an influence to these code difference for illegal copy.

III. Kernel code verification

Linux kernel is open source and it can be downloaded through the internet freely. On the study we downloaded a same kernel and ported to each device. Comparison of each kernel is below a table. Item 1 is open source, item 2 is original source code, and item 3 is illegal kernel source as kernel name and kernel size, the number of files.

Table 1. kernels for comparison

item	Kernel name	size (bytes)	files
1	linux_2.6.28.6	289.0M	26751
2	C-0	400M	26196
3	P-A	1,255M	60379

Comparison results are on the table 2. The result shows 99.3% similarity between original source code and illegal source code and most of kernel codes are open source. This method to compare to all the kernel code is not confidential way as to credits.

Table 2. compare result

kernels			Similar files	similarity(%) based on illegal
comparison		File size (MB)		
origin	C-0	26196 (400M)	25504	97.3
illegal	P-A	25700 (298M)	25540	99.3

Direct comparison result is on table 3. It shows also most of files are the same to 99.5% files, 99.3% file size. And two kernels are to be mostly similar sources.

Table 3. direct compare result

C-0	P-A	Similar files /size	similarity /size (%)
files(size)	files(size)		
26196(400M)	25700(298M)	25578(296M)	99.5(99.3)

As the result, It is clear that the comparison as to all the kernel code is not proper and can make issues to discuss. Therefore best way to compare a kernel source code is classify to each blocks such as device driver, library, and utility.

IV. Conclusions

In this paper, it shows a case study for kernel source code verification as to way of keeping copyright as it uses open source. In case of market released components, vendors release each module driver for supporting a simple handling for special function. And the programmer do simply interface by their input/output characteristics. As developers use this interface to their product, it might be same program code and interface circuit. On the similarity evaluation procedure, kernel source code is an important material, but it can be the same by hardware interface protocols and it can make mistake on valuation. To protect a copy right, comparison would be set up to individual code blocks such as device driver, utility, and library blocks.

References

1. Rajesh K. Gupta, "Introduction to Embedded system", ICS 212, 2002 winter workshop
2. Embedded process system, Hanback electronics , 2003.11.
3. Getting started with HBE-EMPOS II, Hanback electronics, 2004.3
4. Intel PXA255 Processor Developer's Manual
5. Joseph Yiu, ARM Cortex-M3 guide, ITC, 2011

Design of a Multimedia Authoring System using User Location

Hwang Keun Lee
Department of Smartmedia
Jeonju University
Jeonju, Korea
cohere@gmail.com

Geun Ho Lee
Department of Smartmedia
Jeonju University
Jeonju, Korea
ghlee@jj.ac.kr

***Abstract*— In this paper, we design a multimedia authoring tool that can reflect the needs of different users. It is possible to provide contents utilization to user's location information. In addition, it is designed to distinguish the sound field and image field to take advantage of a variety of multimedia elements. It was designed using google maps, google earth plug-in, open API, KML, etc.**

Keywords-multimedia authoring tool; location information; sound field; open API; KML

I. INTRODUCTION

The importance of software resource development has been increasing attention by the rapid development of hardware[1]. Particularly, due to the spread of mobile devices, the demand for detailed information of the location and space has increased explosively. Among them, the amount of search and query which related the location and position are increased constantly. For this reason, Google and Microsoft are providing web-based spatial information in the world to support a variety of software development. Therefore, we develop the soundscape authoring tool based on user emotion using Google Maps, Google Earth Plug-in, open API, KML[2].

II. DESIGN METHOD

A. *Google earth plug-in*

Various function of the google earth which implemented with digital technology can drive on Web page using the google earth plug-in and javascript API that contained herein. In other words, developers can insert google earth on his website, and perform any editing tasks on google earth[3]. Additionally, we can display 3D information depending on the selected menu by integration the google earth plug-in. And also, we can use many other functions of the google earth as a terrain etc.

B. *KML (Keyhole Markup Language)*

KML is a file format that used mainly for displaying geographic information in the google earth, google map, earth browser[4]. The web browser performs tasks similar to HTML processing. But, KML has a structure based on tag that has names and attributes. Therefore, the developer can specify the icon and label by using KML. And it is possible to set the camera position. This is because the developer to define the view.

The authoring tool that can use user location information and multimedia contents was designed using advantages of the feature previously mentioned. The server performs basic tasks such as data storage and security. In addition, it is creating a KML file, and performs the communication between the web servers. The server also performs communication between mobile apps and applications. The client as a mobile app performs the basic data acquisition and transmission in conjunction with the server basically. Clients can represent and select the location information respectively. In addition, the client can perform the event process that depending on the location and behavior of user. Figure 1 shows a block diagram of the designed authoring system.

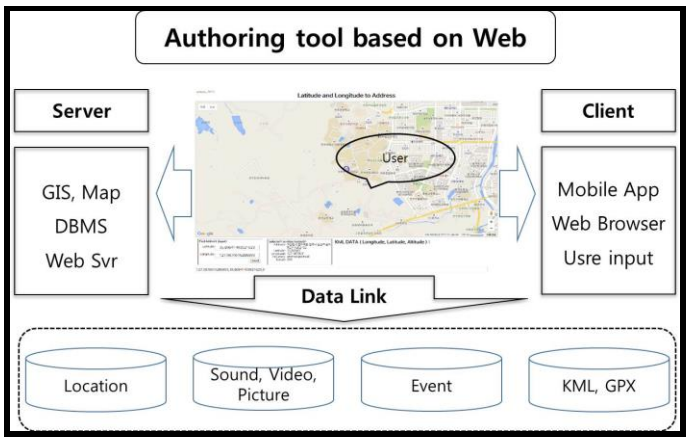

Figure 1 . System architecture

III. SYSTEM DESIGN

It was designed using XML(extensible Markup Language) to a common data structure and configuration. And then KML was used to geographic information modeling. The authoring tool was designed to include a sound file for use soundscape concept. We can play the sound file at any time using <gx:Sound Cue> element. The sound file can be specified in

Identify applicable sponsor/s here. If no sponsors, delete this text box. (sponsors)

the <href> element below, and supported sound types are different depending on the codec installed on your system. The authoring tool was designed to enable the use of MP3 and WAV files. The authoring tool can play multiple sound files at the same time. If the background music and voice have to use in same time at a particular location, it can be useful.

The following is a sample of 15 seconds. The period was defined using <gx:FlyTo> and <gx:Wait>. The first sound clip is played for 15 seconds, and it will be played throughout the entire moving time. The second sound clip is played for 10 seconds with the first file after wait for 5 seconds.

```
soundcue_example.kml
----------------------------------------
<?xml version="1.0" encoding="UTF-8"?>
<kml xmlns="http://www.opengis.net/kml/2.2"
xmlns:gx="http://www.google.com/kml/ext/2.2">
<gx:Tour>
<gx:Playlist>
<gx:SoundCue>
<href>
http://dev.keyhole.com/codesite/AJsBlues.mp3
</href> <!-- 15 second audio clip -->
</gx:SoundCue>
<gx:FlyTo>
<gx:duration>5</gx:duration>
<gx:flyToMode>bounce</gx:flyToMode>
<LookAt>
<longitude>-79.387</longitude>
<latitude>43.643</latitude>
<altitude>0</altitude>
<range>1200</range>
<tilt>10</tilt>
<heading>-172.3</heading>
<altitudeMode>relativeToGround</altitudeMode>
</LookAt> </gx:FlyTo> <gx:SoundCue> <href>
http://dev.keyhole.com/codesite/cntowerfacts.mp3
</href> <!-- 10 second audio clip --> </gx:SoundCue>
<gx:Wait> <gx:duration>10</gx:duration> <!--
continues the tour for 10 seconds --> </gx:Wait> <!--
while audio clip plays --> </gx:Playlist>
</gx:Tour>
</kml>
```

Figure 2 illustrates a screen example of the authoring tool was designed. The main screen which shows the user's location information is located in the center, and the KML data showing the location coordinates has been shown in below. Tool box that can perform the basic operation and input box that can mount multimedia contents are located in the right side.

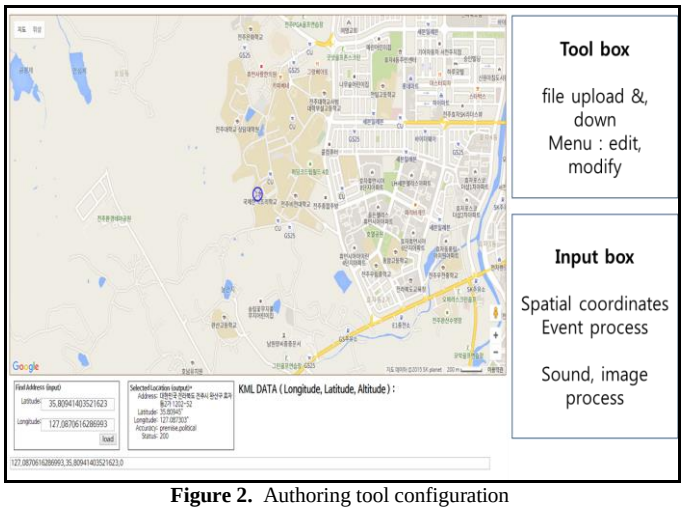

Figure 2. Authoring tool configuration

IV. CONCLUSION

As a result, the performance that can be obtained through the authoring tool design is as follows. First of all, it can be overcome the limitations of existing tour apps using the geographic information system based on soundscape. In addition, the designed system and the database will be able to contribute to the activation of the culture industry and similar applications in the relevant region. And also, it will can be utilized to design a similar authoring system that combines web-based spatial information and multimedia elements.

ACKNOWLEDGMENT

This research is supported by the small and medium business administration (SMBA) 2015.

REFERENCES

[1] Hassan Gomaa, "Software Modeling and Design," Cambridge University press, 2011

[2] Agostino Di Scipio, "Sound Object, Sound Event! Ideologies of Sound and the Biopolitics of Music," The Journal of Acoustic Ecology, vol. 13, No 1, pp.10–14, 2014.

[3] https://developers.google.com/kml/documentation/

[4] https://google-earth-plugin.en.softonic.com/

High-definition polygon computer-generated hologram synthesis with viewing zone separation

Dajeong Im and Hwi Kim*
Department of Electronics and Information Engineering, College of Science and Technology, Korea University,
2511 Sejong-ro, Sejong 339-700, South Korea
*hwikim@korea.ac.kr

***Abstract*—In this paper, we propose a novel method of high-definition (HD) polygon computer-generated hologram synthesis using viewing zone separation.**

Keywords-digital holography; holographic display; computer-generated hologram; high-definition

I. INTRODUCTION

It may be said that computer-generated holograms (CGHs) synthesis algorithm is one of core technology of holographic three-dimensional (3D) display. To achieve the real-time generation of photorealistic holographic 3D scenes, in the field of CGH study, effort is chiefly directed at two directions. The first is the fast calculation method of large-scale CGH, and the second is the extraordinarily realistic description of the 3D object. For improvement of computing speed, parallel computing technique based on the graphics processing unit (GPU) is commonly used. Besides, in polygon CGH, accelerated synthesis algorithm based on theoretical property without any parallel computing hardware is also studied in our previous research [1]. Also, representation theory is as much significant as fast computation in CGH synthesis algorithm. Representation technique includes occlusion culling and rendering such as texturing, shading, etc.

To reconstruct a fine holographic 3D image, computation of large-scale CGH is imperatively necessary. Many techniques for handling of high resolution CGH have been developed, however, it is still very hard and actually impractical. In [2], computation method of large wave fields using the segmented frame buffer is presented without store whole wave field in memory. In the conventional CGH synthesis method, the wave propagation from the object plane to the SLM plane is calculated at one go. Actually, since the diffraction field of the triangle unit in the object plane covers only small region of whole area, the calculation in the object field with additional propagation is faster than the direct calculation in the SLM plane. However, in this method, the maximum diffraction area of each polygon should be calculated, and shifted Fresnel transform for off-axis wave propagations is also required.

In this paper, we propose a novel method of high-definition (HD) polygon computer-generated hologram synthesis using viewing zone separation.

II. LARG3-SCALE CGH CALCULATION

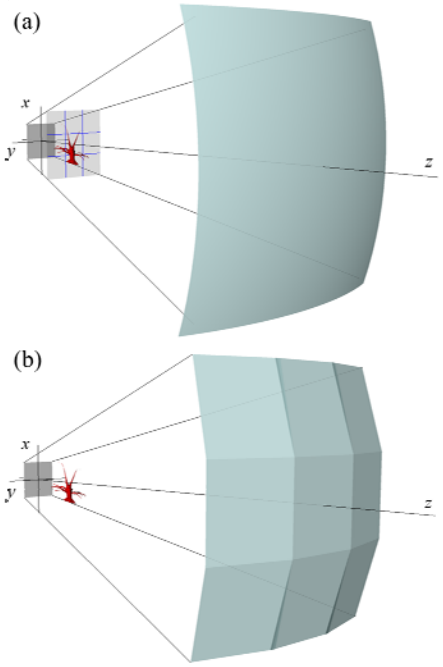

Figure 1. Large-scale CGH segmentation in (a) the conventional and (b) the proposed methods.

The traditional and the proposed methods are compared in Fig. 1. As shown in Fig. 1(a), the conventional method splits the object plane. In the proposed method, the viewing zone is segmentalized as depicted in Fig. 1(b). As a matter of fact, high resolution is necessary to describe carrier wave. In other words, high is unnecessary for representing signal. Therefore, we can calculate total CGH as in (1),

$$CGH_{total} = \sum_{m}\sum_{n} \exp\left(j\left(k_{m,n,x}x + k_{m,n,y}y + k_{m,n,z}z\right)\right) F_{m,n}\left(x,y\right) \tag{1}$$

where m, n is the viewing direction, and $F_{m,n}\left(x,y\right)$ and $\exp\left(j\left(k_{m,n,x}x + k_{m,n,y}y + k_{m,n,z}z\right)\right)$ are signal and carrier

wave respectively. This way facilitates that calculate signal by low resolution without any preconditioning process such as computation of the maximum diffraction area of each triangle.

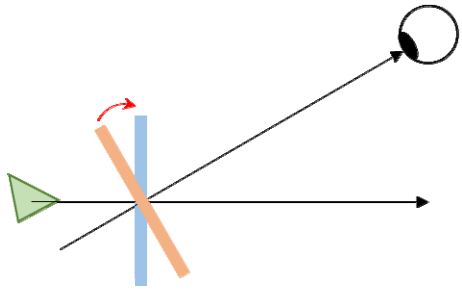

Figure 2. Computation process of the proposed method.

Figure 2 illustrates computation process of the proposed method. From every segmented viewing direction, we calculate signal in the tilted plane expressed orange color without consideration of carrier wave. Since carrier wave is not considered in this step, low resolution signal is computed. Let us assume that total resolution is $10{,}000 \times 10{,}000$ and pixel pitch is $1\ \mu m$. When the number of separated viewing zone is 10×10, signal is calculated at $1{,}000 \times 1{,}000$ resolution and $10\ \mu m$ pixel pitch. Next, light field distribution at the spatial light modulator (SLM) plane expressed blue color is computed using field distribution mapping. We change the resolution into the original resolution, and multiply carrier wave. Lastly, superposition of wave field at every viewing direction is required.

Numerical simulation result is shown in Fig. 3. Figure 3(a) and (b) are amplitude and phase profile of total CGH. Signals at eye lens plane is shown in Fig. 3(c). Because we divide $11{,}011 \times 11{,}011$ resolution into 11×11 views, there are 11×11 signals. Numerically reconstructed holographic image of the center view is in Fig. 3(d).

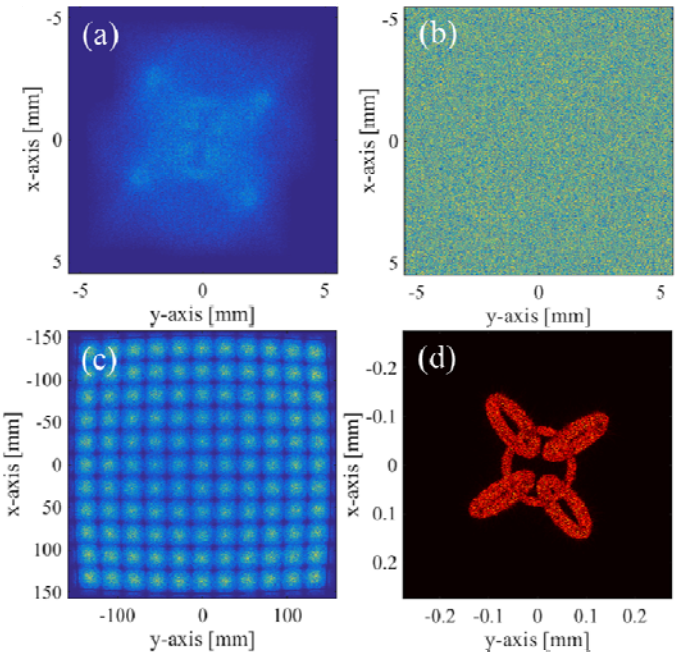

Figure 3. (a) Amplitude profile and (b) phase profile of total CGH. (c) Signals at eye lens plane. (d) Reconstructed holographic image.

III. Conclusion

We proposed a novel method of HD polygon computer-generated hologram synthesis using viewing zone separation. The process of the proposed method is elucidated in detail. The proposed method is demonstrated with numerical simulation.

Acknowledgment

This work was supported by the Industrial Strategic technology development program (10052641, Development of the commercialization platform technology for diffractive optical element based on 3D surface nanostructure for full-color implementation) funded By the Ministry of Trade, industry & Energy (MI, Korea).

References

[1] D. Im, J. Cho, J. Hahn, B. Lee, and H. Kim, "Accelerated synthesis algorithm of polygon computer-generated holograms," Optics Express, vol. 23, pp. 2863-2871, 2015.

[2] K. Matsushima and S. Nakahara, "Extremely high-definition full-parallax computer-generated hologram created by the polygon-based method," Applied optics 48, H54-H63, 2009.

Anti-FP error Oriented Forgery Detection Approach

Yong Soo Choi
Division of Liberal Arts & Teaching, Sungkyul University
Anyang City, Korea
ciechoi@sungkyul.ac.kr

Dessalegn Atnafu AYALNEH
School of Information Security, Korea University
Seoul, Korea
Dessalegn_atne@korea.ac.kr

***Abstract*— Copy-move forgery is one of the most popular tampering artifacts in digital images. In this paper, we present an algorithm to reduce the error (i.e. False Positive) occurring in the forgery detection process. Proposed method uses the perceptual hash string which well known in the field of image processing and also robust against general image processing and geometrical modification. This paper shows how to complement the cons, which existing LBP, MLBP algorithm has, by adopting proposed Anti-False Positive Forgery Detection.**

Keywords- Forensics; False Positive; Perceptual Image Hash;

I. INTRODUCTION (HEADING 1)

The digital image is a very important role in modern society and particularly in accordance with the popularization of SNS network and high-speed network, transmission rate of the video has a very high growth. According to a survey conducted in 1989, 10% of the color image has been published doesn't use as it is and comprises a fake (Transformation). Reason for this increase in the counterfeiting of the digital image is that a lot of software or hardware that can edit an image in a low cost. Of course, this doesn't mean that all of the digital content editing is counterfeit cases, but few of cases lead to social problems such as confusion, personal privacy and political/ military misuse.

II. RELATED WORKS

There is a passive method that can transform the content according to the user's intention and then get the difference between original and modified one. Finally the copyright or secret information might be extracted on it. Passive ways were DCT (Discrete Cosine Transform), SIFT (Scale Invariant Feature Transform), LBP (Local Binary Pattern) and so on[1-3]. Because active ways are using typical insertion and extraction method, it is effective in real applications. But, it is useless in case of extreme circumstance like random operation. In figure 1, it describes how to create a LBP.

$$LBP_{P,R}(x_c,y_c)=\sum_{q=0}^{P-1}s(g_q-g_c)2^q, s(x)=\begin{cases}1: x\geq 0\\ 0: x<0\end{cases}$$ ---- Eq. 1

Where n is the order of the neighbor pixel value and each g_n and g_c refers to a center pixel and the surrounding pixels. P refers to the number of surrounding pixels and R is the distance between the center pixel and the surrounding pixels. Throughout the following equation, histogram is generated using the LBP,.

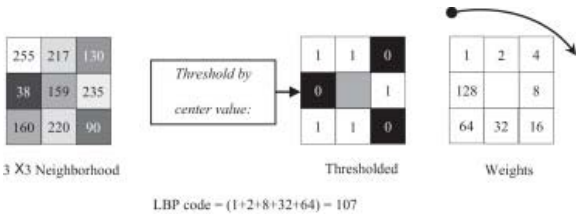

Figure 1. LBP Code Calculation

$$H(t)=\left(\frac{1}{M\times N}\right)\sum_{i-1}^{M}\sum_{i=1}^{N}f(LBP_{P,R}(i,j),t), t\in[0,T]$$ **Eq.2**

$$f(x,y)=\begin{cases}1, x=y\\ 0, otherwise\end{cases}$$ **---- Eq. 3**

Where T is a maximum of LBPs. LBP is invariant to rotational transformation and being obtained by the following equation (4). Normalized LBP can be obtained by the formula (5-6). The equation (7) provides a measurement value of dispersion constant to rotational transformation

$$LBP_{R,R}^{ri}=\min ROR(LBP_{P,R},i)\,|\,i=0,1,\ldots,P-1$$ **---- Eq. 4**

$$LBP_{P,R}^{riu2}=\begin{cases}\sum_{q=0}^{P-1}s(g_q-g_c), U(LBP_{R,R})\leq 2\\ P+1, otherwise\end{cases}$$

---- Eq. 5

$$U(LBP_{P,R})=|s(g_{P-1}-g_c)-s(g_0-g_c)|+\sum_{q=1}^{P-1}|s(g_q-g_c)-s(g_{q-1}-g_c)|$$

---- Eq. 6

$$VAR_{P,R}=\frac{1}{P}\sum_{q=0}^{P-1}(g_q-\mu)^2, \mu=\frac{1}{P}\sum_{q=0}^{P-1}g_q$$ **---- Eq. 7**

Now we select blocks in order from the input image and obtain the each block and LBP value of entire image. Below equation as Feature Matrix(FM) have Vs as a each element.

$$S=\left\{V_{1,m}(j_1)\,|\,\sqrt{(x_q-x_m)^2+(y_q-y_m)^2}\geq Dist\right\}$$ **---- Eq. 8**

This calculates the Euclidean distance between the resulting FMs and generates the CM (Corresponding Matrix) by sorting FMs. If two or more elements of CM have same distance, we

can decide suspected block is copy-moved. In figure 2, it copies some of the image (a) and moves it onto the body of woman of image (b). That is, copied region replaced the body of woman and finally the woman is removed from it. By checking the CM, some blocks, which are considered as the copy-moved block, are connected(c of Figure). Finally we prove two regions of the right (d) have modification generated by copy-move attack.

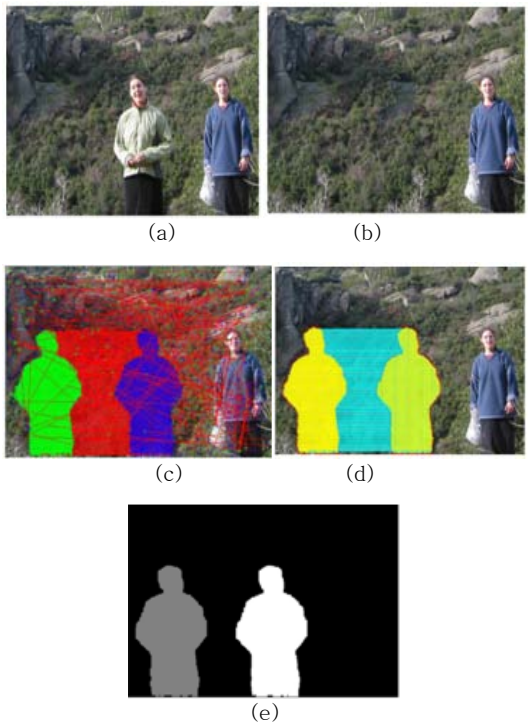

Figure 2. (a)Original (b)Forged Image (c)CM Connection (d) copy-moved region display (e) copy-moved area detection

Figure 3. False Positive Forgery Detectio for similar objects withing image

III. ANTI-FP ERROR DESIGN OF FORGERY DETECTION

In the forgery detection, FP (False Positive) is found to be counterfeit by the software, despite the detection of counterfeit says it is not a forgery. Algorithm for detecting an image forgery due to the damage such as conventional copy-move is being widely studied. But, There is some False Positive conclusion where occurred looking at the example in Figure3.

In figure 3, although there is no forgery operation in image, it detects two aircraft from the forgery detection method using an MLBP.

In this case study, determining, two objects are whether the actual or falsification, is very important. In this paper, it try to solve the FP problem through the application of perceptual hash, as shown in Figure 4, they will proved whether these are same or not. Similar objects are presented in an common image, but perceptual hash generated by detailed region of the image area will be different. Because there were many operations like signal processing and attack.

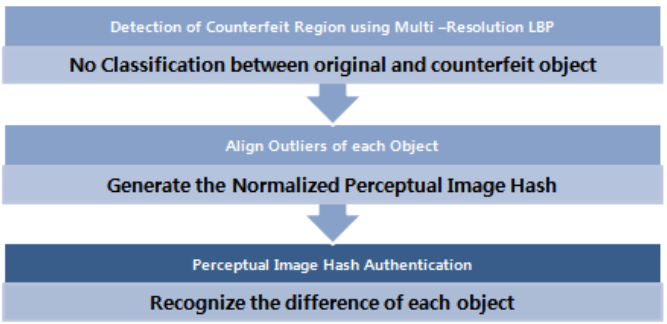

Figure 4. Proposed False Positive error Reduction Approach

IV. CONCLUSION AND FURTHER WORKS

A lot of counterfeit detection research have done in the current digital image forensics. It also has a variety of applications such as a social / military field. However, most current algorithms will determine if a forged image which has the same characteristic value in the image. But it is determine that there were forgery operation even if target image doesn't contain counterfeit on it, the impact by digital decision is very large. Even proposed design does not detect in the case of all the FP, it will be able to reduce the wrong FP error considerabley.

ACKNOWLEDGMENT

This research was supported by Basic Science Research Program through the National Research Foundation of Korea(NRF) funded by the Ministry of Science, ICT & Future Planning(No. 2013R1A1A1013410).

REFERENCES

[1] H. Farid, "A survey of image forgery detection," IEEE Signal Process. Mag., 26 (2) (2009), pp. 16–25

[2] [2] Reza Davarzani, Khashavar Yaghmaje, Saeed Mofaffari, Meysam Tapak, "Copy-move Forgery Detection using Multi-Resolution Local Binary Patterns," Journal of Forensic Science International, Vol 231, Issues 1-3, Sep 2013.

[3] [3] J. Fridrich, D. Soukal, J. Lukas "Detection of copy-move forgery in digital images," Proceedings of the digital forensic research workshop, Cleveland, OH (2003)

Challenges and Research Directions for Multipath TCP Scheduler in Multi-Channel Multi-Radio Wireless Mesh Networks

Eun Jung, Lee
School of Electrical Engineering
KAIST
Daejeon, Rep. of Korea
freakone@kaist.ac.kr

Yong-jun, Seo
School of Electrical Engineering
KAIST
Daejeon, Rep. of Korea
yongjun86@kaist.ac.kr

Hong-Shik, Park
School of Electrical Engineering
KAIST
Daejeon, Rep. of Korea
park1507@kaist.ac.kr

***Abstract*—In this paper, we investigate scheduling algorithms of Multipath TCP (MPTCP) in multi-channel multi-radio (MCMR) wireless mesh networks (WMNs). To do that, we first explore previous works on MPTCP scheduler and analyze them profoundly. After that, we summarize research challenges and directions for MPTCP scheduler in MCMR WMNs. Through this work, we can give a good guideline for network operators when they adapt MPTCP technique to their future 5G network for enhancing the network throughput while minimizing the delay performance.**

***Keywords*—Multipath TCP, Multi-channel multi-radio wireless mesh network, Reordering problem**

I. Introduction

Recently, throughput enhancement has become a critical issue in 5G wireless networks due to high quality (i.e., 4k Ultra HD) video services more prevalently [1]. For enhancing through, the multi-channel multi-radio (MCMR) wireless mesh networks (WMNs) have been paid attention to the 5G networks [2]. Along with this network evolution toward 5G generation, Multipath TCP (MPTCP) has also attracted to a promising solution to improve the application throughput [3]. In general, the previous works on MPTCP only considered the single hop network such as 3G/4G wireless network or WiFi network without considering the multi-hop networks. However, the previous approaches on MPTCP scheduler may face with a reordering problem more seriously in MCMR WMNs, compared with the wired backbone network [4], due to the intensified dynamics of network status in multi-hop wireless environments as shown in Fig. 1. In fact, such heterogeneous nature of wireless environment strengthens the diversity of quality of each path, eventually it results in the degradation of application throughput and end-to-end delay performance [10]. For this reason, we need to consider the network performance and control overhead for the MPTCP scheduler in MCMR WMNs.

To overcome this reordering problem, several works on [5]–[10] have studied during recent years in 3G/4G wireless networks. However, the previous works on the MPTCP scheduler have some limitations applying to the MCMR WMNs directly. For this reason, we need to analyze the existing MPTCP scheduler solutions more deeply for MCMR WMNs.

The objective of this paper is to review the previous literature on the MPTCP scheduler for MCMR WMNs. To do that we analyze the previous works according to two categories: single layer approach and cross layer approach. Based on this analysis, we suggest some challenges and research directions for MPTCP scheduler in MCMR WMNs.

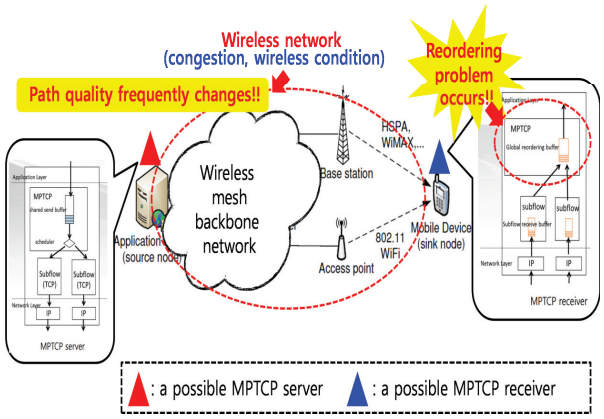

Fig. 1. Multipath scenario and reordering problem in MCMR WMNs.

The remaining of this paper is as follows. First, we analyze the previous works on MPTCP schedulers in 3G/4G wireless networks. After that, we derive some challenges and research direction of it for MCMR WMNs. Finally, we conclude this paper and describe future works.

II. Related Work

To relieve the reordering problem in the MPTCP technique, several existing works on MPTCP scheduler has been proposed [5]-[10]. In particular, the previous works can be divided into two approaches: single layer approach and cross layer approach. Fig. 2 indicates the taxonomy tree of previous works on the MPTCP scheduler.

A. Single layer approach

During the recent ten years, many of the single layer approaches have been proposed to enhance the application throughput [5]-[9]. At first this approach only focused on the MPTCP scheduler. The authors in [5] proposed the MPTCP

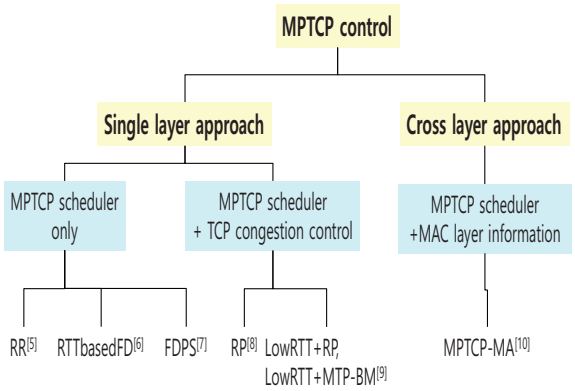

Fig. 2. Taxonomy tree of previous works on the MPTCP scheduler.

scheduler by selecting one sub-flow after the other in round-robin (RR) fashion. Although they can increase the fairness among the sub-flows, the RR scheme occurred ack clock problem when bulk data was transmitted. To solve this problem, some works on [6, 7] began to use the measurement information at the TCP layer. The authors in [6] used the forward delay estimation based on the RTT value for the MPTCP scheduler. However, they assumed that the forward delay was same as the half of the RTT value (symmetric characteristic of the RTT value). To overcome this limitation, the authors in [7] proposed the new forward-delay based packet scheduling algorithm by considering the unsymmetric characteristic of the RTT value (that is, the forward delay is not equal to the backward delay). Different from the previous approach, the authors in [8, 9] try to combine the MPTCP scheduler with the TCP congestion control. Although they successfully achieve their goal, the dynamic delay performance of each path remains.

B. Cross layer approach

In the recent year, some research in [10] began to explore the MPTCP scheduler in cross layer point of view. The authors in [10] first argued the necessary on the other layer information to schedule data segments in MPTCP for heterogeneous wireless networks. They proposed the MPTCP-MA (MAC layer Awareness) to estimate path status. Though using the MAC layer as well as PHY layer information, they can get the quality of each path more accurately at each end node. However, they only proposed the quality estimation for the WiFi sub-flow, and it is only indicated as availability not delay performance.

III. Challenges and Research Directions for MPTCP Scheduler in MCMR WMNs

When accommodating the MPTCP technology, MCMR WMNs still have the problem that the delay performance of each path is not stable like as the 3G/4G wireless networks. In that reason, the buffer bloat problem can occur in the MCMR WMN more seriously [11]. Accordingly, the mitigation of the dynamic delay performance is a critical challenge in the MCMR WMN.

To control the various delay performance of each path more efficiently, the future research on the MPTCP scheduler towards to the cross layer approach. In particular, exploiting the existing routing protocol and its information at MAC layer will be helpful to control the various delay performance. In addition, it will contribute to reduce the computational complexity of MPTCP scheduler in MCMR WMNs. For enhancing the network throughput while reducing the delay performance, the future research on the MPTCP scheduler also should consider the combination of the TCP congestion control.

IV. Conclusion

In this paper, we analyzed the previous works on the MPTCP scheduler to solve the reordering problem in wireless mesh networks. Through this analysis, we propose the future research directions for the MPTCP scheduler in MCMR WMNs. Using this analysis, network operators can get a more possible solution to reduce their management cost and operational cost (OPEXs) caused by computational complexity.

Acknowledgment

This work was supported by the ICT R&D program of MSIP/IITP, Republic of Korea. [1391104001, Research on Communication Technology using Bio-inspired Algorithm].

References

[1] S. Chenand J. Zhao, "The requirements, challenges, and technologies for 5G of terrestrial mobile telecommunication," *IEEE Comm. Magz.*, vol. 52, no. 5, May 2014, pp. 36-43.

[2] M. E. M. Campista, et. al., "Routing Metrics and Protocols for Wireless Mesh Networks," *IEEE Network*, vol. 22, no. 1, Jan/Feb 2008, pp. 6-12.

[3] M. Laor and L. Gendel, "The Effect of Packet Reordering in a Backbone Link on Application Throughput," *IEEE Network*, vol. 16, no. 5, Sep/Oct 2002, pp. 28-36.

[4] F. Yang and P. Amer, "Work in progress: Using one-way communication delay for in-order arrival MPTCP scheduling," *CHINACOM 2014*, pp. 122-125, 2014.

[5] T. Dreibholz, R. Seggelmann, M. Txen, and E.P. Rathgeb, "Transmission Scheduling Optimizations for Concurrent Multipath Transfer," In *PFLDNeT 2010*, 2010.

[6] H. A. Kim, B. H. Oh, and J. Lee, "Improvement of MPTCP performance in heterogeneous network using packet scheduling mechanism," *APCC 2012* 2012.

[7] T. A. Le and L. X. Bui, "Forward Delay-based Packet Scheduling Algorithm for Multipath TCP," 2015. 01 submitted.

[8] C. Raiciu, C. Paasch, S. Barre, A. Ford, M. Honda, F. Duchene, O. Bonaventure, and M. Handley, "How Hard Can It Be? Designing and Implementing a Deployable Multipath TCP," In *USENIX NSDI 2012*, 2012.

[9] C. Paasch, S. Ferlin, O. Alay, and O. Bonaventure, "Experimental Evaluation of Multipath TCP Schedulers," *ACM SIGCOMM workshop on Capacity sharing workshop (CSWS '14)*, pp. 27-32, 2014.

[10] Y. S. Lim, Y. C. Chen, E. M. Nahum, D. Towsley, K. W. Lee, "Cross-layer path management in multi-path transport protocol for mobile devices," *IEEE INFOCOM 2014*, April 27-May 2 2014, Toronto, ON, pp. 1815-1823, 2014.

[11] N. S. Ko, M. H. Kim and H. S. Park, "FD-AQM: Fairness-Aware Delay-Controlled Active Queue Management in 802.11s-Based Multi-Radio Multi-Channel Wireless Mesh Networks," *IEEE Comm. Letters*, vol. 19, no. 5, pp. 839-842, March 2015.

International Conference on Green and Human Information Technology 2016

ICGHIT 2016

Sponsored by_

THE INSTITUTE OF ELECTRONICS AND INFORMATION ENGINEERS
Computer Information Society

Technical co-Sponsored by_

IEEE
SEOUL SECTION

ISSN : 2466-121X